THE DEFORMATION OF THE EARTH DUE TO SURFACE LOADING BY STORM SURGES AND ATMOSPHERIC PRESSURE

F. FRATEPIETRO

Ph.D. 2004

The deformation of the Earth due to surface loading by storm surges and atmospheric pressure

Thesis submitted in accordance with the requirements of the University of Liverpool for the degree of Doctor in Philosophy

by
Federica Fratepietro

November 2004

Abstract

The deformation of the Earth due to surface loading by storm surges and atmospheric pressure

Federica Fratepietro

Models have been developed for computing the loading deformation of the Earth due to storm surges and atmospheric pressure variations. It shown that atmospheric pressure loading and storm surge loading, can cause surface deformations up to several millimeters and changes in the gravity accelerations of a few microGal. The loading effects associated with storm surge events vary faster (within hours) compared with those related with atmospheric pressure fluctuations (within 2-5 days); furthermore non-tidal ocean loading is generally larger (especially at high latitudes) but affects relatively small areas at a time (about 500 km of extension), while pressure variations generally affect very broad areas and the largest deformations are usually registered during the winter periods and mainly derive from an area within 2000 km from the observation point.

The regions situated in the south east of England and along the Dutch-German-Danish coastlines exhibit the largest deformation effects associated with non-tidal ocean loading (up to -30 mm of radial displacement, 10 mm in the tangential north-west direction and gravity changes of about 8μGal during particularly large storm surge events). The effect decreases gradually inland with values of almost -10 mm in the vertical deformation, 1-2 mm in the horizontal and gravity variations of 2-3 μGal at distances of 150 km from the coast. Atmospheric pressure loading and storm surge loading have almost the same magnitude but opposite signs in the northern regions of the British Isles in such extreme meteorological conditions. For stations situated well inland in Europe, atmospheric pressure loading is responsible for most of the deformation induced.

Storm surge and atmospheric pressure loading effects are particularly different when they are associated with winter seasons characterized by opposite NAO indices. When the NAO index is positive (negative) the vertical displacements produced by non-tidal loading are negative (positive) in sign as a consequent sinking (rising) of the areas investigated and the associated gravity variations are positive (negative).

The work described in this thesis is mainly concerned with developing models for better understanding the atmospheric pressure and storm surge loading deformations in the UK and north west Europe. However, as a final

part of this work, comparisons are made with available geodetic observations in this area. The comparison between the gravity measurements performed by an SG at the geophysical station of Membach (Belgium) and the predicted gravity variations induced by non-tidal ocean loading represents a useful validation of our model. On the other hand even if the signal due to the loading deformation induced by atmospheric pressure and storm surges is present in the GPS coordinates and there is some evidence that sub-daily GPS results in particular exhibit a pattern that is similar to the modelled deformation, the observed time series are too noisy at the 5-10 mm level and the comparison with modelled results are generally not conclusive.

Acknowledgments

First I would like to thank my supervisor Prof. Trevor Baker, from the Proudman Oceanographic Laboratory (POL), for guiding me in the right direction from the very first day of the Ph.D., for the support, the numerous enlightening scientific discussions, the constructive criticism and advices. I am also really grateful for the opportunity and the financial support he gave me this year to attend the European Geophysical Union General Assembly in Nice. Working with him has been an honor and a pleasure.

I am deeply indebted to Dr. Simon Williams for advising me in programming and using new computer systems.

I would like to express my gratitude to Dr. R. Flather, Dr. V. Stepanov and Dr. C. Hughes from POL for their help with sea level and atmospheric pressure data.

Dr. M. VanCamp from the Observatoire Royal de Belgique (ORB) is here sincerely acknowledged for processing the observed gravity data for the station of Membach and also Dr. R. Bingley and Alexander Waugh from the Institute of Engineering Surveying & Space Geodesy for providing and processing the GPS data.

Muchas gratias to Dr. A. Souza and in particular to Dr. P. Osuna for taking the time and the effort of helping me out of sticky situations related with typing and for the continuous encouragement.

I would like to take the opportunity to thank all the staff at POL for the assistance and the technical support.

Finally I want to express my gratitude to my friends in Liverpool and in particular to Janany Mahendran for being the good friend and companion that she is.

Un grazie speciale a Raffaella per la sua amicizia, per il supporto morale, i consigli e per aver condiviso con me le gioie e i dolori del dottorato.

Ma soprattutto voglio dire grazie ai miei genitori, ai nonni e ad Alessandro a cui questa tesi *é* dedicata. Siete stati fantastici, grazie per la fiducia e l'appoggio che mi avete dimostrato fin dal primo giorno e soprattutto nei momenti *piú* difficili. Senza il vostro amore, la pazienza e il sostegno tutto questo non sarebbe stato possibile.

Contents

List of Figures

List of Tables

Chapter 1

Introduction

1.1 Background

Dynamical phenomena constantly change the shape of the Earth and consequently cause variations in the position of points on it together with gravity variations. The deformation processes can act on very different time scales and may involve a wide range of wave numbers. In this thesis the deformations associated with surface mass loading, that generally are quasi-periodic or non-periodic phenomena, are studied.

The redistributions of mass at the surface of the Earth are produced by sea level variations (connected with tidal or non-tidal ocean changes of height), the continental groundwater circulation, the horizontal variations of the atmospheric mass distribution and the seasonal melting/accumulation of the snow. These phenomena can determine, through the pressure loading, surface deformations up to several millimeters and changes in the gravity accelerations of a few microGal. The displacements produced are primarily vertical while the horizontal deformations determined are generally about a third or less of the radial variations.

Before the advent of high precision geodetic techniques, centimetric displacements were not directly measurable and it was not necessary to account for them. Because of the rapid development and use of satellite techniques from the 1980's, and their efficacy in measuring deformations with uncertainties of a few millimeters, now the loading deformations induced by surface mass redistributions are able to be detected in the signal derived from the measurements of site positions. They have recently been observed in high precision geodetic data (see for example Van Dam and Herring, 1994; Van Dam et al., 1994; MacMillan and Gibson, 1994; Van Dam et al. 2001).

Also relative gravity observations detected with superconducting gravime-

ters and absolute gravimeters, have achieved the submicroGal precision in revealing the vertical deformations of the surface of our planet.

Since geodetic and gravimetric data are primarily interpreted in terms of geodynamic processes like for example plate tectonics, post glacial rebound or sea level rise, the non-tectonic loading effects connected with mass variations are normally considered as noise and then removed.

Geodetic and gravimetric observations can be corrected by introducing a model of the loading deformation with a precision compatible with the precision of the measurements. If this target is not reached, the accuracy of the measurements is certainly affected by unaccounted site position variations.

Any load at the surface generates regional vertical and horizontal displacements of the crust and associated gravity variations. For example, the crust yields immediately underneath the load and also in the surrounding areas. The deformation is large immediately under the load and it gradually diminishes with increasing distance from it. The relationship between deformation and distance from the load is related with the rheological characteristics of the crust and the mantle as well.

There are different methods for modelling the crustal deformations and the gravity variations induced by different kinds of loading at the Earth's surface. Many procedures consider the response functions of the Earth due to a point mass load (Green's function), and this is indeed the method used here.

In particular the deformation produced will be calculated for the case of atmospheric pressure loading and non-tidal ocean loading i.e. the loading due to storm surges. The two phenomena were chosen since they are strongly inter-connected being driven by the same weather factors. Furthermore the effects of storm surge loading on radial and tangential displacements and the associated gravity variations have never been studied in detail before.

1.2 Research objectives

The aims of this research are to give a better understanding of the loading effects of the horizontal variations of atmospheric pressure and non-tidal ocean mass changes during storm surge events. The two phenomena are driven by the same weather factors and the sum of their loading effects can have a large impact especially in coastal regions.

Accurate atmospheric corrections are provided for some British and north west European sites. The intent is the one of applying the loading calculated in order to reduce the noise in the geodetic observations and in the gravity measurements.

The evaluation of the magnitude and spatial distribution of the loading effects due to storm surge loading can help to spot those areas more sensitive to the non-tidal ocean loading. Since the deformations and the associated gravity variations produced by storm surge loading are particularly large during surge events, also this effect should be removed from the geodetic observations in order to reach a better accuracy in the determination of the long period deformations or for understanding other variations in the data.

1.3 Thesis overview

In Chapter 2, the main geodetic techniques employed for detecting the loading deformations produced by surface mass loads on the Earth will be presented together with the convolution method for loading computations. A short review of the main loading phenomena will be given. The general case of a disc with fixed thickness and variable radius, loading the surface of our planet, will be considered in order to better evaluate the magnitude of the radial deformation produced for a given load and to enable approximate estimates of the deformations achieved by real load distributions.

Chapter 3 deals with the study of the radial loading effects associated with sea level pressure distributions with variable extension in both the hypothesis of an oceanless Earth model and of a non-inverted barometer ocean model.

The aim of Chapter 4 is to study the effects of global pressure distributions on the deformations in the vertical and horizontal directions. Admittance coefficients for high precision displacements are provided and the magnitude of the radial deformations induced by local and regional variations in surface atmospheric pressure at some European sites are given. The time series modelled are compared with those available from other authors (Sherneck, 2002; Petrov, 2003). The convolution results obtained from a worldwide distribution of point loads, are compared with those computed with Rabbel & Zschau (1985) method.

The magnitude of the deformations and the gravity variations in the British Isles and northwest European regions associated with sea mass variations in shallow seas are investigated in Chapter 5. The attention is mainly focused on two large surge events which happened during the period of time investigated. Also the deformations and the gravity changes in these regions are computed for two different winter seasons characterized by opposite North Atlantic Oscillation indices.

In Chapter 6 the total loading deformation in the radial and tangential directions, obtained by summing the effects of both storm surge loading and atmospheric pressure loading is presented. The time series of the radial and

associated tangential deformations, are compared with observational values at some sites of the European Permanent Network (EPN), with continuous GPS at their locations. The time series of the gravity changes induced by storm surge loading modelled for the site of Membach (Belgium) are compared with the observations of the superconducting gravimeter at this station. Finally a further comparison looks at the British GPS station of Lowestoft, where the effect of storm surge and atmospheric pressure loading is investigated in order to assess, by comparing the estimates from GPS solutions with the model predictions, whether the GPS data are sensitive to the loading effects.

The main conclusions are given in Chapter 7.

Chapter 2

Loading on the surface of the Earth

2.1 Geodetic measurements of crustal movements

Deformations and gravity variations are continuously induced within the Earth by different kind of forces. The redistribution of ocean masses due to the tidal forcing or non-tidal ocean forcing (e.g. storm surges), the formation and the melting of the snow and ice coverage, the seasonal changes in the amount of the ground water and the variation in the distribution of the atmospheric masses are responsible for the loading at the surface.

The study of radial and tangential displacements and gravity variations at the surface of the Earth are generally performed in order to provide accurate corrections to space geodetic observations, for correctly interpreting the gravity measurements and for describing with better accuracy the long term crustal movements.

The long term crustal movements can be due to tectonics, post-glacial rebound or more local movements. In the vertical, the measurements of long term crustal movements are particularly important for determining the climate related sea level rise at a tide gauge.

The rising of the sea level is a good indicator of global climate change, it depends upon the thermal expansion of the oceans and the discharge of the polar ice sheets and glaciers at lower latitudes (Etkins & Epstein, 1982). The global mean sea level change is usually determined by the use of tide gauge observations but the measured values contain both a real change in the ocean level and variations connected with vertical movements of the land upon which gauges are situated. Many authors (Peltier & Tushingham,

1989; Peltier & Tushingham, 1991; Douglas, 1991; Nerem & Mitchum, 2001; Donnelly et al., 2004; Wadhams & Munk, 2004), have proposed sea level rising rates for the past centuries but in order to derive good estimates, relative mean sea level observations must be corrected for local, regional and continental vertical land movements (Teferle et al., 2001). To convert the relative into absolute sea level measured at the tide gauges it is necessary to model or measure the vertical land movements (Ashkenazi et al., 1993; Woodworth & Player, 2003).

There are many techniques for measuring radial and horizontal crustal movements such as Very Long Baseline Interferometry (VLBI), Satellite Laser Ranging (SLR) and the Global Positioning System (GPS) (GPS relies on SLR and VLBI for an accurate global reference frame).

For measuring displacements that regard the whole Earth it is necessary to define a reference frame. This is usually realized by the coordinates and velocities of a network of stations connected to the surface of the Earth.

A VLBI network consists of radio telescopes that simultaneously measure the radio signals arriving from space. The signals are processed in order to determine the delays in the arrival times that are used for finding the baseline between two stations. With VLBI the orientation of the Earth is observed relative to quasars.

The SLR technique involves the use of pulses of light that are transmitted from a network of stations on the Earth to several satellites. The travel time of the pulse to return back to the transmitting station is used for determining the distance between station and satellite.

The GPS system can contribute to the study of a variety of phenomena, it makes use of a nominal 24 satellites orbiting about three Earth radii above the surface and at least 4 of them are above horizon at any time. GPS satellites are equipped with powerful radio frequency transmitters. GPS receivers monitor signals emitted by the satellites, in order to obtain precise point positions or relative positions with precisions of millimeters over baselines of several thousands of km. GPS has the potential to detect vertical movements with a precision of 1 mm/yr after 10 years of measurements (Baker et al., 1997; Williams et al.,2004).

The surface deformations of the Earth can also be determined by variations in gravity. The law of gravity states that the strength of gravitational attraction between two masses is inversely proportional to the square of the distance between them. Simplisticly, the changes in elevation of the land create a different distance between the surface and the center of the Earth and hence a change in gravity. Knowing the gravity variations it is possible to obtain the corresponding change in elevation (after making corrections for the redistribution of mass).

Gravity measurements can be relative or absolute. The relative gravimeters can only detect the changes in gravity between two sites and the variation of gravity in time at a certain station. Instead absolute gravimeters measure the gravity value at one site. The technique used for relative measurements uses either a mass on a spring or a superconducting sphere in a magnetic field. Superconducting gravimeters use a sphere levitated by persistent currents in superconducting coils; the vertical position of the coil depends upon the gravity changes measured. The LaCoste & Romberg gravimeter is the most common relative gravimeter, it is based on a zero length spring and it can achieve, depending on the magnitude and the time gap between measurements, a precision as good as 1 μGal in the determination of the gravity differences between two sites (Hopewell, 1999). The technique used for absolute measurements in gravity is the observation of the gravitational acceleration of a mass in free fall in a vacuum. The Micro-g FG5 is a commercial absolute instrument with a precision of $\pm$1-2 μGal and an accuracy of $\pm$1-2 μGal (Sasagawa et al., 1995; Okubo et al., 1997; Williams et al., 2001).

2.2 The elastic deformation of the solid Earth

When external loads are applied at the surface of the solid Earth they cause deformations. A displacement vector having a normal and a tangential component is generated, together with deviations from the local vertical (tilt), variations in the gravity intensities and strain tensors. A description of the method for calculating the deformation of the Earth caused by a mass load placed at its surface is given in Appendix A, it follows Farrell's paper (1972).

In general to calculate surface loading at the surface of the Earth, the equations of equilibrium of the deformed Earth have to be solved, these are derived from the equations of the free oscillations. A different set of boundary conditions with respect to that considered for the body force problem, has to be taken into account (Lanzano, 1982). In fact there is a normal stress acting at the surface of the Earth that is not present in the body force problem.

Since the response of the Earth to mass loading is strongly related to the local properties of the crust and the mantle, a gravitating, elastic Earth model is considered and the elastic parameters (compressibility, rigidity and density) are assumed as functions of depth.

2.3 The convolution method

An efficient way of calculating the vertical and tangential displacement and the variation in gravity due to a distribution of point masses at a certain site is to perform a convolution between the load distribution and the appropriate Green's function for loading.

The Green's functions give the response of the Earth to a point mass load as a function of the angular distance θ from the load.

$$u(\theta) = \frac{r_{Earth}}{m_e} \sum_{n=0}^{\infty} h_n P_n(\cos\theta)$$
$$v(\theta) = \frac{r_{Earth}}{m_e} \sum_{n=1}^{\infty} l_n \frac{\partial P_n(\cos\theta)}{\partial\theta} \tag{2.1}$$

$$g(\theta) = \frac{g}{m_e} \sum_{n=0}^{\infty} (n + 2h_n - (n+1)k_n) P_n(\cos\theta) \tag{2.2}$$

Equation (2.1) represents the Green's functions for the radial and the tangential displacements (see Figure 2.1), while Equation (2.2) describes the gravity Green's function. In particular, h_n, l_n and k_n are the load Love numbers, the terms $P_n(\cos\theta)$ are called the Legendre polynomials with n denoting their degree, m_e and r_{Earth} are the mass and the radius of the Earth and g is the gravitational acceleration (see Appendix A for details).

In Equation (2.2), the first term in brackets is the component of the direct gravitational attraction perpendicular to the surface at the station and is called the Newtonian acceleration g^N.

$$g^N(\theta) = -\frac{g}{4m_e \sin\frac{\theta}{2}} \tag{2.3}$$

The elastic acceleration g^E deriving from the Earth's elastic deformation, is instead defined as follows:

$$g^E = g - g^N \,. \tag{2.4}$$

The convolution procedure should involve an integral over the entire mass loading distribution (Equation 2.5) but for practical purposes is generally approximated by a finite sum.

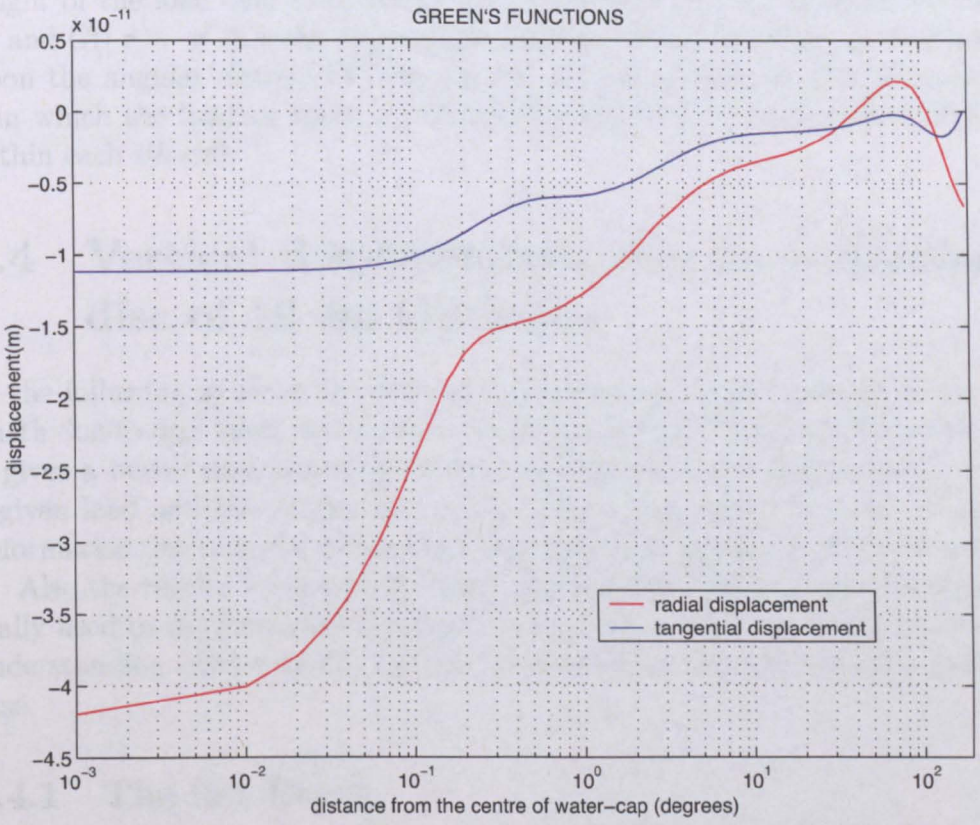

Figure 2.1: Radial (red curve) and tangential (blue curve) surface displacement Green's functions for the Preliminary Reference Earth Model (PREM) (Dziewonski and Anderson,1981). The curves are normalized by the factor $(r_{Earth} \cdot \theta)$, where r_{Earth} is the radius of the Earth $(6.371 \cdot 10^6 m)$ while θ is the distance from the load in radians.

The loading response $L(\mathbf{r})$ at a point on the Earth's surface with position vector $\mathbf{r}$ is:

$$L(\mathbf{r}) = \rho \int \int G(|\mathbf{r} - \mathbf{r}'|)\psi(\mathbf{r}')dA \tag{2.5}$$

where ρ is the density of the matter loading the surface, $\psi(\mathbf{r}')$ is the height of the load over the surface area considered dA at a position vector $\mathbf{r}'$ and $G(|\mathbf{r} - \mathbf{r}'|)$ is the appropriate loading Green's function. It depends upon the angular distance θ between the *ith*-cell considered and the point p in which the loading effect is calculated. The load is considered uniform within each *ith*-cell.

2.4 Vertical displacements due to a circular disc of 10 cm thickness

In the following sections the vertical displacements of the spherical layered Earth due to disc loads of various radii are computed. This is useful because it gives a better understanding of the magnitudes of the displacements for a given load and the results also enable good estimates to be made of the deformation due to a real distributed load (pressure, ground water or ocean).

Also the results for the more simple Boussinesq's Green's function (generally used in the simplified flat Earth case), will be used to obtain a better understanding of the results for the more realistic spherical layered Earth case.

2.4.1 The flat Earth

The Boussinesq formula is used for the calculation of the response of a non-gravitating, elastic half space to a unit surface force. It is assumed that the elastic medium is a half space with depth $z \leqslant 0$ and that the only load is acting vertically at the origin. The loading is assumed symmetric and so it does not depend upon the azimuth θ.

The Boussinesq's solution is generally used in the simplified flat Earth case where the Earth is assumed to be homogeneous so its own characteristics of rigidity, compressibility and density remain constant with increasing depth. It supplies a standard response, convenient for normalizing the spherical Green's function, furthermore near a point load the formula represents the limit of the value of the spherical solution and it can be used for checking the spherical numerical calculations (Farrell, 1972).

For computing the vertical displacement due to a unit force at a distance r from the center of a disc it is necessary to calculate the loading due to an infinitesimal area in the disc dA:

$$dA = r \cdot dr \cdot d\theta$$

where r and θ are the polar co-ordinates of the infinitesimal area inside the disc, and then to integrate over all the disc.

In this particular case the force is not a unit one so it is necessary also to multiply the mass by the gravitational acceleration g.

$$u = \int\int \rho \left[\frac{(\lambda + 2\mu)}{\mu(\lambda + \mu)} \frac{1}{r}\right] \cdot r \cdot dr \cdot d\theta \cdot h \cdot g$$

The term in brackets is the Boussinesq Green's function and λ and μ are the Lamé parameters of the uniform half space.

Evaluating the integral for the displacement at the center of the disc it follows:

$$u = -\frac{\rho h g}{2} \cdot \left[\frac{(\lambda + 2\mu)}{\mu(\lambda + \mu)}\right] \cdot R \tag{2.6}$$

where R is the radius of the disc. The equation is a linear function of R. The negative sign indicates that the observational point is displaced radially downward.

2.4.2 The spherical Earth

A model for calculating the vertical displacement due to a circular disc of water loading on the Earth was developed.

This program helps to solve a very general problem because the thickness of the water h could be extra water in the ground, the increase of the atmospheric pressure over the land, extra water over the ocean due to tidal or non-tidal ocean loading or snow coverage loading.

The thickness of the water h was assumed equal to 10 cm. The density of the water ρ was chosen equal to the density of the pure water (1000 kg/m^3).

The response of the Earth model to disc loads was calculated at the equator, but since a perfect spherical Earth model was used, the response of the vertical displacement results will be identical wherever the disc is placed.

The disc was subdivided into a suitable number of cells and a convolution between Farrell's Green's function (for the Preliminary Reference Earth Model (PREM))(see Dziewonski & Anderson, 1981)) and the mass of each loading element was performed in order to find the total vertical displacement at various distances from the center of the disc i.e. all the results for a certain site were summed up to obtain the value of the vertical displacement due to the circular disc of water at that site. The program uses a subroutine for determining the Green's function at the above distances.

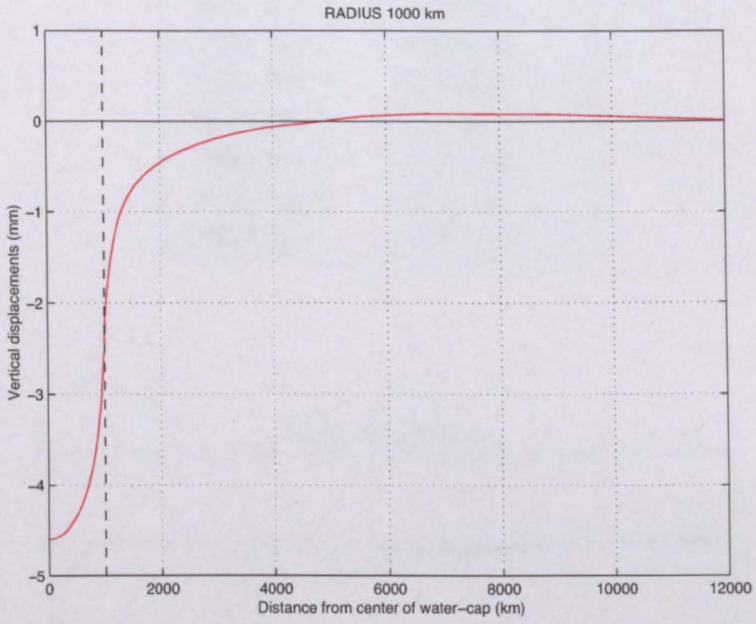

Figure 2.2: Vertical displacements (mm) for a 1000 km radius disc of water. The dotted line is drawn corresponding to the edge of the disc. The thickness of the disc is equal to 10 cm.

For a radius r of the disc equal to 1000 km it was found that the displacement at the central site is around -4.6 mm. The deformation in the vertical at the edge of the disc decreases to -2.8 mm and reaches 0 mm at about 5000 km from the site of interest. For greater distances the radial displacement is slightly positive (see figure 2.2).

In table 2.1, is presented the magnitude of the radial deformation in the center of the watercap when different radii are considered. The displacement is generally bigger when a greater radius is considered (see figures 2.3 and 2.4). However when the disc radius is greater than 50 degrees, the Earth's spherical shape becomes more important, as can be seen in Figure 2.4.

Table 2.1: Vertical displacement in mm at the center of the disc of water with thickness equal to 0.1 m and different radii (km).

RADIUS	DEFORMATION
50 km	-0.6 mm
100 km	-1.0 mm
500 km	-3.2 mm
1000 km	-4.6 mm
2000 km	-6.6 mm
3000 km	-8.0 mm
5000 km	-8.8 mm
7000 km	-7.5 mm
9000 km	-5.5 mm
10000 km	-4.7 mm

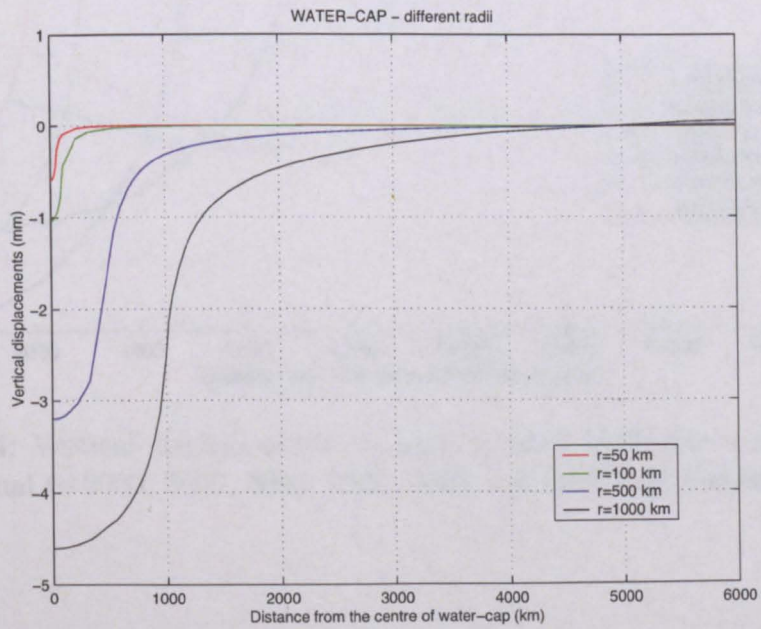

Figure 2.3: Vertical displacements (in mm) induced by a disc of water with radius equal to 50, 100, 500 and 1000 km respectively.

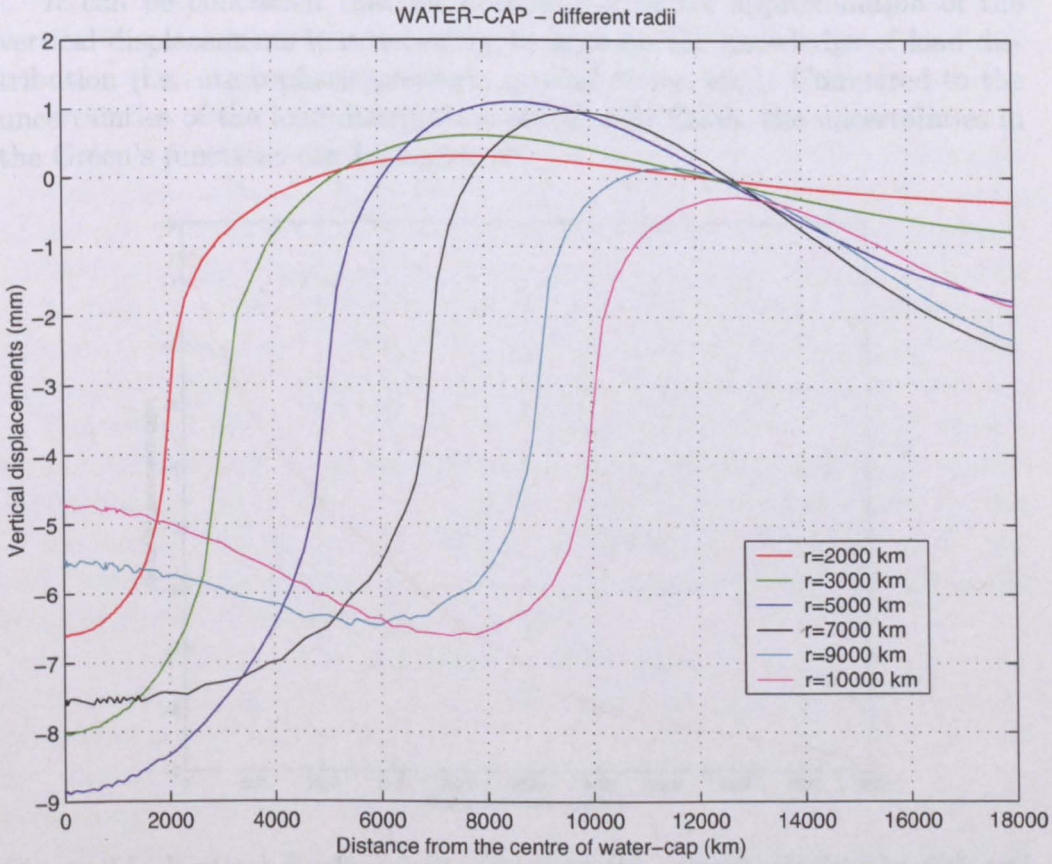

Figure 2.4: Vertical displacements (in mm) induced by a disc of water with radius equal to 2000, 3000, 5000, 7000, 9000 and 10000 km respectively.

The program was also run choosing different Green's functions. In the case of 1000 km of radius, it was found out that the differences between the results using various Green's functions stay between 0.25% and 1% for nearer distances. This fact means that the uncertainties due to the different Earth model (and then different Green's function) are always less than or equal to 1%. In general the vertical displacements are not measured with this accuracy.

It can be concluded that for obtaining a better approximation of the vertical displacements it is necessary to improve the knowledge of load distribution (i.e. atmospheric pressure, ground water, etc.). Compared to the uncertainties of the load distribution on the real Earth, the uncertainties in the Green's functions can be neglected.

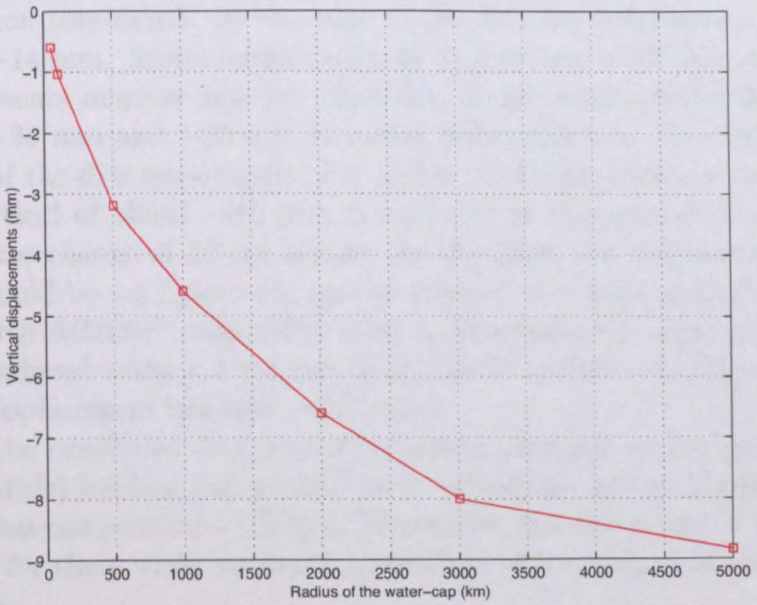

Figure 2.5: Vertical displacements (mm) at the central site for the different radii of the disc

Observing figure 2.5, in which it is presented the curve of the vertical displacement at the central site for the different radii of the disc (see Table 2.1), it is evident that it does not produce a linear behavior as would be predicted by Equation (2.6).

In the Boussinesq's problem the Earth is supposed to be homogeneous, so the values of λ and μ are selected as constant. In fact in an ideal stratified Earth, each layer forming the Earth has its own values of the Lamé parameters. In particular since the Earth becomes less elastic with the increasing

depth, the value of the seismic velocities and the Lamé constants become bigger.

The Green's function chosen for the more realistic spherical and stratified Earth case was not the Boussinesq's formula. This Green's function (PREM) takes into consideration the changes of the magnitude of the Lamé parameters with the depth. In particular the deformation at a distance R from a point load mainly depends upon the values of λ and μ around a depth equivalent to the distance R. As a result the displacement observed for bigger radii is smaller then the one we expect from the Boussinesq's results, since the Earth becomes more rigid with depth and so these parameters become bigger.

From the results of the disc computation (summarized in Table (2.1)), it can be said that a change in pressure of 50 mbar over a 2000 km diameter area can determine a vertical displacement of about -23 mm in the centre of the region considered. At the edge of the disc the deformation produced is about -14 mm. Storm surge residuals of 2 m over a 200 km radius disc, that represents more or less the extension of the southern North Sea, can produce -36 mm and -20 mm of radial deformation at the center and at the edge of the disc respectively. For a disc of 500 km radius a deformation in the vertical of about -3.2 mm is achieved at the central point when a groundwater change of 10 cm occurs. At the edge, the displacement in the vertical would be -1.7 mm. For spatial extensions comparable with the one of the North Atlantic ocean (2000 km), a deformation of almost -0.70 mm can be produced when a 1 cm non-tidal load is applied. At the edge of the disc the displacement becomes -0.35 mm.

It can be concluded that synoptic pressure changes, storm surges, larger scale non-tidal loading and groundwater variations, are all important phenomena that can produce loading deformations. For this reason it is essential to correct for them when we look for precision of few millimeters in GPS observations.

Furthermore, as it was already pointed out by Van Dam (1991), also in our case it was observed that the deformation scales linearly with the mass over the disc and increases, but less than linearly, with the diameter of the disc.

2.5 Different kinds of loading

Dong et al. (2002), have shown that 42% of the observed power (square of the mean amplitude), in the annual vertical variations of site positions, as derived from 4.5 years of global continuous GPS time series, can be explained if various kinds of mass loading are taken into account. In fact, not only the

seasonal signal is important to be considered but also monthly, weekly and even hourly variations in pressure, sea level heights or ground water content have to be taken into account in order to provide accurate corrections to space geodetic observations. For this purpose the convolution method has been extended by various researchers for determining the loading deformations caused by variations in ground water, melting and accumulation of snow and ice, tidal and non-tidal ocean loading and atmospheric pressure loading at various time-scales.

In the following sections the different kinds of loading will be discussed in detail and the magnitude of the corresponding deformations as available from the recent literature will be presented.

2.5.1 Atmospheric pressure loading

Atmospheric pressure changes are caused by the passage of low or high pressure systems. They are regional phenomena and their scale length ranges from several kilometers (tropical cyclones) to a few thousands kilometers (continental anticyclones).

The variations in the horizontal distribution of atmospheric mass deform the Earth's crust in a quasi-periodic way. In fact the local and regional pressure variations influence the measurements of the surface displacements through the loading deformation.

The largest pressure variations are in general those associated with synoptic scale storms, that generally move with periods of a few days but sometimes can be stable for weeks (Stolz & Larden, 1979, MacMillan & Gibson, 1994). They have a spatial distribution of about 2000 km and the largest surface pressure fluctuation (about 40-50 mbar), for these reasons they are expected to contribute the most to the pressure loading.

The displacements caused by atmospheric pressure loading are primarily vertical and the horizontal ones are small but not negligible (generally they are about one third to one tenth of the associated radial displacements(Van Dam & Herring, 1994)). The contribution to surface displacements due to the global seasonal fluctuations of barometric pressure is generally less than 1 cm in the vertical, while vertical displacements associated with pressure variations frequently larger than 20 mm were detected by Van Dam & Wahr (1987).

Sun et al. (1995), pointed out that the deformation generated by variations in the atmospheric pressure distribution is in the order of 20-30 mm in the vertical if a regional pressure change of 50 mbar is considered. For the horizontal deformation instead, corresponding displacement of about 2.0-3.0 mm for the East-West component and 0.5-1.0 mm for the North-South one

can be detected.

It is also known that displacements are generally larger at higher latitudes and during winter months (1-2 cm during each winter month at higher latitudes) this is mainly due to the larger associated pressure variations (Van Dam & Wahr, 1987).

The calculation of the atmospheric pressure surface displacements is mainly influenced by the lateral extension of the considered load, in particular the main contribution comes from the horizontal distribution of the air pressure in a very broad area, so it is necessary to consider a column load of at least 1000 km around the station of interest for accurately determining the loading deformation induced (Sun et al., 1995, Van Dam & Wahr, 1987).

The effects of atmospheric loading at the surface can be computed by performing a convolution sum between the mass loading Green's function and the local and regional barometric data pressure. Commonly the convolution method cannot be replaced by a simple regression between the local air pressure and the vertical displacement (admittance coefficient), since the deformation induced is also determined by the long-wavelength terms of the load distribution (Rabbel & Schuh, 1986).

The air pressure changes gravity data as well because of the direct attraction of the atmosphere, because of the elastic deformation on the Earth's crust and because a variation of the potential due to the mass redistribution (Sun et al., 1994). Green's functions are used as well for evaluating the contribution of global atmospheric pressure variations to local gravity using a column load of a model atmosphere.

Because of the curvature of the Earth, at a gravity site, the attraction of some parts of the atmosphere that are close to the horizon have no contribution to vertical gravity. 90% of the signal comes from a zone of 50 km radius from the gravity site. Between 50 and 250 km the signal is very small. The zone from 250 to 500 km plus the rest of the world, produces the remaining 10% (Merriam, 1992).

It is suggested to divide the globe in 3 different zones: local, regional and global. The first zone is within an area of 50 km from the gravity station. Here the atmospheric pressure is essentially uniform, so a single barometer at the gravimeter site detects the entire signal from this zone, but it is necessary to make hourly observations of pressure and temperature at the gravity site. When a front is passing through, more information on pressure is required. In general the results depend upon the station height above the sea level, on the topography around the station and on temperature variations.

The regional zone extension is from 50 km to 1000 km from the gravity station; a sparse array of hourly samples of pressure and temperature is required. Here the pressure field is related with the one of the local zone.

The global zone is influenced by the pressure variations over the oceans; its extension is greater than 1000 km from the gravity site.

Gravity variations up to 15 μGal peak to peak are common (Sun et al., 1994). Rabbel and Zschau (1985), pointed out that total gravity perturbations may go up to ± 20 μGal for a passing (anti)-cyclone and variations of ± 3 μGal related with seasonal air pressure variability are common. Merriam (1992), concluded that atmospheric pressure can determine gravity changes of about 30 μGal and that most of the signal is produced within an area of 50 km from the gravimeter.

Sun et al. (1994), pointed out that the discrepancies in the results about the contribution of global atmospheric pressure variations to gravity, found by different authors, may have various causes as for example: the model of atmosphere considered, the time and space intervals of the pressure data, the scale height, the lateral scale of the load considered, the distance of the station to the ocean areas or the treatment of the subdivision of the grid elements near the station.

2.5.2 Tidal loading

The surface of the Earth is continuously deformed by the gravitational pull of the Moon and the Sun. This gravitational attraction determines the deformation of the Earth known as the body tide or Earth tide and the periodic rise and fall of the oceans that determines the ocean tides (Garland 1979; Melchior, 1983). As a secondary effect the Earth deforms under the varying tidal water mass load as well and this effect is called ocèan tide loading.

Because of the tidal forces the surface of the Earth moves through a range of over 40 cm in a little over 6 hours and in addition, a periodic load due to the ocean tides determines displacements of over 10 cm in range (Baker, 1984; Baker et al., 1995). These quite large displacements are also associated with variations in gravity.

The body tide deformation can be determined with a very high precision (about 2 mm) (Baker et.al., 1991), the uncertainty that remains is due to the effect of later heterogeneities in structure and inelasticity at tidal periods.

The magnitude of the ocean tide loading deformations depends on the rheological properties of the Earth, crust and mantle. The ocean tide loading has to be removed for studying the body tide and calculation of ocean loading deformations are also required in order to correct the modern high precision space geodetic measurements.

The loading deformation is site dependent because it changes with the spatial distribution of the ocean tide with respect to the observation site and,

nearby and distant ocean tides, are important for the calculation (Baker et al., 1995).

For computing the ocean tide loading a model of the ocean tides and the response functions of an Earth model (Green's functions) are needed. At the moment ocean tide loading calculations can be performed with several available computer programs (Sherneck, 1991; Pagiatakis 1992, Agnew, 1997). All the Earth models derive from seismic observations but we can also note that there does not exist a perfect model describing the real response of the Earth or the tides everywhere. This is because the oceans respond dynamically to the tidal forces and each harmonic has its own spatial variation and the accuracy of the model is related with the bathymetry resolution and the energy dissipation mechanism assumed (Curtis, 1996).

The Earth tides and the ocean tides generated by the tidal potential can be described by an amplitude and phase for each tidal harmonic, which vary spatially over the surface of the Earth. Symbols has been given to the largest harmonics (the principal lunar tide M_2, the principal solar tide S_2, the lunisolar K_1, the lunar declination O_1, ...), each of them represent an astronomical movement.

The computation of the loading displacements and potential involves a summation over an infinite number of spherical harmonics (Baker, 1984 and 1985). Nevertheless this method has some disadvantages since the ocean tide expansion is usually carried out up to a degree $n = 40$. This truncation causes problems for sites nearer to the coast than 1500 km since a higher degree of the expansion would be required.

More easily the ocean tides can be considered as a sum of point loads. For being realistic, the distribution of load points obtained is made progressively denser near the station. The surface of the Earth is divided in cells and it is assumed that the ocean tide is uniform over each cell. For obtaining the ocean tide loading at any distance from the coastline a convolution between the ocean tide and the appropriate loading Green's function is performed. The loading is calculated by summing the deformations produced by each cell.

Ocean tide loading causes gravity variations as well. The causes are related with: the change in gravity due to the vertical displacement of the gravimeter on the deformed Earth, the redistribution of mass of the deformed Earth and the direct gravitational attraction of the ocean tide (see Equation(2.2)).

For gravity stations near the coast it is also very important to include corrections for the additional attraction due to the height above the sea level. The lateral changes in in Earth structure have a very small effect on tidal gravity (Baker et al., 1991).

2.5.3 Continental water loading

Among the loads that are important for correctly evaluating deformations of the Earth's surface, those associated with the continental water storage have to be considered. When we refer to continental water loading, the water stored in the snowpack, in the soil and the groundwater is intended.

Groundwater is defined as the water situated below the Earth's surface and contained in the soil or in the rocks. This amount of water depends upon the porosity, the free air pockets in the material considered and their interconnection (permeability).

A model of global continental water-storage variations due to rainfall, snowmelt and evaporation has to be considered. This is a very difficult target to achieve since the uncertainty of the parameters in the model formulation leads inevitably to significant errors.

Van Dam et al. (2001), found out that the load caused by the variations in the continental water storage is dominantly seasonal but it also presents a significant interannual variability in amplitude. The vertical surface displacement over most of the continental areas reaches values between 9 and 15 mm, but it can be as large as 30 mm in monsoon regions or tropical zones and even in areas covered by ice (southern coast of Alaska and western coast of Canada). The associated tangential deformations have maximum variations of 5 mm in those areas showing the largest vertical signal.

It was demonstrated that continental water loading in areas where the water storage is consistent, can explain some of the long period variability observed in GPS time series previously corrected for atmospheric pressure and non-tidal and tidal loading (Van Dam et al., 2001).

As well as large scale continental water loading, gravity is affected by the attraction of local water masses. Attempts to correlate rainfall events and observed gravity variations have been not completely successful even if variations in groundwater level related with rainfall, would generally have a large effect on gravity. Apparently other factors such as temperature, relative humidity and soil moisture may be important to consider for correctly determining the relationship between rainfall and gravity variations. Goodkind (1986), pointed out that during the heaviest rainfall the gravity at some stations may increase by 0.54 μGal per centimeter of rain. Van Dam & Francis (1998), found out that changes in gravity mostly depend upon the amount of water in the soil beneath the gravimeter rather than on the height of the sheet of water on the surface. Baker (1993), pointed out that variation in ground water at some sites can produce gravity variations that are in excess of 10 μGal.

2.5.4 Non-tidal ocean loading

Non-tidal oceanic loading determines oceanic bottom pressure changes that are responsible for the deformation of the geoid and the nearby crust because of the pressure itself and because of the gravitational attraction of the mass anomaly causing the pressure variation.

Non-tidal ocean loading effects are typically about 5 mm peak to peak in the radial direction for sites situated nearby the coastline, but when large oceanic disturbances happened, the deformation can reach values up to 10 mm at some stations and even more. Horizontal displacements are about one-third of the vertical ones.

The corresponding gravity variations associated are usually in the order of 2-3 μGal but changes about 5 μGal peak-to peak are also predicted (Van Dam et al., 1997).

It was also noticed that a large number of GPS stations of the IGS global network are located in areas very close to the coast or nearby the water and this fact makes it very important to properly evaluate the vertical and tangential deformations and the gravity variations induced by this kind of loading, in order to remove them from the observations.

Munekane & Matsuzaka (2004) have considered the effects of non-tidal ocean loading on the seasonal variability observed in the coordinates of some GPS stations in the Pacific region. They found variations of up to several millimeters in the vertical components for GPS sites surrounded by water. At these locations the non-tidal ocean loading was found to be more significant than the atmospheric pressure and the snow/soil moisture mass loading.

Storm surges are a particular type of non-tidal ocean loading. They affect areas of extensive shallow water on wide shelves. Storm surge loading effects have not so far been considered in the literature and for this reason, in this thesis an entire Chapter (Chapter 5), will be dedicated to the study and the determination of the magnitude of the deformation and gravity changes associated with sea mass variations, in particular in the North Sea.

2.6 Conclusions

In this chapter the main geodetic techniques currently used for detecting the deformation on the Earth due to the loading at its surface were presented.

The convolution method, generally employed for the calculating the deformation induced, was also introduced and a detailed description of the theory at the base of the methodology was given. Since the convolution method has been extended to calculate the effects caused by different kinds of loading, a

short review of all the main loading phenomena was presented together with the magnitude of the vertical and horizontal deformation induced and the associated gravity variations as available from the recent literature.

The formulation was also used in the general case of a disc with fixed thickness and variable radius loading the surface of our planet. This gives a better understanding of the magnitude of the radial deformation produced for a given load and enables good estimates of the deformation achieved by a real load distribution when a progressively broader area is responsible for the loading at a certain location. It was noticed that when the radius of the disc is greater that 5000 km, the spherical shape of the Earth becomes important.

It was pointed out that the choice of different Green's functions did in general, not matter so much in the definition of the final result because the differences reached stayed between 0.25% and 1% for the nearer distances. It was concluded that it is necessary first to improve the knowledge of the loading distribution for obtaining more accurate values of the radial deformation induced. In fact compared with the uncertainties in the load distribution, the uncertainties in the Green's functions can be neglected.

From the results of the Boussinesq's Green's function for vertical displacements, generally used in the simplified flat, homogeneous Earth case, a better understanding of the results for a spherical layered Earth was achieved. It was pointed out that when the radius of the disc becomes bigger, also the Lamé parameters should became bigger as a consequence of the increased rigidity of the Earth with depth.

Chapter 3

Atmospheric pressure loading using a sea level pressure model

Since among the different causes that produce loading on the Earth's surface, the atmospheric pressure variations are one of the most important, in the last few years different methods were developed for computing air pressure corrections for surface displacements and gravity measurements. Pressure loading is then removed from astronomical and geodetic observations in order to determine the long period deformation at the Earth's surface (typically1 or 2 mm/year in the radial direction) with greater accuracy.

The vertical displacements at the Earth's surface known as atmospheric pressure loading, are those associated with the variations in barometric pressure due to the change of the weight of the column of atmosphere. For computing the deformation at a site, information about the global distribution of atmospheric pressure and the response of the ocean surface driven by atmosphere forcing are needed in detail.

Generally the pressure distribution around a site has to be known with particular accuracy within an area extending about 1000-2000 km from the station considered. In fact, the main contribution to pressure loading is caused by synoptic weather patterns. Synoptic storms commonly have a life span of approximately 5 days and scale pressure systems of 1000-2000 km. They do not contribute appreciably to the seasonal variability in global pressure (Van Dam et Wahr, 1987), but they have the largest surface pressure variations and therefore are expected to contribute the most to pressure loading (Van Dam et al., 1994; MacMillan & Gibson, 1994). Their effect can reach 10% of the total signal due to the astronomical forces, so this signal must be removed for correctly studying the geophysical and geodynamical problems of the solid Earth (Sun et al., 1994).

The aim of this chapter is to study the effects on the vertical displace-

ment associated, with different lateral extensions of pressure distributions. Air pressure correction values (admittance coefficients), for high precision displacement measurements are provided and an idea about the magnitude of the surface displacements produced by local and regional variations in atmospheric pressure at some UK sites is given.

The deformation induced is calculated following two different approaches. First the radial displacement is calculated performing a convolution (CONV method) between the pressure distribution and the appropriate Farrell's (1972) Green's function in the hypothesis of an oceanless Earth model or Non-Inverted Barometer Ocean (NIBO) model; second an Inverted Barometer Ocean model (IBO) is assumed. Some important conclusions are derived from the comparison of the results achieved.

Also the methodology of Rabbel & Zschau (1985) that used the Two Coefficients Correction Equation (TCCE method), is performed for calculating the deformation at a site. A comparison of these latest results with those obtained from both the hypotheses considered (NIBO and IBO), is performed. The results of the comparison are discussed in order to understand which is the most convenient method to be used when high accuracy is required in the determination of the loading deformation.

3.1 Numerical modeling of atmospheric pressure and deformation induced

Atmospheric pressure data at zero height above mean sea level for the entire world were available from the National Center for Atmospheric Research (NCAR). They were computed every six hours during the period of time investigated (January 1998 - December 2000).

The atmospheric effects on vertical displacements were computed by performing a convolution between the local and the regional barometric pressure data and the mass loading Green's function (CONV method). The surface pressure load determining the deformation was reduced to a distribution of point loads and the displacement produced by each of them was summed up for calculating the final result.

The deformation was evaluated at Sheerness, Lowestoft and Herstmonceux, situated on the south east coast of the British Isles. These sites were chosen since they have a continuous GPS station at their location.

Two models of atmospheric pressure loading effect on vertical deformation of the Earth's surface were developed. In both the models a more detailed grid, coinciding with the Proudman Oceanographic Laboratory Storm Surge

Model (POLSSM) grid, was considered for the area of the UK and the North European coasts. This sub-grid covers 25 degrees of extension in longitude (between 12 W and 13 E) and 15 degrees in latitude (between 63 N and 48 N) with a resolution of 0.16 degrees in longitude and 0.11 degrees in latitude (see Figure 5.1). For the rest of the world a new 1 degree x 1 degree spherical grid system was considered.

The loading elements closer to the site of interest were smaller than those used for the rest of the world, since a denser distribution of point loads near the station of interest generally achieves more realistic results.

Since our interest was just focused on the atmospheric pressure variations, the International Standard Atmospheric pressure (ISA) value at the sea level (1013.25 mbar) was removed from each pressure datum.

The mass of each cell was evaluated by multiplying the pressure value at the center of the cell by the area of the loading element previously computed and then dividing by the gravitational acceleration g_0. The correct value of g_0 (since it is a function of latitude θ), was determined using the International Gravity Formula (IGF) (Vanicek and Krakiwsky, 1986).

$$\begin{aligned} g_0 &= 978.0327[1 + 0.0052790414 \sin 2\theta + \\ &\quad + 0.0000232718 \sin 4\theta + 0.0000001262 \sin 6\theta] \end{aligned} \tag{3.1}$$

3.2 Non-Inverted Barometer Ocean model (NIBO)

The first model of the radial displacement induced by atmospheric pressure variations considered was an oceanless Earth or Non-Inverted Barometer Ocean (NIBO) model since the resulting vertical deformations at the chosen sites arose from the contribution of pressure loading over both the land and the ocean areas i.e. the contribution to the radial deformation of all the loading elements of the interpolation grid in which the world was subdivided were considered.

On the sea level pressure grid from NCAR, covering the whole of the world, longitude values were set every 1.875 degrees but for the latitude the interval between two data points was not regular (it varied between 1.880 and 1.905 degrees).

Sea level pressure data were first interpolated onto the sub-grid (POLSSM grid) covering the British Isles because of the smaller dimensions of the cells considered. In fact for achieving a better accuracy in the determination of the loading deformation, many authors (Van Dam & Wahr, 1987; Sun et al., 1995) have suggested such a subdivision of those grid elements closer

to the site in which the deformation has to be computed. Then, another interpolation onto the 1 degree x 1 degree grid was used for the further regions.

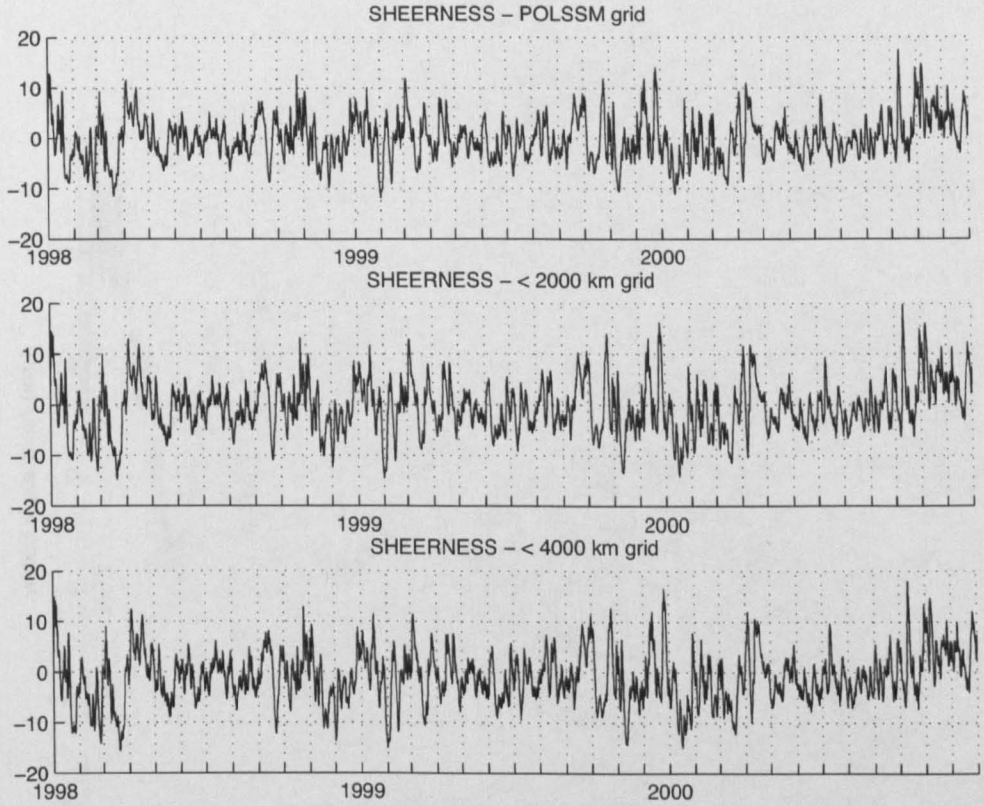

Figure 3.1: Radial displacements (in mm) for the site of Sheerness during the period of time investigated (1998-2000). The first plot from the top represents the vertical displacement induced by atmospheric pressure when just the cells in the POLSSM grid are considered to contribute to the deformation. The second and third plot represent instead the deformation at the site when the contributions of all the loading elements within a radius of respectively 2000 and 4000 km from the station are summed up.

The radial displacement at the British sites of Sheerness, Lowestoft and Herstmonceux was evaluated for three different cases. The contributions to the displacement were computed due to the cells of the sub-grid and also due to all the cells to a distance of up to 2000 km and 4000 km from the site of interest. The limit of 4000 km of radius was set after the conclusions derived from Van Dam & Wahr, (1987) and Sun et al.(1995).

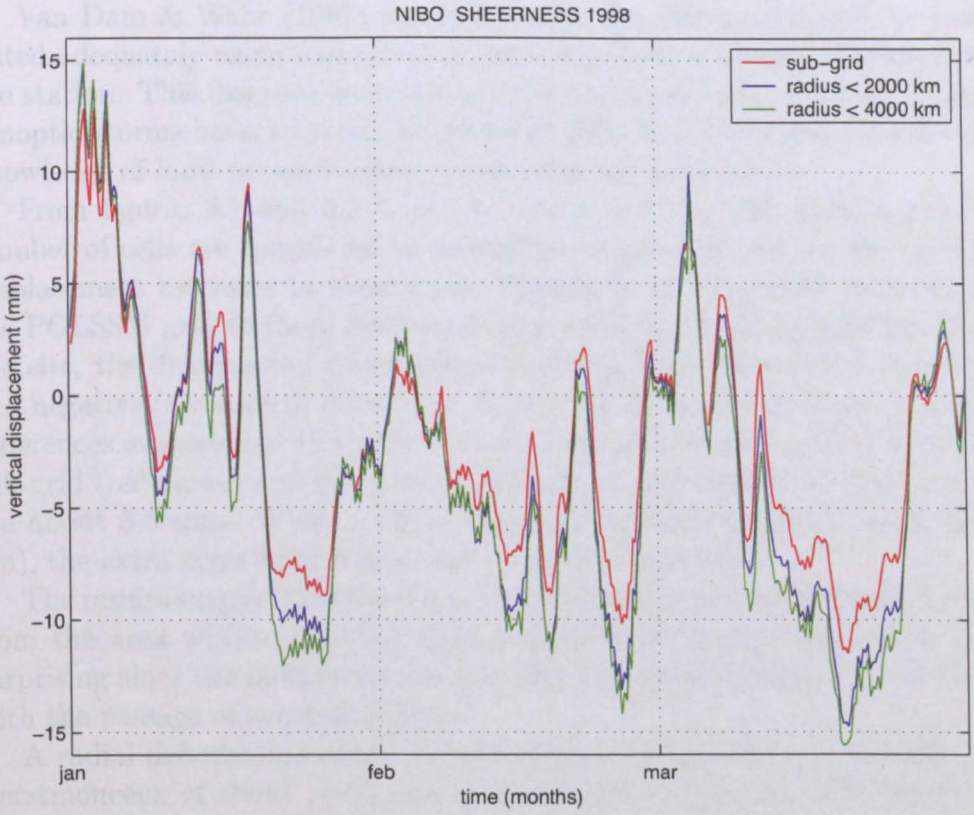

Figure 3.2: Comparison of the vertical displacements for the site of Sheerness for the first three months of 1998. In red is drawn the deformation due to the contribution of the loading elements in the sub-grid, in blue is drawn the contribution due to the cells in the surrounding 2000 km area and in green the contribution of the grid units in the surrounding 4000 km area is presented.

The choice of calculating the vertical deformation considering three different radial extensions around the location of interest, was also made in order to study the effects on the deformation of the lateral pressure distribution and to determine the distance at which the result starts to converge. This would indicate which is a reasonable area to be accounted for achieving accurate results.

Van Dam & Wahr (1987) concluded that the deformation can be computed adequately using real pressure data from points within 1000 km from the station. This distance is consistent with the observation that the largest synoptic storms have a spatial extension of 2000 km across and because the knowledge of local pressure alone is generally not sufficient.

From figures 3.1 and 3.2 it can be easily noticed that when a greater number of cells are considered to contribute to the deformation the vertical displacement increases in magnitude. Passing from the results achieved on the POLSSM grid to those estimated from an area extending 4000 km from the site, the deformation shows larger peaks in both the positive (upward) and negative (downward) directions. Figure 3.2 in particular, shows that the differences evaluated at the peaks, between the deformation arising from the sub-grid (red curve) and the area of 2000 km around Sheerness (blue curve) are about 3-5 mm. When a larger region is considered (radius equal 4000 km), the extra contribution is about 1-2 mm on average.

The results suggest that the main contribution to the displacement derives from the area within 2000 km from the point of interest and this is not surprising since the distance represents also the spatial extension associated with the passage of synoptic storms.

A radial deformation of the Earth's surface at Sheerness, Lowestoft and Herstmonceux of about 15-25 mm (peak to peak) can occur. The perturbation is bigger in amplitude during winter months when atmospheric pressure variations are bigger, while smaller fluctuations are modelled for the summer period (between -5 and $+10$ mm). These conclusions are in accordance with the results of other authors (Van Dam, 1991).

In Figures 3.3, 3.4 and 3.5 are presented in red the vertical displacement in millimeters and in blue the pressure variations in millibar at Sheerness. It appears that an air pressure correction of -0.5 mm/mbar could be considered in a first approximation as a proper coefficient for passing from atmospheric pressure values at the station to the vertical displacement induced. In this particular case the pressure value at the station is not exactly the one in the site considered but it is instead the pressure at the center of the cell in which the station is situated. The curves show almost the same course for the three years accounted when a factor of -0.5 mm/mbar is considered. Small discrepancies (about 1-2 mm), are detected at the minimums and maximums

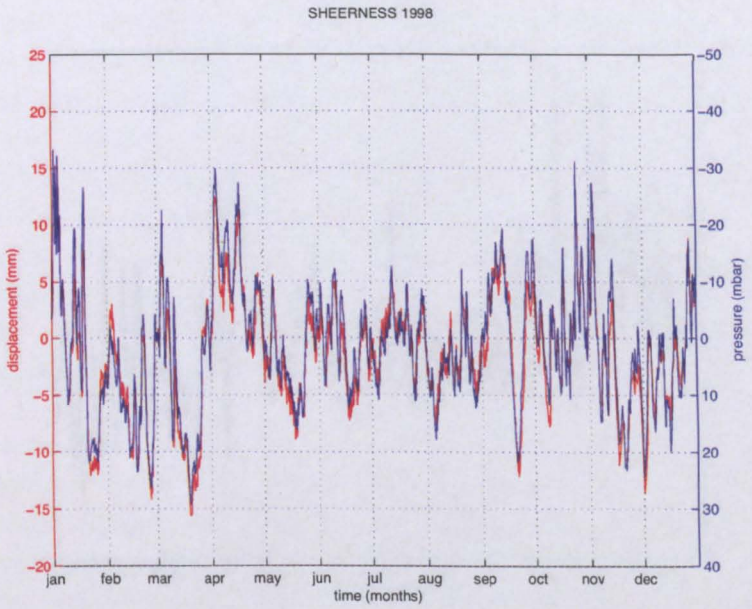

Figure 3.3: Vertical displacement and pressure variations at Sheerness during 1998. The red curve represents the vertical displacement in millimeters during 1998 from all the cells within an area of 4000 km from Sheerness, while the blue one refers to the pressure variation at Sheerness (NIBO hypothesis).

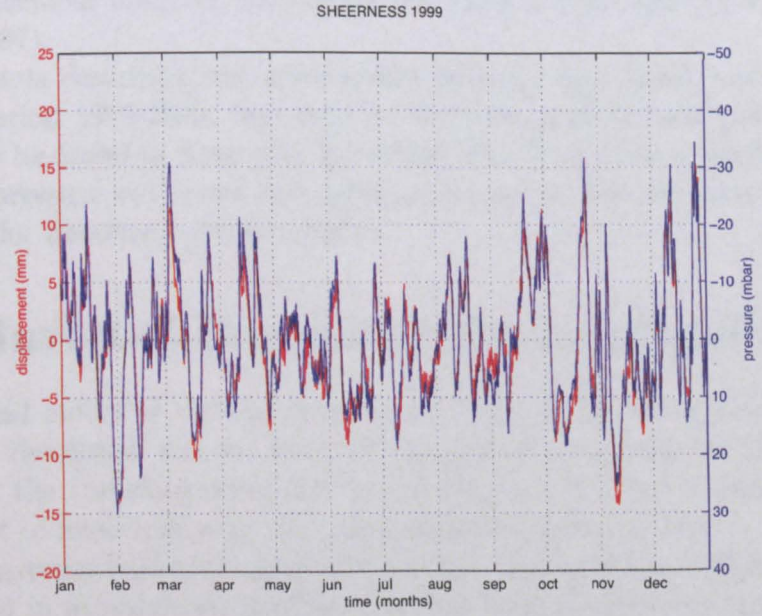

Figure 3.4: Same as figure 3.3 but for the year 1999.

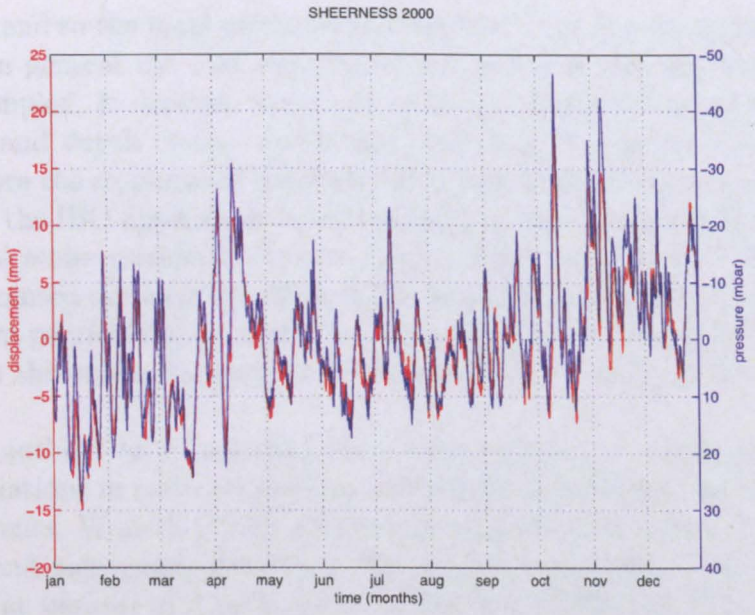

Figure 3.5: Same as figure 3.3 but for the year 2000.

of the time series indicating that when extreme barometric variations are registered the local pressure alone is not adequate for evaluating correctly the displacement induced. This consideration was also made by van Dam & Wahr (1987).

The plots describing the relationship between deformation and pressure for the period 1998-2000, that refer to the sites of Herstmonceux and Lowestoft can be found in Appendix B, section B1. They show a similar relation between pressure at the site and deformation induced so the same coefficient assumed for Sheerness can be applied.

3.3 Inverted Barometer Ocean model (IBO)

The second model of vertical deformation induced by atmospheric pressure variation developed was an Inverted Barometer Ocean model (IBO). This time just the contribution of the land areas was considered since the total increment of mass load over the ocean regions was set to zero.

The inverted barometer hypothesis states that for every millibar increase (decrease) in atmospheric pressure, the sea surface depresses (rises) locally by 1.01 cm (see for example Dickman, 1988; Sun, 1995). Thus the ocean floors do not experience any of the forces associated with barometric pressure

variations and so the total incremental mass load over the ocean basins is set to zero. In general the real response of the ocean to atmospheric pressure is very complex; it depends upon the coastline shape, the wind stress, the geometry and depth of the continental shelf and the presence of currents. Furthermore the response of the sea level to barometric forcing and then the validity of the IBO approximation are strongly dependent upon the temporal and spatial scale considered (Ponte, 1992). Carrere and Lyard (2003), have recently pointed out that the effect of the wind forcing in the ocean response is dominant particularly around a ten days period while for periods less than three days the ocean response to pressure forcing generally differs from the IBO.

Many authors have analyzed the ocean response to atmospheric pressure fluctuations in order to perform corrections to observations and gravity measurements. Wunsch (1972) concluded from the comparison of local data pressure and tide gauge data that the inverted barometer response is appropriate at periods of 3 or 4 days. In fact it is likely that the ocean does respond to pressure as an inverted barometer at the periods of weeks. But the global response is certainly not an inverted barometer at period close to 1 day. Ponte et al. (1991), have given estimates of the sea level using the IBO relation and they concluded that at low frequencies the assumption is fairly accurate but at periods shorter than 2.5 days the departures from the inverted barometer behavior are large so below 2 days IBO is not reliable. Mathers & Woodworth (2001), pointed out that the local IBO provides a reasonable representation of the response of the ocean to pressure forcing outside tropical areas with coefficients that go from -0.5 to -0.9 cm/mbar as the time scale increases from several days to several weeks. Boy et al. (2002), concluded that for computing the loading of a global atmospheric model the optimal choice is to consider the IBO assumption for the response of the ocean to the pressure forcing since the NIBO hypothesis is generally inadequate at seasonal timescales.

For the second model of vertical displacement induced by barometric variations an IBO hypothesis was chosen since this is the most commonly used method in the literature for atmospheric pressure loading computations. The geographical distribution of the land areas was derived for our model from a 1 degree x 1 degree ocean land mask. Sea cells were then excluded from the computation. The sea level pressure data were interpolated first on the POLSSM grid and then on the 1 degree x 1 degree spherical grid system. The radial displacement was evaluated at Sheerness, Lowestoft and Herstmonceux in the three different cases already seen.

For the IBO assumption, since there is a reduced number of cells, the radial deformation of the Earth's surface associated with pressure loading

was obviously smaller than the one detected in the NIBO hypothesis. A displacement of about 10-15 mm (peak to peak) was determined for the three sites investigated.

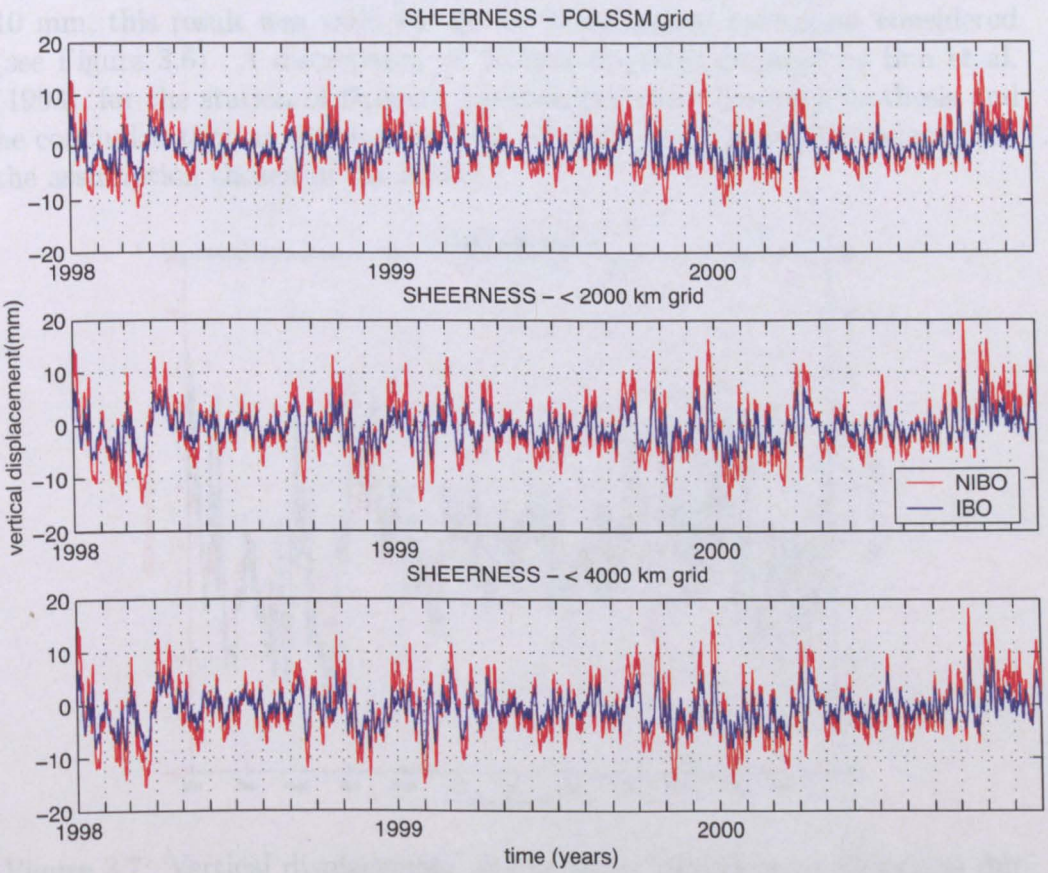

Figure 3.6: Vertical displacements at Sheerness from the NIBO and IBO models. In red are the vertical displacements in millimeters from the NIBO model for the period of time investigated (1998-2000), they are presented as results from the contribution of the cells in the POLSSM grid, in the area within 2000 km and 4000 km from the Sheerness respectively. In blue are drawn the curves obtained from the IBO model.

Also in this case the perturbation results were bigger in amplitude during the winter months when atmospheric pressure variations are bigger while summer periods showed smaller variations peak to peak.

In general the correct model that have to be assumed for accurate evaluations of the deformation due to atmospheric pressure loading should be something in between NIBO and IBO assumptions and this would depend

upon the distance of the station considered from the coast. In our case the sites chosen for the computation were not inland sites so great differences were obtained considering an oceanless model or not. Passing from NIBO to IBO assumption, the radial displacement at Sheerness reduced by about 10 mm, this result was valid for all the three spatial extensions considered (see Figure 3.6). A discrepancy of 10 mm was also detected by Sun et al. (1993), for the station of Brussels between the two opposite hypothesis and he concluded that at the site the load response was significantly affected by the assumption chosen in the model.

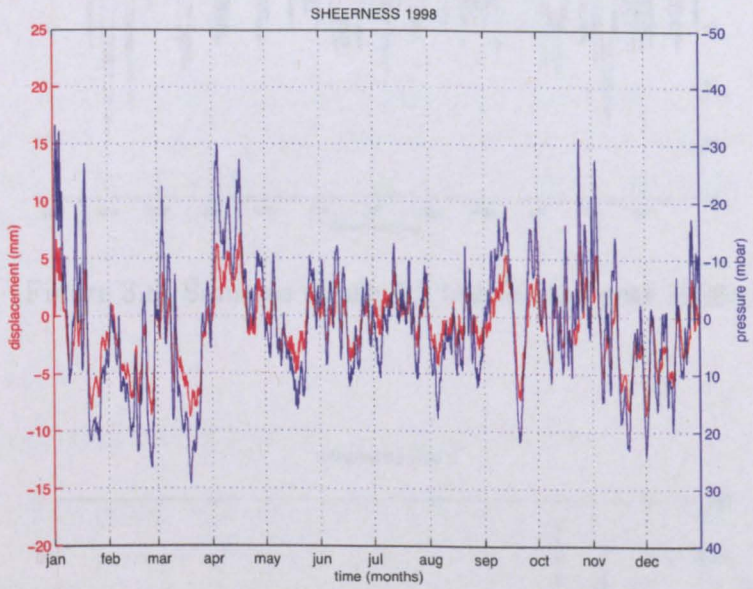

Figure 3.7: Vertical displacement and pressure variations at Sheerness during 1998. The red curve represents the vertical displacement in millimeters during 1998 from all the cells within an area of 4000 km from Sheerness, while the blue one refers to the pressure variation in millibar at Sheerness (IBO hypothesis).

In figure 3.7, 3.8 and 3.9 are presented in red the values of the vertical displacement induced in Sheerness by the contribution of the atmospheric pressure variations of the land cells within an area of 4000 km from the site considered. The blue curves represent the pressure variations in millibar at the center of the cell in which the site is located. Making a comparison between these three figures and the previous ones (figures 3.3, 3.4 and 3.5) for the NIBO hypothesis, it is evident that the radial deformation is still related with the pressure variations at Sheerness but that the magnitude of

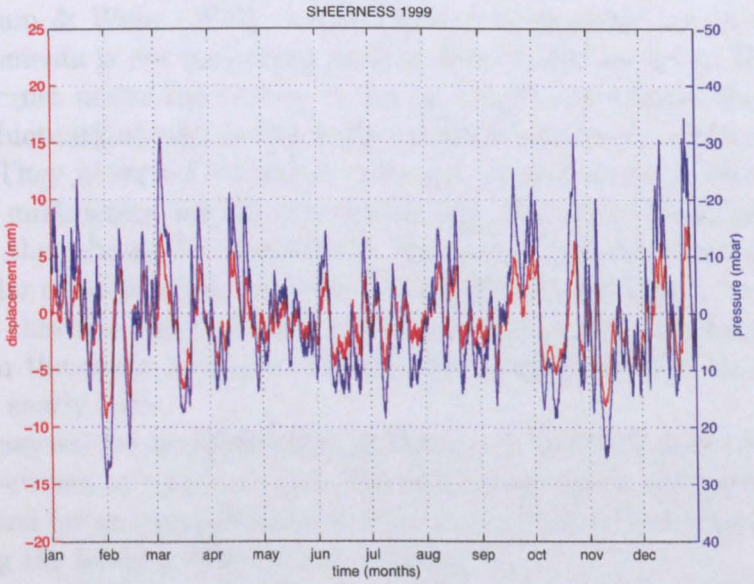

Figure 3.8: Same as figure 3.7 but for the year 1999.

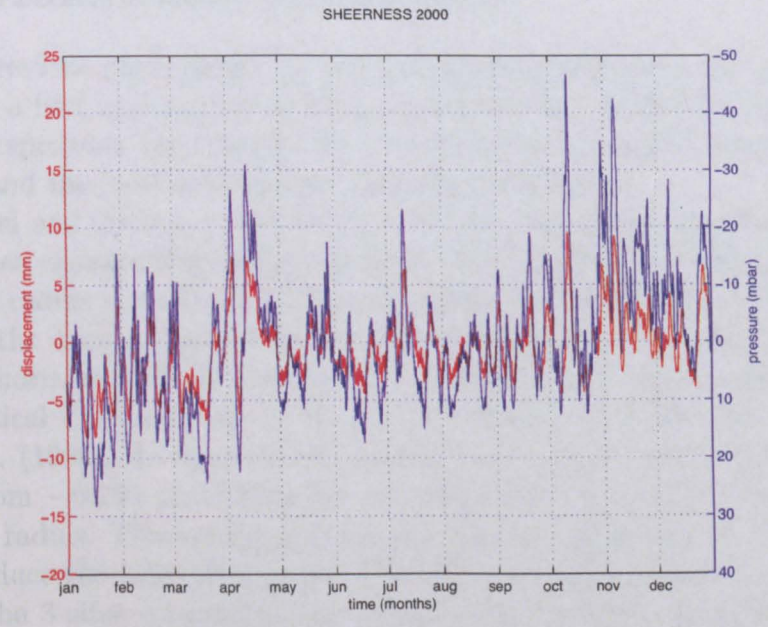

Figure 3.9: Same as figure 3.7 but for the year 2000.

the displacement is smaller than before.

Van Dam & Wahr (1987), noticed that a large reduction in the values of displacements is not surprising passing from NIBO model to IBO model, since the crust under the nearby ocean no longer experiences the effects of pressure fluctuations and so no longer contributes to the deformations at the site. They observed a smaller reduction in the vertical deformation of about few millimeters, for the non-coastal site of Boulder (Colorado). It was concluded that the addition of IBO to their model affects inland sites less.

A similar consideration was made by MacMillan and Gibson (1994). They concluded that the effect of the inverted barometer will decrease as the distance from the coast increases therefore the displacement of an island site should be nearly zero.

It can anyway be concluded that in the case of the IBO model the transfer function between air pressure and deformation is smaller compared with the one obtained for an oceanless Earth since the number of cells summed up for calculating the loading effect is also smaller.

The same kind of consideration is valid for the sites of Lowestoft and Herstmonceux. The relative plots are inserted for completeness in Appendix B, section B.1.

3.4 Admittance coefficients

As the previous plots show, the vertical displacements at a site can be obtained in a first approximation from the admittance coefficient for that station. It represents the transfer function between the radial deformation at the site and the local atmospheric pressure variations.

Rabbel and Zschau (1985) found that for the radial displacements the admittance changes from approximately -0.1 mm/mbar for a pressure system with radius r_0=160 km to -0.9 mm/mbar at r_0=5500 km. They pointed out that the displacement of the surface is primarily vertical and air pressure induced horizontal displacements are less significant. Their results suggest that vertical displacements of the Earth's surface of 10-20 mm can occur. Sun et al. (1995), showed that the transfer function for vertical deformations varies from -0.250 mm/mbar for 100 km radius to -0.539 mm/mbar for 1000 km radius. This means that the air pressure variations of a very broad area produce the most of the contribution to the deformation.

For the 3 sites considered, the admittances were computed by fitting a linear curve to the data obtained from the CONV method in both NIBO and IBO hypothesis. A period of one year and the contribution of all the cells with a maximum distance of 2000 and 4000 km from the station were

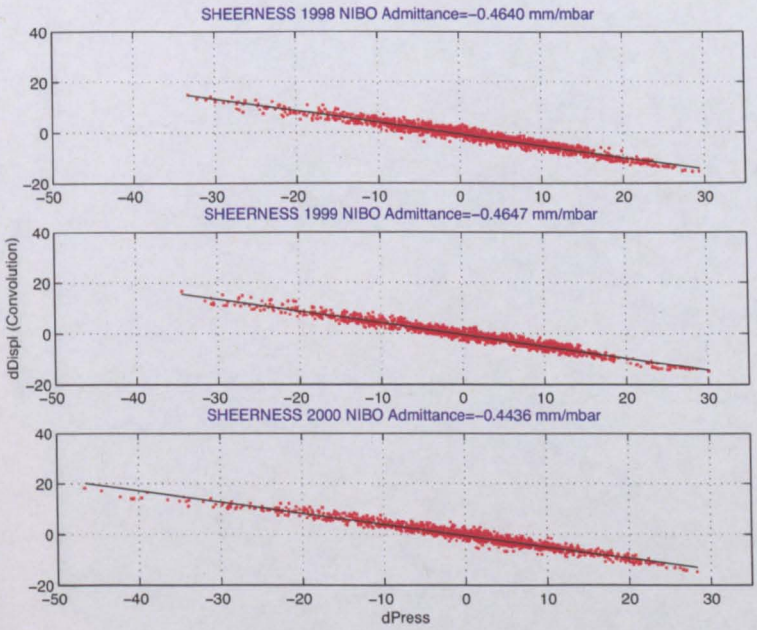

Figure 3.10: Admittance coefficients for the period considered for the site of Sheerness (CONV method applied to an area of 4000 km from the site - NIBO hypothesis).

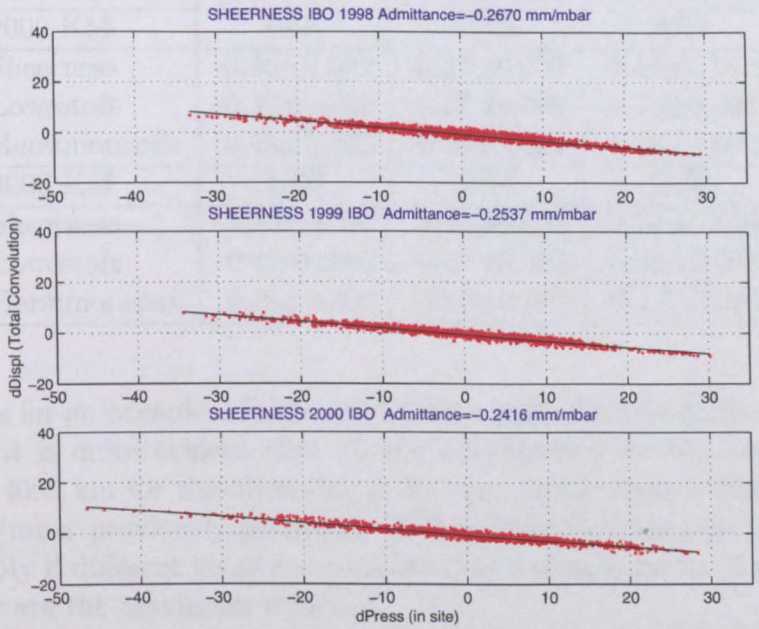

Figure 3.11: Admittance coefficients for the period considered for the site of Sheerness (CONV method applied to an area of 4000 km from the site - IBO hypothesis).

considered. Also the admittances from the POLSSM grid were calculated.

Table 3.1: Admittance coefficients (in mm/mbar) and relative error bars for the three stations considered during the period 1998-2000. (CONV method - NIBO hypothesis).

SUBGRID	1998	1999	2000
Sheerness	-0.39±0.001	-0.39±0.001	-0.38±0.001
Lowestoft	-0.40±0.001	-0.41±0.001	-0.40±0.001
Herstmonceux	-0.38±0.001	-0.38±0.001	-0.37±0.001
2000 KM	1998	1999	2000
Sheerness	-0.46±0.002	-0.47±0.002	-0.46±0.002
Lowestoft	-0.47±0.002	-0.47±0.002	-0.46±0.002
Herstmonceux	-0.45±0.002	-0.46±0.002	-0.45±0.002
4000 KM	1998	1999	2000
Sheerness	-0.46±0.003	-0.46±0.003	-0.44±0.003
Lowestoft	-0.47±0.003	-0.47±0.003	-0.45±0.003
Herstmonceux	-0.46±0.003	-0.46±0.003	-0.44±0.003

Results for an oceanless Earth model are summarized in Table 3.1. From the table it is quite evident that all the admittances for the areas within 2000 and 4000 km for the observing point, are pretty close to the factor of -0.5 mm/mbar previously proposed. The transfer functions do not change considerably if different years are considered and discrepancies of about 0.02 mm/mbar are the maximum achieved.

The admittances calculated from the contribution of the grid elements of the sub-grid are smaller in magnitude compared with those computed for larger regions in both the hypotheses assumed. Sun et al. (1993), pointed out that the transfer functions between radial deformation and air pressure changes increases from 0.12 mm/mbar for loads extending up to 160 km to loads at 1000 km distance from the station of interest (Brussels). Our differences are generally larger (0.13 - 0.16 mm/mbar) especially for an oceanless Earth model.

In the case of Table 3.2 the admittance coefficients proposed are smaller than those calculated using an oceanless Earth model, but this is in accordance with the use of an IBO hypothesis in our program.

Even if in general it is not possible to produce a unique admittance coefficient for a certain location valid for different timescales because of the changes in the weather pattern that continuously modify the barometric pressure field, it can be concluded that admittances between -0.24 and -0.27

Table 3.2: Admittance coefficients (in mm/mbar) and relative error bars for the three stations considered during the period 1998-2000. (CONV method - IBO hypothesis).

SUBGRID	1998	1999	2000
Sheerness	-0.21±0.001	-0.21±0.001	-0.20±0.001
Lowestoft	-0.17±0.001	-0.17±0.001	-0.17±0.001
Herstmonceux	-0.20±0.001	-0.20±0.001	-0.20±0.001
2000 KM	1998	1999	2000
Sheerness	-0.26±0.001	-0.25±0.001	-0.25±0.001
Lowestoft	-0.22±0.001	-0.21±0.001	-0.21±0.001
Herstmonceux	-0.26±0.001	-0.25±0.001	-0.25±0.001
4000 KM	1998	1999	2000
Sheerness	-0.27±0.002	-0.25±0.002	-0.24±0.002
Lowestoft	-0.22±0.002	-0.21±0.002	-0.20±0.002
Herstmonceux	-0.27±0.002	-0.25±0.002	-0.24±0.002

mm/mbar are pretty common if the IBO hypothesis is considered and an area of 4000 km from the location of interest (Sheerness). For an oceanless Earth model admittances between -0.44 and -0.46 mm/mbar are common.

3.5 Rabbel & Zschau method

There are various methods for evaluating the deformations on the Earth due to a surface load distribution. Here the method proposed by Rabbel and Zschau (1985), is investigated since it is the recommended method in the IERS (International Earth Rotation and Reference Systems Service) conventions since 1996.

Rabbel and Zschau (1985) estimated the deformation caused by synoptic storms by modelling pressure disturbances as Gaussian functions of radius around a central point. They provided a Two Coefficient Correction Equations (TCCE method) and they estimated the deformations and the gravity changes at the Earth's surface caused by regional and global air pressure variations.

A geometrically simple pressure distribution of cyclones or anticyclones was considered were the isobars were assumed to be nearly circular and the anomalous pressure could be described in a first approximation by a simple formula:

$$p(r) = p_{max} \cdot e^{-\frac{r^2}{r_0^2}} \tag{3.2}$$

here r was the distance from the center of the (anti-)cyclone, p_{max} was the maximum pressure anomaly at the center and r_0 the distance at which the anomaly has dropped to $\frac{p_{max}}{e}$ (e=2.718). The expression in Equation 3.2, can just be applied to barometric variations far from the coastline. Near the sea the pressure distribution is complicated because of the dynamical reaction of the sea water to the passing cyclone.

Vertical displacements and gravity changes at the Earth's surface due to the anomalous pressure distribution were computed setting r_0 to three different values. Tropical cyclones were modelled with r_0=160 km or 400 km (steep pressure gradient and small spatial extension) while continental anticyclones were modelled with r_0=1000 km (small pressure gradient and large spatial extension). All the calculated deformations and gravity changes were normalized to p_{max}=1 mbar.

Since the magnitude of the displacements is critically dependent on the spatial extension of the pressure anomaly, a unique regression coefficient between the local displacements and the local air pressure changes is not sufficient for achieving a precise air pressure correction.

Rabbel and Zschau (1985) proposed the following two coefficient correction equation one belonging to the long wavelength loading and the other belonging to the short wavelength loading for the case of the vertical loading deformation (Equation (3.3)).

The short wavelength loads were obtained from the measured pressure variations at the surface point under investigation. The long-wavelength contributions were computed by averaging the pressure variations in a surrounding area of 2000 km and setting to zero the pressure changes for the oceanic regions.

In the case of the vertical displacements the corrections of Rabbel and Zschau are given by the following formula:

$$u = -0.90p_l - 0.35(p_s - p_l) \tag{3.3}$$

where u is the radial displacement in mm, p_s is the local pressure variation in mbar, p_l is the average of the pressure variation in a surrounding area of 2000 km (in mbar) except for setting the pressure value equal to zero over ocean areas. This contrivance was assumed in order to model the influence of an Inverted Barometer Ocean model (IBO).

Since it is known that Equation (3.3) allows to estimate vertical seasonal deformation with errors of less than 1 mm (Rabbel & Schuh,1986), as a

further step, our results from the convolution method were compared with those obtained using the TCCE method (Rabbel & Zschau, 1985).

For this purpose the averaged value of pressure within an area of radius 2000 km from the site was computed and also the pressure value at Sheerness, Herstmonceux and Lowestoft were evaluated. The pressure at the sites of interest was obtained interpolating the pressure data available from the atmospheric pressure grid at the exact location of the sites considered i.e. it did not correspond anymore with the pressure variations at the center of the grid element in which the stations were located. In particular, the formula in Equation (3.3) was used but it was slightly modified for the oceanless hypothesis since p_l (the average of the pressure variation in the surrounding area of 2000 km), was calculated without setting to zero the pressure value over the ocean areas.

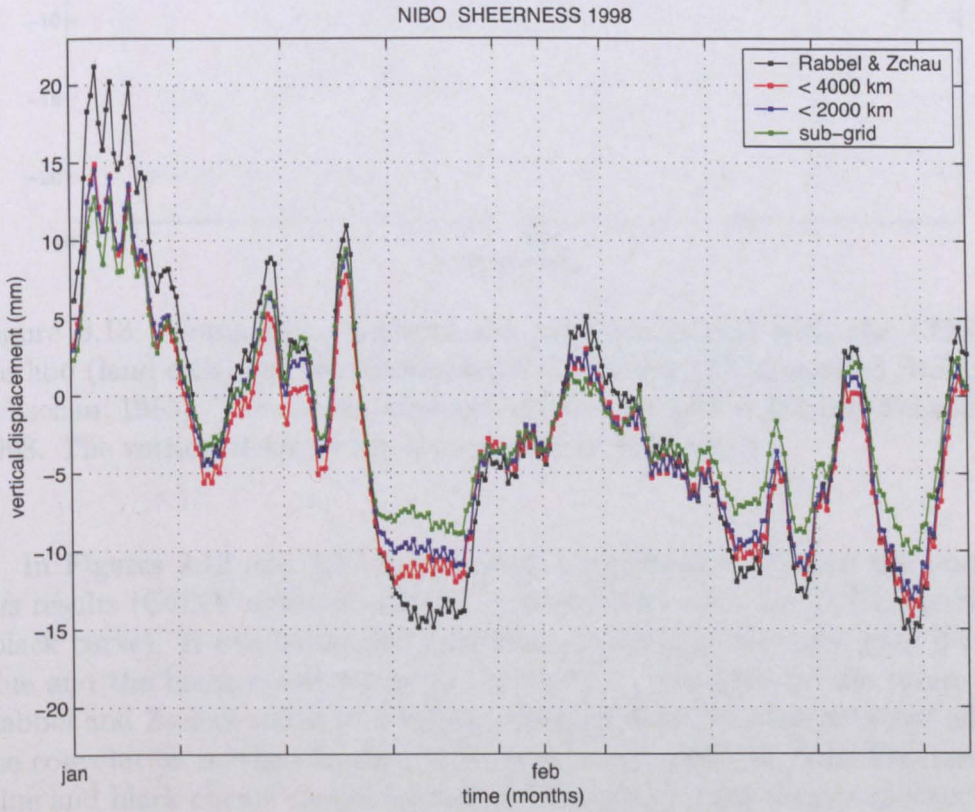

Figure 3.12: Comparison between the results obtained with the CONV method (land and sea cells) and the ones evaluated with the TCCE method (Rabbel & Zschau, 1985). The curves presented refer to the period January-February 1998. The vertical deformation is expressed in millimeters.

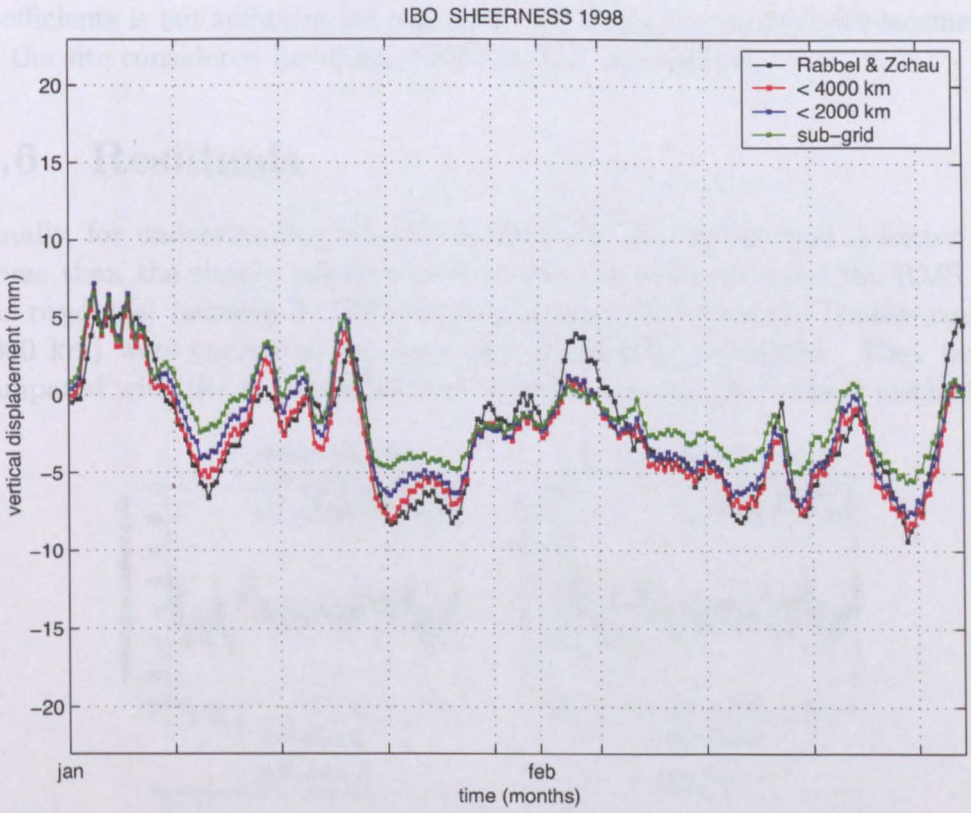

Figure 3.13: Comparison between the results obtained with the CONV method (land cells) and the ones evaluated with the TCCE method (Rabbel & Zschau, 1985). The curves presented refer to the period January-February 1998. The vertical deformation is expressed in millimeters.

In Figures 3.12 and 3.13 is presented a comparison between the previous results (CONV method) and the ones obtained with the TCCE method (black curve). It can be noticed that the agreement is not very good if the blue and the black curve values are compared. In particular the values of Rabbel and Zschau result in a bigger variation than the ones obtained with the convolution method applied to an area within 2000 km from Sheerness. Blue and black curves should be much more similar since they both refer to an area of 2000 km from the site of interest.

The TCCE formula was mainly designed for a NIBO ocean model but Rabbel & Zschau pointed out that in this assumption and in particular for sites close to the sea, many complications arise from the dynamical reaction of the water mass of the sea and other factors should be accounted for. From the results (see Figures 3.12 and 3.13), it was concluded that the use of two

coefficients is not sufficient for correctly evaluating the vertical displacement at the site considered for either NIBO or IBO assumption.

3.6 Residuals

Finally, for understanding whether Rabbel and Zschau method is better or worse than the simple admittance formula, the residuals (and the RMS of the residuals) between TCCE results and convolution results (radius equal 4000 km) were computed for each year previously considered. They were compared with the residuals between convolution and admittance method.

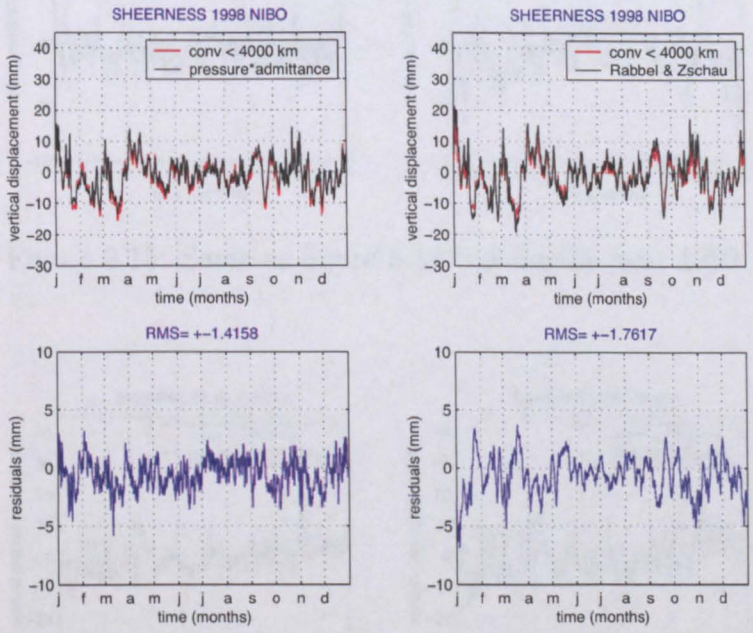

Figure 3.14: Residuals between TCCE results and convolution results and between convolution and admittance method. In red are the vertical displacement calculated from the CONV method (radius equal 4000 km) NIBO hypothesis for 1998 and for the site of Sheerness. In black are alternatively represented on the left, the radial displacements obtained by multiplying the admittance characteristic for the station and for the year considered (-0.46 mm/mbar) by the local derived pressure (pressure value of the cell in which Sheerness is situated), and on the right, the vertical displacements obtained from the TCCE method. In blue are presented the residuals (and the RMS of the residuals) between convolution and admittance (left) and convolution and TCCE method (right).

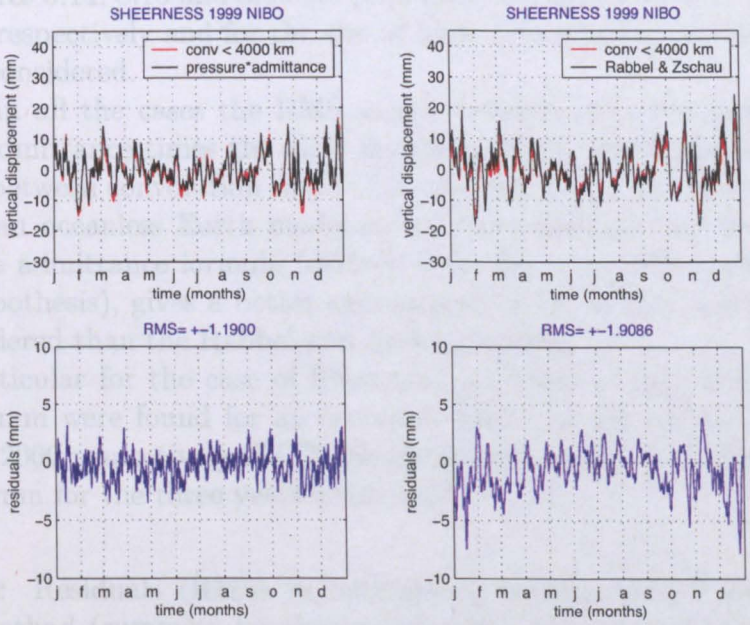

Figure 3.15: Same as figure 3.14 but for the year 1999.

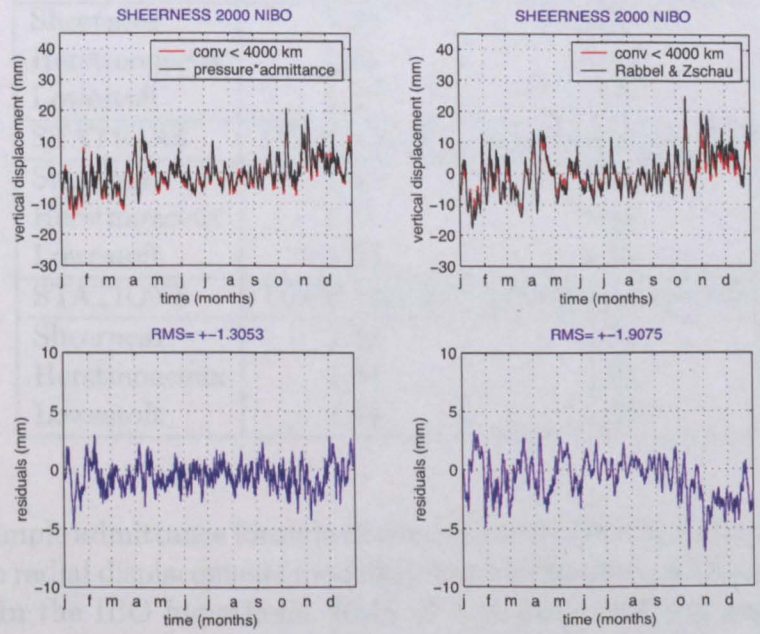

Figure 3.16: Same as figure 3.14 but for the year 2000.

In figures 3.14, 3.15 and 3.16 are presented the results for year 1998, 1999 and 2000 respectively and for the site of Sheerness when an oceanless Earth model is considered.

Since in all the cases the RMS values between the convolution results and the admittance times the local derived pressure were smaller than the residuals between convolution and TCCE method results, it can be concluded that, for an oceanless Earth model and for the stations here investigated, the simple admittance formula (derived from the convolution results in the NIBO hypothesis), gives a better approximation of the displacement at the site considered than the Rabbel and Zschau formula.

In particular for the case of Sheerness, residuals of 1.41 mm, 1.19 mm and 1.30 mm were found for an oceanless Earth model and for year 1998, 1999 and 2000 respectively. TCCE residuals were about 1.76 mm, 1.91 mm and 1.91 mm for the three years considered.

Table 3.3: Residuals (RMS) in millimeters between TCCE method and CONV method (summing up the contribution from the cells within a distance of 4000 km from the site) and between admittance and CONV method for the three stations considered during the period 1998-2000.

STATIONS	TCCE rms 98	Admittance rms 98
Sheerness	1.40	1.19
Herstmonceux	1.38	1.13
Lowestoft	1.49	1.28
STATIONS	TCCE rms 99	Admittance rms 99
Sheerness	1.44	1.03
Herstmonceux	1.41	0.98
Lowestoft	1.53	1.12
STATIONS	TCCE rms 00	Admittance rms 00
Sheerness	1.39	1.14
Herstmonceux	1.34	1.08
Lowestoft	1.44	1.22

The simple admittance formula derived from the IBO model approximates better the radial displacements modelled than the Rabbel and Zschau method as well. In the IBO hypothesis, RMS of 1.19 mm, 1.03 mm and 1.14 mm were found for the three years previously considered and the site of Sheerness (see figures 3.17, 3.18 and 3.19). TCCE residuals of 1.40 mm, 1.44 mm and 1.39 mm were calculated.

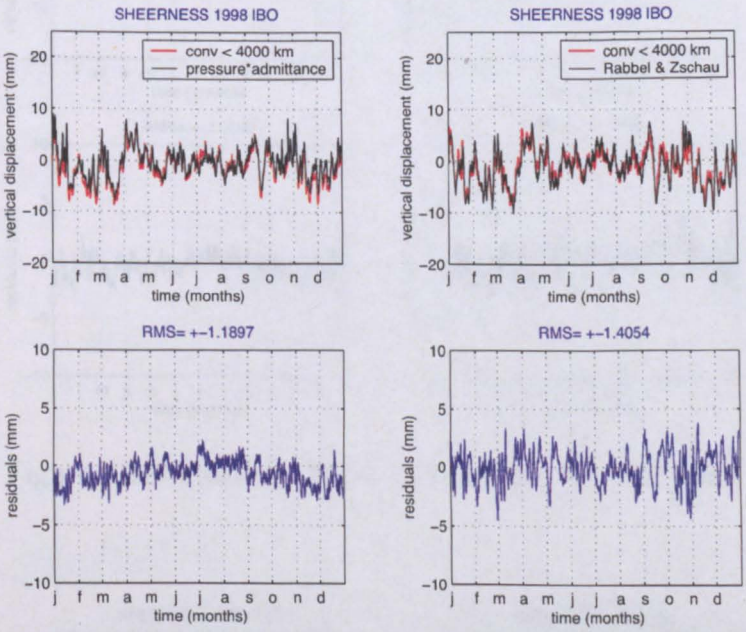

Figure 3.17: Residuals between TCCE results and convolution results and between convolution and admittance method. In red are the vertical displacement calculated from the CONV method (radius equal 4000 km) IBO hypothesis for 1998 and for the site of Sheerness. In black are alternatively represented on the left, the radial displacements obtained by multiplying the admittance characteristic for the station and for the year considered (-0.27 mm/mbar) by the local derived pressure (pressure value of the cell in which Sheerness is situated), and on the right, the vertical displacements obtained from the TCCE method. In blue are presented the residuals (and the RMS of the residuals) between convolution and admittance (left) and convolution and TCCE method (right).

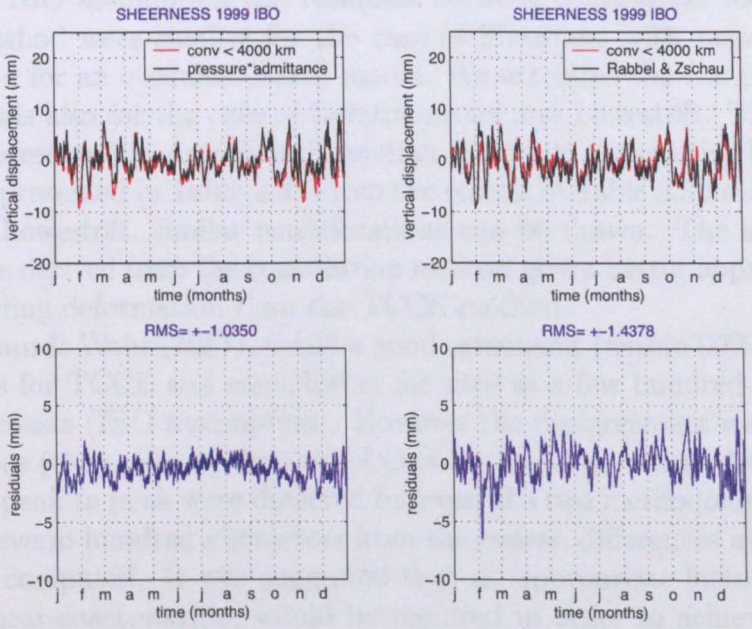

Figure 3.18: Same as figure 3.17 but for the year 1999.

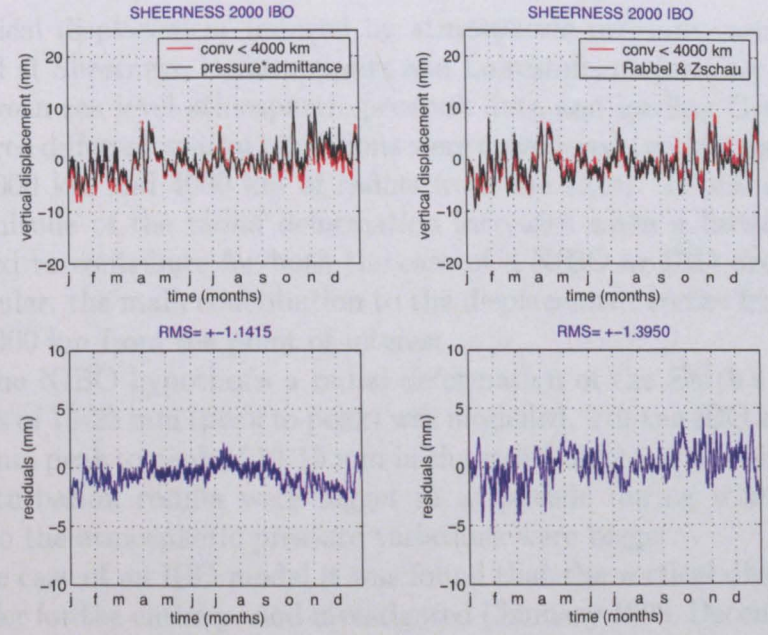

Figure 3.19: Same as figure 3.17 but for the year 2000.

In the IBO assumption the residuals between convolution method and TCCE method were smaller for the case of Sheerness with respect to the RMS found for an oceanless Earth model. We extended the computation of the residuals also for the case of Herstmonceux and Lowestoft. The relative plots are presented in Appendix B, section B.3 while the relative RMS computed are presented in Table 3.3. From the results of Table 3.3 for Herstmonceux and Lowestoft, similar considerations can be drawn. The admittance coefficients derived from the convolution method give a better approximation of the loading deformation than the TCCE method.

Van Dam & Wahr (1987), found a good agreement (within 90%), between the results for TCCE and convolution for sites at a few hundred kilometers from the coasts (IBO assumption). However the disagreement was large for coastal sites (they refer to the case of Onsala (Sweden), where discrepancies of 10 mm peak to peak were detected between the two methodologies). Even for sites several hundred kilometers from the coasts, differences as large as 5 mm were computed. It was suggested that an appropriate factor, different for each near-coast station, would be required in order to achieve a better agreement.

3.7 Conclusions

The vertical displacement induced by atmospheric pressure variations was evaluated at Sheerness, Herstmonceux and Lowestoft, performing a convolution between sea level atmospheric pressure data and loading Green's function. Three different spatial extensions were considered (within the sub-grid, within 2000 km and 4000 km of radius from the sites). It was noted that the magnitude of the radial deformation increases when a broader area is considered to contribute for both the case of a NIBO or IBO ocean model. In particular, the main contribution to the displacement comes from an area within 2000 km from the point of interest.

For the NIBO hypothesis a radial deformation of the Earth's surface at Sheerness of 15-25 mm (peak to peak) was modelled. For the IBO assumption a maximum peak to peak of 10-15 mm in the radial deformation was detected. The perturbation results were bigger in amplitude during winter months when also the atmospheric pressure variations were bigger.

In the case of an IBO model it was found that the vertical displacements are smaller for the entire period investigated (January 1998 December 2000), if compared with the results for an oceanless Earth model. This fact can be explained since in the IBO hypothesis ocean floors do not experience any of the forces associated with barometric pressure variations and so the total

incremental mass load over the ocean basins is set to zero i.e. it does not contribute to the deformation.

From the visual relationship between local pressure variations and the deformation associated, a factor of −0.5 mm/mbar was detected for the 3 stations and for the periods considered in an oceanless Earth model. The coefficient represents in a first approximation, the dependency of the deformation induced from the pressure variations. For the IBO hypothesis the magnitudes of the displacements were smaller with respect to those previously modelled.

Since the magnitude of the radial displacement at a site can be determined in a first approximation from the transfer function between vertical displacement and local atmospheric pressure variations, also the admittance was calculated for the site of Sheerness, Herstmonceux and Lowetoft considering the contribution of the three spatial extensions and a period of one year each time. For both the hypotheses assumed in the model, the admittances derived from an area of 2000 and 4000 km from the observation points were pretty similar among them. Admittances to local pressure between −0.47 and −0.44 mm/mbar were calculated at Sheerness in the NIBO assumption. Values between −0.27 and −0.24 mm/mbar were computed in the IBO hypothesis. A general decrease in the transfer functions moving from a NIBO to a IBO hypothesis was detected for all the 3 spatial extensions.

The highest accuracy in the loading model results can be obtained with the global convolution but also the methodology of Rabbel and Zschau (1985), was used for calculating the deformation at the sites since this is the recommended method in the IERS conventions. For understanding whether Rabbel and Zschau method is better or worse than the simple admittance formula, the residuals (indicated here as RMS) between TCCE results and convolution results (radius equal 4000 km) were computed for each year previously considered. They were compared with the residuals between the results from convolution and admittance method. It was concluded that, for both oceanless Earth model and IBO model the simple admittance formula, gives a better approximation of the displacement at the sites considered than the Rabbel and Zschau formula and that the use of the two coefficient equation is generally not sufficient for correctly evaluating the vertical displacement at the coastal stations examined. In particular, RMS residuals from the simple admittance formula of 1.41 mm, 1.19 mm and 1.30 mm were found for an oceanless Earth model and for year 1998, 1999 and 2000 respectively at Sheerness. In the IBO hypothesis, RMS residuals of 1.19 mm, 1.03 mm and 1.14 mm were found for the three years previously considered.

Chapter 4

Global atmospheric pressure loading models

The aim of this chapter is to study the effects of large pressure distributions on the deformations in the vertical and horizontal directions so the barometric pressure field considered covers the whole Earth. Air pressure correction values for high precision displacements measurements are provided and the magnitude of the radial deformation induced by local and regional variations in atmospheric pressure at some European sites is given.

The time series of surface displacements modelled are compared with those available from other authors (Sherneck, 2002; Petrov, 2003), and the differences among the results are investigated. Particular attention is given to the causes of the discrepancies.

Moreover a comparison between the modelled transfer functions between deformation and pressure and the admittances for the same sites available from the literature (Van Dam and Herring, 1994; Manabe et al., 1991; Van Dam et al., 1994; Van Dam and Wahr 1987, Van Dam 2002) is presented. Admittance coefficients are also computed for further European stations (mainly British sites).

The results, obtained by performing a convolution between the local and the regional barometric pressure data and the mass loading Green's functions (Farrell, 1972), are also compared with those computed using the Two Coefficient Correction Equation method (TCCE) of Rabbel & Zschau (1985). The target is of understanding which method gives a better approximation of the radial deformation at a site when the convolution performed considers a worldwide load distribution.

4.1 Radial and tangential deformations induced at four European sites

The vertical and horizontal crustal displacements induced by atmospheric pressure variations at the European sites of Wettzell (Germany), Onsala (Sweden), Herstmonceux (United Kingdom) and Metsahovi (Finland) were calculated performing a convolution between the local and the regional barometric pressure data and the mass loading Green's functions (Farrell, 1972).

The period of time investigated was between January 1998 and December 2000. Sea level pressure data were available for the entire world from the National Center for Atmospheric Research (NCAR) and surface pressure data were accessible from the Climate Diagnostic Center (CDC) web site (Petrov, 2003). They were derived from NCEP/NCAR Reanalysis numerical model, with a correction for inadequate diurnal/semidiurnal atmospheric tides.

Two models of surface displacement due to atmospheric pressure variations were considered and for both a detailed sub-grid coinciding with that of the Proudman Oceanographic Laboratory Storm Surge Model (POLSSM), that covers the British Isles and the North European coasts, was used.

For the site of Herstmonceux, since the station is located inside the POLSSM sub-grid, pressure data were interpolated first on the sub-grid and then on the additional 1 degree x 1 degree grid covering the rest of the world.

For the stations of Onsala and Wettzell, since their geographical position is very close to the eastern edge of the POLSSM grid, a further subdivision of the loading elements within an area of 1000 km from the sites and outside the sub-grid was considered.

Just for the case of Metsahovi (the site is completely outside the POLSSM grid), a grid of 0.1 degrees x 0.1 degrees was used for the area within 1000 km from the location and then a grid of 1 degree x 1 degree for the rest of the world.

In both the programs an Inverted Barometer Ocean (IBO) model was used. This hypothesis was assumed in order to perform a more realistic comparison with the time series available from other authors.

It was already pointed out in Chapter 3, that generally, when the loading effects induced by barometric pressure changes are investigated, the IBO assumption works quite well for inland sites while at coastal stations the agreement is not as good. In particular the effects of IBO decreases as the distance from the coasts increases, so the deformation at a coastal site is commonly half of the displacement of an inland site when the same pressure forcing is given. The deformation at an island site should be nearly zero (MacMillan and Gibson, 1994).

In the first program, the atmospheric pressure variation was obtained by removing from each sea level pressure datum the International Standard Atmosphere (ISA) pressure value at sea level (1013.25 mbar).

The sea level pressure data from NCAR were computed by a numerical weather model and estimated at various levels in the atmosphere, including the Earth's surface. The surface pressure on the topography is then converted by NCAR to sea level pressure by making some assumptions about the fictitious column of air between the Earth's surface and the sea level (when the pressure value over mountain areas is extrapolated to sea level, it obviously leads to fictitious pressure).

The conversion from surface pressure to sea level pressure can be performed using the hydrostatic balance condition that gives the pressure variation dp as a function of altitude variation dz:

$$dp = -g \cdot \rho \cdot dz$$

where g is the mean surface gravity that is a function of the latitude and ρ is the density of the atmosphere that is a function of the height.

Substituting the equation of state ($p = \rho RT$) in the hydrostatic equation gives:

$$\frac{dp}{p} = -g\frac{dz}{RT}$$

the integration of this expression between the surface z_0 and the level z leads to:

$$p(z) = p_0 exp\Big[-\int_{z_0}^{z} g\frac{dz}{RT}\Big]$$

for an isothermal atmosphere ($T(Z) = T_0$) we obtain (Boy et al., 2002):

$$p(z) = p_0 exp\Big[-\frac{g \cdot dz}{RT_0}\Big]$$

Thus, the determination of the sea level pressure field, depends upon the accuracy of the assumptions made in the weather model.

The input pressure field of the second model of radial deformation, were the surface pressure data available from CDC web site. The accuracy of the atmospheric loading computation was improved averaging over different

periods of time (3 years, 10 years and 23 years), the surface pressure value for each grid element and subtracting the mean cell by cell before performing the interpolation. This method was adopted for determining the surface pressure variations that are responsible for the different loading effects.

In both the cases an ocean land mask of 1 degree x 1 degree, was used for deriving the geographical distribution of the land areas. The only exception was represented by the areas within POLSSM grid where the ocean land mask adopted was more detailed (0.16 degrees x 0.11 degrees).

Table 4.1: Geographical positions in degrees of latitude and longitude of the four stations considered in the computation.

STATION	LATITUDE	LONGITUDE
Herstmonceux (UK)	50.8673 N	0.3362 E
Onsala (Sweden)	57.3947 N	11.9263 E
Wettzell (Germany)	49.1437 N	12.8774 E
Metsahovi (Finland)	60.2420 N	24.3841 E

4.1.1 Differences among the time series calculated with the second model

The time series of the vertical and horizontal displacements induced by atmosphere pressure loading were calculated at the four European sites previously indicated, by both the models. In the second model, the deformations were computed using the atmospheric pressure variations after removing the mean pressure in each cell. Three different mean pressure fields were used:

(a) the mean over 3 years (1998-2000)

(b) the mean over 10 years (1993-2002)

(c) the mean over 23 years (1980-2002).

It is evident from figure 4.1 (that presents the radial displacements at the site of Onsala at the beginning of 1998 and 1999 respectively), that in general, it does not make so much difference if the mean pressure subtracted is obtained by averaging over 3, 10 or 23 years. In fact the resulting curves representing the deformation are quite similar.

In this particular case the period between 1980 and 2002 was chosen since, as will be seen better in the next section, averaging over this period of time

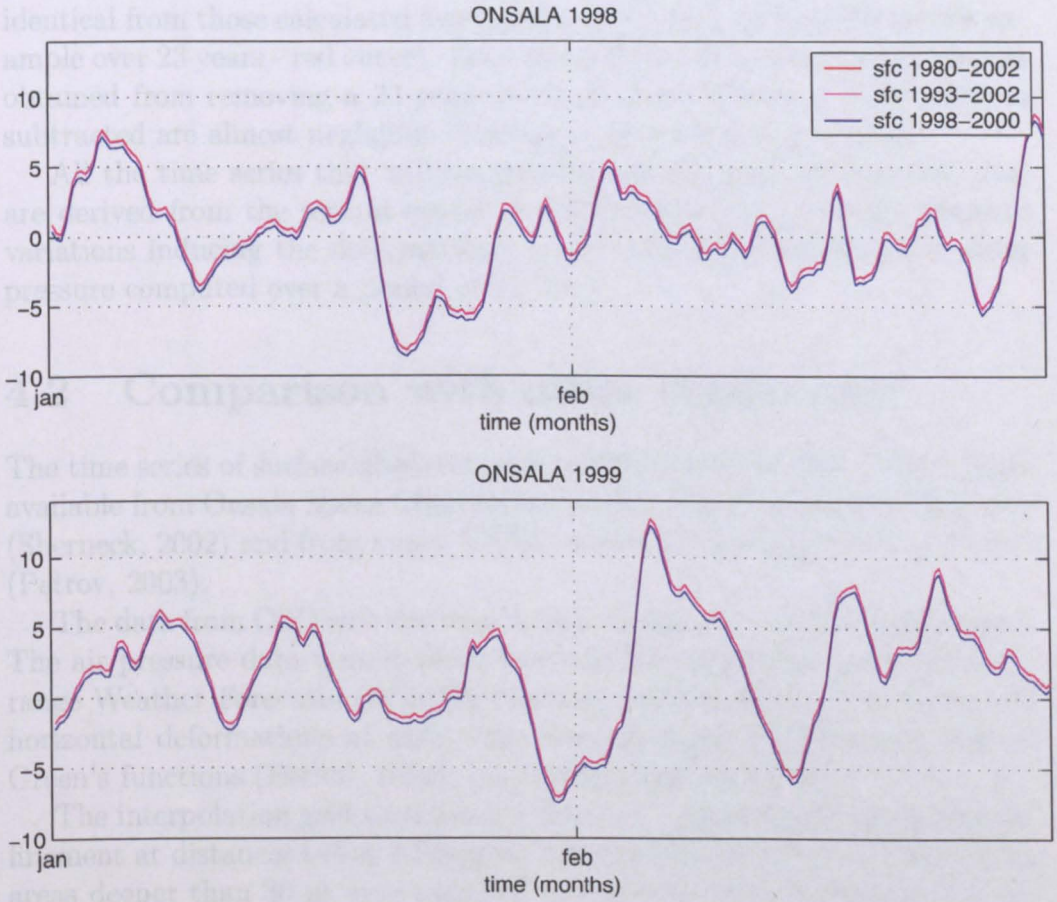

Figure 4.1: Vertical displacements obtained at the site of Onsala at the beginning of 1998 and 1999 respectively. The results were calculated for the case in which the deformation is induced by surface pressure field. The mean averaged over 3 years (producing the blue curve), 10 years (producing the magenta curve) and 23 years (producing the red curve) is removed from the pressure data cell by cell before performing the convolution. It can be noticed that the magenta and the red curves that refer to 10 and 23 years of averaged values removed, are superimposed.

makes the time series in this way obtained comparable with those proposed by Petrov (2003).

It can be concluded that averaging the pressure data over a period of 10 years (magenta curve in figure 4.1) is sufficient for obtaining results almost identical from those calculated averaging over a longer period of time (for example over 23 years - red curve). Even the differences between displacements obtained from removing a 23 years mean to those when a 3 years mean is subtracted are almost negligible (discrepancies are less than 1 mm).

All the time series that will be presented in the next sections and that are derived from the second model of radial deformation (surface pressure variations inducing the deformations), were achieved subtracting the mean pressure computed over a period of 23 years.

4.2 Comparison with other time-series

The time series of surface displacements modelled were compared with those available from Onsala Space Observatory (OSO) web site edited by Sherneck (Sherneck, 2002) and from a new NASA website on loading edited by Petrov (Petrov, 2003).

The data from OSO web site were 6 hour samples of surface displacement. The air pressure data were derived from the European Center for Medium-range Weather Forecasts (ECMWF) surface pressure fields. The radial and horizontal deformations at some sites were obtained by convolving Farrell Green's functions (Farrell, 1972), with surface pressure data.

The interpolation grid used was a 1 degree x 1 degree grid with a finer refinement at distances below 10 degrees from the site of interest. The oceanic areas deeper than 30 m were assumed to respond instantaneously as an inverted barometer. All other areas were loaded by the full air pressure effect.

Since the assumption in space geodesy concurrent with the present International Terrestrial Reference Systems is that there is no permanent pressure loading effect, the mean (derived from a four years period) of the time series from OSO was subtracted before the ordinates are applied as corrections to estimated positions.

The time series of vertical displacement induced by atmospheric pressure loading from NASA web site were obtained by convolving the difference between the surface pressure field and the mean surface pressure, with Farrell Green's functions derived on the basis of the Preliminary Reference Earth Model (PREM).

Pressure data were available every 6 hours. The mean surface pressure was calculated by averaging NCEP reanalysis surface pressure field over a

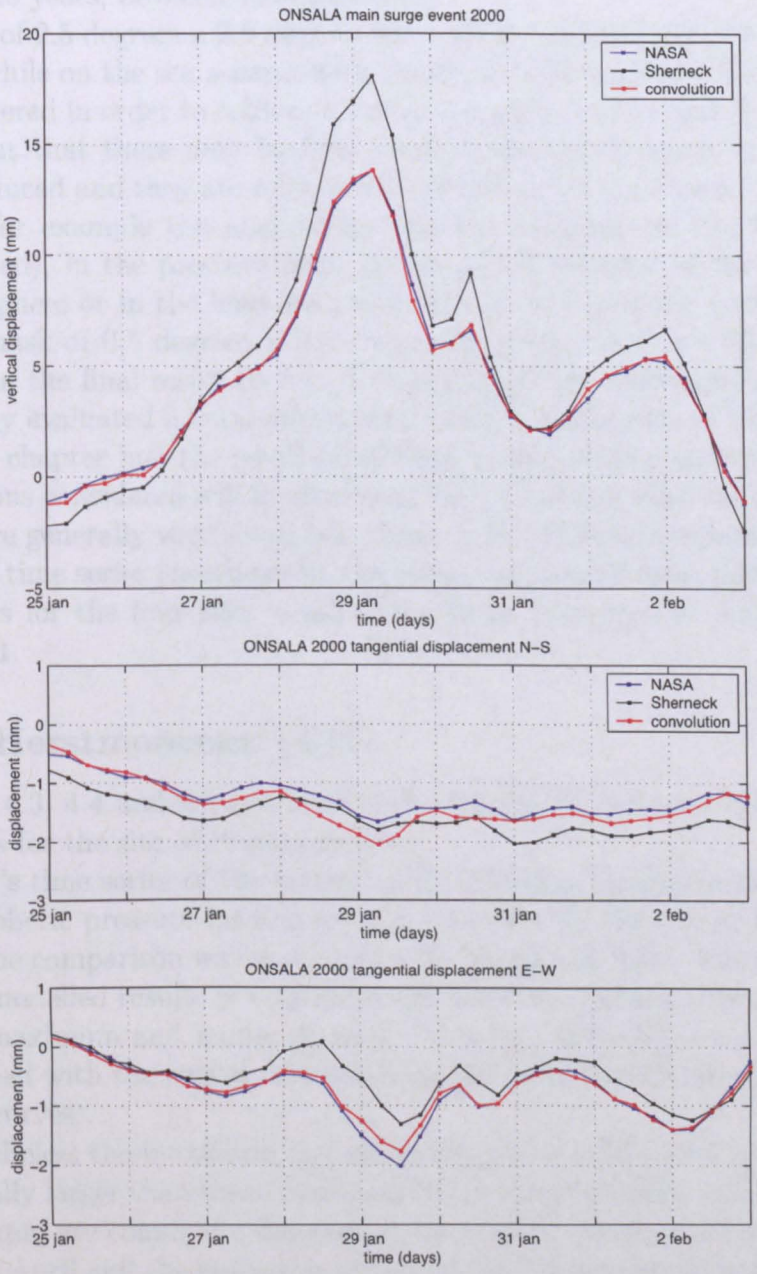

Figure 4.2: Vertical and horizontal deformation modelled for the site of Onsala at the beginning of 2000. The results were calculated for the case in which the deformation is induced by surface pressure field. The mean averaged over 23 years was removed from the pressure data before performing the convolution.

period of 23 years, between 1980 and 2002.

A grid of 2.5 degrees x 2.5 degrees was used for interpolating the data on the land while on the sea a mask with resolution 0.25 degrees x 0.25 degrees was considered in order to achieve a better accuracy. Petrov and Boy (2004), pointed out that there may be four possible sources of errors in the time series produced and they are related with deficiency in the Green's functions (because for example the anelasticity and the ellipticity of the Earth are not included), in the pressure field, in the model response of the ocean to the atmosphere or in the land-sea mask chosen. In particular considering a land-sea mask of 0.5 degrees x 0.5 degrees instead of 0.25 x 0.25 increases the error in the final result by 5%. Combining all the mentioned sources of errors, they evaluated a total uncertainty in their time series of 15%.

In this chapter just the results modelled for the vertical deformations at the locations considered will be discussed since the tangential displacements induced are generally very small (see Figure 4.2). The plots representing the tangential time series (north-south and east-west components) calculated by the models for the four sites considered will be presented in Appendix C, section C.1.

4.2.1 Herstmonceux (UK)

In figures 4.3, 4.4 and 4.5 are presented comparisons between the different time series for the site of Herstmonceux.

Petrov's time series of the vertical and horizontal displacements induced by atmospheric pressure loading are not available for the site of Herstmonceux, so the comparison was made just with Sherneck's data. The agreement with the modelled results is very good and there is a perfect correspondence between maximum and minimum peaks in time, especially if a comparison is performed with the curves achieved from the second model (see figures 4.3 - 4.5 red curves).

Nevertheless the maximum and minimum peaks in Sherneck's time series are generally larger than those calculated by both our models, and differences up to 4-5 mm are commonly detected in the vertical. During the period from the end of April and the beginning of September the agreement improves and the discrepancies revealed are smaller (about 2-3 mm on average).

When the deformation is induced by sea level pressure field, an obvious diurnal variation that is more evident during the summer months (see figures 4.3 - 4.5 green curves) is seen. This oscillation is probably related with the daily temperature excursion that is particularly big between May and August. Diurnal and semidiurnal variations are a features of the pressure field (Ponte & Ray, 2002), however since they do not appear in the other

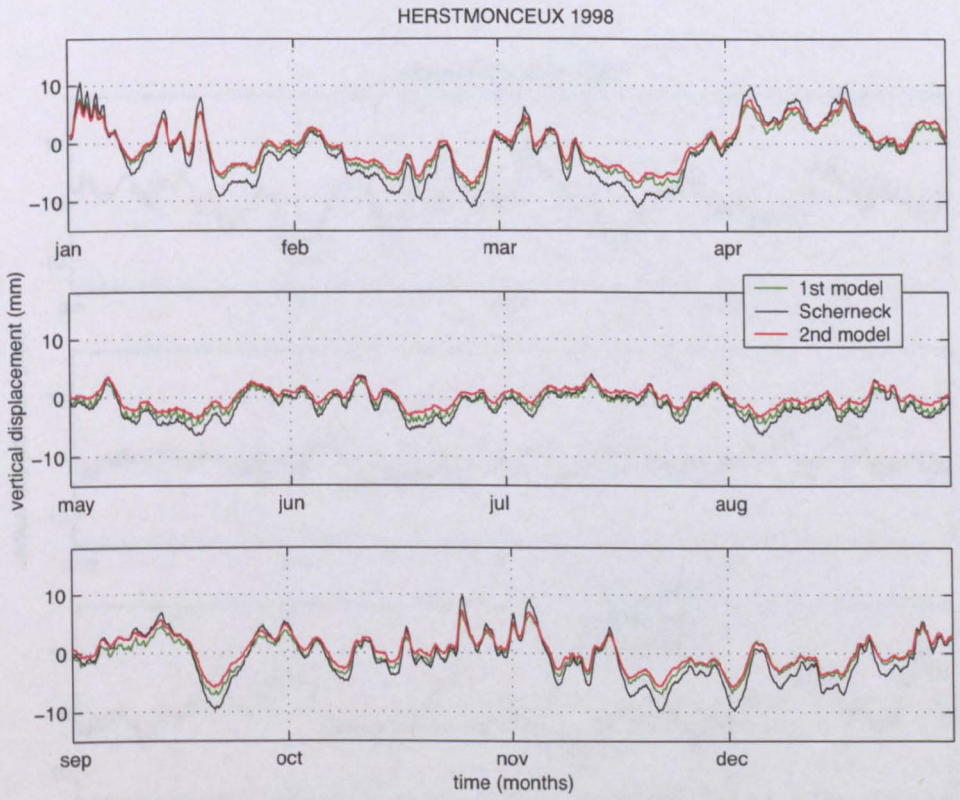

Figure 4.3: Radial deformation induced by atmospheric pressure loading at Herstmonceux during 1998. The modelled results from the second (red curve) and the first model (green curve) are compared with those available from OSO web site (black curve).

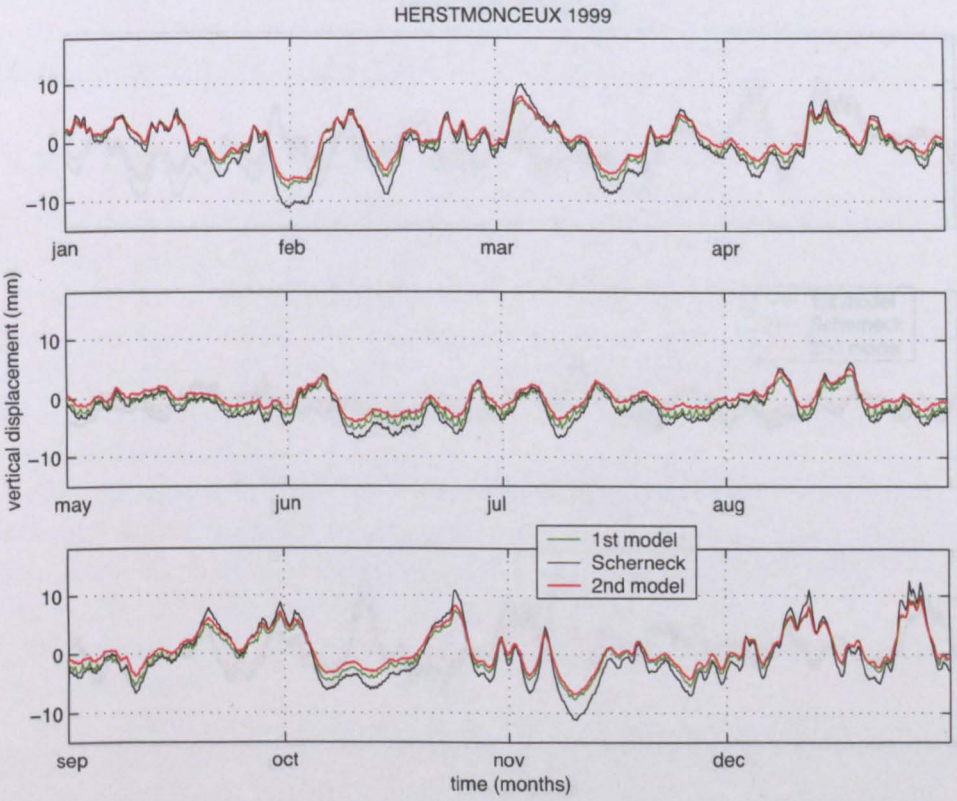

Figure 4.4: Same as figure 4.3 but for year 1999

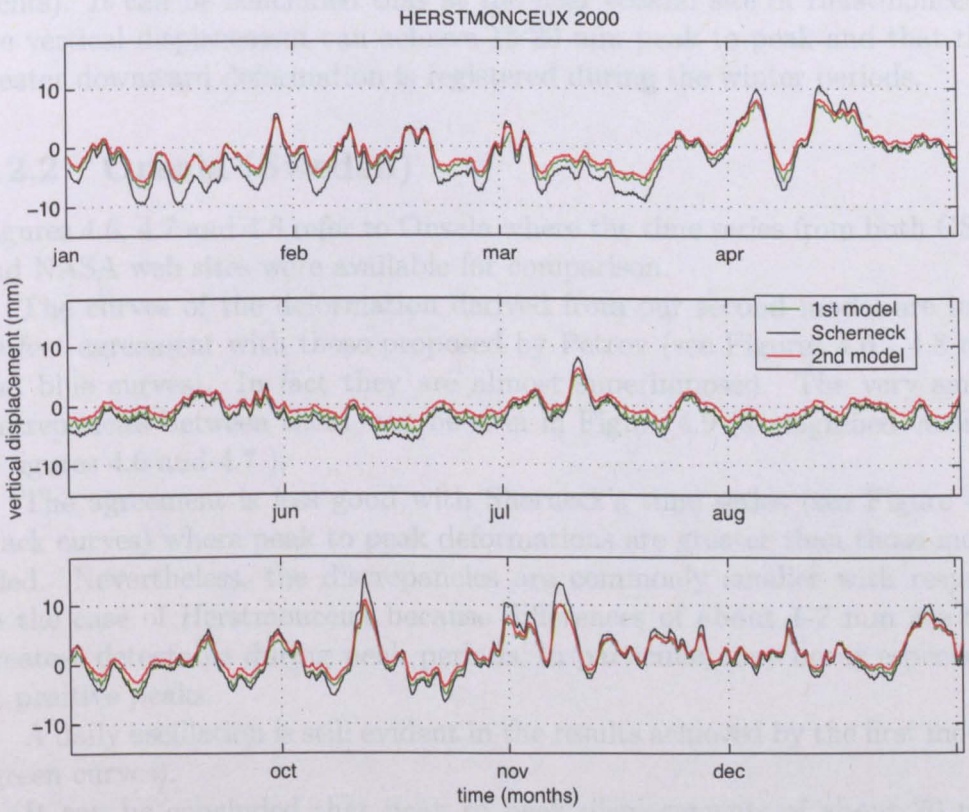

Figure 4.5: Same as figure 4.3 but for year 2000

time series considered, it can be concluded that the oscillation is related to some anomaly in the sea level pressure data set.

As was already noted by Van Dam and Wahr (1987), the radial displacements appear to be bigger during the winter period than during the summer season, this fact is related with the greater atmospheric pressure variations during colder months.

The results modelled are in a reasonably good agreement with those proposed by Sherneck (his time series showed a greater peak to peak displacements). It can be concluded that at the near coastal site of Herstmonceux the vertical displacement can achieve 15-20 mm peak to peak and that the greater downward deformation is registered during the winter periods.

4.2.2 Onsala (Sweden)

Figures 4.6, 4.7 and 4.8 refer to Onsala where the time series from both OSO and NASA web sites were available for comparison.

The curves of the deformation derived from our second model are in a perfect agreement with those proposed by Petrov (see Figures 4.6 - 4.8 red and blue curves). In fact they are almost superimposed. The very small discrepancies between them, can be seen in Figure 4.9 (a magnified version of figures 4.6 and 4.7).

The agreement is less good with Sherneck's time series (see Figure 4.9 black curves) where peak to peak deformations are greater than those modelled. Nevertheless, the discrepancies are commonly smaller with respect to the case of Herstmonceux because differences of about 1-2 mm are the greatest detectable during peak periods, in particular they occur especially at positive peaks.

A daily oscillation is still evident in the results achieved by the first model (green curves).

It can be concluded that peak to peak displacements of about 20 mm occur at the station of Onsala and that minimum variations are generally found during the summer period.

4.2.3 Wettzell (Germany)

Figures 4.10, 4.11 and 4.12 refer to Wettzell. It can be noted that Sherneck's time series are shifted in time compared with our modelled curves and the NASA results during the period between the middle of January and the beginning of April 1998; moreover, data are not available for the year 2000 so the comparison for this year can just be performed with Petrov's time series.

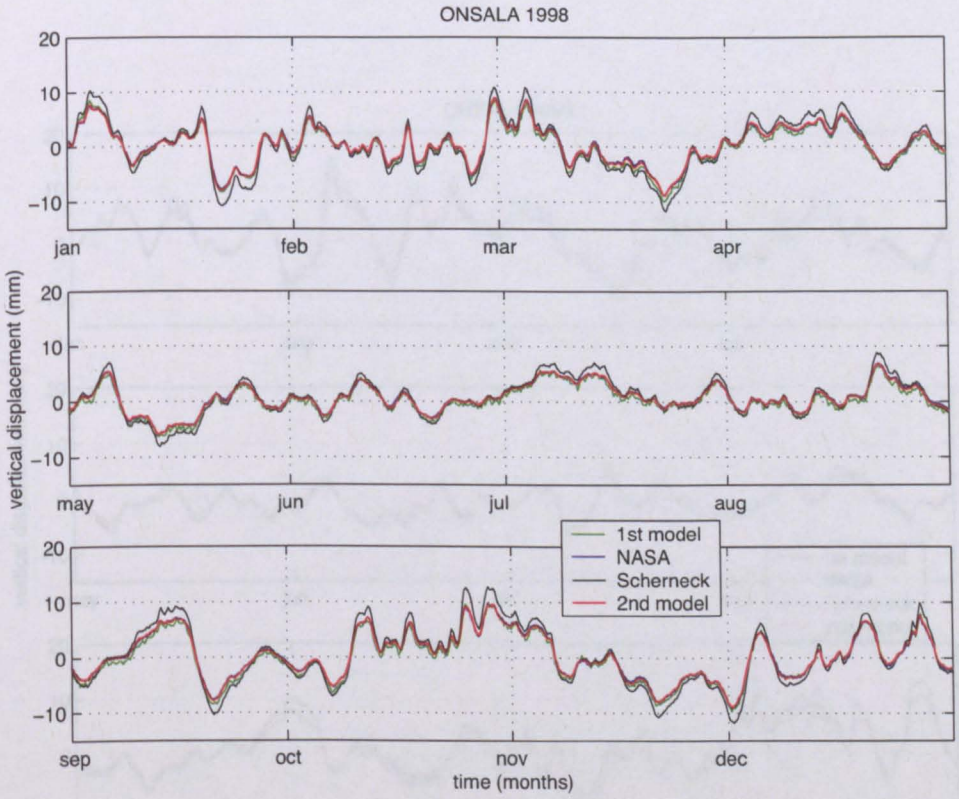

Figure 4.6: Radial deformation induced by atmospheric pressure loading at Onsala during 1998. The modelled results from the second (red curve) and the first model (green curve) are compared with those available from OSO web site (black curve) and NASA web site (blue curve). It can be noticed that NASA's time series (blue curve) and our second model results (red curve) are in a nearly perfect agreement, the curves being almost superimposed.

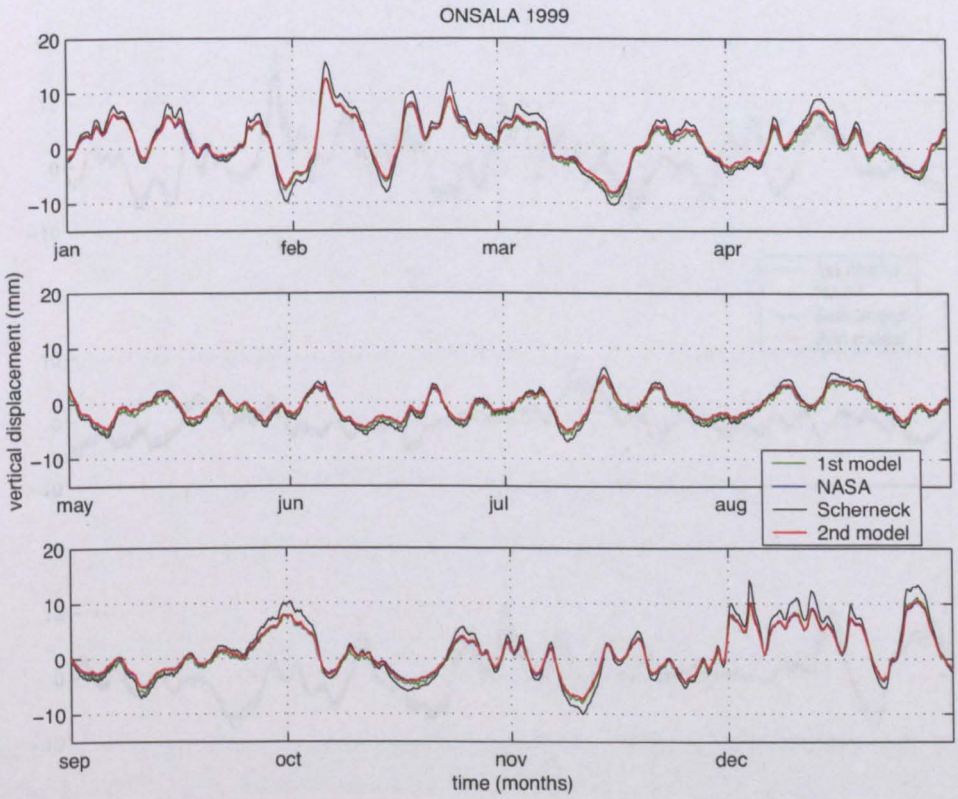

Figure 4.7: Same as figure 4.6 but for year 1999

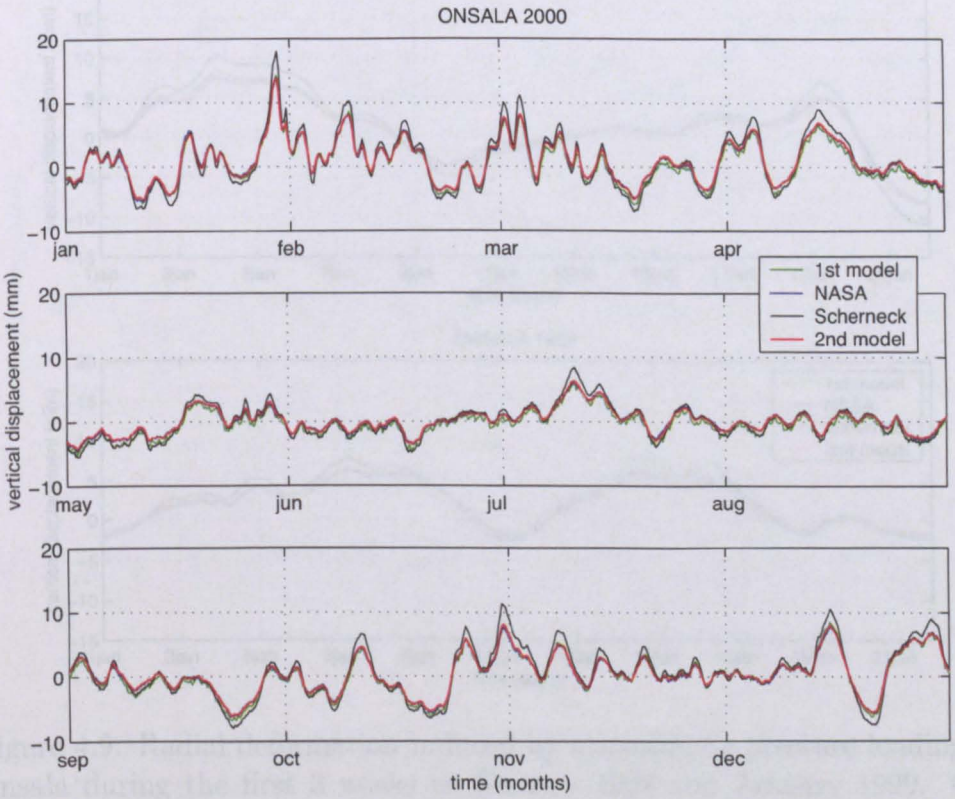

Figure 4.8: Same as figure 4.6 but for year 2000

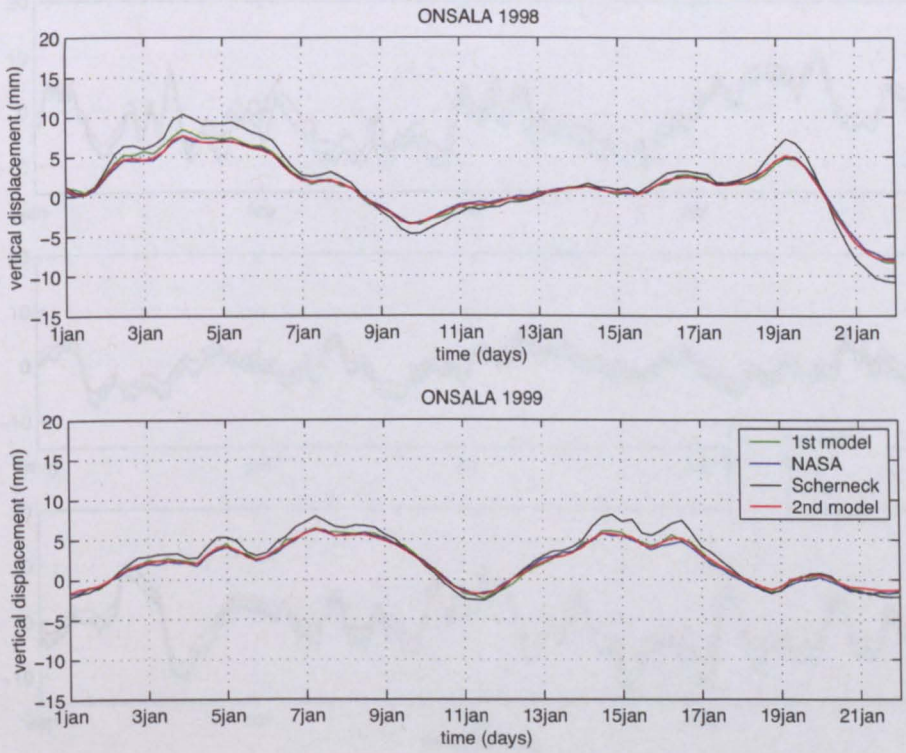

Figure 4.9: Radial deformation induced by atmospheric pressure loading at Onsala during the first 3 weeks of January 1998 and January 1999. Our results from the second (red curve) and the first model (green curve) are compared with those available from OSO web site (black curve) and NASA web site (blue curve).

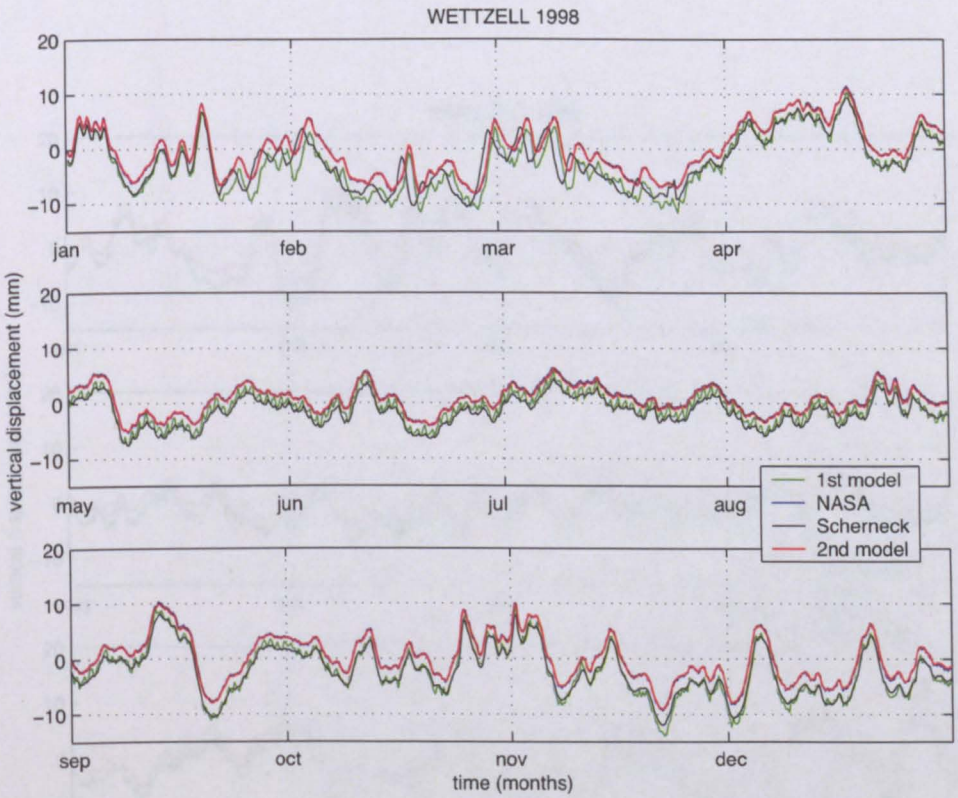

Figure 4.10: Radial deformation induced by atmospheric pressure loading at Wettzell during 1998. The modelled results from the second (red curve) and the first model (green curve) are compared with those available from OSO web site (black curve) and NASA web site (blue curve). It can be noticed that NASA's time series (blue curve) and our second model results (red curve) are in a nearly perfect agreement, the curves being almost superimposed.

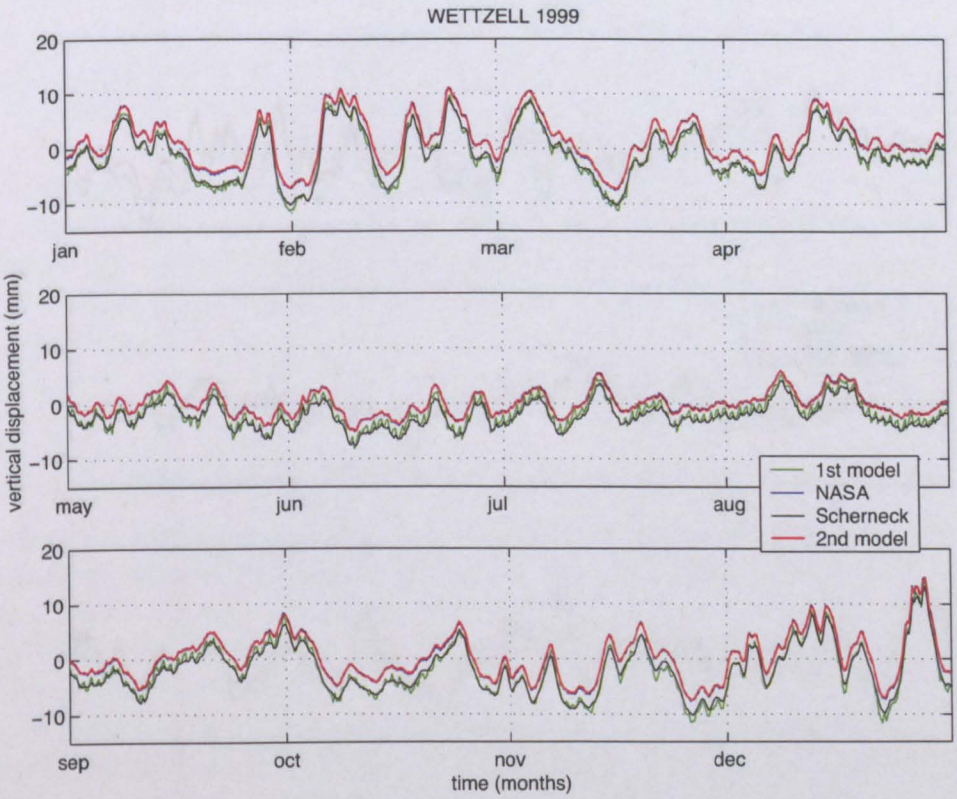

Figure 4.11: Same as figure 4.10 but for year 1999

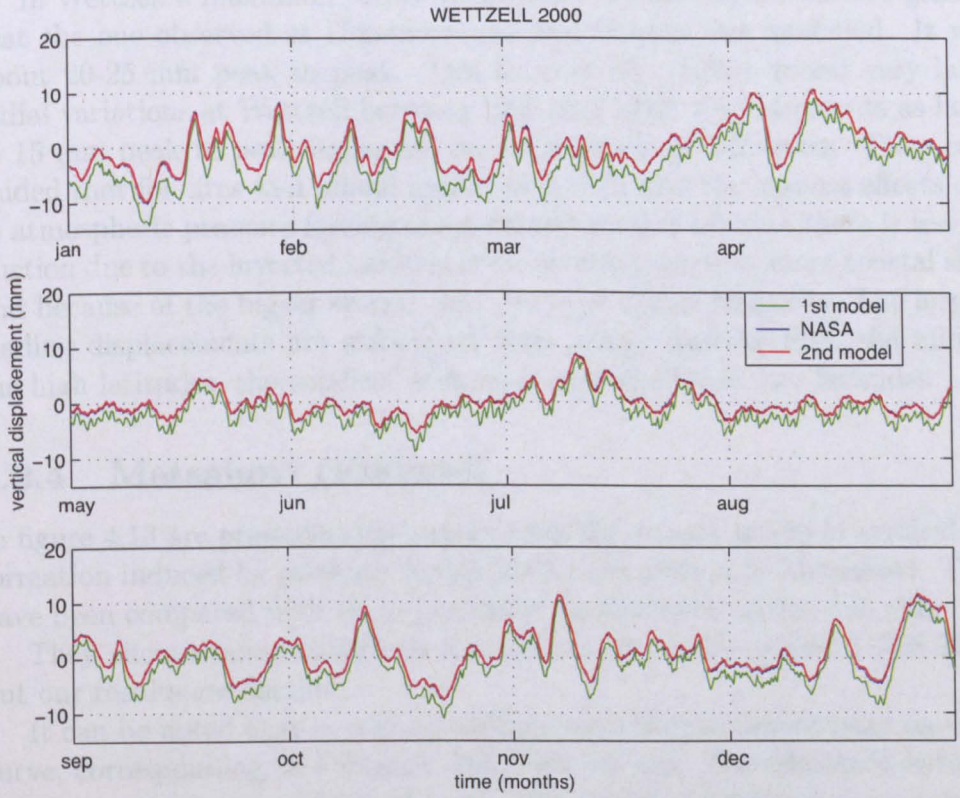

Figure 4.12: Same as figure 4.10 but for year 2000

It can be noted a general upward shift (about 3 mm) of our results if compared with those of Sherneck's for the whole period of time considered (figures 4.10 and 4.11 black curves). This disagreement is probably not related with errors in our programs of the modelled deformation since the accordance with Petrov's time series is very good.

The daily oscillation observed also for the sites of Herstmonceux and Onsala from the time series derived from the first model is still present at this location (see Figures 4.10, 4.11 and 4.12 green curves).

In Wettzell a maximum radial deformation of the Earth's surface greater that the one observed at Herstmonceux and Onsala was modelled. It was about 20-25 mm peak to peak. Van Dam et al. (1994), found very large radial variations at Wettzell between 1992 and 1993. Displacements as large as 15 mm peak to peak happened on a time-scale of 1-2 weeks. They concluded that for sites well inland and at high latitudes the loading effects due to atmospheric pressure forcing are generally greater because there is less reduction due to the inverted barometer ocean component to more coastal sites and because of the bigger storms that occur at higher latitudes. The largest loading displacements are associated with inland stations from the mid to the high latitudes, the smallest with near-coastal sites at low latitudes.

4.2.4 Metsahovi (Finland)

In figure 4.13 are presented the results from the second model of vertical deformation induced by pressure variations for the station of Metsahovi. They have been compared with those presented by Sherneck on his web site.

They show similar variations throughout the whole period (1998-2000) but our results are smaller.

It can be noted that in correspondence with the maximum peak on OSO curve, corresponding to February, 5th 1999 - 6 a.m., the difference between the two curves is quite big (5.28 mm). The values of Sherneck show a maximum displacement of 25.22 mm, we found a value of the radial deformation of 19.94 mm.

If a comparison between the time series of the radial deformation calculated from the first model (sea level pressure field as inducing the deformation) and OSO curves is performed (not shown), it can be noted a discrepancy between the maximums of the two curves (corresponding to February, 5th 1999 6 a.m.), of 5.56 mm (peak of 19.66 mm).

It can be concluded from both the curves that a radial displacement of 25-30 mm peak to peak can occur at this site.

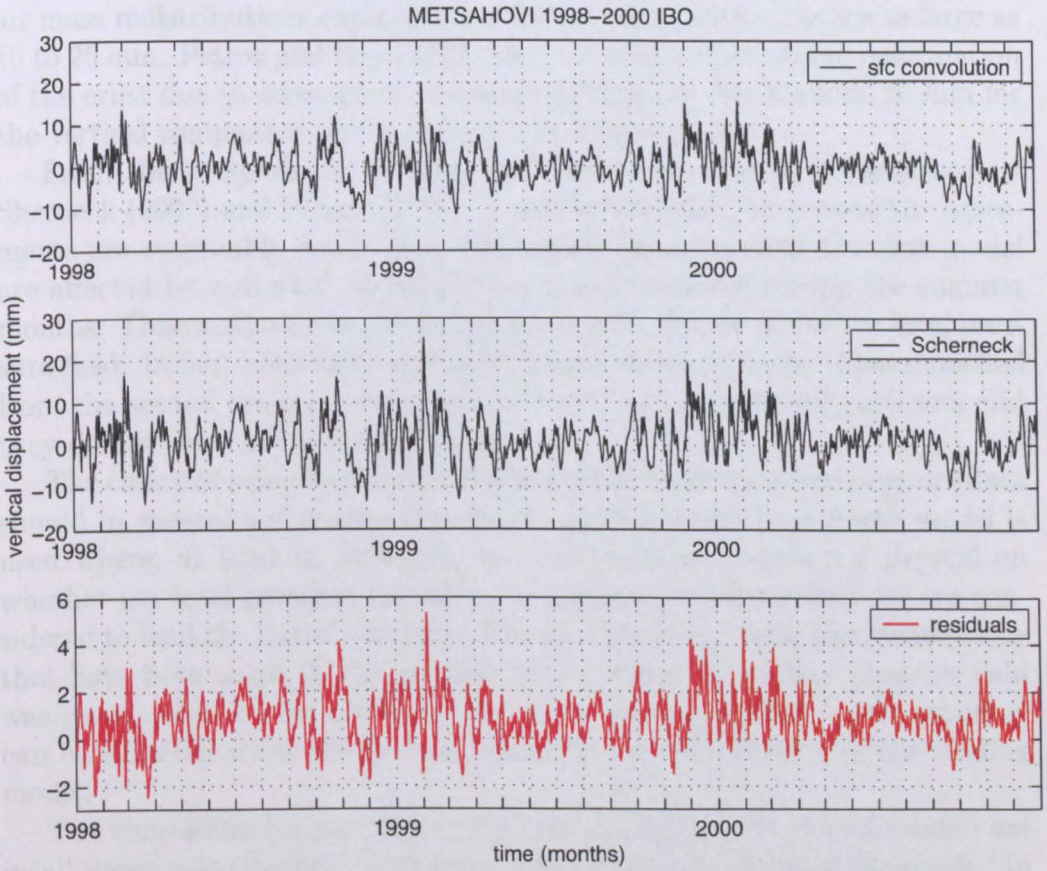

Figure 4.13: Radial deformation induced by atmospheric pressure loading at Metsahovi during the period between 1998 and 2000. The modeled results from the second program (surface pressure field input) are compared with those available from OSO web site. The time series in red represents the difference between the two curves.

4.3 Discussion

Vertical deformation of 15-20 mm peak to peak can occur at Herstmonceux and even larger displacements can be detected for the other sites considered (in particular Wettzell and Metsahovi). These results are in a good agreement with the numerical analysis of Van Dam et al. (1994). They suggested that air mass redistributions cause deformations of the Earth's surface as large as 10 to 25 mm. Petrov and Boy (2004) have noted that the loading deformation of the crust due to atmospheric pressure forcing can reach about 20 mm for the vertical component and 3 mm for the tangential one.

From the comparisons between our time series and those proposed by Sherneck (2002) and Petrov (2003), it can be said that, in general the agreements are reasonably good. Just the results obtained from the first model are affected by a diurnal variation that is more evident during the summer months. This oscillation is certainly related with the use of the sea level pressure field. In fact both OSO and NASA time series and also those modelled from the second program were derived from surface pressure data sets and they do not show any daily oscillations.

The choice of using sea level pressure data instead of surface pressure data should in general not matter very much. In fact a spherical Earth model is used where, at least in principle, the deformations should not depend on whether sea level pressure variations or surface pressure variations are considered to load the Earth's surface. The problem arises from the assumptions that have been made in the weather model when the surface pressure field was interpolated to the sea level. It can be concluded that better accuracy can be achieved when the surface pressures are used directly in the loading model.

The time series (in particular those obtained from the second model) are in all cases more similar to those of Petrov than to those of Sherneck. In particular the displacements found at the site of Wettzell differ from those proposed by Petrov by less than 0.1 mm. For the case of Onsala the discrepancies are, on average, less than 0.7 mm.

The diurnal amplitude taken from the sea level pressure field (derived from NCEP/NCAR surface pressure) is between 4 and 33 times larger than the surface pressure from ECMWF (used by Sherneck) and NCEP (used by Petrov). Furthermore, Sherneck's model is different from the other models by a scale factor ranging between 1.0 and 1.5. Caution should therefore be applied before attempting to use the sea level pressure field from NCEP/NCAR

The differences between our results for the same sites and Sherneck's results reach values of 2-3 mm. The reason of this fact depends mainly upon the pressure data sets that were used. Sherneck has used the ECMWF

surface pressure field while Petrov's and our time series were derived from the NCEP/NCAR Reanalysis Numerical Model.

For the first computation of the vertical displacements at a site, the International Standard Atmospheric Pressure (ISA) value at the sea level (1013.25 mbar) was removed. For our second model (surface pressure field input) (red curves), the pressure averaged over a certain period of time (1980-2002), was removed from each pressure datum. This was done since we were only interested in atmospheric pressure variations. This same method was used by Petrov and a different one was adopted by Sherneck who removed the mean of the loading time series computed over a period of 4 years (i.e. there is no mean in each cell). In fact, as it was already shown in the previous section, it does not matter so much if the mean pressure removed is averaged over 3, 10 or 23 years; but part of the very close similarity of our time series with NASA's curves is due to the fact that also our mean pressure was averaged over the same period of time (1980-2002).

As a final consideration, it has to be pointed out that even if the grid of interpolation chosen by Sherneck was very close to that used by us (1 degree x 1 degree with finer refinement closer to the site), our modelled displacement results were more similar to those proposed on the NASA web site, where Petrov used a less detailed grid (2.5 degrees x 2.5 degrees) for his computation. This fact suggests that the dimensions of the grid of interpolation are not as significant as the choice of the pressure field used in the calculation.

4.4 Admittance coefficients

It is important to emphasize that for obtaining the highest accuracy of the loading model results, the global convolution is generally recommended (as described in the previous section). However, in order to reduce the computational burden, a method that has been widely used considers the atmospheric pressure time series at the chosen location, together with the admittance coefficient, that represents the transfer function between the radial deformation at the site and the local atmospheric pressure variations.

The admittances for the four stations considered were computed by fitting a linear curve to the data obtained from the convolution method. The contribution for one year of all the loading elements of the grid that covers the entire world was taken into account.

It was already pointed out (Section 3.4), that in general, it is not possible to produce a unique admittance coefficient for a certain station since this coefficient slightly changes with time for the same site mainly because of the variation of the weather pattern that continuously changes the pressure

field. On the other hand it has to be said that comparing the results for different years, it has been noted that the coefficients uncertainties is only about ± 0.01mm/mbar. This fact allows to propose an averaged admittance coefficient for each station.

Table 4.2: Averaged admittances (in mm/mbar), obtained from our models of radial deformation induced by sea level pressure (slp) and surface pressure (sfc) variations, for the four European stations considered during the period 1998-2000.

STATION	ADMITTANCE (slp)	ADMITTANCE (sfc)
Herstmonceux	-0.25 mm/mbar	-0.25 mm/mbar
Onsala	-0.28 mm/mbar	-0.27 mm/mbar
Wettzell	-0.44 mm/mbar	-0.46 mm/mbar
Metsahovi	-0.34 mm/mbar	-0.34 mm/mbar

The averaged results obtained for the three years considered, from the first and the second model are presented in Table 4.2. They include the contribution from the grid elements covering the whole planet.

For the site of Herstmonceux (UK), an admittance of -0.25 mm/mbar was found. For the station of Onsala in Sweden the admittance varies between -0.28 mm/mbar and -0.27 mm/mbar, the value depends upon the model considered. The transfer function between the vertical displacement and the local atmospheric pressure variation at Wettzell (Germany) was between -0.46 mm/mbar and -0.44 mm/mbar, while at the site of Metsahovi (Finland) it was equal to -0.34 mm/mbar.

Comparing the results presented in Table 4.2 it can be noted that the use of a different pressure field does not affect significantly the admittance coefficients and maximum discrepancies of 0.02 mm/mbar are only detected at the continental site of Wettzell. It seems that the use of the surface pressure field instead of sea level pressure has increased the value of the transfer function. For the case of this German site, the transfer functions computed by the second model are more accurate than those obtained from the model of radial deformation induced by sea level pressure variations. In fact, among the four sites considered, Wettzell is the only continental site at high elevation, since its distance from the coasts is bigger than 500 km. As a consequence, when the surface pressure field is extrapolated to the sea level it leads to fictitious pressure. When the sea level pressure data are used for calculating the radial displacement, the results are inevitably more uncertain. This inaccuracy affects less coastal sites or stations with a very

low-level terrain (Peixoto and Oort, 1992).

The transfer functions for the inland site of Wettzell are larger than the admittances derived for the coastal sites of Herstmonceux, Onsala and Metsahovi i.e. -0.25 mm/mbar to -0.34 mm/mbar compared to -0.46 mm/mbar. This difference in admittance magnitudes between inland and coastal sites is what is expected for the inverted barometer ocean model and was already pointed out by Van Dam and Herring (1994). They have noted that even if a regression between the local pressure and the estimated radial displacement may provide a viable means for obtaining approximate load corrections, for coastal or island sites the use of the local pressure alone does not always offer a practical solution for computing the load contribution. In fact the inverted barometer effect is likely to reduce the contribution of the local pressure variations to the total load displacements at coastal sites.

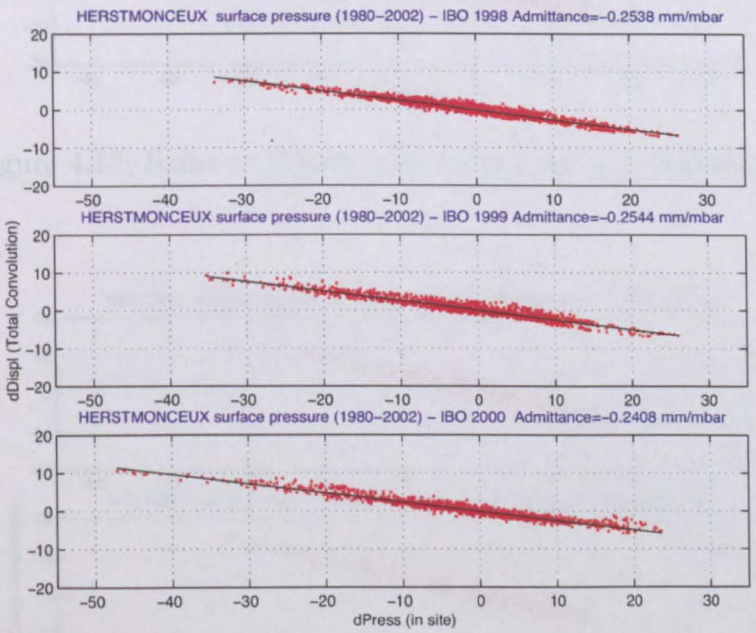

Figure 4.14: Linear curves representing the admittance for the three different years considered (CONV method IBO hypothesis) at Herstmonceux. The data were obtained from the model of radial deformation induced by surface pressure variations.

In the Figures 4.14-4.17 are presented the linear curves of the admittances for the four different stations in the three years considered obtained from the model of radial deformation induced by the surface pressure variations.

The values of the admittance found with our models were then compared

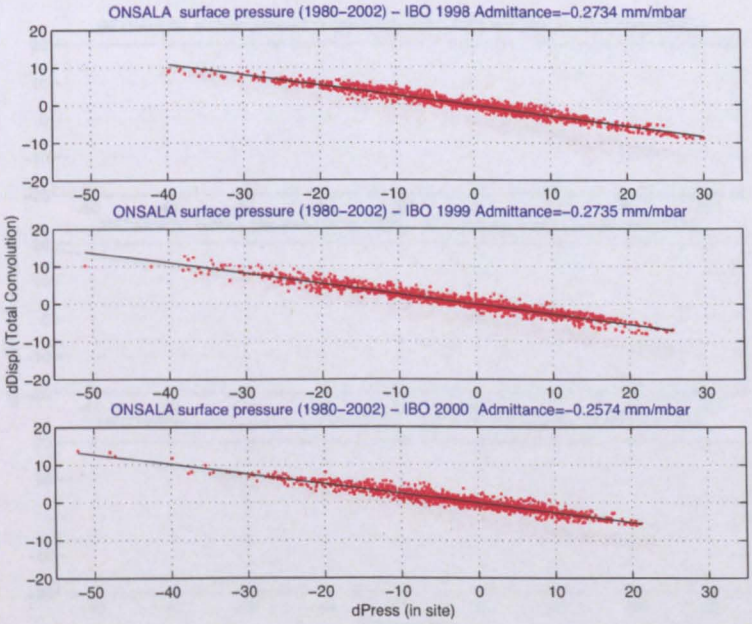

Figure 4.15: Same as Figure 4.14 but for the site of Onsala.

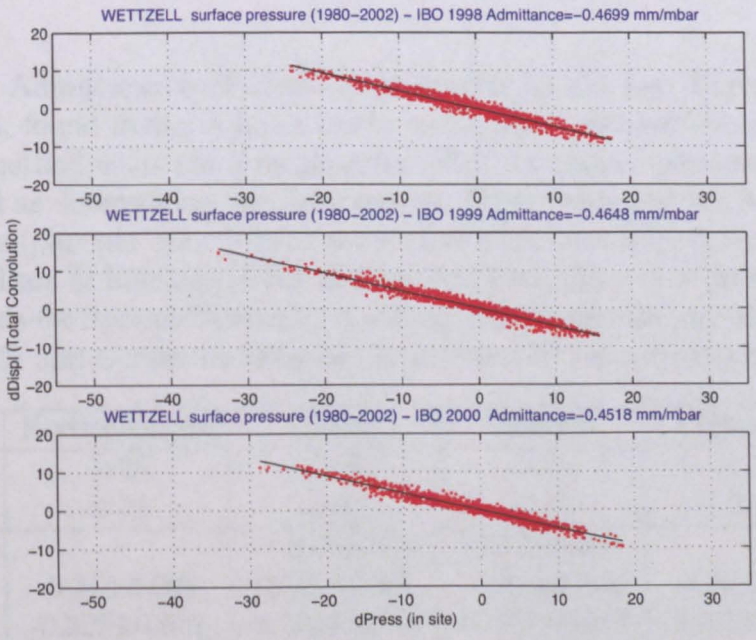

Figure 4.16: Same as Figure 4.14 but for the site of Wettzell.

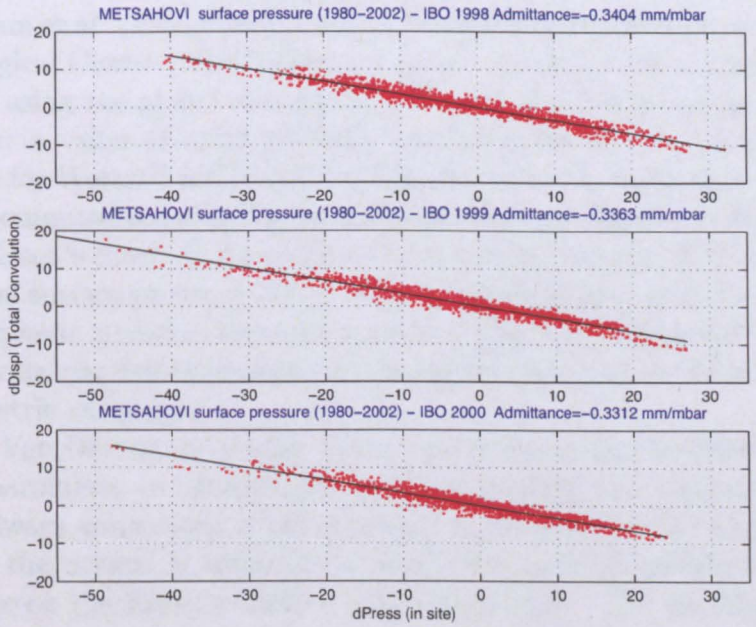

Figure 4.17: Same as Figure 4.14 but for the site of Metsahovi.

Table 4.3: Admittance coefficients in mm/mbar for the four European sites considered, found fitting a linear curve to the data obtained from the convolution method when sea level pressure (SLP) or surface pressure (SFC) is considered as determining the deformation. Other values of the admittance coefficients (plus the error bars in some cases), are shown for comparison. A from Van Dam & Herring (1994); B from Van Dam, Blewitt & Heflin (1994), SBL stands for Special Bureau for Loading, the results are provided by Van Dam (2002) and C refer to Manabe, Sato, Sakai & Yokoyama (1991)

	Herstmonceux	Onsala	Wettzell	Metsahovi
SLP	-0.25	-0.28	-0.44	-0.34
SFC	-0.25	-0.27	-0.46	-0.34
A	–	-0.32±0.001	-0.46±0.002	–
B	-0.36±0.008	-0.29±0.005	-0.43±0.008	-0.39±0.005
SBL	-0.327±0.001	-0.344±0.001	-0.442±0.001	-0.375±0.001
C	–	-0.254	-0.442	–

with those available from the literature (see Table 4.3).

Van Dam et al. (1994), proposed a regression coefficient between National Meteorological Center (NMC) pressure data and local vertical displacement, estimated using the global convolution, of -0.36 ± 0.008 mm/mbar for Herstmonceux; a value of -0.29 ± 0.005 mm/mbar for Onsala; -0.43 ± 0.008 mm/mbar for Wettzell and -0.39 ± 0.005 mm/mbar for Metsahovi.

They computed the effects of atmospheric pressure loading convolving the Farrell's Green's function for vertical deformation (Farrell, 1972) with twice daily global surface pressure values on a 2.5 x 2.5 degrees grid. In particular the atmospheric pressure from an arbitrary day was subtracted from each twice daily datum before performing the convolution in order to account just for barometric variations.

In the Van Dam et al. model, the oceans respond as a so called modified inverted barometer to atmospheric pressure loading i.e. since the oceanic mass is always conserved, a net increase or decrease in the total mass of air above the oceans is consider to produce a uniform pressure D acting everywhere on the Earth's surface under the oceans. The uniform pressure D is equal to:

$$D = \int_A \Delta P \frac{dS}{A} \tag{4.1}$$

where ΔP is the local change in pressure, A is the surface area of the oceans, and the integral is taken over the ocean surface.

The agreement between our results and the results published by Van Dam et al., (1994) is very good for the site of Wettzell. The difference with the admittance coefficients obtained from our models is between +0.01 and +0.03 mm/mbar, depending upon the pressure data set considered. Also for the case of Onsala the discrepancies are about -0.02 and -0.01 mm/mbar. The agreement is not as good for Metsahovi (divergence up to -0.05 mm/mbar) and Herstmonceux (up to -0.11 mm/mbar).

Van Dam and Herring (1994), have published the results of the local regression coefficients between radial surface displacements and local surface pressure for Wettzell and Onsala (-0.46± 0.002 mm/mbar for Wettzell and -0.32 ± 0.001 mm/mbar for Onsala) (see Table 4.3). These coefficients differ by -0.03 mm/mbar from those of Van Dam et al., (1994).

The differences between our results and Van Dam et al., (1994), are certainly not related with their modified IBO assumption since when we computed the effect of atmospheric pressure loading with a modified inverted barometer hypothesis, the contribution of the extra uniform pressure D from ocean areas was always positive and so its effect was the only one of shifting

upward the time series of vertical displacement induced. Certainly it does not increase the differences peak to peak of the deformation and thus the admittances. Van Dam and Wahr (1987) have indicated that the effect of the uniform pressure D on radial deformations are no more than 3 mm for coastal geodetic stations and are even smaller at inland points. In this case the contribution was about 1 mm or even less.

The regression coefficients calculated between the modelled loading effects and the local pressure derived by Manabe et al. (1991) for the sites of Onsala and Wettzell lead to values of -0.254 mm/mbar and -0.442 mm/mbar respectively (see Table 4.3). A comparison between these results and ours shows differences of about +0.02 mm/mbar for both the stations. For his computation Manabe et al. used surface pressure derived from the Global Objective Analysis (GANL) and obtained from the Japanese Meteorological Agency.

Further air pressure coefficients were available also from the web site of the International Earth Rotation Service (IERS) Special Bureau for Loading (SBL), they were provided by Van Dam (2002). Surface pressure from 18 years of the NCEP Reanalysis data set (1980-1997) on a 2.5 x 2.5 degrees grid and available every six hours were used for computing the regression coefficients.

The admittance coefficients from our models differ from the SBLs coefficients by about -0.07 mm/mbar for the station of Onsala and by -0.08 mm/mbar for Herstmonceux. For the site of Metsahovi the values of the transfer functions are closer (-0.03 mm/mbar), while for Wettzell the discrepancies are only about +0.02 mm/mbar.

It can be concluded that in general there is a reasonably good agreement between our results and those available from the literature and especially for the sites of Wettzell and Onsala. In particular, the results proposed by other authors are very consistent for the site of Wettzell (i.e. -0.43 mm/mbar to -0.46 mm/mbar).

The close agreement of all the results for Wettzell suggests that the differences between distinct published results for more coastal sites are due to the dissimilar resolutions of the land-ocean mask used by different authors. For a near coastal site, the reduction in the magnitude of the admittance coefficient due to the inverted barometer response of the ocean will depend upon the land-ocean mask.

The excellent agreement between the time series and those provided by Petrov (2003) supplies with an important validation of the model. It should be noted that Petrov recommended that the convolution model results are used directly rather than using admittance coefficients and the local pressure.

4.5 Admittance coefficients at some UK stations

Table 4.4: Averaged admittances over the period 1998-2000 (in mm/mbar) for some British sites. The transfer functions were obtained from the model of radial deformation induced by surface pressure (sfp) (IBO hypothesis).

STATIONS	ADMITTANCE COEFFICIENT
Lerwick	-0.08 mm/mbar
Aberdeen	-0.14 mm/mbar
Morpeth	-0.19 mm/mbar
North Shields	-0.18 mm/mbar
Hemsby	-0.20 mm/mbar
Lowestoft	-0.20 mm/mbar
Barking	-0.26 mm/mbar
Sheerness	-0.25 mm/mbar
Dover	-0.24 mm/mbar
Herstmonceux	-0.25 mm/mbar
Portsmouth	-0.23 mm/mbar
Hurn	-0.23 mm/mbar
Newlyn	-0.13 mm/mbar
Camborne	-0.14 mm/mbar
Brest (France)	-0.16 mm/mbar
Aberystwyth	-0.21 mm/mbar
Holyhead	-0.18 mm/mbar
Liverpool	-0.22 mm/mbar
Dunkeswell	-0.23 mm/mbar
Sunbury	-0.26 mm/mbar
Pershore	-0.27 mm/mbar
Nottingham	-0.27 mm/mbar
Portpatrick	-0.16 mm/mbar
Millport	-0.18 mm/mbar
Stornoway	-0.11 mm/mbar

In Table 4.4 are presented the admittance coefficients for some European stations mainly located in the British Isles and along the North European coasts. They were obtained with the same methodology proposed for the previous stations (i.e. fitting a linear curve to the data obtained from the

convolution method applied to the whole planet, when surface pressure data are considered. The hypothesis of an inverted barometer ocean model was assumed). For completeness, in Appendix C is presented a table with the transfer functions for the same sites first, when an oceanless Earth model is considered and then when the NIBO hypothesis is assumed inside the POLSSM grid while an IBO model is used for the further regions.

From Table 4.4 it can be noted that a very small admittance coefficient was obtained for the island site of Lerwick (−0.08 mm/mbar).

For stations located near the ocean like Newlyn, Camborne, Brest, Aberdeen and Stornoway the transfer function between vertical deformation at the location and the local atmospheric pressure variations increases slightly (−0.11 to −0.16 mm/mbar).

Finally, in the center of the country (Dunkeswell, Sunbury, Nottingham and Pershore), the admittance coefficients are the largest with a maximum of -0.27 mm/mbar at Nottingham and Pershore. This fact confirms what was already pointed out by Van Dam and Herring (1994), i.e. the transfer functions for inland sites are generally bigger when compared with those derived for coastal sites. For this case, inland stations coefficients are still less than the admittance calculated at the continental site of Wettzell where it reached −0.46 mm/mbar.

Figure 4.18: Geographical positions of the stations for which the admittance coefficients were determined.

4.6 Residuals

The radial displacements derived from the admittance coefficients obtained using the convolution method were compared with the deformations evaluated with Rabbel and Zschau method (TCCE method)(1985). This time the transfer functions were derived from the contribution of all the loading elements of the grid of interpolation that covered the entire world.

Rabbel and Zschau proposed a Two Coefficient Correction Equations (TCCE) method as a fast alternative to the convolution since it allowed saving a lot of computational time.

It was already concluded in Chapter 3, that the admittance coefficients approximate the deformation better than the TCCE formula, but in the previous case a smaller grid was considered (it extended about 4000 km from the observation point). Here it will be investigated if a similar result is valid also when bigger regions are considered to contribute to the deformation.

Table 4.5: RMS Residuals in millimeters between TCCE method and CONV method applied to the entire planet and between admittance (derived from the time series evaluated by the first model) and CONV method for the four stations considered during the period 1998-2000. SLP stands for sea level pressure.

STATIONS	TCCE rms 98	Admittance SLP rms 98
Herstmonceux	1.73	0.88
Onsala	1.24	1.09
Wettzell	1.97	1.05
Metsahovi	3.64	1.46
STATIONS	TCCE rms 99	Admittance SLP rms 99
Herstmonceux	1.55	1.04
Onsala	1.23	1.17
Wettzell	1.87	1.11
Metsahovi	3.46	1.39
STATIONS	TCCE rms 00	Admittance SLP rms 00
Herstmonceux	1.67	0.92
Onsala	1.35	1.14
Wettzell	1.92	0.98
Metsahovi	3.07	1.37

In general, when high accuracy is required in the determination of the radial deformation, the whole convolution method has to be applied but when

the precision requested is not high the methodology of Rabbel & Zschau can provide a good approximation of the displacement at a site (Rabbel and Schuh, 1986). This is still one of the recommended methods in the IERS Conventions and therefore the TCCE is investigated further in this section.

The residuals (and the RMS of the residuals) estimated between TCCE results and convolution results were always bigger than those calculated between the convolution and the admittance results. This fact indicates that the admittances we computed on the basis of the results produced by the first model, approximate the displacements at the sites considered better that the Rabbel and Zschau formula even when the pressure variations for the whole world are included (see Table 4.5). In particular, if a comparison is made between the results in Table 3.3 and Table 4.5, it can be noticed that, for the station of Herstmonceux the residuals between TCCE method and the convolution method get slightly worst when the latter methodology is applied to the entire planet and not just to an area of 4000 km from the site. This fact can be easily explained since the TCCE time series were calculated using the formula in Equation (3.3) that only involves the cells up to 2000 km from the station. Since in Table 4.5 the comparison with the convolution data regards a broader area, the RMS become slightly bigger respect with those that refer to 4000 km area from the observation point (Table 3.3).

Van Dam and Wahr (1987) have concluded that Rabbel and Zschau equation is useful for calculating atmospheric corrections for inland points (few hundred kilometers from the coast), but the agreement with the results from the convolution, is not as good for coastal sites. In particular in their case referred to Onsala (winter 1980), the dissimilarities between the two time series (one derived from the convolution and the second from TCCE equation), reached up to 10 mm and differences as large as 5 mm or more persisted for sites several hundred kilometers inland. It was suggested that coastal sites and near coastal stations need to extend the regression equations including a factor appropriate to each site. In this case even for the continental site of Wettzell the admittance modelled from the convolution formulation worked better than the TCCE formula.

The admittance residuals obtained from the displacements produced by surface pressure data set were, in general, smaller than those obtained from the admittance produced when pressure interpolated to sea level is determining the deformation. This leads to the conclusion that considering the pressure field at the surface as inducing the displacements, allowed us to achieve more accurate results in determining the transfer function representative for a site. On the other hand, as expected, considering the mean of surface pressure over different periods of time does not affect significantly the magnitude of the RMS. In fact the residuals due to the admittances are very

Table 4.6: RMS Residuals in millimeters between admittance (derived from the time series evaluated by the second model) and CONV method for the four stations considered during the period 1998-2000. SFC3 stands for surface pressure when the mean over 3 years is removed from the data set. SFC23 stands for surface pressure when the mean over 23 years is removed from the data set.

STATIONS	Admittance SFC3 rms 98	Admittance SFC23 rms 98
Herstmonceux	0.74	0.76
Onsala	0.84	0.85
Wettzell	0.99	0.99
Metsahovi	1.12	1.12
STATIONS	Admittance SFC3 rms 99	Admittance SFC23 rms 99
Herstmonceux	0.79	0.80
Onsala	0.94	0.93
Wettzell	0.89	0.89
Metsahovi	1.12	1.12
STATIONS	Admittance SFC3 rms 00	Admittance SFC23 rms 00
Herstmonceux	0.74	0.71
Onsala	0.90	0.91
Wettzell	0.88	0.87
Metsahovi	1.11	1.11

similar (maximum discrepancies of ±0.01 were detected), even if the mean removed is averaged over a different period of time (Table 4.6).

A comparison between admittance residuals and TCCE residuals in the surface pressure case was not performed since TCCE formula was specifically derived for sea level pressure and the local pressure variation p_s and the pressure change in a surrounding area of 2000 km from the observation point p_l were with respect to 1013.25 mbar.

4.7 Conclusions

Time series of vertical and horizontal displacements were computed at the four different European stations of Herstmonceux (UK), Onsala (Sweden), Wettzell (Germany) and Metsahovi (Finland) in the period between January 1998 and December 2000. These stations were chosen since the model results could be compared with model results already published for these sites.

Two different models of the radial and tangential deformation induced by sea level (first model) and surface pressure variations (second model) respectively were developed and the associated radial displacements were calculated by performing a convolution between the pressure field and the mass loading Green's functions and assuming an inverted barometer response for the ocean.

Since the interest was only focused on the deformations due to pressure variations, the ISA pressure value at the sea level (1013.25 mbar) was removed from the sea level pressure field before performing the convolution. For the second model, that considers surface pressure data, a similar procedure was followed by removing the mean pressure averaged over a period of 3, 10 and 23 years. It was noted that the differences in the time series of the radial deformation obtained using different files of mean pressure are negligible.

From the results it was concluded that the maximum in the radial deformation of the surface that can occur at the site of Herstmonceux is about 15-20 mm peak to peak; for Onsala peak to peak displacements of about 20 mm can occur. In Wettzell a maximum radial deformation of the Earth's surface of 20-25 mm peak to peak is common and a radial displacement of 25-30 mm peak to peak can occur at Metsahovi.

When the deformation is induced by the sea level pressure field, our time series of the radial displacements are affected by a diurnal variation that is more evident during the summer months. This oscillation is probably related with the daily temperature excursion that is particularly big between May and August and since it does not appear in the time series considered for comparison computed by Sherneck (2002) and Petrov (2003) for the same

sites and periods, we concluded that it is related to the sea level pressure data set.

The time series that we obtained from the second model of radial deformation were in a very good agreement with those proposed by Petrov (2003), while the curves of Sherneck (2002) showed, in general, a greater peak to peak displacement.

The discrepancies between these results and those of Sherneck are mainly due to the different surface pressure data sets used (i.e. NCEP and ECMWF), and less significantly by the smaller period of time on which the mean pressure was averaged (4 years). The times series derived from the second model of radial deformation and those proposed by Petrov were obtained from the same pressure data set and a mean pressure over the period 1980-2002 was removed from the pressure field. The perfect agreement achieved leads also to the conclusion that the dissimilarities between the grids of interpolation have negligible effects on the final deformation results.

Although the convolution model is the recommended method, it was decided to investigate also the methodology based on admittance coefficients, since they are widely used in space geodesy. Even if in general it is not possible to produce a unique admittance coefficient for a certain station (this coefficient slightly changes with time for the same site), it has been noted, comparing the results from different years, that the coefficient uncertainty is only about ± 0.01 mm/mbar. Because of this fact, mean admittances over the period considered can be given for different stations.

Fitting a linear curve to the time series obtained from the models and averaging the results for the period 1998-2000, admittance of -0.25 mm/mbar was found for the site of Herstmonceux (UK). For the station of Onsala in Sweden the admittance varies between -0.28 mm/mbar and -0.27 mm/mbar. The transfer function between the vertical displacement and the local atmospheric pressure variation at Wettzell was between -0.46 mm/mbar and -0.44 mm/mbar, while at the site of Metsahovi (Finland) it was equal to -0.34 mm/mbar. It was noted that the use of a different pressure field does not affect significantly the admittance coefficients.

In general there is always a reasonable agreement between our coefficients and those available from the literature (Van Dam and Herring, 1994; Manabe et al., 1991; Van Dam et al., 1994; Van Dam and Wahr 1987, Van Dam 2002), especially for the sites of Wettzell and Onsala. Probably the small discrepancies detected can be due to a different source, time and quality of the surface pressure data, to the different grids of interpolation used and to the different size of the elements in them. The resolution of the land-ocean mask is particularly important. The differences are certainly not related with the modified IBO assumption.

From the analysis of the residuals (and the RMS of the residuals) between admittance and convolution and the TCCE method and convolution, it can be concluded that the transfer functions calculated on the basis of the results produced by the first model, approximate the deformations at the sites considered better than the Rabbel and Zschau formula, even when larger regions contribute to the deformation.

When the pressure field at the surface is considered as inducing the displacements, the admittances calculated from the convolution are very accurate and the residuals computed are smaller than those observed when sea level pressure is inducing the deformation.

Chapter 5

Non-tidal ocean loading due to storm surges

So far, in the previous Chapters on atmospheric loading the standard procedures in the geodetic literature have been followed i.e. it has been assumed that either there is no ocean and the atmospheric pressure directly loads the ocean floor (NIBO model) or the ocean responds as an inverse barometer, so that there is no loading on the ocean floor (IBO model). In reality the ocean responds dynamically to atmospheric pressure changes and the associated wind fields. This is particularly true on the shallow continental shelves, where the associated sea level variations are called surges.

The aim of this chapter is to evaluate the magnitude of the vertical and tangential displacements of the British Isles and northwest European regions by the loading due to sea mass variations in the shelf seas. Also the gravity changes produced by the loading deformation are investigated.

Firstly, the main aspects and characteristics of storm surges are described in terms of the response of sea level to pressure and wind forcing. Also a general description of the phenomenon on the west and east coasts of British Isles is given.

The results from the model of the vertical and tangential deformations and associated gravity variations of the UK due to loading by surges are provided. In particular, the attention is focused on two main storm events which happened during the period of time investigated.

Finally the effect on the vertical and tangential deformations and the associated gravity changes in the British Isles and in the north west Europe related with two different winter seasons characterized by opposite North Atlantic Oscillation indices are examined. Some conclusions are made concerning the inter-annual variability of displacements that may be observed with continuous GPS (and SLR, VLBI or gravity) measurements between

two such years, with large variations in winter mean sea levels.

5.1 Storm surges

The regular tidal rise and fall of the sea could be accurately predicted by the tidal theory if it was not continuously disturbed by irregular weather factors such as the variations in the surface pressure and the wind stress on the sea surface. In fact, when the sea level $X(t)$ is estimated, the measurement contains a tidal component $T(t)$ (or astronomical component) that is a periodic movement related in amplitude and phase with the gravitational effects of the Moon and the Sun, and a non-tidal component $S(t)$, that is usually called the meteorological residual, dependent upon the weather factors.

$$X(t) = Z_0(t) + T(t) + S(t)$$

here $Z_0(t)$ is the mean sea level that slowly changes with time.

Generally the non-tidal component has magnitude of about a few decimeters so it goes almost unnoticed, but occasionally the residuals are of the order of 1 meter or even more and this may cause flooding events in coastal regions.

The term surge commonly refers to a sudden movement of water quickly generated but which is soon over while a storm surge is usually defined as a particular meteorological event during which a very large non-tidal component is generated. As a result there is a raising (positive surge) or a lowering (negative surge) of the sea level. The same storm can be responsible for a positive and negative surge as it develops and progresses. Positive surges can then be preceded by a negative surge. At higher latitudes the weather effects of lowering or rising the observed sea level compared with the level predicted, are greater during cold stormy months.

The prediction of positive surges is generally very important for warning in time those areas located near the coasts that could be subjected to floods. Although forecasting negative surges can be equally important in order to ensure a safe navigation.

It was pointed out by Pugh (Pugh, 1987), that statistically there is a tendency for large positive residuals to occur more frequently than large negative residuals. In general the non-tidal residuals markedly depend on the seasonal cycle of the weather. In fact around the UK, the greater surge events usually occur between November and February while the period May - September is generally quite. The importance of these components is also related with the local bathymetry since the greatest effects are registered when they act on semi-enclosed shallow seas or coincide with high water on

spring tides (tides that occur approximately twice a month when the Moon is either new or full).

There are two main categories of storms depending upon the extension of their effects: tropical and extratropical. Tropical storms are small but intense, they produce high floods in a region that usually extends about 10 km; extratropical storms extend over hundreds of kilometers and are relatively slow moving.

Commonly the duration of a passing storm surge lies between a few hours and two or three days, for example North sea surges are diurnal in character while surges on the west coasts of the British Isles are much shorter and have a life span of about 9 to 15 hours (Heaps 1967).

The main causes of storm surges are the reduction in atmospheric pressure that produce changes in the forces acting vertically on the sea surface (the effects are felt immediately at all depths) and the wind stress on the sea surface. When a barometric depression is passing through an ocean area there is a decrease in the atmospheric pressure acting on that zone and as a consequence the sea level rises. The depth below the surface at which the wind effect is felt depends upon the length of time it acts for and the vertical variation of density of the water column.

Generally it is not possible to completely separate the effects of winds and air pressure but it is known that their effects are both important during an extratropical storm while a surface wind stress can alone account for a higher elevation of the sea level than the atmospheric pressure variation associated in the case of a tropical storm (Wells, 1997). The pressure variation is normally responsible for a slowly varying contribution to the meteorological residuals at a given site.

Around the British Isles deep low pressure systems are liable to cause surges and since these phenomena act for longer periods and involve a larger region, the Earth's rotation becomes important in determining the sea response.

5.1.1 Sea level response to atmospheric pressure

The inverse relationship between sea level and pressure forcing can be modelled theoretically. When the sea level is in equilibrium conditions with respect to the atmospheric pressure acting i.e in absence of currents, it follows:

$$\frac{\partial P}{\partial x} = 0$$

If ρ represents the constant density of the water, the pressure P is defined

by the sum of the atmospheric pressure P_A and the sea level ζ. z is the depth of water (N.B. z is negative). x is the direction of integration.

$$P = P_A - \rho \cdot g(z - \zeta)$$

Differentiating respect to x it becomes:

$$\frac{\partial P_A}{\partial x} + \rho \cdot g \frac{\partial \zeta}{\partial x} = 0$$

So the sum of the atmospheric pressure and the pressure due to variations in sea level is constant:

$$P_A + \rho g \zeta = constant$$

It can be concluded that when small variations of P_A with respect to the mean atmospheric pressure forcing happen, the sea level ζ varies relative to the mean sea level according to:

$$\Delta\zeta = -\frac{\Delta P_A}{\rho g}$$

Assuming a density ρ of 1026 kg/m^3 and a gravitational acceleration g of 9.80 m/s^2:

$$\Delta\zeta = -0.993 \Delta P_A \qquad (5.1)$$

where $\Delta\zeta$ is in centimeters and ΔP_A in millibar. This response is called the inverted barometer effect (previously already discussed) and it means that if the sea level would completely adjust to the pressure forcing, there would be no changes in the observed bottom pressure.

As previously anticipated (Chapters 3 and 4), the inverted barometer effect is rarely found in practice because of the dynamical response of the sea especially on continental shelf areas.

For describing the dynamical response of the sea level to the atmospheric pressure and wind stress, the hydrodynamical equations have to be solved on a computer (Flather & Davies 1976; Flather 1984; Pugh 1987).

5.2 Storm surges in UK

Around the UK the main storm surges are due to low pressure systems and the dynamical characteristics of storms surges on the west coast are quite different from those on the east coast.

In the North Sea the surges are generated by cyclonic depressions and winds acting to the north and north west of Scotland. Entering the North Sea, the water is affected by dynamical effects, by the Earth's rotation and by the very shallow depth of water along the coasts of the southern North sea.

Since the south east of England and the North Sea are experiencing a gradual subsidence (Sclater & Christie, 1980, de la Vega-Leinert & Nicholls, 2000), it is evident how vulnerable these zones are to flooding. Fortunately, because the travel directions of the surges are from north to south, reliable warnings are generally possible. The storm surge on the east coast of Britain can usually be predicted some 6-12 hours in advance. The technique of forecasting flooding patterns consists of the observation of tidal residuals on the north east coasts of Scotland and particularly with computer models of the hydrodynamics (see next section).

The direction of propagation of the North sea surges is related with the Coriolis force that produces a rotation of the current driven by the wind to the right in the northern hemisphere (to the left in the southern hemisphere). As a consequence northerly wind is responsible for water transport toward the eastern coast of the British Isles, inducing a rise in the sea level.

In February 1953 a great storm surge happened in the North sea. Meteorological residuals of 2-4 meters above the predicted sea level were reached and large areas of the eastern coast of the UK and Holland were inundated. The surge caused a considerable loss of life and damages to the land and properties (Flather, 1984; Wells, 1997).

Reviewing the effects of storm surges on UK coasts, Heaps (Heaps, 1967) pointed out that there is a marked tendency for a maximum raising of water near Southend.

On the west coast of British Isles, the most effective wind directions in creating large surges in the Irish Sea and the Celtic Sea are the south and southwest direction (Amin, 1982) and, because of a nearly resonant response of the Irish Sea and Bristol Channel to tidal forcing from the Atlantic, the surges are quickly and intensively generated and very short lived (i.e. a single semidiurnal tidal cycle).

The Dover Strait is entered by only a small part of the North Sea surge energy while the main part of the surge is reflected and amplified traveling towards the coasts of Holland and Germany.

Surges in the English Channel are usually smaller than elsewhere in the region (Pugh, 1987).

5.3 Numerical modelling of the loading due to storm surges

Numerical models of surges are generally developed for forecasting flooding patterns but they find large applications also in the hydrodynamic interpolation of arrays of sparse observational data and in the simulation of particular conditions in a controlled environment (wind speed, atmospheric pressure forcing, etc.). In our particular case, the height of the sea level at hourly intervals, available from Proudman Oceanographic Laboratory Storm Surge Model (POLSSM), was used as the input for a new loading program (Flather & Williams, 2001; Flather et al., 2001). The vertical and horizontal displacements and associated gravity changes associated due to storm surge loading were computed using this model. POLSSM is driven by winds and air pressure that are derived from a further atmospheric model. The wind stress is considered to increase as the square of the wind speed while the barometric disturbance is exerting its influence on a very large scale. At the coastlines the flow of water is assumed parallel to the boundary and the main loss of energy is due to bottom friction.

The gravity loading effect can be separated into two different parts the Newtonian and the elastic (see Equation 2.2). The elastic part of the loading contains the gravity changes due to the vertical displacement of the station on the deformed Earth that moves the station through the gravity field. It also includes the gravity change induced by the redistribution of the mass within the Earth. The Newtonian part of the loading is the direct gravitational attraction of the extra water mass near the site of interest. The total loading effect consists of the sum of the two components, Newtonian and elastic.

As a first stage, the grid of the loading model coincided with POLSSM one. It covered 25 degrees of extension in longitude (between 12 W and 13 E) and 15 degrees in latitude (between 63 N and 48 N) with a resolution of 0.16 degrees in longitude and 0.11 degrees in latitude (Figure 5.1). The PREM Green's function is convolved with the sea level heights from POLSSM (see Equation 2.5). The small dimensions for the grid elements is a very key factor because for smaller cells the numerical approximation achieved using point masses is more accurate (Bos, 2000).

Deformations and gravity variations were estimated at the sites of Sheerness and Lowestoft on the east coast of England between January 1997 and

December 2003. These sites were chosen because they are situated in the area of maximum surge elevation and have continuous GPS at the tide gauges.

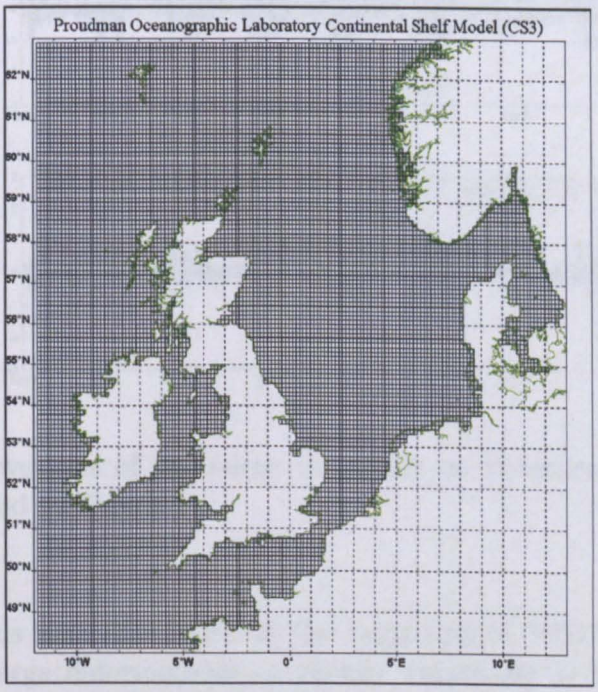

Figure 5.1: Proudman Oceanographic Laboratory Storm Surge Model grid. The model grid has an extension of 25 degrees in longitude and 15 degrees in latitude and a resolution of 0.16 in longitude and 0.11 in latitude.

In Figure 5.2 are presented the heights of the surge at Sheerness and Lowestoft during the time interval 1997-2003 calculated by POLSSM. The non-tidal modelled residuals in meters are generally quite large (up to 1 – 2 meters) for both the locations considered. It can be noticed that the surge elevation at the site of Sheerness is always slightly higher compared with the elevation reached at Lowestoft at the same time. This fact is quite surprising since the two stations are geographically very close. This result can be explained by the lower depths near Sheerness and the shape of the coastline. There is an obvious tendency for storm surges to occur during winter months (i.e. from December to February) while spring and summer periods are by comparison relatively calm.

During the period of time investigated, two particularly large storm surges events occurred. The first one was on February 4th 1999 and the second one, with greater magnitude in surge elevation on January 30th 2000. High

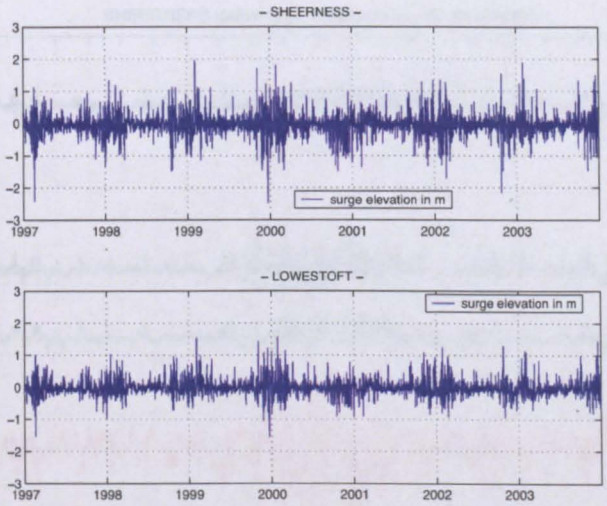

Figure 5.2: Elevations of the surge in meters at Sheerness and Lowestoft during the period 1997-2003.

positive residuals were also found at the beginning of 2003 but they did not produce such large deformations or gravity variations as these two events (see for completeness Figures 5.7 - 5.10).

Figures 5.3 and 5.4 show the elevation of the surge at Sheerness and Lowestoft during the period 1999-2000. Also the vertical and the horizontal deformations induced are presented. The two peaks in the blue curves at the beginning of February 1999 and at the end of January 2000 correspond to the elevation of the surge during the main surge events of the interval of time considered. In red are represented the radial displacements generated in millimeters, while in black and green respectively are represented the tangential deformation associated (north-south component and east-west component). It can easily be noticed that the tangential displacements calculated are generally not negligible but are much smaller than the vertical deformations produced. In the lower part of the figures are described the deformation on the 29th and 30th of January 2000.

There is an inverse relationship between surge elevation and land vertical deformation movements, i.e. a positive storm surge event determines a consequent negative displacement in the radial direction on the Earth's surface. In this particular case the extra water in the North Sea exerted an extra loading over the Earth's crust and the displacement is found in and around the British Isles and as a consequence there is a significant downward movement of these areas.

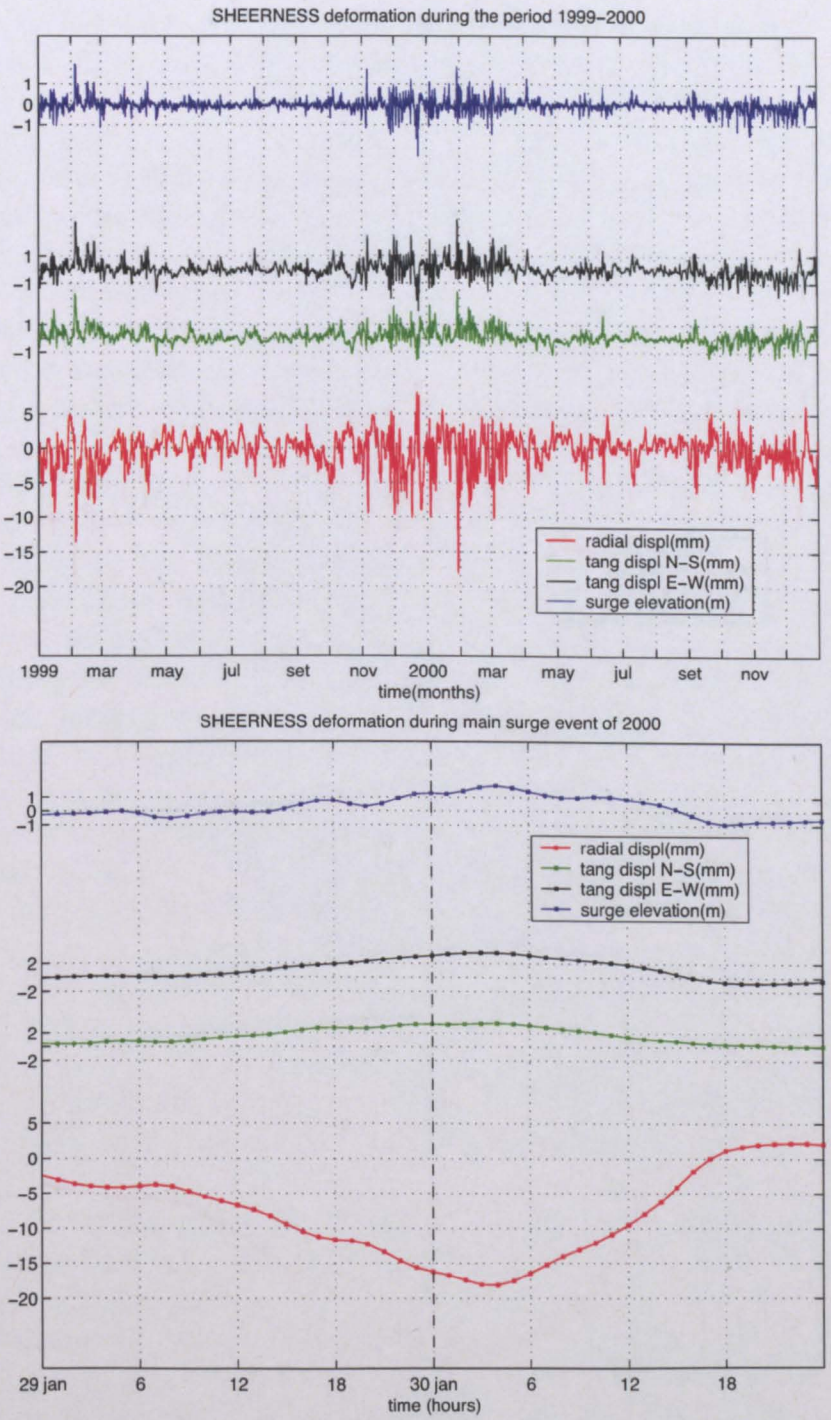

Figure 5.3: Elevations in meters (blue curve) and corresponding vertical (red curve) and tangential deformations (green and black curves) in millimetres at Sheerness (North and East directions are positive). The maximum downward radial displacement corresponds to the main surge event of January, 30th 2000. In the lower part of the figure a plot describing the deformation on the 29th and 30th of January 2000 is presented.

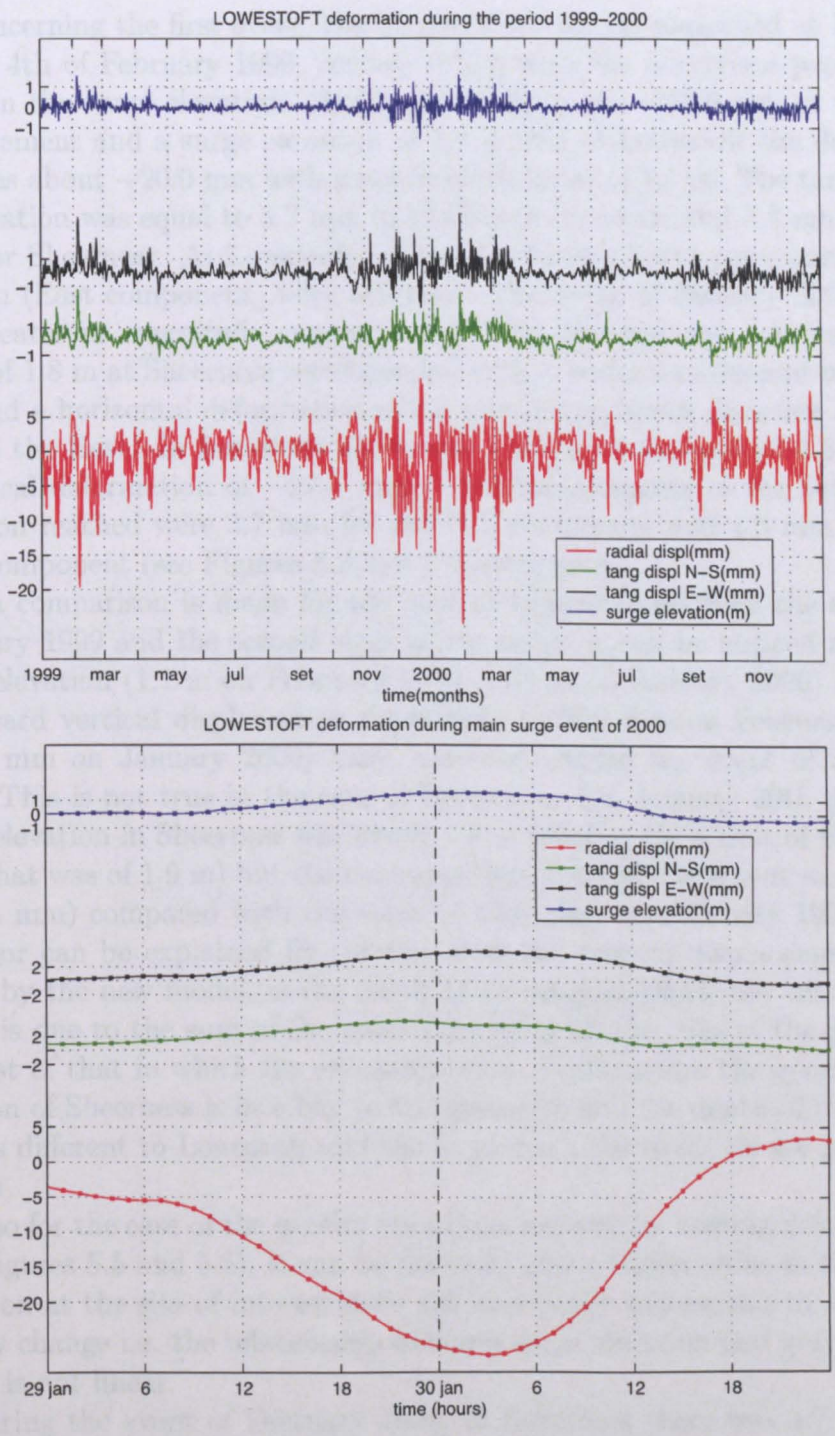

Figure 5.4: Elevations in meters (blue curve) and corresponding vertical (red curve) and tangential deformations (green and black curves) in millimetres at Lowestoft (North and East directions are positive). The maximum downward radial displacement corresponds to the main surge event of January, 30th 2000. In the lower part of the figure a plot describing the deformation on the 29th and 30th of January 2000 is presented.

Concerning the first event, the biggest deformation happened at 11 p.m. on the 4th of February 1999, corresponding with the maximum peak measured in the surge elevation. At Sheerness there was −13.6 mm of vertical displacement and a surge elevation of 1.9 m and at Lowestoft the deformation was about −20.0 mm with a sea level elevation of 1.1 m. The tangential deformation was equal to 3.2 mm in the North direction and 3.8 mm in the East for Sheerness. At Lowestoft values of 3.0 mm (North component) and 3.7 mm (East component) were achieved. The event of January 30th, 2000 was greater in magnitude compared with the previous one. A maximum surge of 1.8 m at Sheerness corresponded with a vertical movement of −18.1 mm and a horizontal deformation of 3.3 mm in the North direction and 3.6 mm to the East. In Lowestoft there was a sea level increase of 1.5 m and a vertical deformation of −27.5 mm. The displacements in the tangential direction reached were 3.7 mm for the N-S component and 4.3 mm for the E-W component (see Figures 5.3 and 5.4 lower part).

If a comparison is made for the case of Lowestoft between the event of February 1999 and the second large storm surge, it can be noticed that the surge elevation (1.1 m on February 1999, 1.55 m on January 2000) and the downward vertical displacement magnitude (−20.0 mm on February 1999, −27.5 mm on January 2000) have increased during the event of January 2000. This is not true in the case of Sheerness. On January 30th 2000 the surge elevation in Sheerness was about 1.8 m (smaller than that of February 2000 that was of 1.9 m) but the corresponding vertical movement was bigger (−18.1 mm) compared with the value (−13.6 mm) on February 1999. This behavior can be explained by the fact that the vertical displacement computed by the new model, is the result of an integral effect over all the grid i.e. it is due to the sum of the contributions of all the cells of the grid and not just of that in which the site is situated. Furthermore the geographical position of Sheerness is in a bay so the geometry and the depth of the ocean floor is different to Lowestoft and the local non-tidal residuals are generally greater.

Also for the case of the gravity variations induced by loading deformation (see Figures 5.5 and 5.6), it can be noticed, that a bigger value in the surge elevation at the site of interest does not necessarily correspond to a greater gravity change i.e. the relationship between surge elevation and gravity variations is not linear.

During the event of February 1999, at Sheerness there was 3.7 μGal of gravity change. The contribution of the Newtonian component of the gravity was of 0.7 μGal and the one of the elastic component was about 3.0 μGal. At Lowestoft the effect was 5.4 μGal (almost 1.0 μGal from the Newtonian part and 4.4 μGal from the elastic one). The total gravity variation was

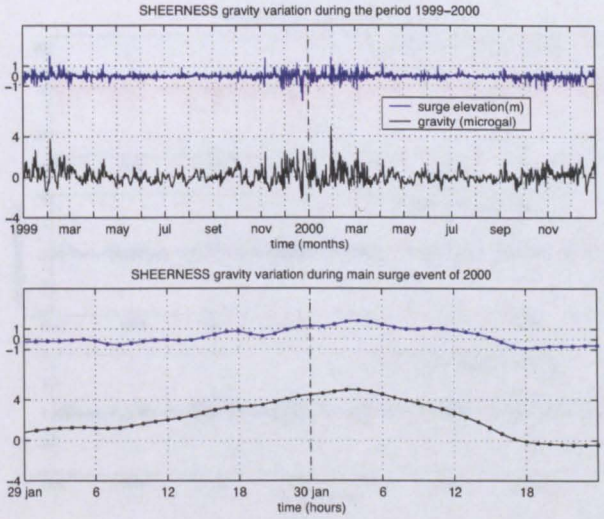

Figure 5.5: Elevations in meters (blue curve) and corresponding gravity variations (black curves) in μGal at Sheerness. The maximum peak in the gravity variation corresponds to the main surge event of January, 30th 2000. This event is shown in the lower part of the figure. [1 μGal = $10^{-8} m/s^2$.]

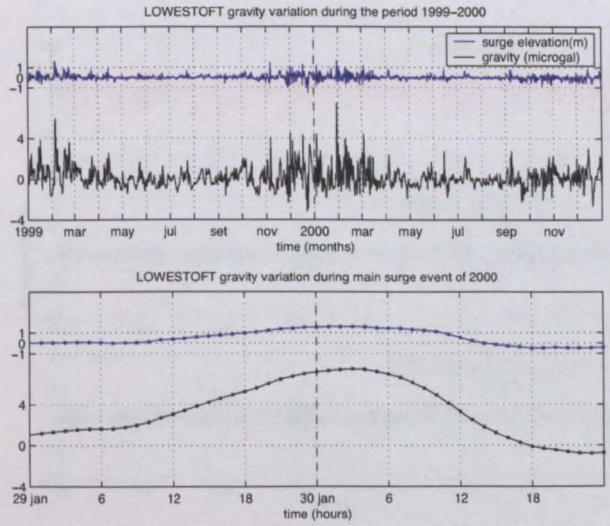

Figure 5.6: Elevations in meters (blue curve) and corresponding gravity variations (black curves) in μGal at Lowestoft. The maximum peak in the gravity variation corresponds to the main surge event of January, 30th 2000. This event is shown in the lower part of the figure.[1 μGal = $10^{-8} m/s^2$.]

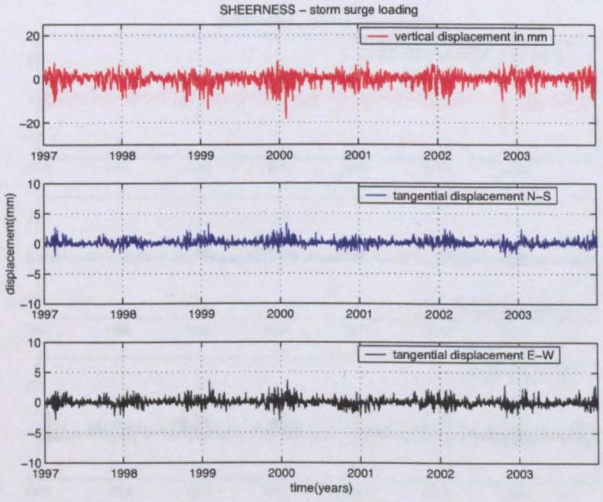

Figure 5.7: Radial deformation (in red) and associated tangential displacement as a North-South component (blue curve) and East-West component (in black) during the period of time investigated. The results refer to the station of Sheerness.

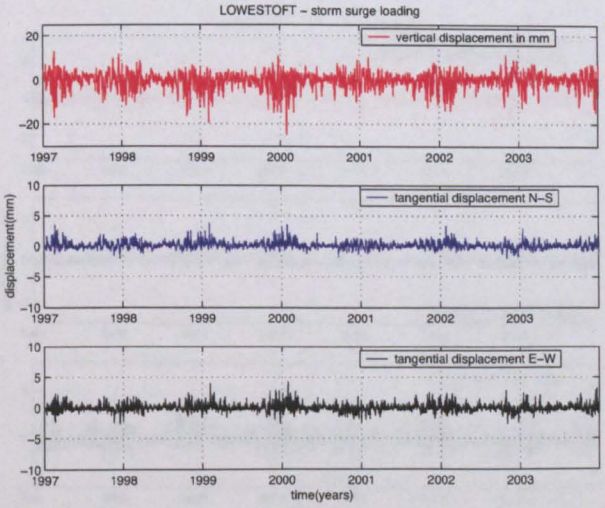

Figure 5.8: Radial deformation (in red) and associated tangential displacement as a North-South component (blue curve) and East-West component (in black) during the period of time investigated. The results refer to the station of Lowestoft.

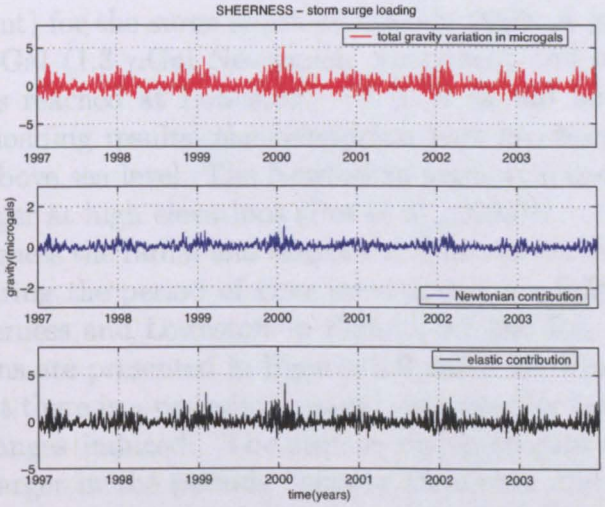

Figure 5.9: Total gravity variation (in red) at Sheerness during the period of time investigated. In blue is presented the Newtonian component of the gravity change while the elastic component is shown in black.

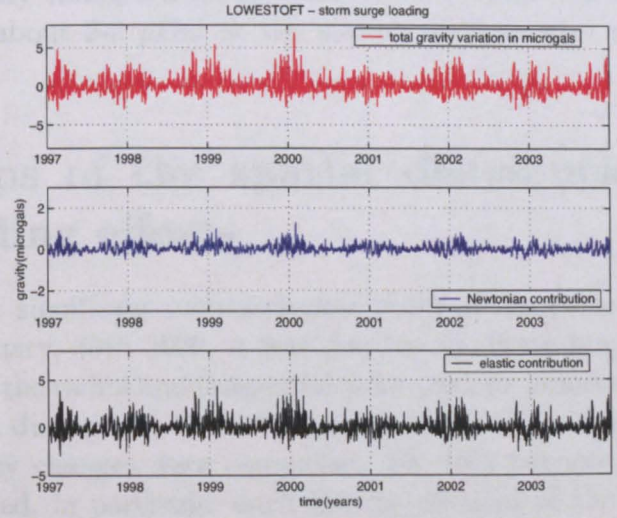

Figure 5.10: Total gravity variation (in red) at Lowestoft during the period of time investigated. In blue is presented the Newtonian component of the gravity change while the elastic component is shown in black.

equal to 5.0 μGal at Sheerness (1.0 μGal Newtonian component, 4.0 μGal elastic component) for the surge storm of January 2000. A gravity variation of almost 7.5 μGal (1.3 μGal Newtonian component and 6.2 μGal elastic component) was reached at Lowestoft. (N.B. It should be noted that for all the gravity loading results, the Newtonian part has been computed for zero elevation above sea level. The Newtonian attraction component can be significantly larger at high elevations (Bos et al., 2002)).

For completeness the radial and tangential deformation induced by storm surge events during the period of time investigated are fully shown for the stations of Sheerness and Lowestoft in Figures 5.7 and 5.8. The associated gravity variations are presented in Figures 5.9 and 5.10. From all four plots it is evident that there is a periodic seasonal character for both deformations and gravity changes induced. The surface displacements and the gravity variations are larger in the periods between December and February while summer and spring periods do not show significant large non-tidal residuals (both positive and negative). Vertical displacements are always bigger than the horizontal deformations induced while elastic gravity variations are generally larger than the Newtonian components of the gravity changes.

Radial displacements induced by surge storm loading of about 15 mm peak to peak are very common in Sheerness. In Lowestoft the deformation that could be reached is even greater on average (20 mm peak to peak). The total gravity changes associated with the deformation have an average magnitude of about 2-3 μGal at the station of Sheerness and 3-4 μGal at Lowestoft.

5.4 Maps of the spatial distribution of the loading effects

Since the most significant meteorological event of the period 1997-2003 occurred on January, 30th 2000, it was decided to create maps of the spatial distribution of the radial and tangential deformations induced by storm surge loading before, during and after the passing storm. Also the maps of the associated gravity changes were computed. For this purpose, the model was slightly modified, in particular each loading element of the grid (cell), corresponded to an observational point at which the deformation has to be computed at a certain chosen epoch. The contribution to the deformation or to the gravity change due to all the cells of the grid was summed up at each n^{th} station (corresponding with the center of the n^{th} loading element).

In the next Figures (5.11 - 5.22), are shown the plots representing the

spatial distribution of the loading deformation and gravity variations for four particular epochs of the main surge event (0 a.m. and 2 p.m. on January 29th and 3 a.m. and 4 p.m. on January 30th 2000). In this way it was possible to observe the development of the surge in terms of the magnitude of the deformations induced and to show those areas causing the loading due to the extra mass of water in the North sea. The maps were generated using the Generic Mapping Tool (GMT) (Wessel and Smith,1991; Wessel and Smith, 1995).

As it can be seen in Figure 5.13, the downward vertical displacement arrived at its maximum in Lowestoft and Sheerness at 3 a.m. January 30th, when the height of the surge had its maximum. The effect is evident on the north European coasts as well. A maximum was also found at the same time in the tangential deformation and in the induced gravity variation.

The body of water progressed from the northern part of the North sea and the first areas that experienced the deformation were in Scotland. Residuals in the sea level of about 40 cm produced a vertical movement of the land of about 12 mm downward and gravity variations of 2-3 μGal at the site of Lerwick. This happened 27 hours before the event reached its maximum in the south east of the British Isles (Figures 5.11 and 5.19). It should be noted, however, that a large part of the oceanic response in this area is like an inverted barometer. Therefore, when atmospheric pressure loading is added in order to obtain the total loading, the deformations will be much smaller. This will be discussed later in this Chapter.

Just 14 hours later, the eastern coasts of the UK were affected by the deformation with displacements in the radial direction between -12 and -15 mm and gravity changes of about 3-4 μGal on average. Observing the heights of the surge producing the deformation it can be seen that the main body of water has moved toward the north-west coasts of mainland Europe (Denmark and Holland in particular with maximum of 2.6 m), producing large effects in these regions (Figures 5.12 and 5.20).

At 3 a.m. the storm surge reached its maximum striking the areas surrounding the southern part of the North sea. The non-meteorological residuals had values greater than 3 m, producing deformation of -27 to -30 mm in the radial and gravity changes up to 8 μGal. In UK the effects were mainly felt in the south-east of England with vertical displacements of -21 to -24 mm and variations of 6-7 μGal (Figures 5.13 and 5.21).

After 13 hours the situation came back to "normality" indicating that the storm event had a life span of less that 40 hours (Figures 5.14 and 5.22).

Observing Figures 5.15 to 5.18, it can be noticed that the tangential deformation induced by the storm surge event displaced the land toward the center of the North sea and had its greatest effect along the north-west

European coasts with movements up to 10 mm at sites situated along the Danish and German coasts.

It can be concluded that during the period of time investigated (1997-2003), the greatest effect of the deformation was felt on the Dutch-German-Danish coastlines at 3 a.m. of January 30th 2000, with about -30 mm of displacement in the radial direction and 10 mm in the tangential (toward the north-west direction). The gravity changes were of about 8μGal. The effect decreased gradually inland with values of almost -10 mm in the vertical deformation, 1-2 mm in the horizontal and gravity variations of 2-3 μGal at distances of 150 km from the coast. The regions most sensitive to flooding events due to storm surges in the North sea are those situated in the south east of England and along the Dutch-German-Danish coastlines and these are the areas where the deformation effects were at their maximum.

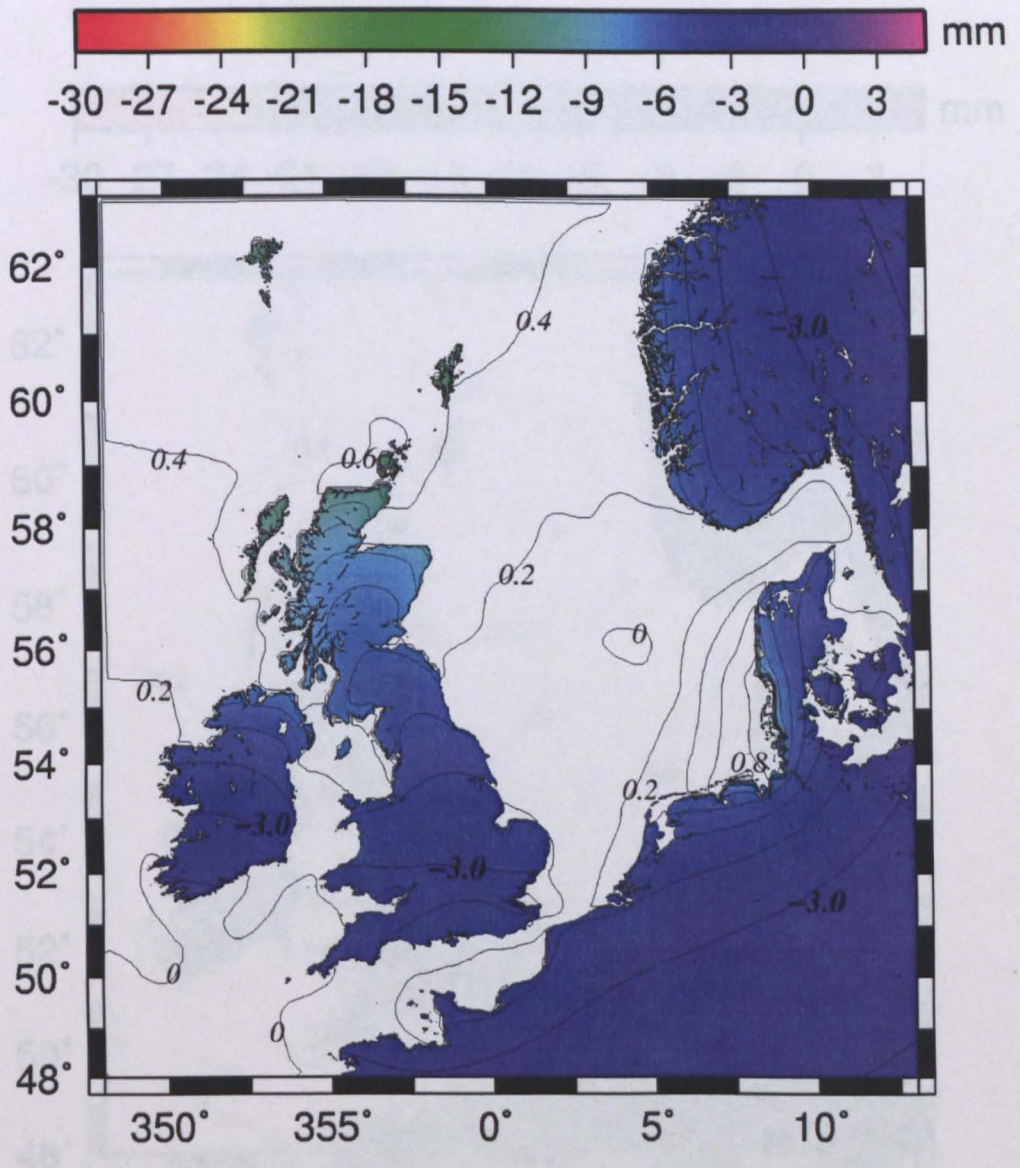

Figure 5.11: Vertical displacement and storm surge elevation at 0 a.m. on January 29th 2000.The curves on the land represent the vertical displacement in millimeters at 0 a.m. on January 29th 2000, they are drawn every millimeter. The curves on the sea show the surge elevation in meters at the same time. They are marked every 20 cm.

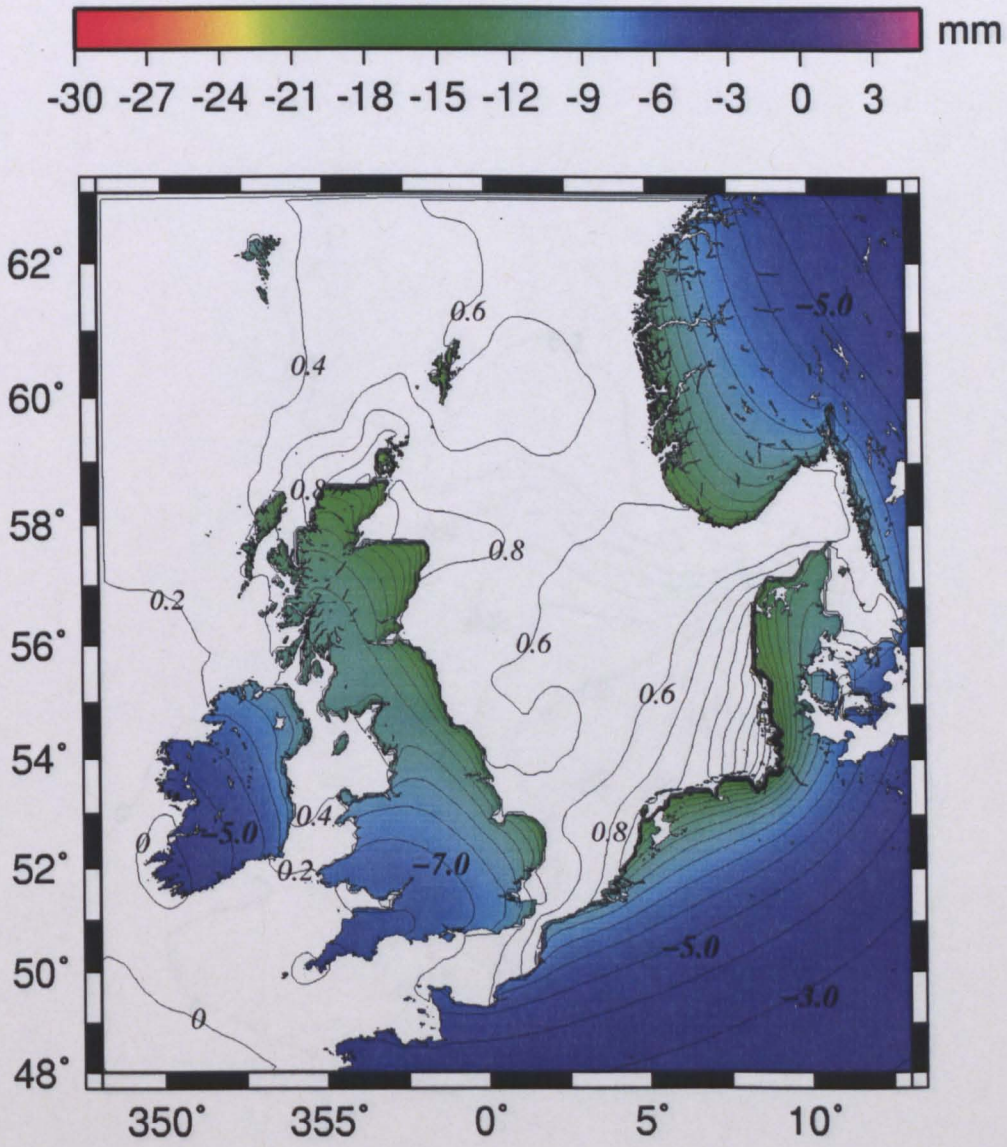

Figure 5.12: Same as Figure 5.11 but at 2 p.m. on January 29th 2000.

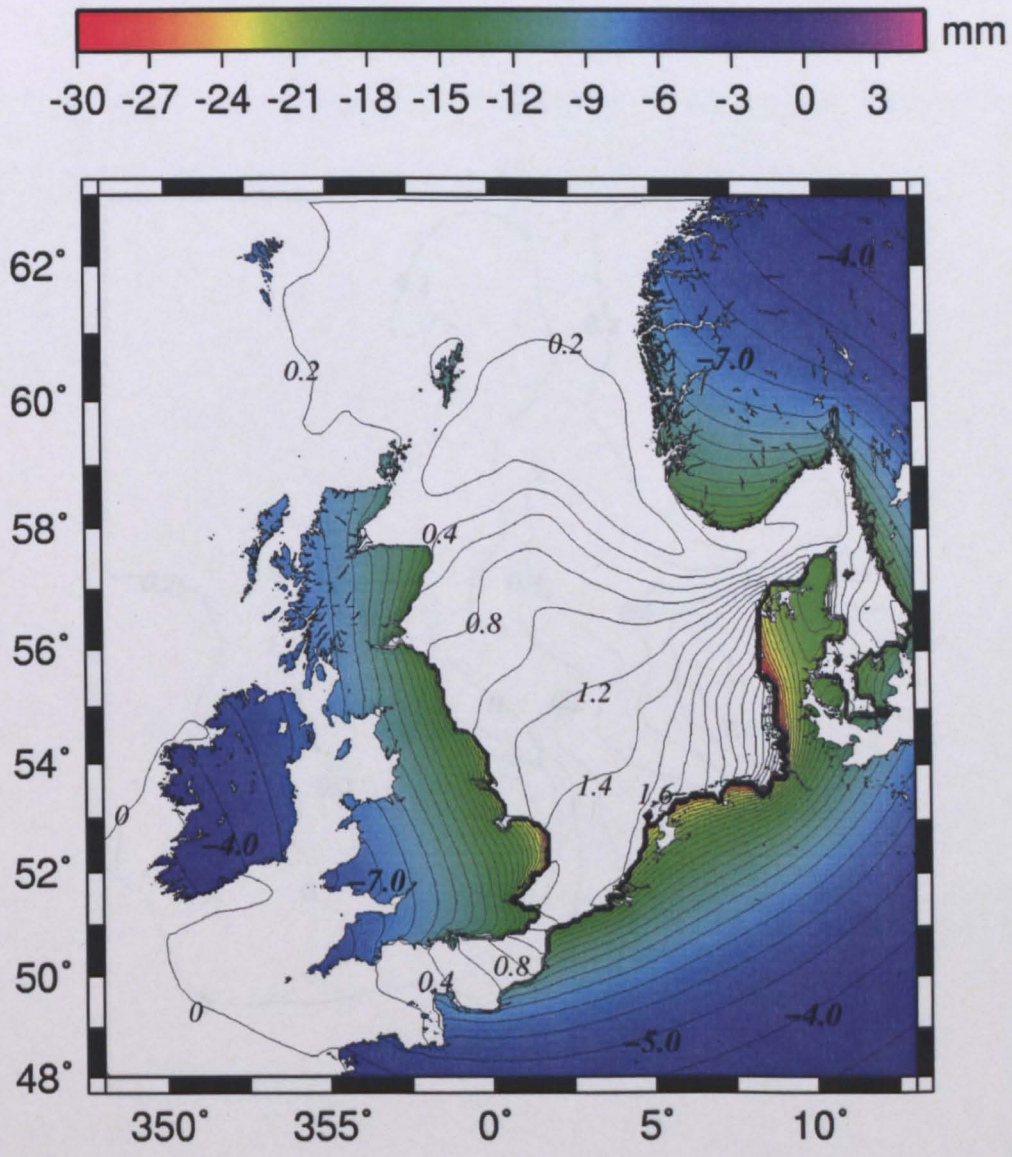

Figure 5.13: Same as Figure 5.11 but at 3 a.m. on January 30th 2000.

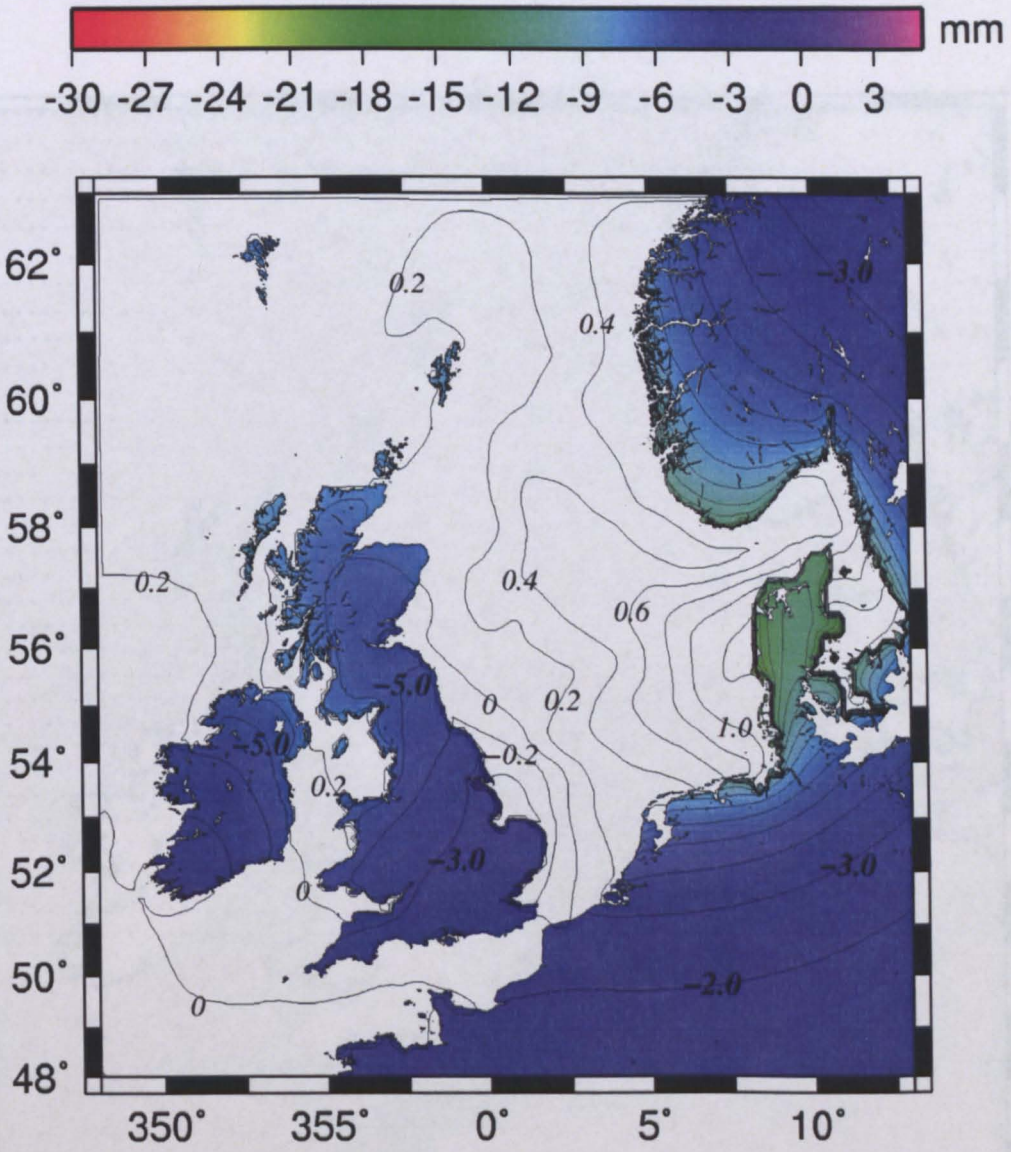

Figure 5.14: Same as Figure 5.11 but at 4 p.m. on January 30th 2000.

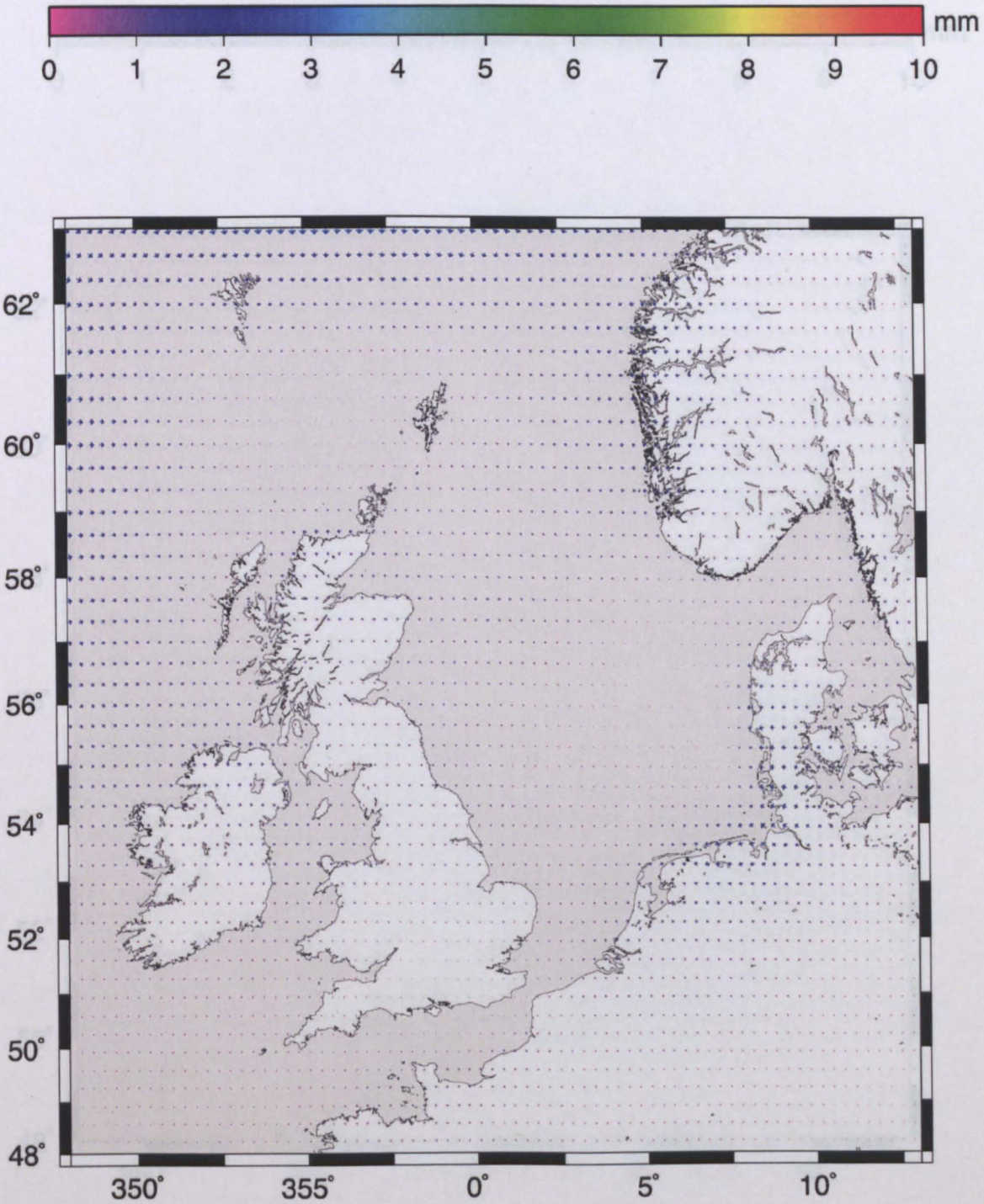

Figure 5.15: Tangential displacement at 0 a.m. on January 29th 2000. The arrow's length and color were scaled with the deformation.

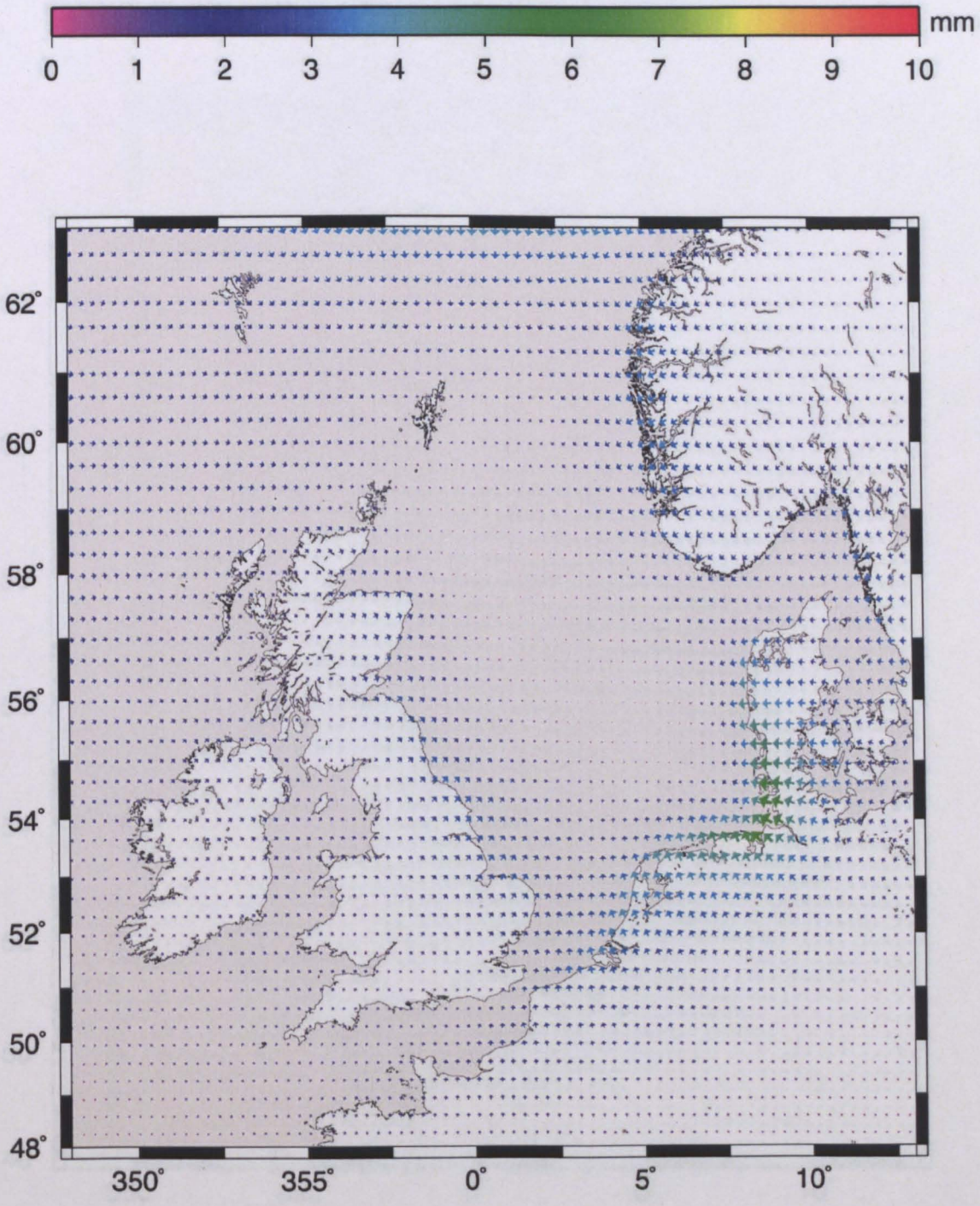

Figure 5.16: Same as Figure 5.15 but at 2 p.m on January 29th 2000.

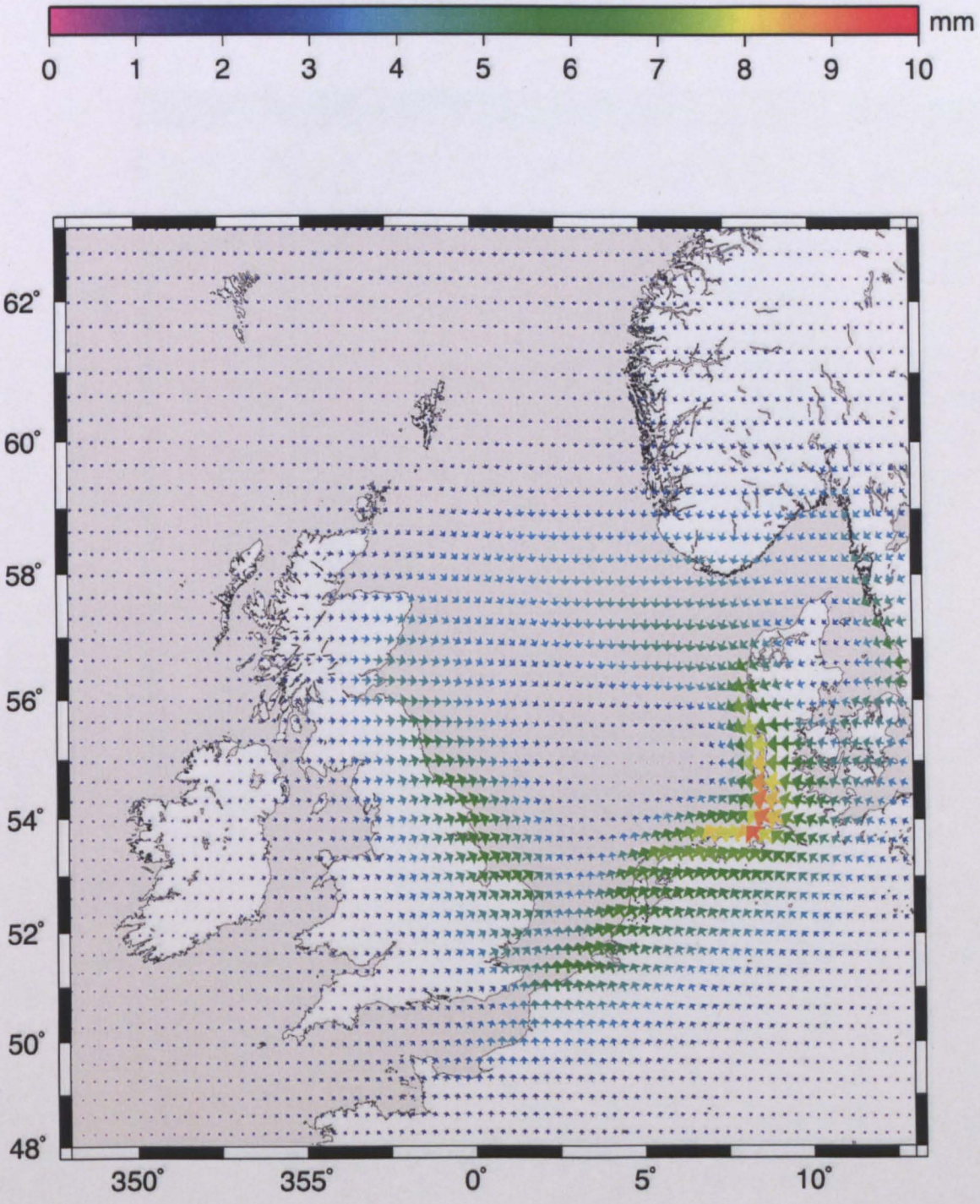

Figure 5.17: Same as Figure 5.15 but at 3 a.m on January 30th 2000.

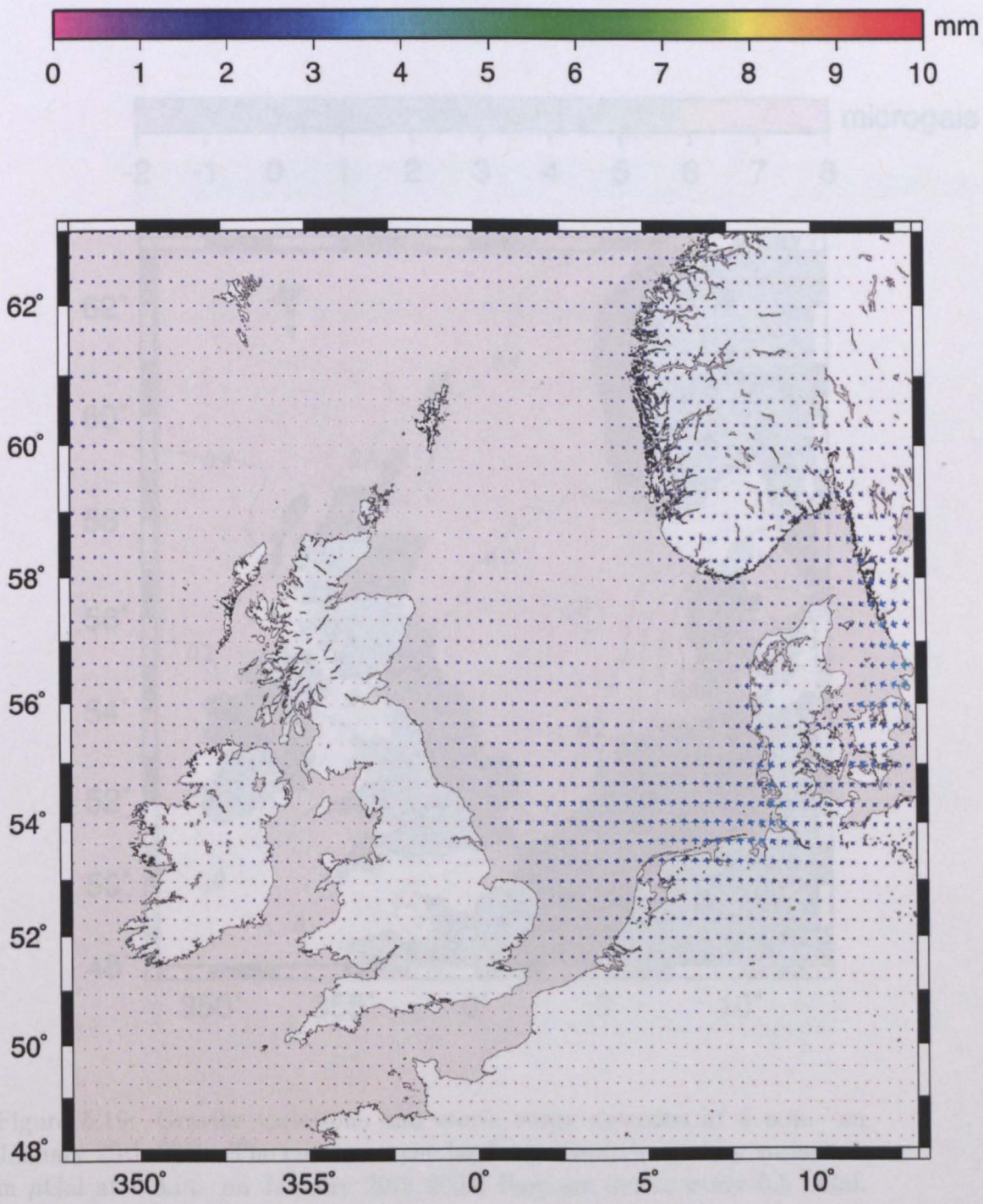

Figure 5.18: Same as Figure 5.15 but at 4 p.m on January 30th 2000.

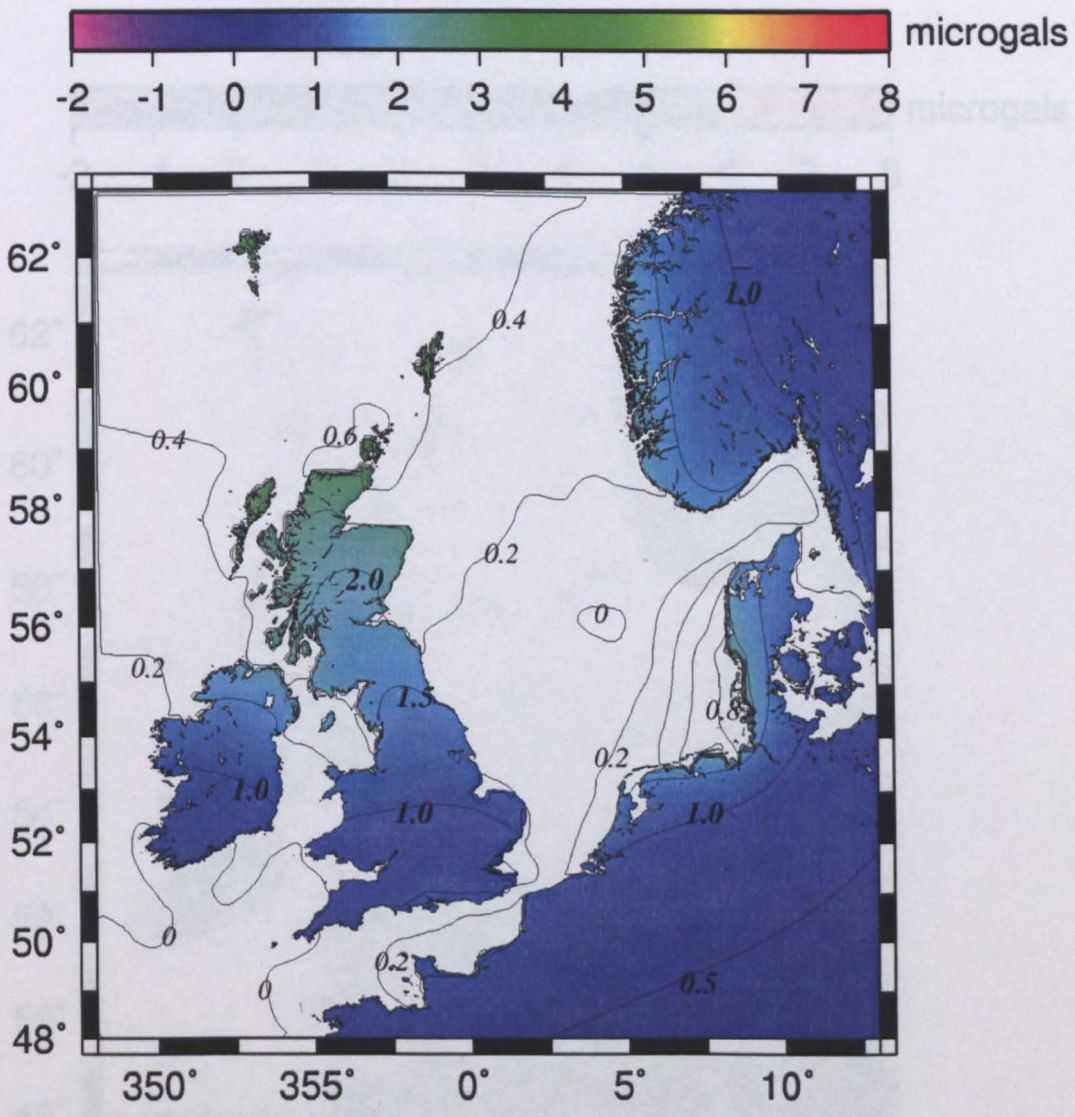

Figure 5.19: Gravity variations and storm surge elevation at 0 a.m. on January 29th 2000. The curves on the land represent the gravity variations in μGal at 0 a.m. on January 29th 2000, they are drawn every 0.5 μGal. The curves on the sea show the surge elevation in meters at the same time. They are marked every 20 cm.

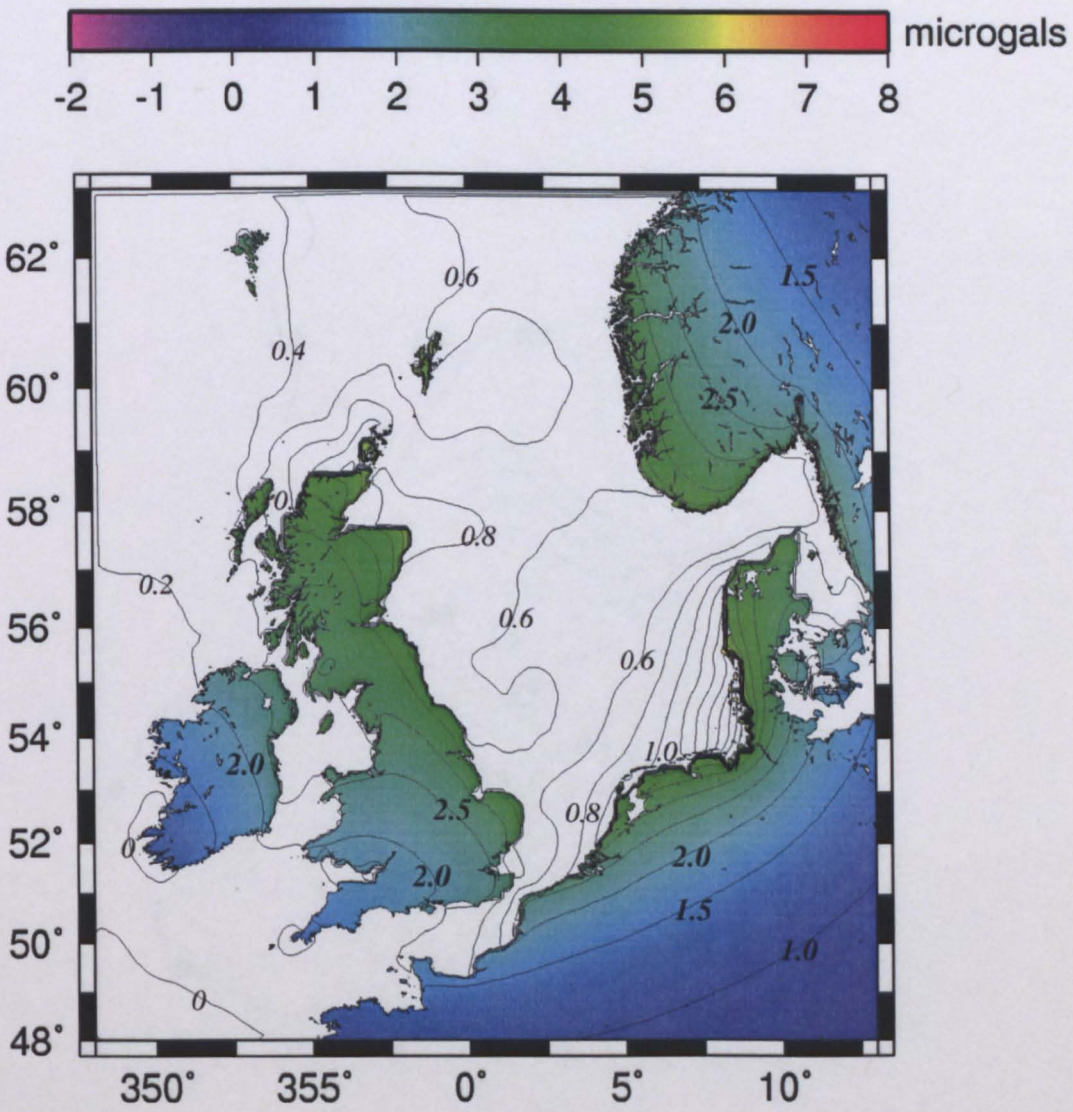

Figure 5.20: Same as Figure 5.19 but at 2 p.m on January 29th 2000.

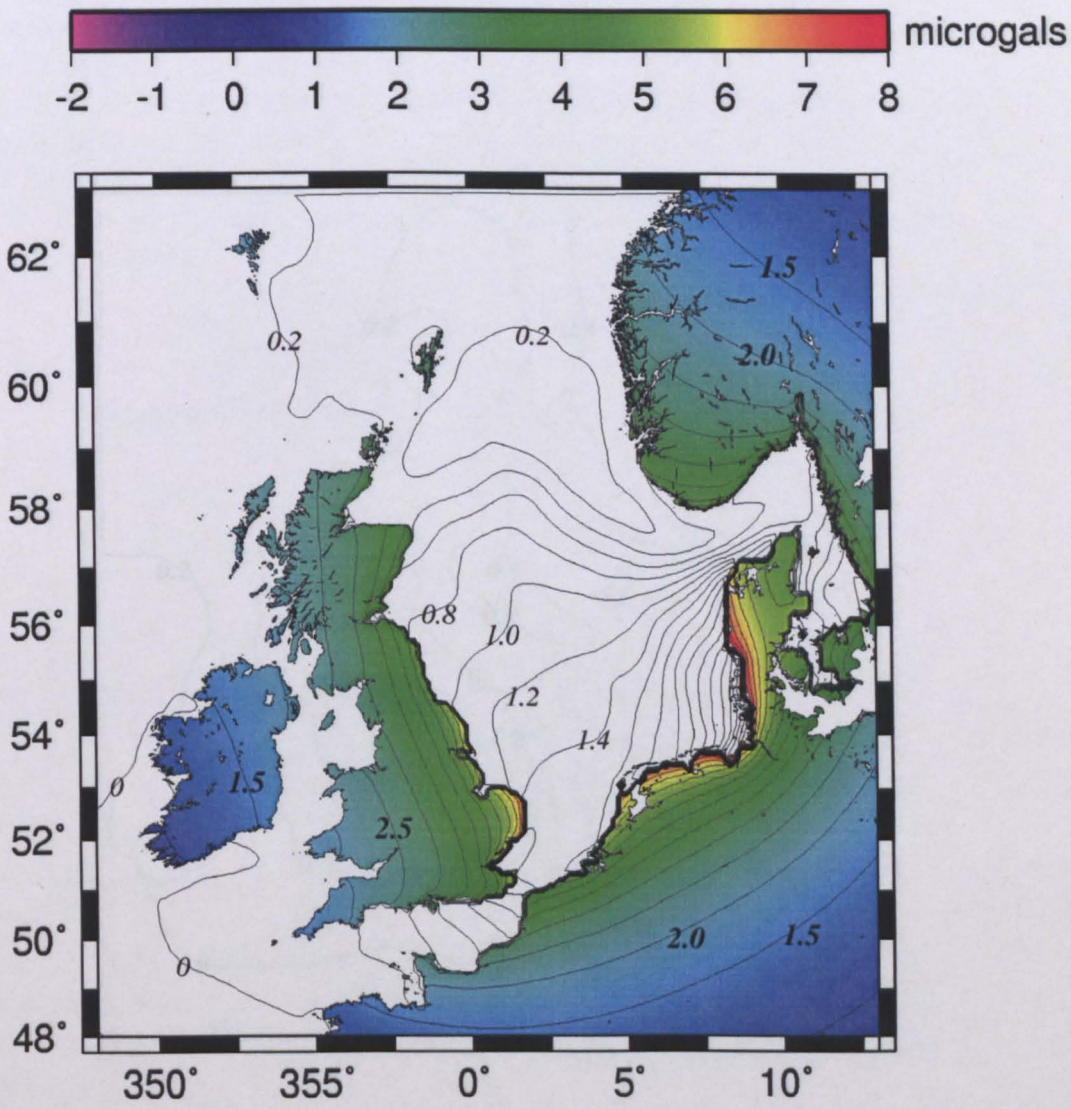

Figure 5.21: Same as Figure 5.19 but at 3 a.m on January 30th 2000.

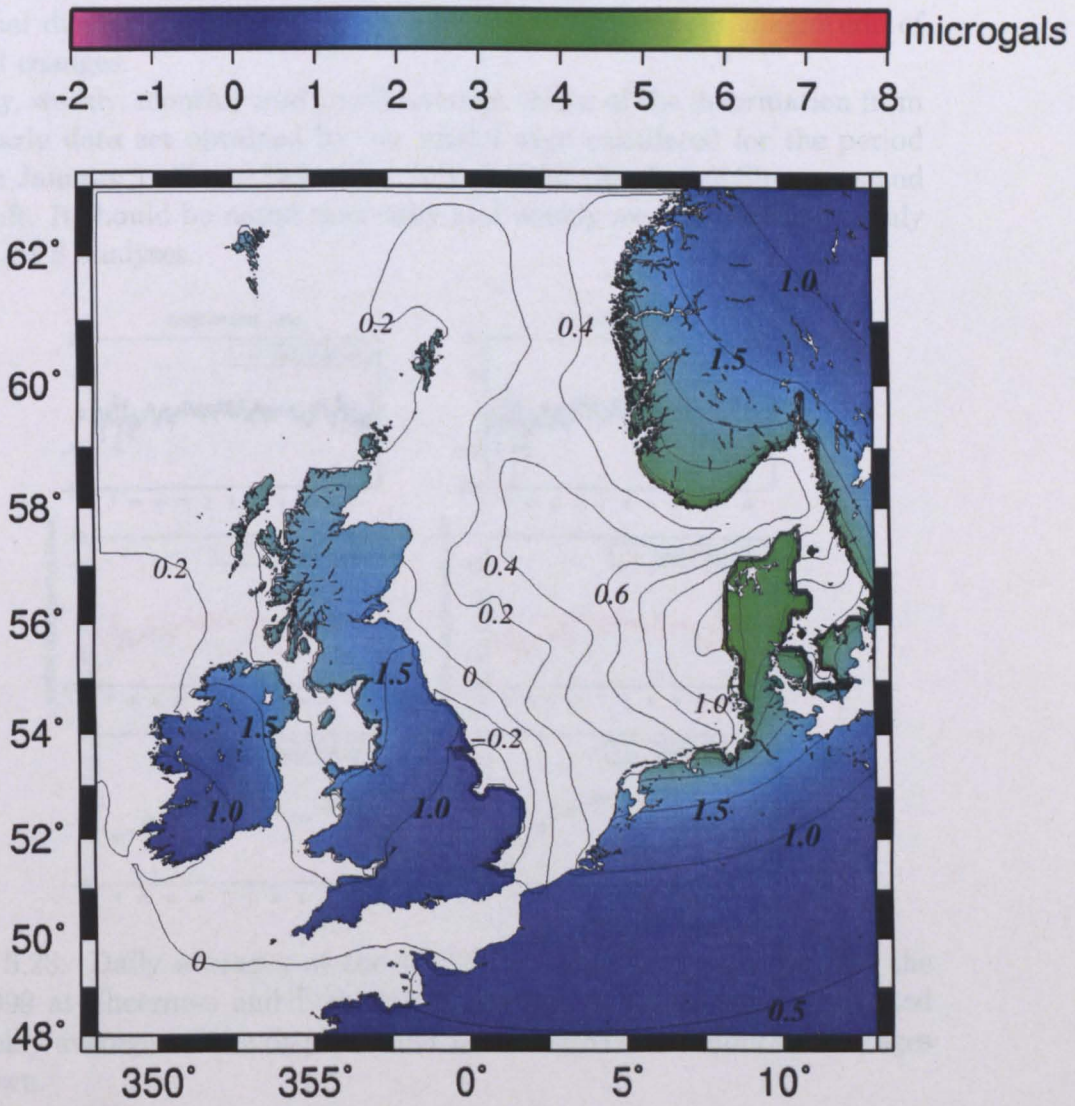

Figure 5.22: Same as Figure 5.19 but at 4 p.m on January 30th 2000.

5.4.1 Seasonal and longer period deformation

Finally the seasonal and longer period vertical deformations due to storm surge loading were computed together with the seasonal and longer period gravity variations. The seasonal variations in the tangential direction were not considered because of their small values (they are about one third of the radial displacements) and as a consequence the reduced magnitude of seasonal changes.

Daily, weekly, monthly and yearly average values of the deformation from each yearly data set obtained by our model were calculated for the period between January 1997 and December 2003 and for the sites of Sheerness and Lowestoft. It should be noted that daily and weekly averages are commonly used in GPS analyses.

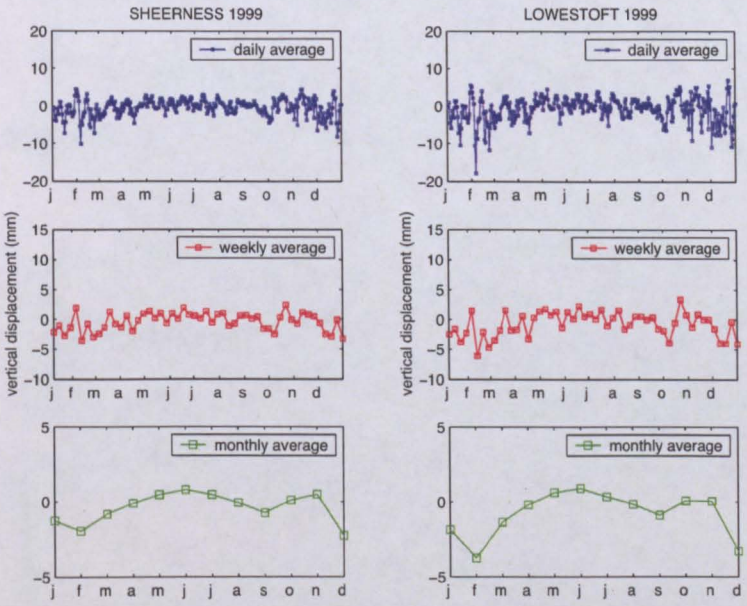

Figure 5.23: Daily averages of the vertical displacement (in blue) for the year 1999 at Sheerness and Lowestoft respectively. In red are represented the weekly averages of the displacement while in green the monthly averages are shown.

From Figures 5.23 -5.26 it can be seen that the curves representing the averaged vertical displacement and the associated gravity variation become smoother when the mean is calculated for a longer period of time, i.e. passing from daily to monthly averaged values. This means that if the long period deformation is considered for extended periods of time i.e. more than ten

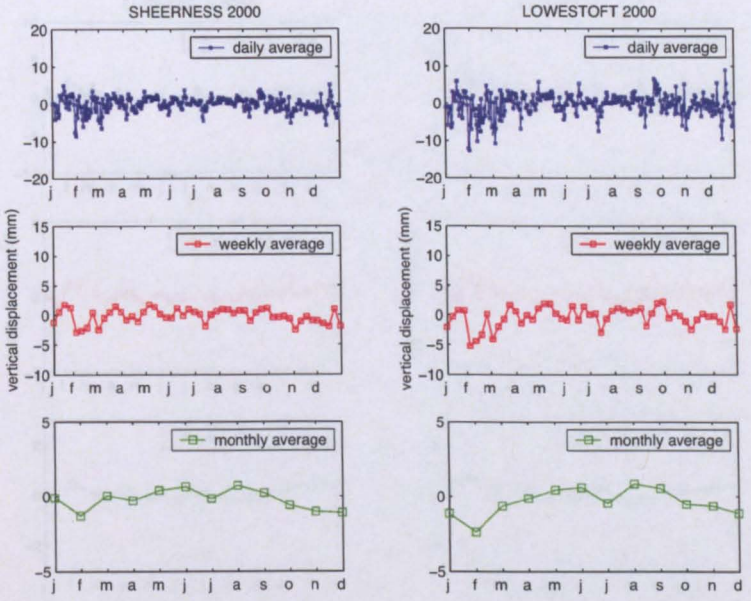

Figure 5.24: Same as Figure 5.23 but for the year 2000.

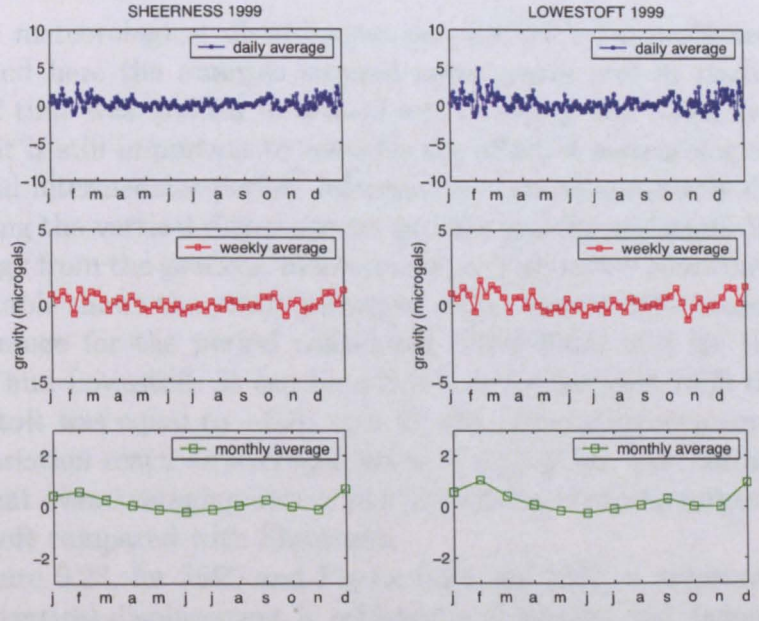

Figure 5.25: Daily averages of the total gravity variation (in blue) for the year 1999 at Sheerness and Lowestoft respectively. In red are represented the weekly averages of the gravity chance while in green the monthly averages are shown.

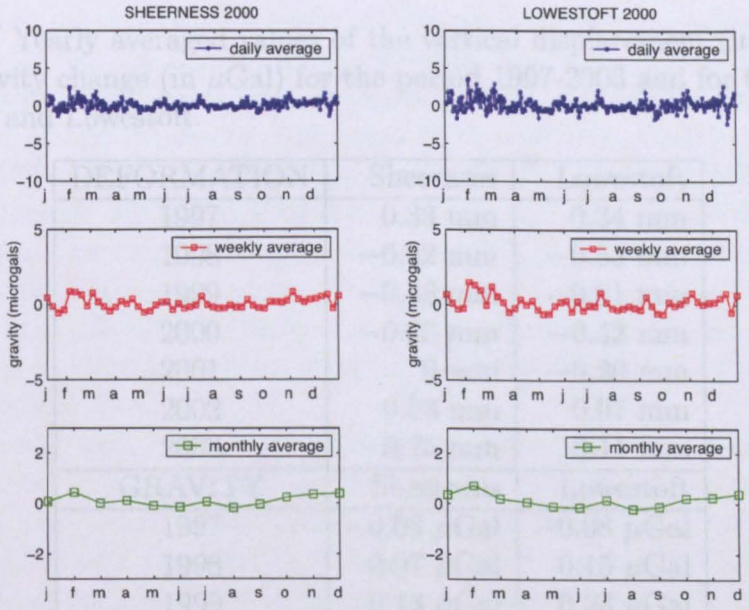

Figure 5.26: Same as Figure 5.25 but for the year 2000.

years, the meteorological disturbances can probably be neglected. In the case studied here the analysis covered seven years and in particular this interval of time was divided in several sets of yearly and monthly data. At this level it is still important to consider the effect of meteorological factors, so long and intermediate period deformations can be accurately determined by removing the vertical displacement and the gravity variations induced by meteorology from the geodetic measurements. This fact is confirmed in Table 5.1. The table shows the yearly averages of the vertical deformation and the gravity change for the period considered (1997-2003) and for the sites of Sheerness and Lowestoft. It can be noted that for the year 1999 the average for Lowestoft was equal to -0.81 mm for the radial displacement while the gravity variation reach an averaged value of 0.23 μGal. Furthermore, it can be seen that even averaging over a year the effects of storm surges are larger at Lowestoft compared with Sheerness.

In Figure 5.23, for 1999 and Figure 5.24, for 2000, a minimum in daily averaged vertical displacement is achieved in February and January respectively and it obviously coincides with the large east coast surge events just considered. In particular a monthly average of -3.77 mm in Lowestoft and -1.96 mm in Sheerness were found during February 1999. The average was smaller in magnitude for February 2000 with values of -2.40 mm at Lowestoft and -1.32 mm at Sheerness. This is apparently in contradiction with the

Table 5.1: Yearly averaged values of the vertical displacement (in mm) and of the gravity change (in μGal) for the period 1997-2003 and for the sites of Sheerness and Lowestoft.

DEFORMATION	Sheerness	Lowestoft
1997	0.33 mm	0.34 mm
1998	−0.22 mm	−0.53 mm
1999	−0.43 mm	−0.81 mm
2000	−0.23 mm	−0.42 mm
2001	0 mm	−0.20 mm
2002	0.03 mm	0.07 mm
2003	0.25 mm	0.11 mm
GRAVITY	Sheerness	Lowestoft
1997	−0.08 μGal	−0.08 μGal
1998	0.07 μGal	0.15 μGal
1999	0.13 μGal	0.23 μGal
2000	0.08 μGal	0.13 μGal
2001	0 μGal	0.05 μGal
2002	0 μGal	0 μGal
2003	−0.06 μGal	−0.03 μGal

fact that the main event and consequently the main deformations produced were achieved during the second storm surge. What has to be said is that generally a low monthly mean can also be achieved when several surge events happen in the same averaged period. A similar consideration is valid for the plots that refer to the gravity changes. In particular values of 1.03 μGal and 0.7 μGal were averaged at Lowestoft in February 1999 and February 2000 respectively. At Sheerness the monthly mean reached 0.56 μGal in 1999 and 0.41 μGal in 2000.

For completeness the plots representing the seasonal and longer period deformation and gravity variation for the other years considered are presented in Appendix D.

5.5 The North Atlantic Oscillation (NAO)

The North Atlantic Oscillation (NAO), is generating a great interest in meteorology at the moment because of its climatic importance. In fact the weather of the Atlantic region and the surrounding areas exhibit a wide range

of variability on various time scales and in order to better understand, and eventually predict the future climate changes, it is important to improve the techniques for comprehending the causes of these fluctuations and as well the impact of anthropogenic factors on the variability (Paeth et al., 1999; Ulbrich & Christoph, 1999). Woolf et al. (2003), have concluded that in the next decades the behavior of the NAO will be a very important regional factor to consider for determining the sea level rise and the coastal vulnerability of some European regions. Furthermore there is evidence of a recent change in the link between NAO and Arctic sea ice export even if it is not understand whether the phenomena are significantly related in a long term context (Hilmer & Jung, 2000).

During the past 15 years the winter temperatures over western Europe have been milder than normal because of a meridional oscillation in the atmospheric mass center near Iceland and over the subtropical Atlantic. This substantial climate variability is associated with the NAO, that is a large scale mode of natural weather change with a great impact on the weather and climate in the North Atlantic region and surrounding continents. NAO influences atmospheric variables such as rainfall, temperature, wind, ice accumulation rates and also other meteorological parameters (Hurrell, 1995, Appenzeller et al., 1998).

The NAO can be characterized by indices that represent its phase. Commonly the NAO index is based on the difference in surface pressure between the subtropical areas and subpolar regions. Usually the difference in pressure is computed between one station in Iceland and another site either at the Azores, or the station of Lisbon or Gibraltar (Jones et al., 1997).

Since 1965 the trend of the NAO has been from negative to positive values and this is unusual in the observational records (Hurrell, 1995). In particular the positive winter index (e.g. winter of 1989), has some very important impacts on the winter climate of Europe and the United States east coast. Lu and Greatbock (2002), pointed out that the strong upward trend of the NAO index may be related with the eastward shift in the NAO centers of action but it is not clear at this stage whether this behavior is simply part of the natural internal variability of the climate system or it is rather related with anthropogenic factors.

When the NAO is in a positive phase (high index), there are lower than normal low pressure systems over the Iceland region and part of the Arctic and simultaneously higher than normal high pressure systems over the region extending from the Azores across the Iberian peninsula. The increased difference in pressure generates stronger winter storms over the northern Atlantic ocean. Very intense west winds are produced and consequently warmer weather over northern Europe coupled with wetter conditions from Iceland

through Scandinavia and drier weather over southern Europe. During the negative phase, the reduced gradient of pressure results in weaker mean westerlies over the North Atlantic Ocean, colder winter conditions over Europe with weaker winter storms and moister air in the Mediterranean area.

Also the US east coasts are affected by mild conditions associated with a positive winter NAO index. The weather is not as wet as it is during a negative phase of the oscillation and as consequence it snows less. Canada and Greenland are subjected to colder and drier winters than normal. During winters characterized by a negative NAO index, the US east coast experiences cold and wet weather conditions that lead to snowy winters. Milder winter temperatures affect Greenland and Canada.

Recently the influence of NAO on sea level variability has been demonstrated (Wakelin et al., 2003). It was shown that the sensitivity of the sea level to the NAO is very strong in the southern North sea (up to 96 mm per unit NAO index) and in the Baltic region of Europe. The variability is mostly present in the non-hydrostatic component of the sea level i.e. after correcting for the inverted barometer effect on sea level, even if both hydrostatic and non-hydrostatic contributions to the sea level respond to the NAO. For the non-hydrostatic component in particular, the effects of pressure and wind appear to be largely decoupled and it was concluded that it mostly depends upon the strength and the direction of the wind field. Yan et al. (2004), have recently pointed out that for the regions of the northern Europe the relationship between higher sea level and positive NAO conditions associated with the cold season is very strong. A negative relation instead characterizes the southwest of England. These relationships are variable in time and this fact is probably related with movements that affect the pressure centers underlying the NAO. They linked the NAO and the sea level also in the frequency domain, concluding that the long term trend in the sea level does not appear to be related with NAO. Analysis of NAO and sea level variability have instead shown that the relation is stronger at annual and interannual time scale. In particular the sea level does not simply respond to NAO related pressure forcing but also to the variations in the thermal conditions and fluxes associated with it.

Lutherbacher et al. (1999), have provided the most reliable reconstruction of the NAO indices back to the 1675, these values can be used for long-term testing of proxy-based indices on the monthly to decadal timescales (Schmutz et al., 2000). Rodwell et al. (1999), have shown that much of the multiannual and multidecadal variability of the winter NAO over the last fifty years can be correctly reconstructed from the data of the sea surface temperature of the North Atlantic. They pointed out that variations in the sea surface temperatures can influence the change in atmospheric temperature,

precipitation and storminess over Europe as well. Therefore, the ability to forecast climate variations over the north Atlantic Europe and North America is strongly related with the capacity of predicting sea surface temperature patterns associated with the NAO variability (Mehta et al., 2000).

Even if the scientific research about NAO has made some steps forward in the past decades, the mechanism that drives this phenomenon is still unclear and in particular why the NAO has become more positive during the past 30 years.

5.5.1 Deformations and gravity changes during two winter seasons characterized by opposite NAO indices

Usually the NAO index is constructed by performing an average over the winter period of the surface pressure data available. A useful winter season is considered to be the period between December and March.

Table 5.2: Recent values of the NAO index averaged over the winter period i.e. between December and March. Just the value for the winter 2003-2004 refers to the average over the months December-February (Stephenson, 1999).

WINTER	NAO index
1994-1995	+2.44
1995-1996	−2.32
1996-1997	+0.18
1997-1998	+0.80
1998-1999	+0.98
1999-2000	+1.85
2000-2001	−0.50
2001-2002	+0.79
2002-2003	+0.40
2003-2004	−0.63

In Table 5.2 are presented some of the recent indices. Most of them are positive as a consequence of the positive phase in the NAO over the past decades. Negative values were only found over the winter 1995-1996, 2000-2001 and 2003-2004. What is important to notice is that between the winter 1994-1995 and the following one (1995-1996), the index has suffered a dramatic variation passing from a positive +2.44 in 1994-1995 to a negative

−2.32 the subsequent year. This is also evident from Figure 5.27. The sea surface height variability for the north Atlantic ocean can be represented with a dipole structure between the subtropical and the subpolar North Atlantic. Esselborn and Eden (2001), pointed out that the variation in signal of the NAO index between winter 1994-1995 and the following coincided with a change in the sea surface height dipole pattern, caused by variations in the ocean heat transport and in the wind stress curl.

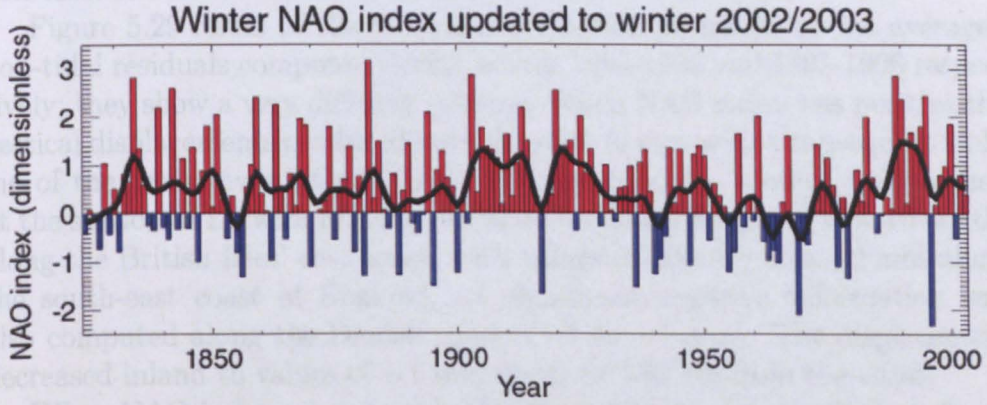

Figure 5.27: NAO index variations through the winter between the period 1825-2003.The solid line represents the index smoothed over a period of five years (Stephenson, 1999).

This large variation in NAO index passing from one winter to the other was associated with very different climatic scenarios. In particular, the marked dramatic switch in the NAO index between winter seasons 1994-1995 and 1995-1996 is the greatest change recorded since winter 1823 (Jones et al., 1997).

It was decided to investigate the impacts of such contrasting weather conditions on the deformation and gravity variations produced in the British Isles and in the north-western parts of Europe since there is a proven influence of the NAO on non-tidal residuals of the sea level (Wakelin et al., 2003) and on the increase of storm track activity over the east Atlantic and the western Europe (Ulbrich & Christoph, 1999). With this target in mind, sea level data for the winter 1994-1995 and 1995-1996 were averaged over each cell of the POLSSM grid and two different data files were computed. The surge elevation for each cell of the grid corresponded to the averaged residual for that element computed over the entire winter season investigated. The same method was applied to the atmospheric pressure data.

Maps of the spatial distribution of the vertical and tangential deformation

and the associated gravity variations were produced. The differences between the deformation modelled during the two winter seasons were investigated.

Figure 5.28 represents the averaged surge residuals causing the deformations and gravity variations during the two winter periods considered. Positive residuals were registered for winter 1994-1995 with maximum values of 20 cm in the northern part of the North Sea (in the Shetland and Scotland areas) and values up to 40 cm along the Danish coastlines. Negative non-tidal sea level residuals were found in winter 1995-1996.

Figure 5.29 refers to the vertical deformation produced by the averaged non-tidal residuals computed during winter 1994-1995 and 1995-1996 respectively; they show a very different picture. When NAO index was positive the vertical displacements produced were negative in sign with a consequent sinking of the areas investigated. The maximum (about -6 mm), was reached at the station of Lerwick and the radial deformation decreased toward south, along the British Isles' east coast, with values of about -3 to -2 mm along the south-east coast of England. A significant negative deformation was also computed along the Danish coasts (-5 to -4 mm). The displacement decreased inland to values of -1 mm at about 150 km from the coast.

When NAO index was negative (Figure 5.29), the deformation produced by non-tidal loading was generally positive with a consequent rise of the areas investigated. The maximum (about 4 mm) affected the Danish-German-Dutch coastlines while along the east coasts of British Isles positive displacements of about 1-2 mm were modelled. The deformation was smaller toward the center of the European continent with values close to 0 mm i.e. on average those areas did not experience any radial deformation associated with non-tidal loading during the winter period considered.

In winter 1994-1995, the downward deformation along the north German and Danish coasts is clearly due to the increased sea levels in the German Bight due to the increase in westerly winds during the positive phase of NAO. However, the downward displacements in the Shetland Islands and northern Scotland are due to the increase in the sea levels due to the inverted barometer response of the deep ocean to the lower atmospheric pressure in the north (Figure 5.28). The total deformation in this area (non-tidal plus atmospheric pressure loading) will be much smaller. Therefore as a further step, the vertical deformation produced, was calculated summing the effects due to atmospheric pressure loading and non-tidal residuals loading (pressure variations and non-tidal residuals changes were averaged over the two winter periods). From Figure 5.30, it is clear that during winter 1994-1995, the greatest negative radial displacement (about -2.5 mm), was modelled along the Danish-German-Dutch coastlines while the Scotland and Shetland Islands regions experienced a considerable reduction in the deformation com-

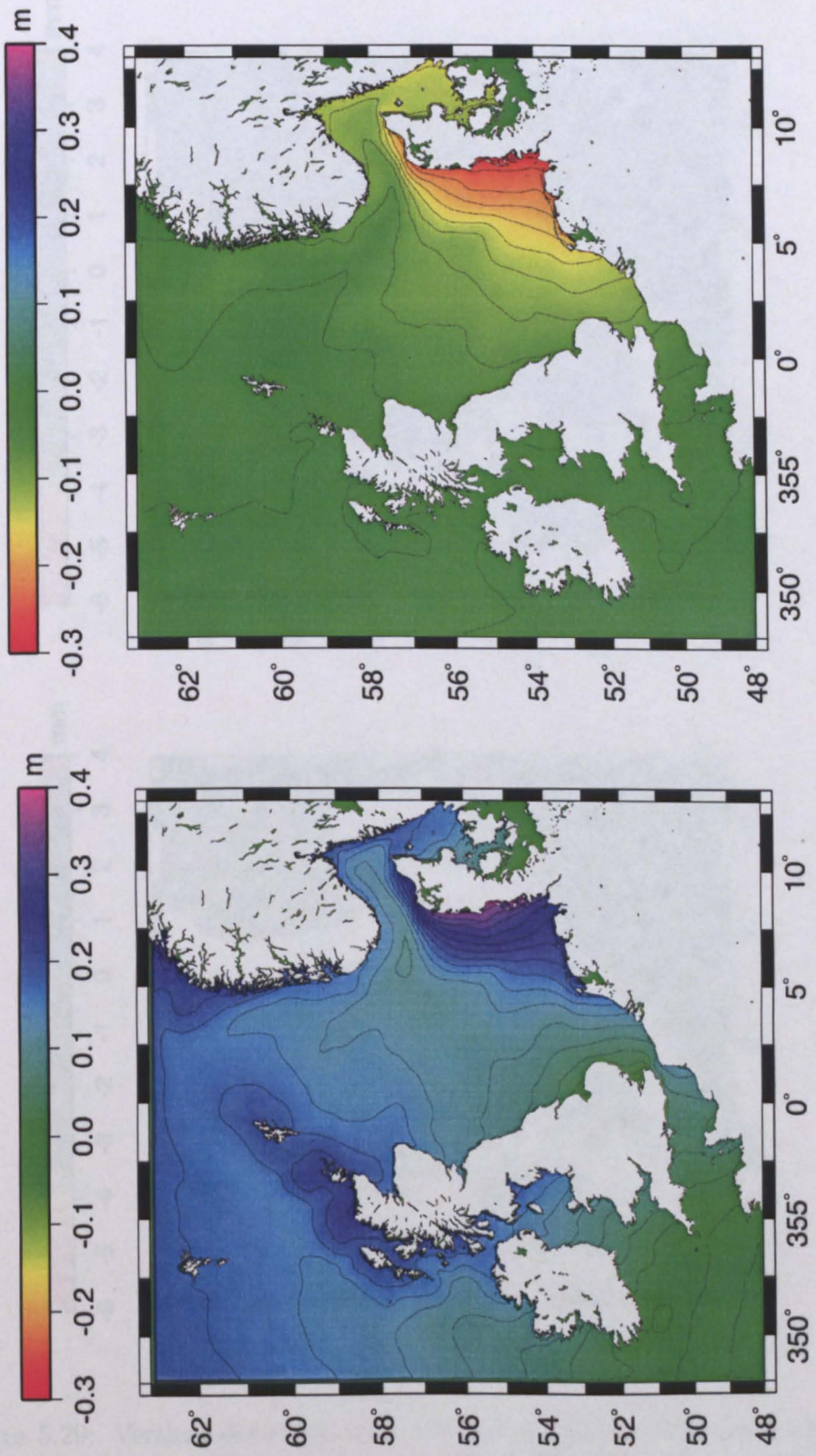

Figure 5.28: Non-tidal residuals in meters averaged over the winter 1994-1995 on the left and 1995-1996 on the right (period between December and March).

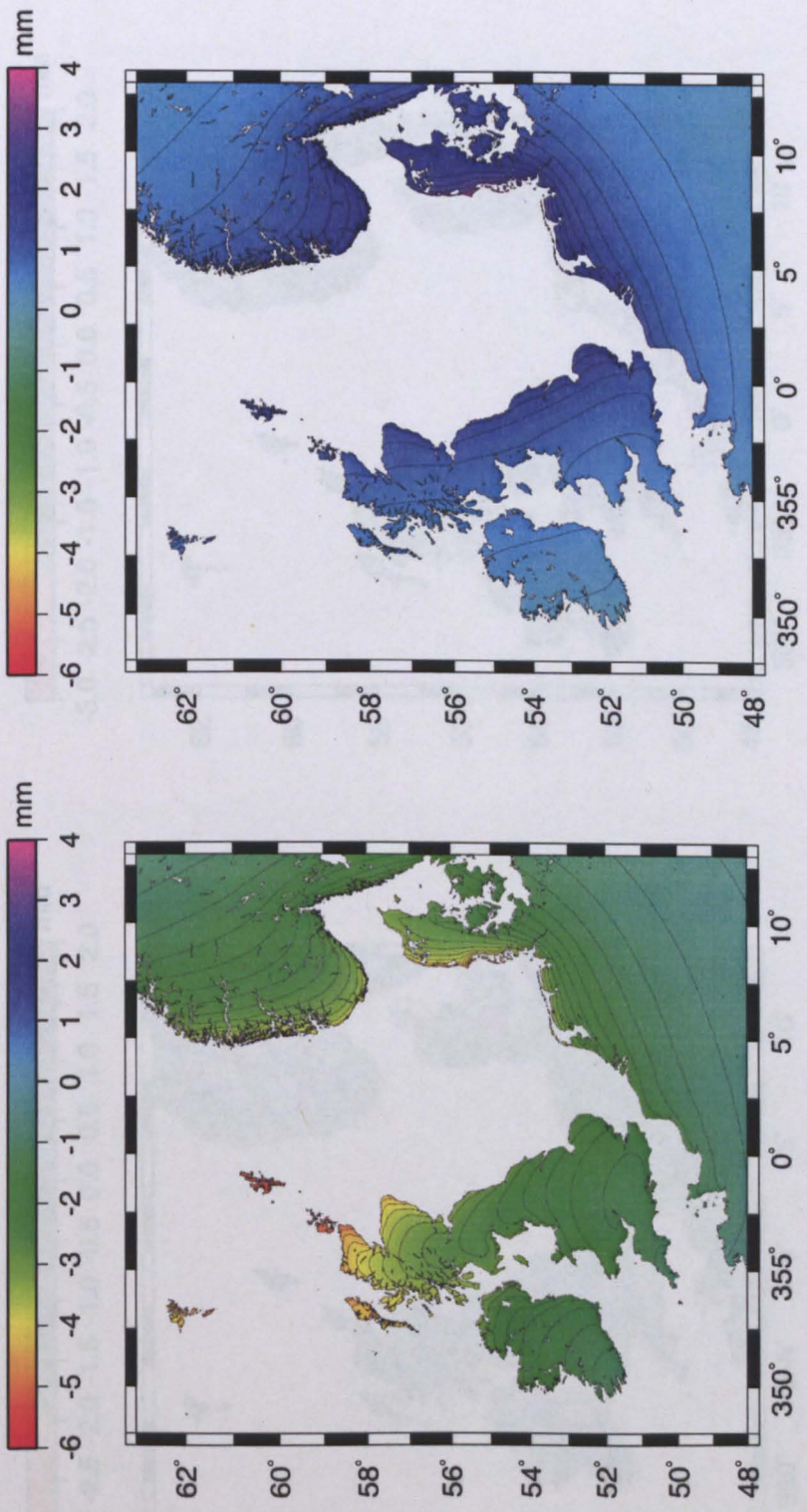

Figure 5.29: Vertical deformation in millimeters induced by sea level non-tidal residuals averaged over the winter 1994-1995 on the left and 1995-1996 on the right (period between December and March).

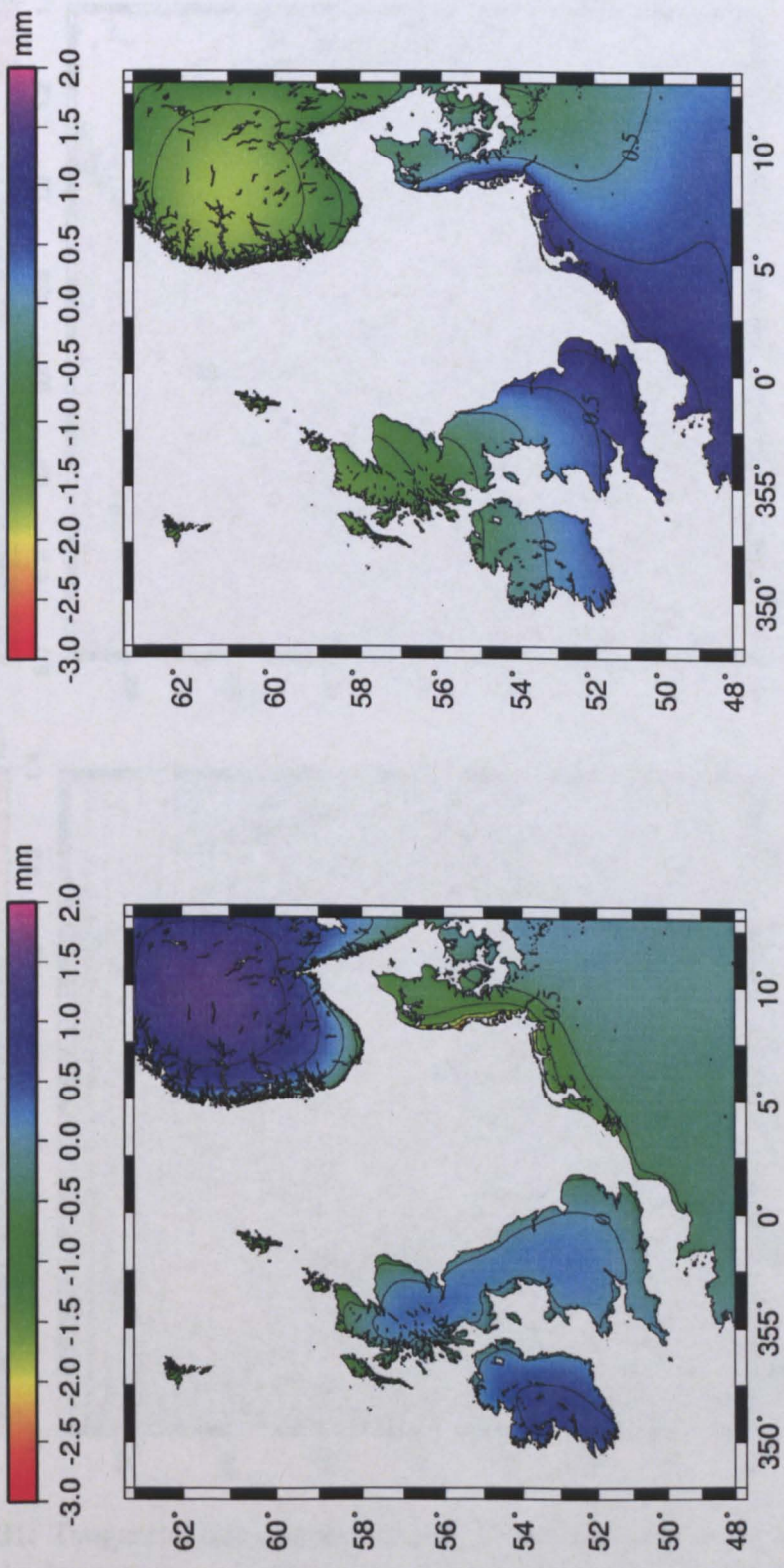

Figure 5.30: Total averaged vertical deformation in millimeters induced by sea level non-tidal residuals and atmospheric pressure loading over the winter 1994-1995 on the left and 1995-1996 on the right (period between December and March).

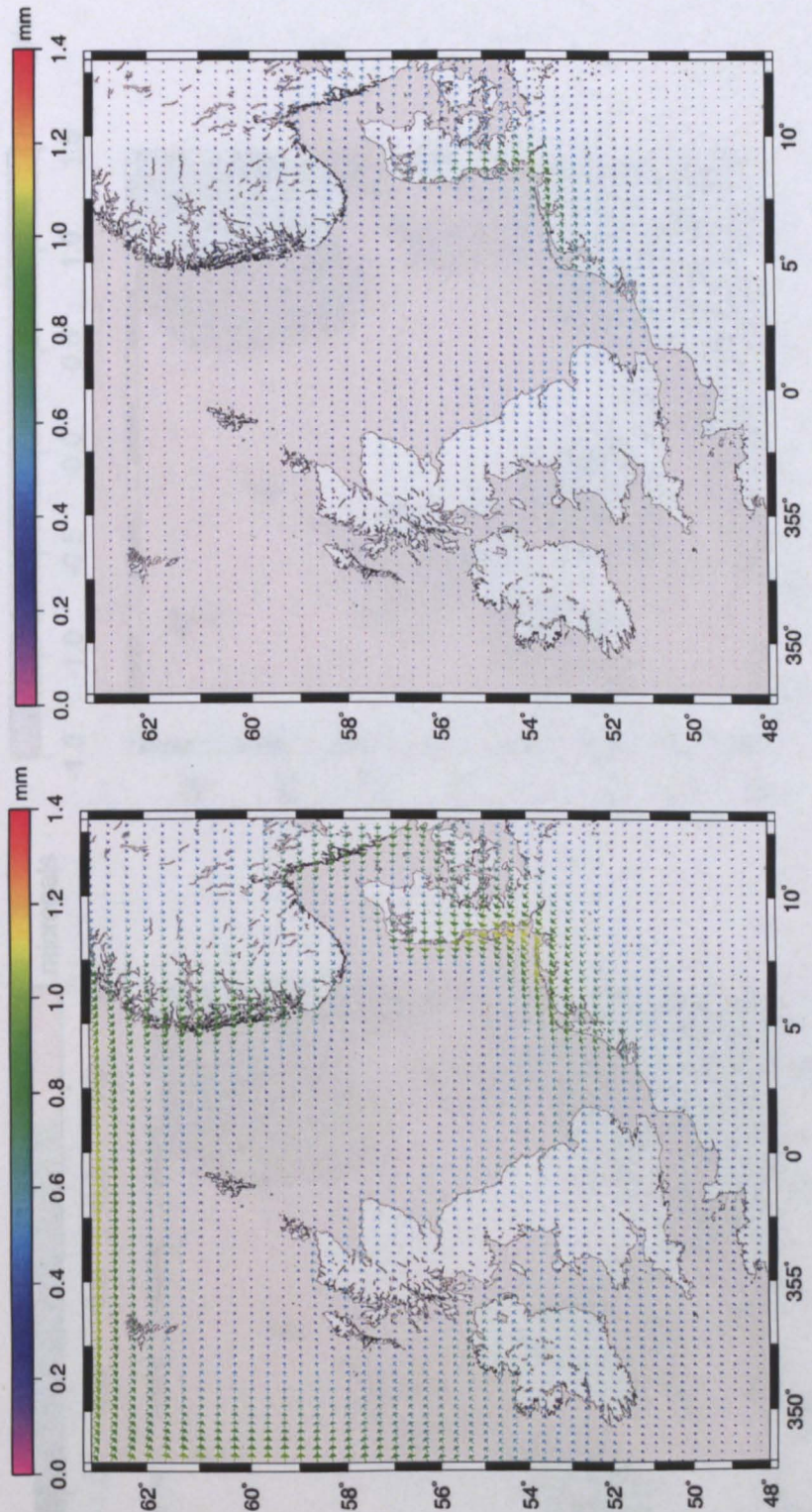

Figure 5.31: Tangential deformation in millimeters induced by sea level non-tidal residuals averaged over the winter 1994-1995 on the left and 1995-1996 on the right (period between December and March).

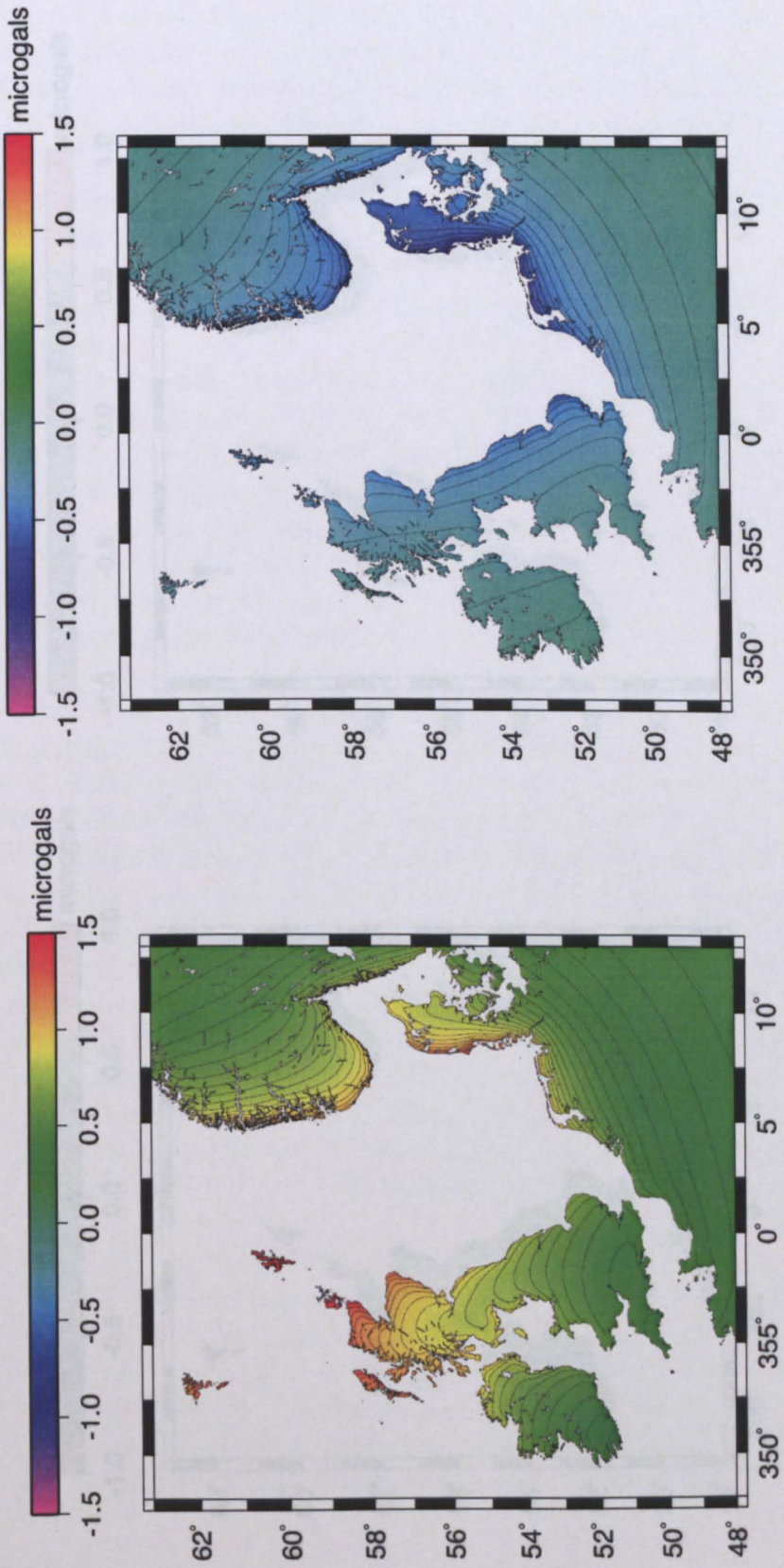

Figure 5.32: Gravity variations in μGal induced by sea level non-tidal residuals averaged over the winter 1994-1995 on the left and 1995-1996 on the right (period between December and March).

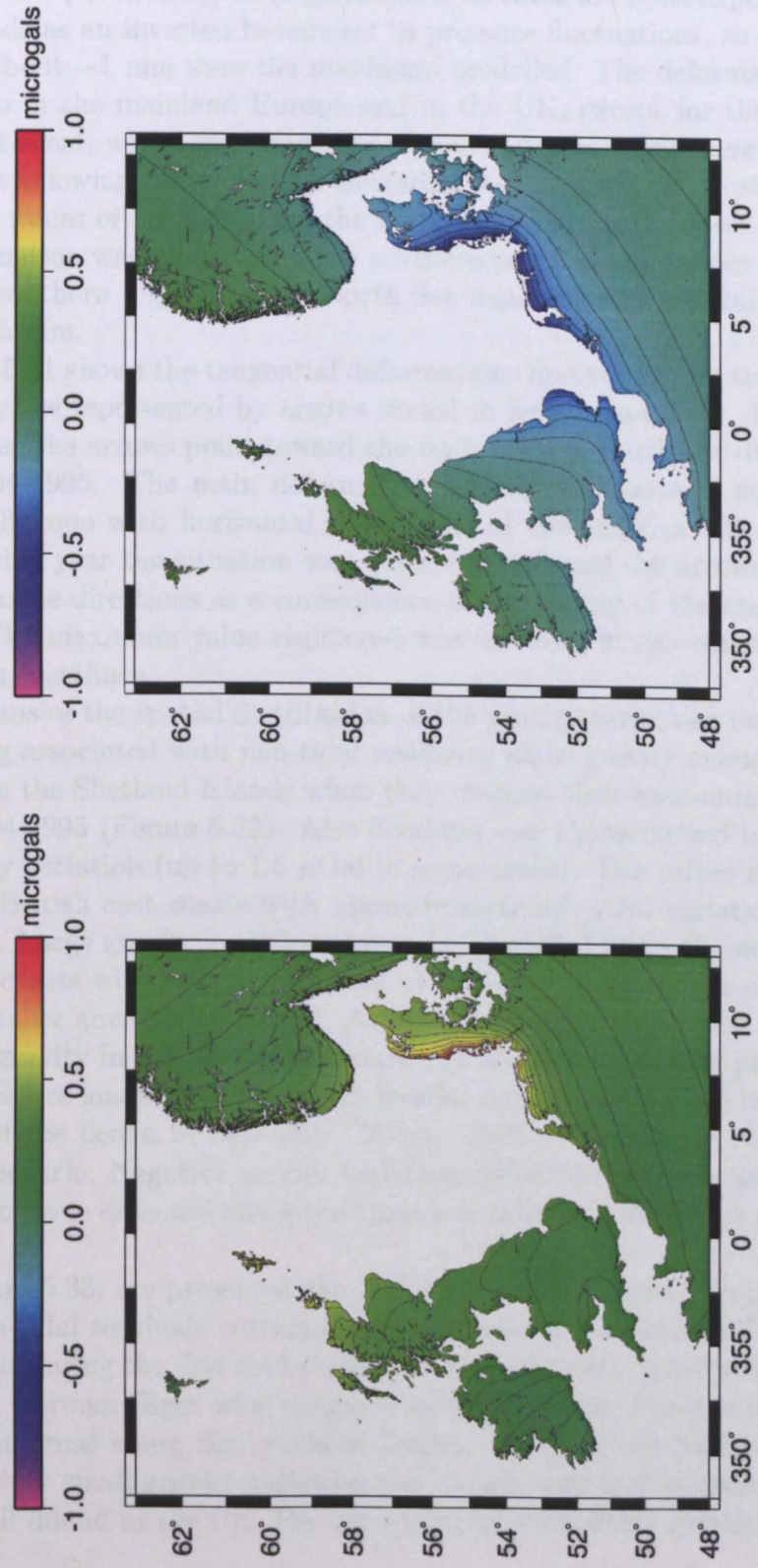

Figure 5.33: Total averaged gravity variations in μGal induced by sea level non-tidal residuals corrected for the inverted barometer effect over the winter 1994-1995 on the left and 1995-1996 on the right (period between December and March).

pared with the previous figure (Figure 5.29). In these areas, as expected, the sea responds as an inverted barometer to pressure fluctuations, so displacements of about -1 mm were the maximum modelled. The deformation was nearly zero in the mainland Europe and in the UK, except for those areas on the east coast, where displacements of about -0.5 to -1 mm were reached. During the following winter season, the radial displacement was positive with maximum values of 1.8 mm along the north-west European coasts. A negative deformation was modelled in the northern parts of UK (about -1 mm) while the southern regions by the North Sea experienced a general uplift of about 1-1.5 mm.

Figure 5.31 shows the tangential deformations due to the non-tidal residuals. They are represented by arrows scaled in length and color. It can be noticed that the arrows point toward the center of the North sea during the winter 1994-1995. The main deformation affects the coasts of north-west mainland Europe with horizontal movements of the order of 1.0 -1.2 mm. The following year the situation was quite different and the arrows pointed in the opposite directions as a consequence of the raising of the areas investigated. The maximum value registered was 0.8 mm, it was reached along the Danish coastlines.

The maps of the spatial distribution of the gravity variations induced by the loading associated with non-tidal residuals, show gravity changes up to 1.5 μGal in the Shetland Islands when they reached their maximum peak in winter 1994-1995 (Figure 5.32). Also Scotland was characterized by a positive gravity variation (up to 1.5 μGal in some areas). The values decreased along the British east coasts with approximately 0.5 μGal variation in the south-east. Large gravity variations were also modelled along the north-west European coasts with maximum values of 1.5 μGal. The change of gravity became smaller and smaller inland. Again, it should be noted that the total change in gravity in the Shetland Islands and Scotland (sea level plus atmospheric pressure loading) will be much smaller due to the inverted barometer response of the ocean in this area. Winter 1995-1996 shows a completely different scenario. Negative gravity variations affected the whole area; maximum peaks were detected along the Danish coastlines with values up to -1 μGal.

In Figure 5.33, are presented the gravity variations derived from the averaged non-tidal residuals corrected for the inverted barometer effect. It is evident that during the first cold season the most dramatic gravity change regarded the German Bight with values of about 0.9 μGal. Positive variations affected the areas along the northern British coasts by the North Sea (0.5 μGal). A very small gravity variation was experienced in the mainland Europe or well inland in the UK. For the winter 1995-1996 the gravity changes

were negative along the Danish-German-Dutch coastlines (-0.5 μGal) and along the eastern coasts of England.

It can be concluded that opposite NAO indices have a significant impact over the winter periods, on the deformation in the radial and the tangential directions and in the gravity changes of the UK regions together with the northwestern European areas. In fact a positive index is generally associated with stormy winter conditions and consequently a broad downward deformation and a positive gravity variation are on average, induced in the regions affected by storm surge loading. On the contrary, when a negative index characterizes the colder season, the weather conditions over the UK and the north west Europe are generally drier and the occurrence of storm surges is very limited. Consequently a general upward displacement and negative gravity variations are found in the regions affected.

When the effects on the deformations and gravity changes due to atmospheric pressure loading are also considered, a general reduction in the magnitude of the radial deformation and the gravity variation is commonly found during both the winter seasons. In particular in Scotland and in the Shetland Islands the deformation and the gravity variation is reduced since in these regions the sea responds as an inverted barometer to the pressure forcing i.e. the storm surge loading and the atmospheric pressure loading deformations and gravity changes generally cancel each other.

5.6 Conclusions

A model for evaluating the magnitude in the British Isles and in the northwest European regions of vertical and tangential displacements and associated gravity variations induced by sea mass changes in the shelf seas was developed. The deformation was estimated at the sites of Sheerness and Lowestoft, chosen because of their location in the area where the effects of the storm surges of the North Sea are among the largest and because they have a continuous GPS at their stations. During the period of time investigated (1997-2003) two larger surge storm events happened, the first in February 1999 and the second (bigger in magnitude compared with the previous), in January 2000.

From the results achieved it can be concluded that in Sheerness radial displacements of about 15 mm peak to peak are very common. In Lowestoft the deformations generally reach even greater values with displacements of 20 mm peak to peak. The tangential deformations calculated are generally not negligible but much smaller than the radial displacements produced. The total gravity changes associated with the deformation have an average

magnitude of about 2-3 μGal at the station of Sheerness and 3-4 μGal at Lowestoft.

It was concluded that the surface displacements and the gravity variations produced are larger during winter periods (between December and February), while summer and spring periods are relatively calm and hence the effects are smaller.

The development and evolution of the surge event of January 2000, in terms of magnitude of deformation induced was investigated through maps covering the British Isles and the north-west European regions and representing the spatial distribution of the loading effects due to the passing storm. The downward vertical displacement arrived at its maximum in Lowestoft and Sheerness at 3 a.m. on January 30th, when the height of the surge was greatest. A peak was registered at the same time also in the tangential deformation and in the gravity variation induced. The greatest effect of the deformation was felt on the Dutch-German-Danish coastlines with about -30 mm of displacement in the radial direction, 10 mm in the tangential (toward the north-west direction) and gravity changes of about 8 μGal. The effect decreased gradually inland with values of almost -10 mm in the vertical deformation, 1-2 mm in the horizontal and gravity variations of 2-3 μGal at distances of 150 km from the coast.

From the maps of the spatial distribution of the loading effects, it was deduced that the regions more sensitive to flooding events due to storm surges in the North Sea i.e. those situated in south east of England and along the Dutch-German-Danish coastlines have the largest deformation effects.

The seasonal and longer period vertical deformations due to storm surge loading were computed, together with the seasonal and longer period gravity variations. If the long period deformation is considered for very extended periods of time, the meteorological disturbances can probably be neglected but in the cases studied here it is still important to consider the effect of meteorological factors, in order to remove them from the geodetic measurements. It was pointed out that generally a low monthly mean can also be achieved when several surge events happen in the same averaged period.

Finally the large variation in NAO index passing from winter 1994-1995 to winter 1995-1996 associated with two very different climatic scenarios was investigated. Positive surge residuals were registered for winter 1994-1995 (characterized by a positive NAO index) with maximum values up to 40 cm along the Danish coastlines. Negative residuals of about -30 cm were achieved in the area of the maximum upward deformation (along north-west European coasts) during the following cold season (the NAO index associated was negative). From the maps of the spatial distribution of the vertical and tangential deformation and the associated gravity variations induced by

storm surge loading, it was concluded that when the NAO index is positive the vertical displacements produced are negative in sign as a consequent sinking of the areas investigated. A tangential movement towards the center of the North Sea is also detected. The gravity variations associated are positive. When NAO index is negative the deformation produced is positive indicating a general rise of the affected regions. The tangential deformation has opposite direction and the gravity change associated is negative. When the effects of atmospheric pressure loading are also considered, a general reduction in the deformation and gravity variation is modelled. In particular, in Scotland and in the Shetland Islands a significant decrease in the vertical displacement and in the gravity change is associated with the inverted barometer response of the sea in these regions to pressure fluctuations. The inter-annual variability between such extreme years as 1994-1995 and 1995-1996 should be detectable in the vertical displacements measured by GPS, VLBI and SLR, particularly near the coasts of Germany and Denmark.

Chapter 6

The total deformation due to atmospheric pressure loading and storm surge loading

In the previous chapters the deformations on the Earth's surface due to atmospheric pressure variations and storm surge loading were discussed. In this chapter, as a further step, the total loading deformation in the radial and tangential directions, obtained by summing the effects of storm surge loading and atmospheric pressure loading will be presented. The time series will be calculated at some stations located either in UK or in the north-west of Europe, where the storm surge loading has its maximum effects. The attention will be focused on the epochs of the main surge events of 1999 and 2000.

A comparison will be performed for the site of Membach (Belgium), between the time series of the gravity changes modelled during the two storm surge events and the observed gravity variations (from the superconducting gravimeter operating at the location), previously corrected for different effects. The discrepancies between observed and modelled time series will be investigated. In this way the validity of the loading model will be tested.

Finally, an estimate of the magnitude of the total loading signal moving from the north-western coast of Europe toward the center of the continent will be presented, taking as examples the vertical deformations induced at a few German sites. Moreover, the time series of the radial and tangential deformation associated, will be compared with observational values at the British site of Lowestoft and at few stations of the European Permanent Network (EPN), with continuous GPS at their locations. The target will be to understand how much of the loading signal due to atmospheric pressure loading and storm surge loading is present in the detected values.

6.1 Improving the model

For computing the vertical and horizontal displacements associated with both the loading effects of atmospheric pressure and storm surges, our computational models needed to be implemented.

The contribution of the non-tidal loading was calculated for the entire world and not just for the cells of the POLSSM grid. An additional 1 degree x 1 degree grid was used for the rest of the world i.e. for the deep ocean regions, using a new global barotropic model developed at POL (Stepanov & Hughes, 2004). The contribution to the deformation due to the sea level variability for the deep ocean regions is always smaller than the contribution related with shallow continental shelves i.e. sea cells from POLSSM grid in our particular case. This depends upon the greater distance between the observational point and the loading cell and mainly upon the fact that the deep ocean responds as an inverted barometer to the pressure variations and then the atmospheric pressure loading of ocean cells nearly cancels the sea level loading.

The atmospheric pressure contribution was already calculated at some sites considering the contribution of the whole Earth. A detailed sub-grid coinciding with POLSSM grid was used for the area of the British Isles and the north west European regions while an additional 1 degree x 1 degree grid was considered for the rest of the world. In this way, for both the loading contributions the same interpolation net was used and this fact allowed a direct summation of the two contributions after a proper interpolation of the data in time. Furthermore the inverted barometer hypothesis assumed in the previous calculation concerning the atmospheric pressure loading (Chapter 4), has to be reconsidered when computing the total loading.

Inside the POLSSM grid

The effect on the displacements due to storm surge loading was evaluated considering just those cells in the grid that are situated on the sea and then exhibit a certain surge elevation. Sea level residuals were available from POLSSM, they were calculated without removing the inverted barometer effects i.e. the complete sea level variation was included.

The effect on the deformation due to atmospheric pressure loading calculated by our model was computed in the previous chapter using the IBO hypothesis, thus the contribution to the loading comes just from the land areas while the mass of the ocean regions (atmosphere + sea level), was set to zero. The IBO assumption is not correct when both the effects of atmospheric pressure and storm surge loading have to be summed up. In fact,

when atmospheric pressure effects on loading are considered, also the contribution due to the atmospheric pressure loading over the sea has to be taken into account in order to obtain the total loading on the sea floor.

If a sea cell is considered inside the POLSSM grid, the total pressure variation dP acting at the bottom of the ocean floor is:

$$dP = \frac{m \cdot g}{A}$$

where g is the gravitational acceleration in m/s^2, A is the area of the cell in m^2 and m the mass in kilograms. The mass m is the sum of the mass variation of water m_{water} and the mass variation of the column of air above the water m_{air}:

$$m = m_{water} + m_{air}$$

This means that the total pressure dP acting at the bottom of the cell is not just due to the contribution of the water mass, but also to the one due to the air mass.

It can be concluded that the correct way for obtaining the total loading effect in the sub-grid examined is summing the radial or the tangential deformation caused by storm surge loading plus that due to atmospheric pressure loading in a Non Inverted Barometer (NIBO) hypothesis i.e. the contribution to the displacements from the atmospheric pressure over the sea cells has also to be accounted for.

Outside the POLSSM grid

Outside the POLSSM grid, sea level residuals are available once a day from a new global barotropic model developed at POL (Stepanov & Hughes, 2004). In the output of the model the inverted barometer effect was already removed. As a consequence the computation of the atmospheric pressure loading is not required over the oceans and only the loading over the land has to be computed.

6.2 Total vertical deformation at some UK sites

The total vertical deformation produced by both storm surges and atmospheric pressure loading was computed for 24 distinct British sites plus the

French station of Brest, summing the two different effects. The epochs of the two main surge events of the period investigated (4th and 5th February 1999 and 29th and 30th January 2000) were considered.

The data from the time series of vertical and tangential displacement caused by surface pressure variations, available every six hours, were interpolated every hour. The same was done for the loading effect determined by sea level residuals outside POLSSM grid since data were available once a day. In this way it was possible to sum the atmospheric pressure loading with the storm surges contribution (available hourly inside the POLSSM grid) and then to generate a smoother curve of the entire radial and horizontal deformation. Here just the results that refer to the vertical displacements are discussed since the tangential deformations associated are fairly small even if not negligible. Figure 6.1 shows the geographical positions of the sites considered for the computation.

It was observed that the magnitude of the total radial deformation increases moving from north toward south along the east coast of the British Isles, i.e. from Lerwick to Hemsby and this is very evident especially if the event of January 2000 is considered (see Figures 6.2 - 6.8 and those in Appendix E).

At the northern British stations of Lerwick, Aberdeen, Morpeth and North Shields on the east coast, and Stornoway, Portpatrick and Millport on the west side, the vertical displacement caused by atmospheric pressure loading was quite big. It has values of about 23 mm at Lerwick between 29th and 30th of January 2000. Since at this site the magnitude of the two different loading effects during the surge event of 2000 was almost the same but with opposite sign (deformation due to storm surge loading has a negative peak of about -20 mm), and the peaks happened almost at the same time, the resulting total radial displacement was positive with values between 0 and 5 mm. Also for the event of February 1999, the opposite peaks of storm surge and barometric pressure contributions were almost equal in magnitude (non-tidal loading effect was slightly greater), and contemporary. The total displacement achieved in the radial direction was about -3 to -4 mm (Figure 6.2). A similar situation happened at the stations of Stornoway (Figures 6.3) and Portpatrick (Appendix E), where the two distinct loading effects almost cancelled each other. It can therefore be seen that for these sites, which are near the deep ocean, the IBO assumption is almost correct i.e. the storm surge loading and atmospheric pressure loading approximately cancel.

The coincidence in time of the main peaks due to the two distinct effects did not happen at the other northern sites considered so the total radial deformation reaches values of about -10 mm at these stations (the plots that refer to these stations and some others are shown in Appendix E).

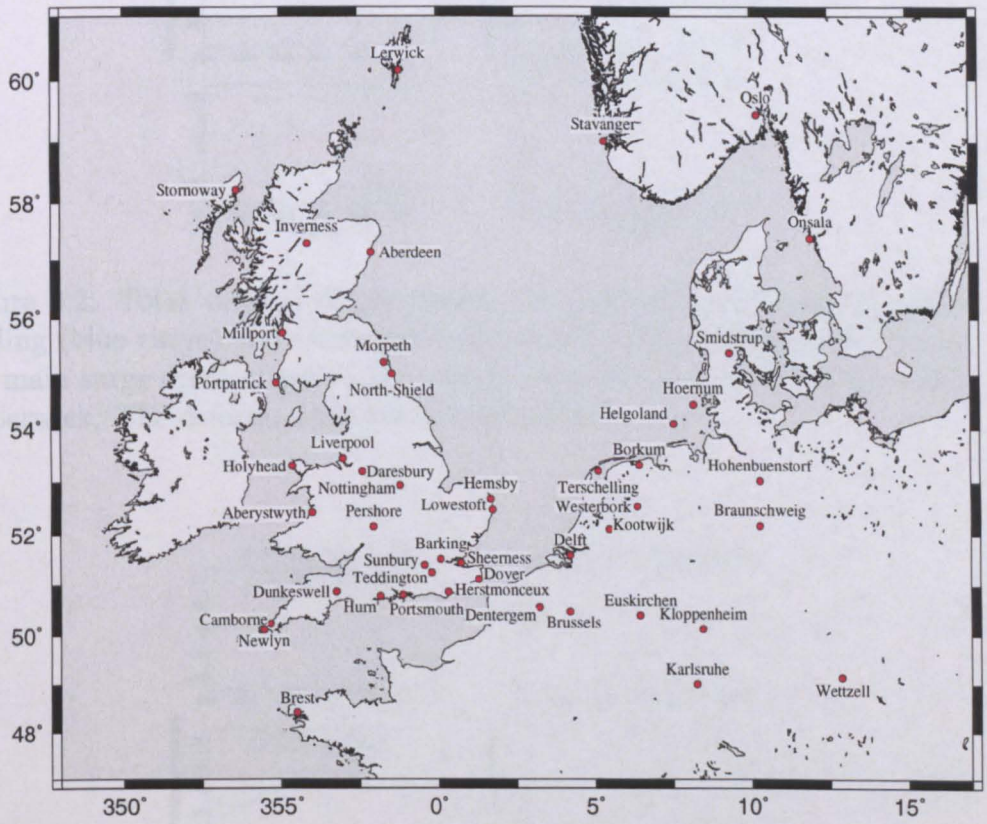

Figure 6.1: Geographical positions of the stations for which the total vertical and tangential deformations (surge storm loading + atmospheric pressure loading) were computed.

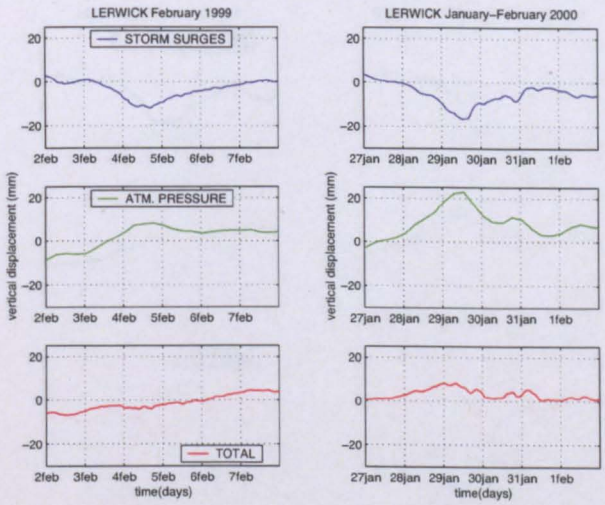

Figure 6.2: Total vertical displacements (in red) induced by storm surges loading (blue curve) and atmospheric pressure loading (green curve) during the main surge event of year 1999 (on the left) and year 2000 (on the right) at Lerwick. The deformations are in millimeters.

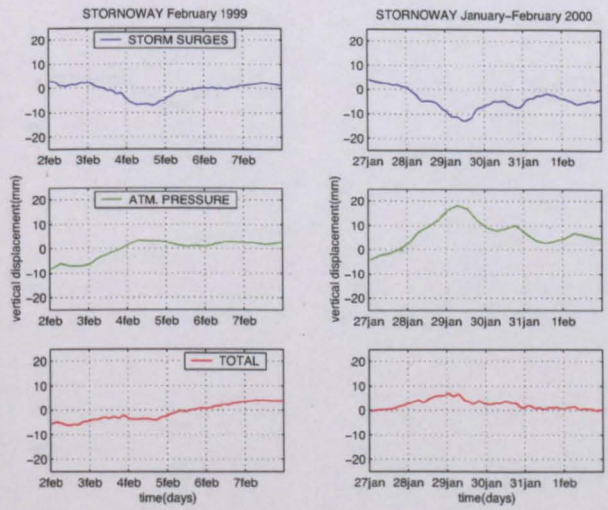

Figure 6.3: Total vertical displacements (in red) induced by storm surges loading (blue curve) and atmospheric pressure loading (green curve) during the main surge event of year 1999 (on the left) and year 2000 (on the right) at Stornoway. The deformations are in millimeters.

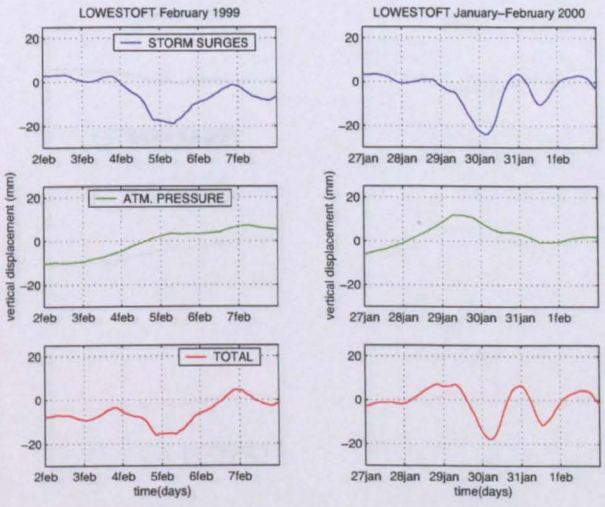

Figure 6.4: Total vertical displacements (in red) induced by storm surges loading (blue curve) and atmospheric pressure loading (green curve) during the main surge event of year 1999 (on the left) and year 2000 (on the right) at Lowestoft. The deformations are in millimeters.

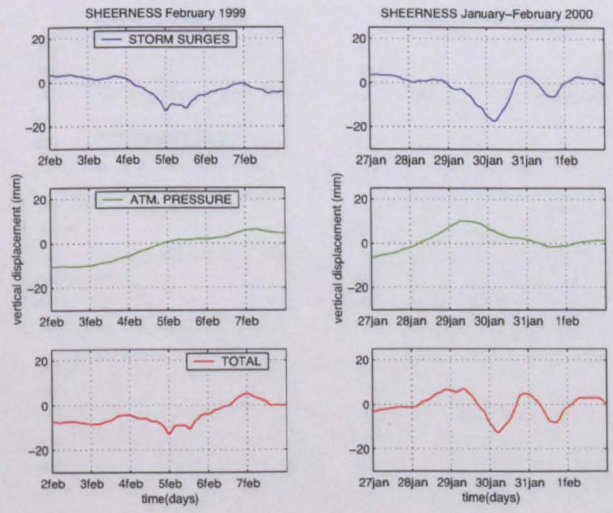

Figure 6.5: Total vertical displacements (in red) induced by storm surges loading (blue curve) and atmospheric pressure loading (green curve) during the main surge event of year 1999 (on the left) and year 2000 (on the right) at Sheerness. The deformations are in millimeters.

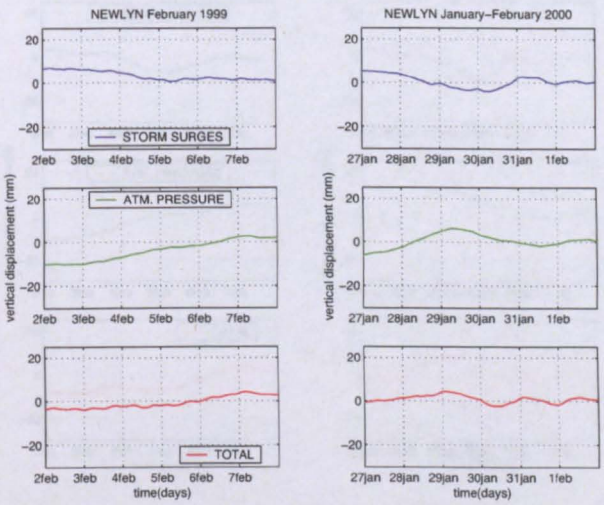

Figure 6.6: Total vertical displacements (in red) induced by storm surges loading (blue curve) and atmospheric pressure loading (green curve) during the main surge event of year 1999 (on the left) and year 2000 (on the right) at Newlyn. The deformations are in millimeters.

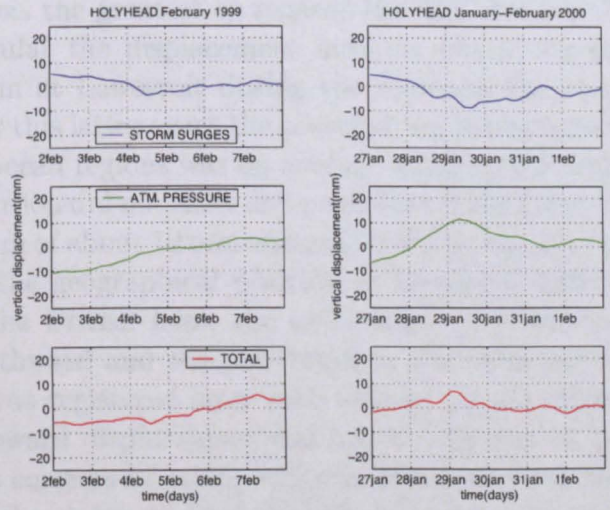

Figure 6.7: Total vertical displacements (in red) induced by storm surges loading (blue curve) and atmospheric pressure loading (green curve) during the main surge event of year 1999 (on the left) and year 2000 (on the right) at Holyhead. The deformations are in millimeters.

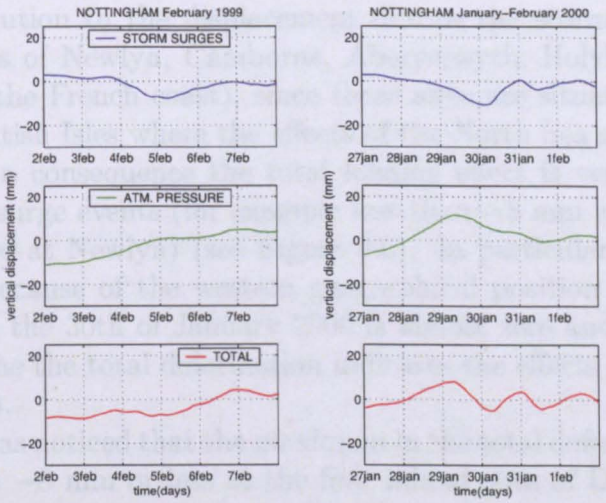

Figure 6.8: Total vertical displacements (in red) induced by storm surges loading (blue curve) and atmospheric pressure loading (green curve) during the main surge event of year 1999 (on the left) and year 2000 (on the right) at Nottingham. The deformations are in millimeters.

At the sites of Lowestoft and Sheerness the displacement due to storm surge loading was the greatest as regards the UK stations (Figures 6.4 and 6.5). In particular the displacement induced was at its maximum of -19 mm and -23 mm at Lowestoft during the first and the second surge event respectively (for this latter event the contribution to the vertical displacement from the deep ocean regions was on average equal to 0.8 mm). The pressure loading contribution did not show any peak during the event of February 1999 while a maximum of about 10 mm was registered on the 29th of January 2000.

Because of the geographical position of Lowestoft and Sheerness in the south east of the British Isles, the extra mass of water took a few hours for moving southward and the maximum in the deformation due to storm surge loading was registered later with respect to the other northern sites. The total downward displacement was about -18 mm at Lowestoft during both the events considered, while -15 mm of deformation were modelled for Sheerness. Total maximum displacements between -10 and -20 mm were also found at Hemsby, Barking, Dover and Herstmonceux.

Portsmouth and Hurn are situated along the south coast of the UK. Here the contribution to the deformation due to storm surges has a minor effect, so the total radial deformation modelled at these stations was less than -10 mm.

The contribution to the displacement due to the storm surges, affects less the stations of Newlyn, Camborne, Aberystwyth, Holyhead, Liverpool and Brest (on the French coast), since those sites are situated on the west coast of the British Isles where the effects of the North Sea storms is almost negligible. As a consequence the total loading effect is very small during both the main surge events (for example less than −8 mm at Liverpool and slightly negative at Newlyn) (see Figure 6.6). In particular, at the station of Holyhead, because of the western geographical position of the site, the deformation on the 30th of January 2000 is almost zero and nothing in the time series of the the total deformation indicates the effects of a surge event (see Figure 6.7).

Finally, it was noticed that the maximum in the total deformation reached values of about −8 mm or less at the four inland sites of Dunkeswell, Sunbury, Pershore and Nottingham during the first surge event (1999). The deformation produced was even less for the event of 2000 (−5 mm) (see Figure 6.8). The storm surge effect at these inland sites did not produce any great deformation since, as it will be shown and in the next section, the non-tidal loading effect decreases moving from the coast toward the land. This fact is caused by the increasing distance between the observation point and the grid elements that contribute to the loading. The pressure contribution to the deformation was comparable to that modelled in other UK sites i.e. about few millimeters for the event of 1999 and between 10 - 15 mm for the storm surge event of 2000.

The main contribution to the variation in the vertical deformation at a station situated in the south regions of the UK is generally due to the storm surges effects, especially for those sites located nearby the North Sea (in particular on the east coast of the British Isles). For those sites situated in the northern regions, atmospheric pressure loading and storm surge loading have almost the same magnitude but opposite signs (i.e. sea level responds nearly as an inverted barometer). As a consequence their combination reduces the magnitude of the total effect, especially when the peaks in the deformation happen at the same time.

Storm surge and atmospheric pressure loading peaks were contemporary at Lerwick, Stornoway and Portpatrick while, moving toward the south of the country, the peaks in the non-tidal deformation were registered a few hours later.

It can be concluded that, the loading effect induced by storm surges, varies faster (within hours), compared with that due to the atmospheric pressure loading (the largest pressure variations are associated with synoptic storm and have a life span of about 2-5 days). Furthermore, the spatial impact of storm surge loading is smaller than the one associated with barometric

pressure variations. Such non-tidal effects are generally larger (especially at high latitudes) but they affect small regions at a time (about 500 km of extension). Pressure variations usually affect very broad areas (1000-2000 km of extension).

6.3 Total vertical and tangential deformation at some European sites

The contribution of storm surge loading to vertical deformation decreases when moving from the north-west European coast toward the center of the continent during the event of January 2000, i.e. from Helgoland Island (Germany) to Wettzell (Germany), passing from −38.55 mm to −2.73 mm well inland (see Table 6.1).

Table 6.1: Vertical (up) and tangential (N-S and E-W components) deformation induced by storm surge loading at the sites considered. The displacements refer to the peak in the main surge event of January 2000.

STATION	UP	N-S	E-W
Helgoland	-38.55 mm	3.55 mm	-3.01 mm
Westerbork	-15.35 mm	4.74 mm	-2.50 mm
Kootwijk Observatory	-14.71 mm	4.45 mm	-2.46 mm
Brussels	-8.86 mm	3.46 mm	-0.94 mm
Euskirchen	-6.46 mm	2.49 mm	-0.99 mm
Kloppenheim	-4.93 mm	1.77 mm	-0.09 mm
Karlsruhe	-3.83 mm	1.41 mm	-0.57 mm
Wettzell	-2.73 mm	0.78 mm	-0.63 mm

The two components of the tangential displacements associated with such non-tidal ocean loading are small but not negligible. They show an horizontal deformation toward the north-west direction for all the sites considered (Helgoland Island, Westerbork, Kootwijk Observatory, Brussels (Belgium), Euskirchen, Kloppenheim, Karlsruhe and Wettzell) (see Table 6.1). The magnitude of the northern tangential component increases from Wettzell (0.78 mm) toward the coast and reaches 3.55 mm at Helgoland Island. The east-west component is negative at the coast (−3.01 mm), indicating a westward movement of the stations located in the area. The rate of deformation diminishes moving toward the center of the European continent.

Table 6.2: Vertical (up) and tangential (N-S and E-W components) deformation induced by atmospheric pressure loading at the sites considered. The displacements refer to the peak in the main surge event of January 2000.

STATION	UP	N-S	E-W
Helgoland	11.98 mm	-2.21 mm	-0.80 mm
Westerbork	9.31 mm	-2.24 mm	-0.79 mm
Kootwijk Observatory	8.36 mm	-2.23 mm	-0.78 mm
Brussels	5.95 mm	-2.26 mm	-0.71 mm
Euskirchen	6.71 mm	-2.30 mm	-0.68 mm
Kloppenheim	7.38 mm	-2.36 mm	-0.59 mm
Karlsruhe	5.88 mm	-2.33 mm	-0.57 mm
Wettzell	7.86 mm	-2.40 mm	-0.30 mm

Table 6.3: Total vertical (up) and tangential (N-S and E-W components) deformation induced by both storm surges and atmospheric pressure loading at the sites considered. The displacements refer to the peak in the main surge event of January 2000.

STATION	UP	N-S	E-W
Helgoland	-26.57 mm	1.34 mm	-3.81 mm
Westerbork	-6.04 mm	2.50 mm	-3.29 mm
Kootwijk Observatory	-6.35 mm	2.22 mm	-3.24 mm
Brussels	-2.91 mm	1.20 mm	-1.65 mm
Euskirchen	0.25 mm	0.19 mm	-1.67 mm
Kloppenheim	2.45 mm	-0.59 mm	-0.68 mm
Karlsruhe	2.05 mm	-0.92 mm	-1.14 mm
Wettzell	5.13 mm	-1.62 mm	-0.93 mm

The atmospheric pressure loading effect is radially positive at Helgoland Island (almost 12 mm) and the tangential deformation modelled indicates a movement of the station toward south-west. The vertical displacement induced is generally smaller inland while the magnitude of the horizontal deformation remains almost constant for all the stations considered (see Table 6.2).

The total deformation achieved summing up both the effects modelled for the epoch of the main surge of 2000, indicates that passing from the sites situated nearby the north-west European coastline to sites well inland, the displacement decreases and at distances of about 100-150 km from the coasts (between Brussels and Euskirchen), it changes to positive values (upward movement), because the pressure contribution becomes more important than the non-tidal one (see Table 6.3). In particular the site of Euskirchen seems to experience a very small vertical and tangential deformation during the storm event considered since the two distinct loading effects tend to cancel each other.

A general westward deformation affects all the German sites considered and the station of Brussels, while the northern horizontal displacement decreases until changing direction for sites well inland (between Euskirchen and Kloppenheim).

It can be concluded that for sites situated along the north-west European coastlines or with distances from the North Sea of about 50 - 100 km and less, the storm surge loading contribution to the vertical and tangential deformation is more important than the atmospheric pressure effect.

On the other hand, the deformation of stations located well inland (like Kloppenheim and Wettzell), reflects mainly the contribution of the barometric pressure variations and the effects of storm surge loading are mitigated as a result of the greater distance from the coastline.

6.4 Comparison between modelled and observed time series of the deformation

In the previous part (Chapter 5), it was pointed out that the vertical and tangential displacements induced by storm surge and atmospheric pressure loading should be detectable by the modern geodetic techniques.

In this section a comparison will be performed for the site of Membach (Belgium), between the time series of the gravity changes modelled during the two storm surge events and the observed gravity variations (from the superconducting gravimeter operating at the location). It is well known

that such observations are capable of detecting the deformations induced by different kinds of loading, for this reason they can be employed in detecting the loading deformations produced by storm surges as well. The discrepancies between observed and modelled time series will be investigated.

A further comparison will be performed between the time series of sites of the European Permanent Network (EPN) with continuous GPS at their location and the British GPS station of Lowestoft, where the effect of storm surge and atmospheric pressure loading over the period of the main surge event of year 2000 will be investigated. It will be assessed whether the GPS data are sensitive to the loading effects, by comparing the estimates from sub-daily, daily, weekly and monthly solutions with the model predictions.

6.4.1 Comparison with Membach's superconducting gravimeter data

A superconducting gravimeter (SG) is operating at the geophysical station of Membach, situated in the Eastern part of Belgium. The Membach laboratory is located within a 140 meter long tunnel cut into the side of a hill. The SG is located 49 m below the surface. The station of Membach was chosen since, it has the nearest superconducting gravimeter to the North Sea coasts.

The SG measures continuously the gravity at the site with a precision of 0.001 μGal (i.e.1 nanoGal) and an accuracy of 0.1 μGal (Crossley et al., 1999). The SG is a relative gravimeter so for eliminating the uncertainties in the observed gravity variations due to instrumental drift it is necessary to make parallel absolute gravimeter (AG) measurements every few weeks.

An SG consists of a superconducting sphere levitating in a persistent magnetic field. When the sphere moves vertically a change in voltage is registered by the nulling feedback system. It is proportional to the gravity variation. This instrument allows the study of a wide range of geophysical phenomena like for example ocean loading, Earth tides, polar motion and slow tectonic deformations.

Van Camp et al. (2003), have observed a small gravity trend of -0.6 $\pm$ 0.1 μGal/year at the station of Membach that should indicate that the site is going up by about 3 mm/year, this fact appears to be consistent with GPS observations performed at 3 km from Membach.

Depending upon the meteorological factors (mainly the rain), the residual amplitude in gravity i.e. after removing tides, polar motion and pressure effects, is usually about 5 μGal but it can vary a bit from year to year. Even if the rainfall is quite uniform in the areas surrounding the site during the entire year the gravity registers a decrease in winter season as a consequence

of the reduction in evapo-transpiration. At a first sight this relationship may appear surprising since an increase in water mass in the ground should lead to an increase in gravity as well. For explaining this apparent contradiction the location of the site has to be taken into account. The water mass is actually above the instrument and this makes the gravity diminish.

A comparison was performed between the gravity variations at Membach detected by the SG and the gravity changes computed by our model during the periods in which the two main surge events previously investigated happened. The target was understanding if the gravity changes induced by non-tidal sea level residuals are detectable from real observational data. In this case also the validity of the modelled gravity time series could be assessed.

The gravity residuals at Membach were obtained by correcting for Earth tides (computed by a synthetic model based on observed tidal parameters), polar motion effect and linear instrumental drift (estimated by comparison with the absolute gravity measurements). For removing the air pressure effect, the air pressure data (available from the Baratron pressure transducer working in the same room of the SG at Membach), were fitted with the gravity residuals. Two fits were performed, one for the period between the 29th of January and the 12th of February 1999 and one for the period between the 23rd of January and the 6th of February 2000. The fitted air pressure admittances for the two periods considered were, -0.268 μGal/mbar for 1999 and -0.288 μGal/mbar for 2000. (In Appendix E, section E.3, are presented for completeness the time series of the gravity residuals at Membach before removing the air pressure effect).

In Figure 6.9 is presented a comparison between the gravity variations calculated by our model of storm surge loading and the gravity residuals available from the SG at Membach. In both of the plots in can be noticed that there is some similarity between the observed and modelled gravity.

It should be noted that the zero for the observed gravity residuals is arbitrary. A better agreement during the surge events could be obtained by shifting the observations upwards by 1 to 1.5 μGal, but no attempt has been made to do this. The general agreement between the model and observations is encouraging, both for the main surge events and the smaller surge event on the following days.

Other variability of around 1 μGal can also be seen in the SG data in Figure 6.9 and is likely to be due to the effects of rainfall.

Since the Membach geophysical station is not located near the coast, it can be concluded that if the SG station was about 100 km closer to the coastline the storm surge signal would stand out much more clearly above the other noise in the data and a better agreement between modelled and

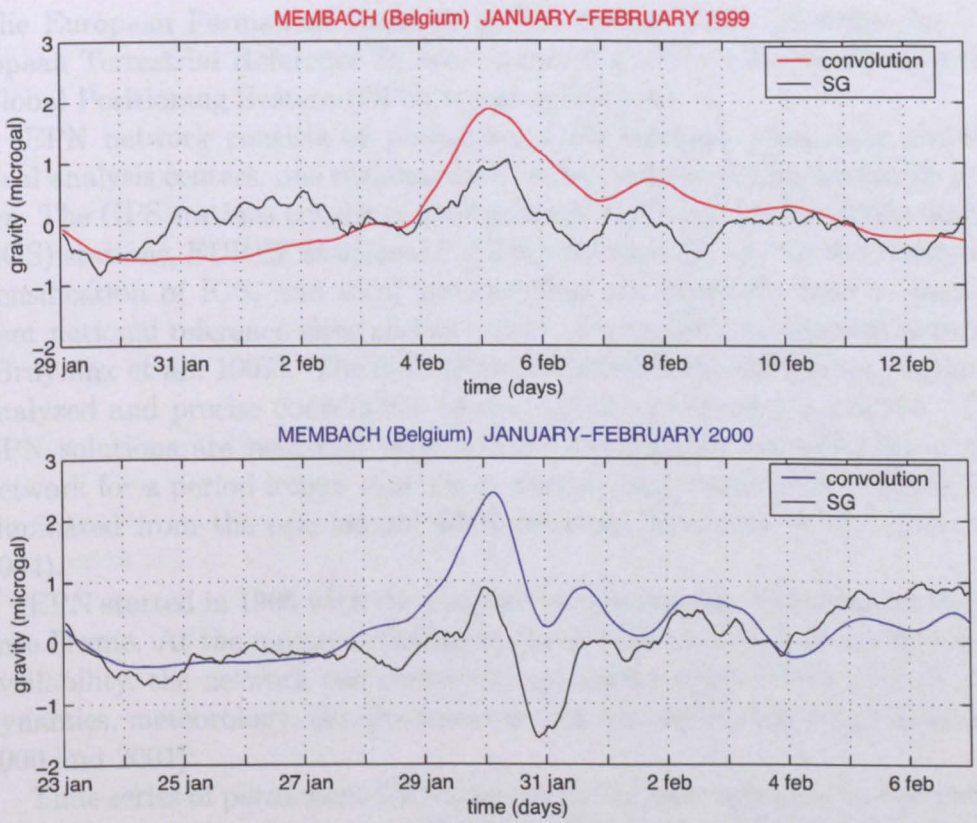

Figure 6.9: Comparison between the gravity residuals at Membach observed by a SG (black curves) and the gravity variations modelled for the two periods of the main surge events previously investigated (red and blue curves for 1999 and 2000 respectively). The gravity residuals are in μGal. Note that for the gravity observations the zero is arbitrary.

observed data would be easier to achieve.

6.4.2 Comparison with the time series of continuous GPS stations of the European Permanent Network

The European Permanent Network (EPN) realizes and maintains the European Terrestrial Reference System computing the weekly positions of the Global Positioning System (GPS) tracking stations.

EPN network consists of permanent GPS stations, local data centers, local analysis centers, one regional data center and one regional analysis center. The GPS stations consist of International GPS Service for Geodynamics (IGS) stations, EUREF stations i.e. GPS sites that are part of the European densification of IGS, and local stations that are generally used as permanent national reference sites and as a part of a geodetic permanent network (Bruyninx et al., 1997). The data from the network of stations are routinely analyzed and precise coordinates of the stations involved are realized. The EPN solutions are near-real time and all the stations not included in the network for a period longer than three months, are classified as inactive and eliminated from the operational EPN network (Bruyninx et al., 2003 and 2004).

EPN started in 1995 with the purpose of maintaining the European Reference Frame. At the moment, thanks to the densification and to the fast data availability, the network can contribute to further applications such as geodynamics, meteorology, climate research and sea level monitoring (Bruyninx 2000 and 2001).

Time series of permanent GPS stations are increasingly used to determine displacements of points at the Earth's surface for practical and scientific purposes. In this case, EPN time series were compared with the total vertical and tangential deformation elaborated by our model for a sample of stations. Our comparison was performed considering the standard coordinates time series created with the purpose of detecting outliers and coordinates jumps (Bruyninx et al., 2003a).

The target was to understand how much of the total loading deformation due to atmospheric pressure and storm surge loading might be seen in the signal detected by GPS. This attempt was not very successful, particularly as only weekly values were available for the EPN stations. The results from just 3 representative stations are shown here, mainly to show the overall variability in the available data.

Since in general a comparison between the tangential components ob-

served and modelled is very hard to perform also during the storm event peaks, because of the small magnitude associated, the following discussion will regard just the vertical components of the deformation induced. The modelled vertical and tangential deformations for different stations and for longer periods of times are presented in the Appendix E, section E.2, for completeness.

Helgoland Island (Germany) For the site of Helgoland Island, a negative peak in the vertical displacement was modelled (about -26 mm; Figure 6.10), in correspondence with the main surge event of the 2000.

The station of Helgoland Island is very sensitive to the contribution of the storm surges of the North Sea, to the vertical and tangential deformation, in fact it is situated in the area in which the non-tidal loading effect has its maximum.

EPN's data were not available for the year 1999, so no comparison was performed for the epoch of the first storm surge.

Westerbork (Holland) At the station of Westerbork during the surge event of 1999 a total deformation of -6 mm in the vertical was calculated by the model (Figure 6.11). In particular, the total deformation resulting from the summation of atmospheric pressure and storm surge loading, did not represent a proper peak in the time series. In fact the maximum peaks of the two distinct loading effects almost cancelled each other, being contemporary but opposite in phase. The minimum was instead modelled few days before (between the 2nd and the 3rd of February), when a low pressure system affected the region considered.

The following year a deformation of -6 mm was modelled. At this epoch the peaks due to the modelled loading effects did not happen at the same time (Figure 6.11 upper part). A maximum positive deformation of over 10 mm was caused by pressure variations a few hours before the main surge event.

Wettzell (Germany) Finally at Wettzell, the modelled deformation in the vertical was equal to 5.13 mm during the storm event of 2000 and positive (about 4-5 mm) for the event of 1999. The station is well inland and is not sensitive to the effect of storm surges so atmospheric pressure loading account for most of the displacements calculated (see Figure 6.12).

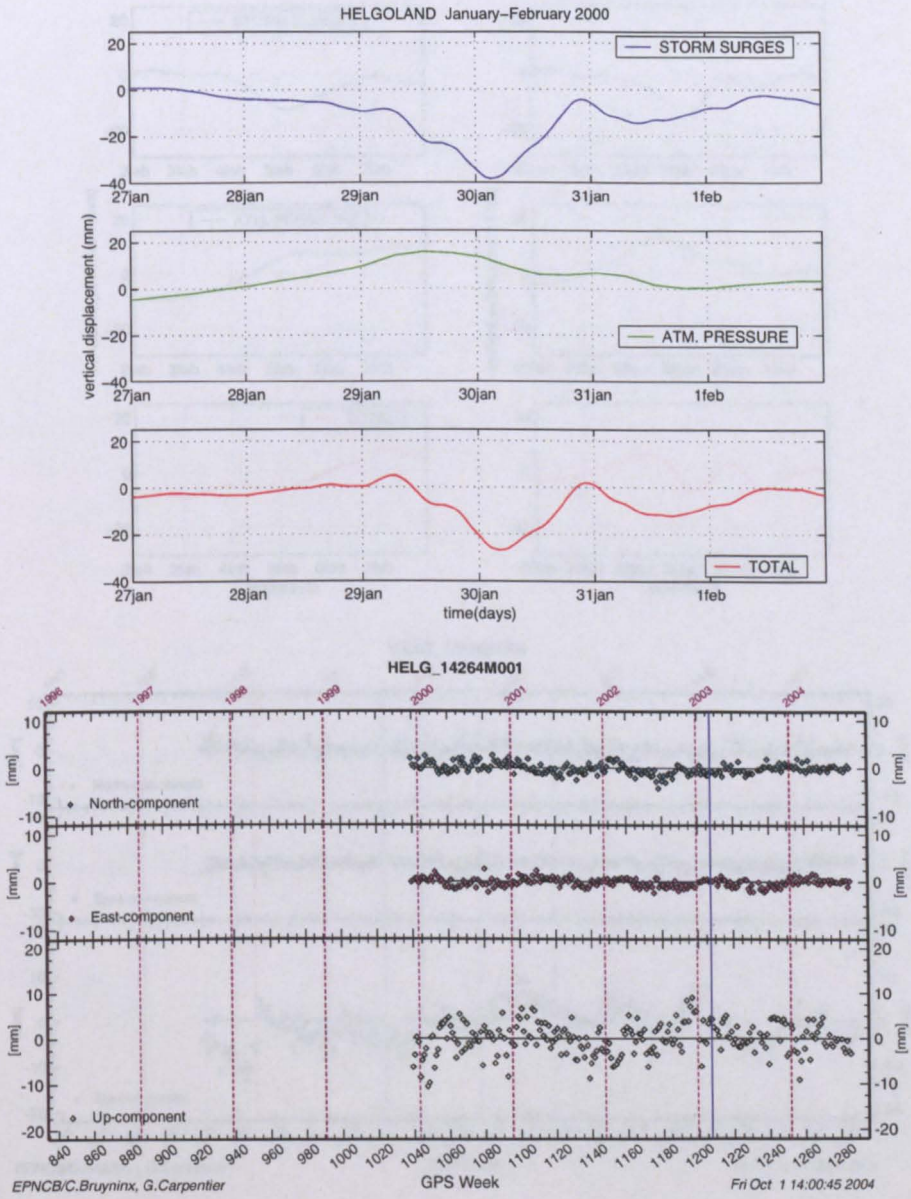

Figure 6.10: Modelled total vertical deformation induced at Helgoland Island by atmospheric pressure and non-tidal ocean loading (upper part) during the storm events of 2000. In the lower part is presented the standard EPN time series for the site considered (Bruyninx & Carpentier, 2004).

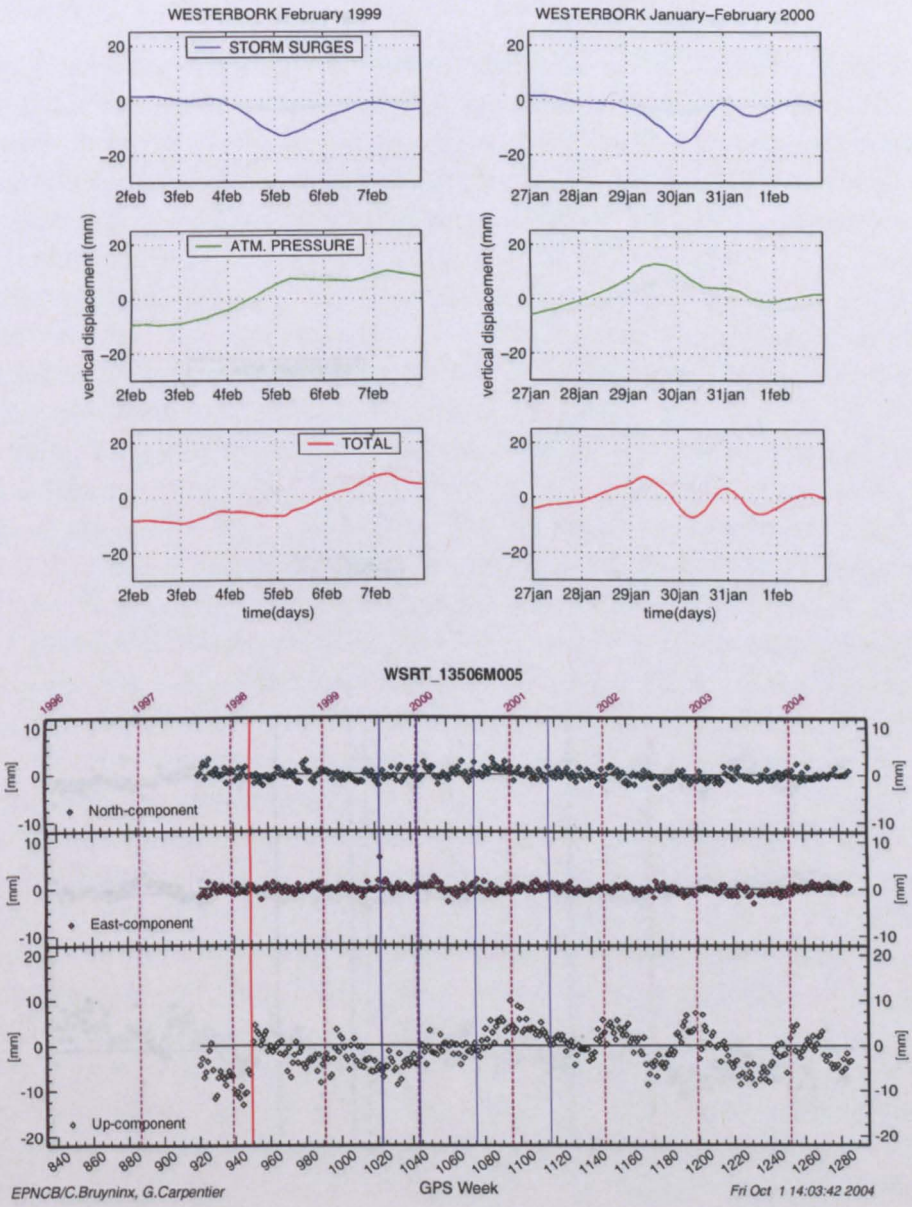

Figure 6.11: Modelled total vertical deformation induced at Westerbork by atmospheric pressure and non-tidal ocean loading (upper part) during the storm events of 1999 (left) and 2000 (right) respectively. In the lower part is presented the standard EPN time series for the site considered (Bruyninx & Carpentier, 2004).

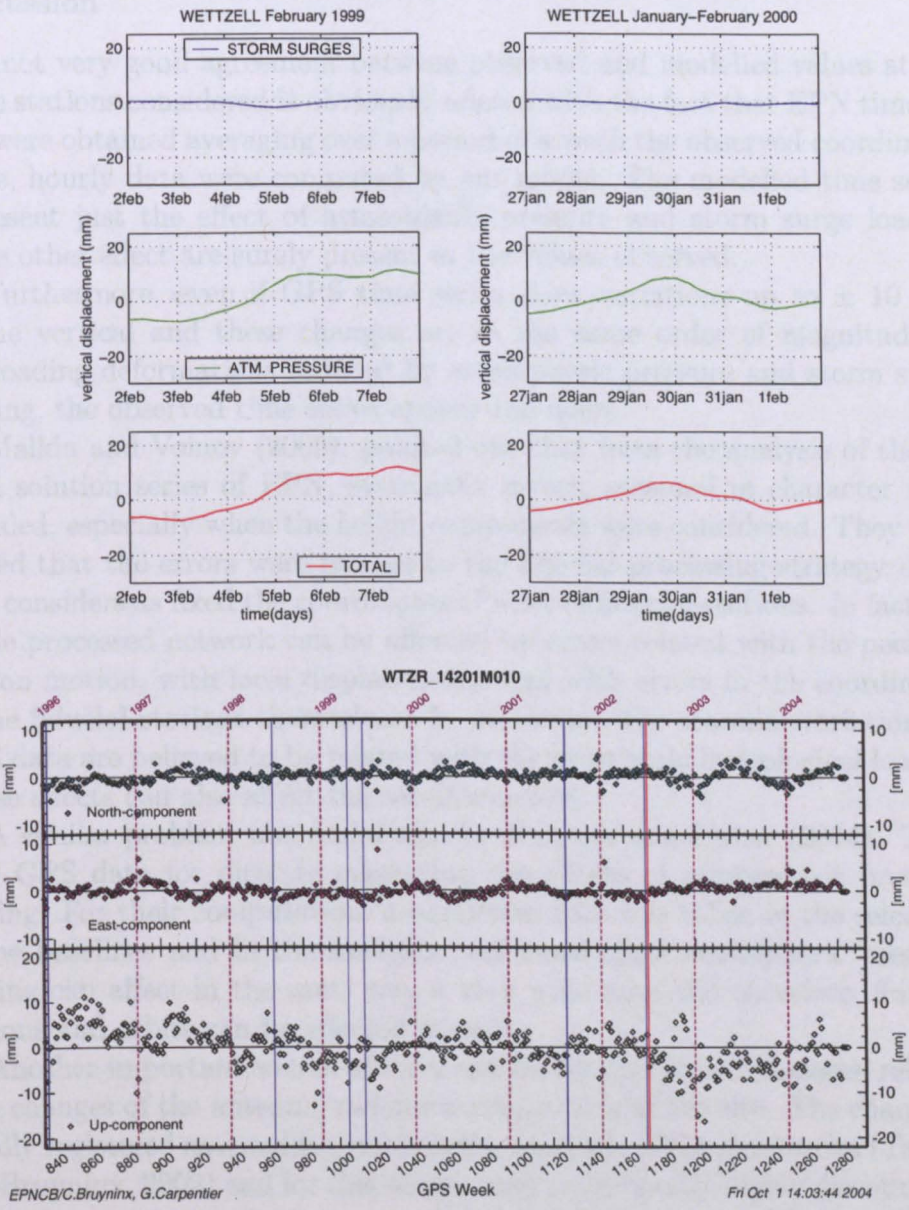

Figure 6.12: Modelled total vertical deformation induced at Wettzell by atmospheric pressure and non-tidal ocean loading (upper part) during the storm events of 1999 (left) and 2000 (right) respectively. In the lower part is presented the standard EPN time series for the site considered (Bruyninx & Carpentier, 2004).

Discussion

The not very good agreement between observed and modelled values at the three stations considered is obviously related with the fact that EPN time series were obtained averaging over a period of a week the observed coordinates while, hourly data were computed by our model. The modelled time series represent just the effect of atmospheric pressure and storm surge loading while other effect are surely present in the values observed.

Furthermore, even if GPS time series show variations up to $\pm$ 10 mm in the vertical and these changes are in the same order of magnitude as the loading deformations induced by atmospheric pressure and storm surge loading, the observed time series appear too noisy.

Malkin and Voinov (2000), pointed out that from the analysis of the official solution series of EPN, systematic errors, seasonal in character were revealed, especially when the height components were considered. They concluded that the errors were related to the fiducial processing strategy used, that considers as fixed the coordinates of a set of fiducial stations. In fact the whole processed network can be affected by errors related with the peculiar station motion, with local displacements and with errors in the coordinates of the fiducial stations themselves. In particular, the seasonal variations in GPS data are believed to be related with the large scale hydrological loading whose effects can also affect the satellite orbits.

A similar problem was found also by Kaniuth and Huber (2004). They used GPS data for directly measuring the effects of atmospheric pressure loading. For their computation, a particular care was taken in the selection of the baselines and in the analysis performed since atmospheric pressure loading can affect in the same way a very wide area and therefore, fiducial stations and orbits can be affected as well.

Another important source of error can be the equipment changes, related with changes of the antenna/radome configuration of the site. The change is usually registered as a sudden jump in the residuals of the time series (Takacs and Bruyninx, 2002) and for this reason they are generally highly discouraged unless necessary. In the lower part of the previous figures (Figures 6.10 - 6.12), a blue line always indicates a receiver change or a firmware update and a red one refers to a replace of the antenna (Bruyninx & Roosbeek, 2002).

It can be concluded that even if the signal due to the loading deformation induced by atmospheric pressure and storm surge is present in the GPS coordinates, it is very difficult to directly measure it mainly because of the confusing signals (noise) in the observed time series at the 5 - 10 mm level.

6.4.3 Comparison with IESSG's GPS solutions

A further more detailed analysis was carried out in collaboration with the Institute of Engineering Surveying & Space Geodesy (IESSG) of the University of Nottingham. The effect of storm surge and atmospheric pressure loading at the UK CGPS station of Lowestoft (LOWE) over the period of the large storm surge event of 2000 (between 27th January and 1st February), was investigated. The target was to assess whether the GPS data were sensitive or not to the loading effects produced.

A first test was performed comparing the 12 and 24 hours GPS solutions with our hourly model predictions considering the effects of storm surge loading and atmospheric pressure loading (Figures 6.13). In this analysys, GPS time series were processed on the baseline between Nottingham and Lowestoft (designed as i2l). From the Figure it can be noticed that when the 12 hours sub-daily GPS solutions are considered, there is some similarity between modelled and GPS data, but the deformation observed is between -25 and 10 mm which is slightly greater than the values predicted. On the other hand the 24 hours daily GPS solutions do not show the deformations induced in a high resolution but it is still possible to detect the main features of the displacement. Furthermore the RMS values for the GPS minus the model are lower compared with the RMS for the GPS alone, in both the cases studied. This fact indicates a small improvement in GPS values when they are corrected for both the loading effects.

A second test was performed comparing GPS data with daily, weekly and monthly predicted deformations. The GPS time series were computed in an ITRF2000 reference frame based on Kootwijk, Onsala, Villafranca and Wettzell (KOVW).

In Figure 6.14 are plotted the results of the comparison between GPS and modelled time series. Also the RMS for GPS and GPS minus the model (calculated removing the daily, weekly and monthly mean of the loading results from daily, weekly and monthly mean GPS heights) are presented. On the daily and weekly plots are included the monthly RMS for the GPS and the GPS minus the model. It can be seen that correcting the observed GPS time series for the loading model results averaged over different periods of time has not improved the final results. In particular this fact is confirmed by the computation of the monthly and yearly residuals that generally become larger when model data are removed from GPS time series. These results were confirmed by a further test that compared GPS time series on the re-processed single baseline i2l, with daily, weekly and monthly predicted deformations (not shown). In particular it should be noted that the GPS daily results show a significant variability in summer (May to August), when

there is only a small variability in the loading deformation. This fact show that there are other effects present in the GPS observations, which makes it difficult to clearly observe the loading signals, even during the winter months.

It can be concluded that in Figure 6.13 there is some evidence that daily and sub-daily GPS results exhibit a pattern that follows the vertical deformation predicted at Lowestoft summing the hourly loading effects due to storm surge loading and atmospheric pressure loading. On the other hand the results are not conclusive when the daily, weekly and monthly modelled time series are compared with daily, weekly and monthly GPS time series. It was already pointed out in the previous section that GPS data are generally quite complex to be analyzed because the signals may be affected by the processing strategy used, the satellite orbits and multipath and the tropospheric delay models. Furthermore, atmospheric pressure variations may affect an area that extends up to 1000-2000 km, then particular attention has to be paid in the choice of the reference frame or baseline of stations.

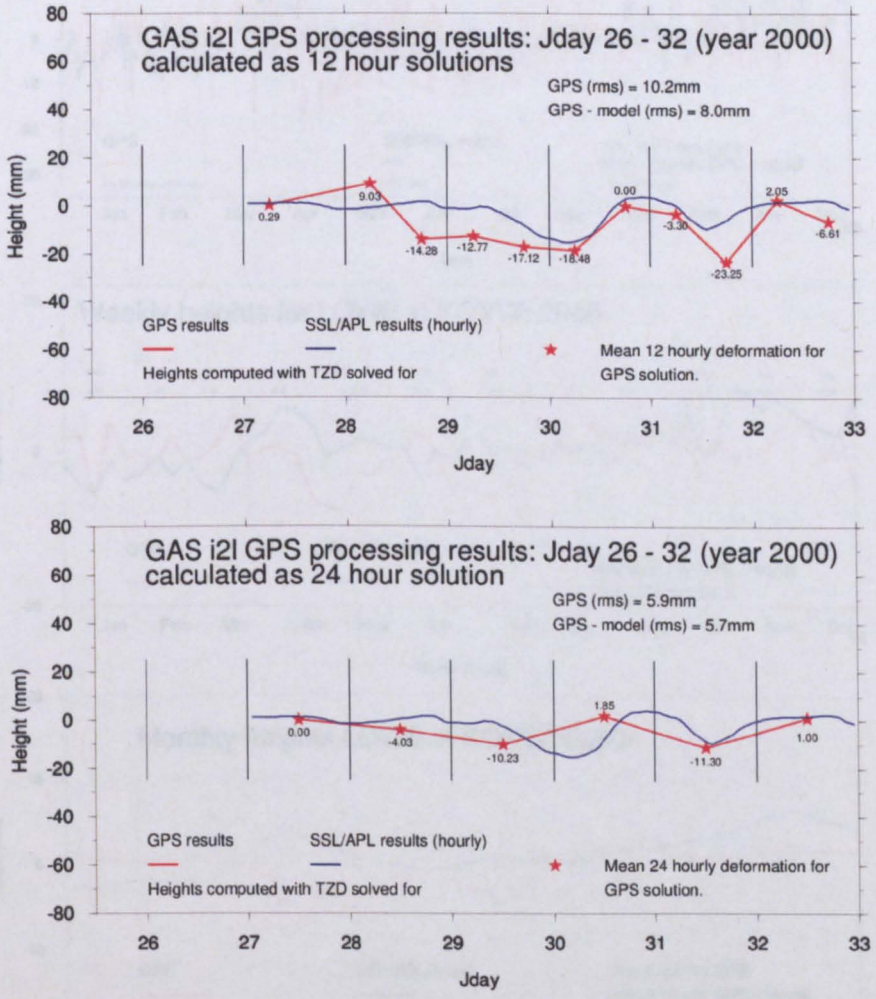

Figure 6.13: Comparison between GPS solutions and predicted radial displacements. In red are the 12 hours (upper part) and 24 hours (lower part) GPS solutions and in blue are the modelled vertical deformations induced by atmospheric pressure loading and storm surge loading (the predicted time series for the site of Nottingham were removed from the time series for the station of Lowestoft).

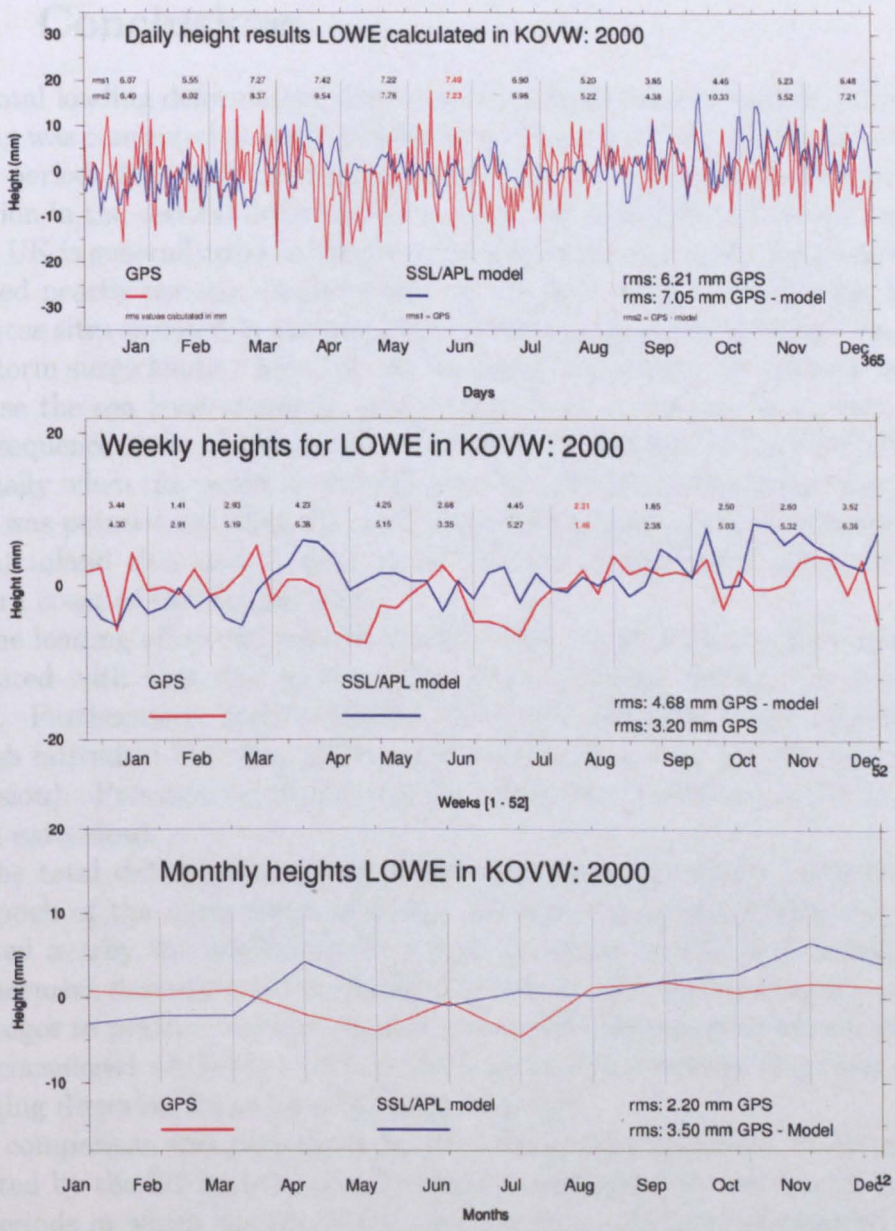

Figure 6.14: Comparison between mean GPS heights and modelled mean radial dispalcements. In red are the daily (top), weekly (middle) and monthly (bottom) mean GPS heights computed in an ITRF2000 reference frame based on Kootwijk, Onsala, Villafranca and Wettzell (KOVW), while in blue are represented the daily (top), weekly (middle) and monthly (bottom) mean model values for the station of Lowestoft (year 2000). The RMS for the whole year and for each individual month are also included; in particular the top line refers to GPS and the second line refers to GPS minus model.

6.5 Conclusions

The total loading deformation due to storm surges and atmospheric pressure loading was computed at some British sites during the two main surge events of the period 1997-2003. It was concluded that the main contribution to the variation in the vertical deformation at a station situated in the south region of the UK is generally due to the storm surges effects especially for those sites situated nearby the sea, in particular on the east coast of the British Isles. For those sites situated in the northern regions, atmospheric pressure loading and storm surge loading have almost the same magnitude but opposite signs because the sea level responds approximately as an inverse barometer. As a consequence their combination reduced the magnitude of the total effect, especially when the peaks in the deformation happen at the same time.

It was pointed out that the total deformation reaches values of about -5 mm at inland sites and it goes up to -20 mm at stations situated on the Eastern coast of the British Isles.

The loading effect induced by storm surges, varies faster (within hours), compared with that due to the atmospheric pressure loading (within 2-5 days). Furthermore, such non-tidal effects are generally larger (especially at high latitudes) but they affect small regions at a time (about 500 km of extension). Pressure variations usually affect very broad areas (1000-2000 km of extension).

The total deformation achieved summing both the effects modelled for the epoch of the main surge of 2000, indicates that passing from the sites situated nearby the north-west European coastline to sites well inland, the displacement decreases and at distances of about 100-150 km from the coasts it changes to positive values. A general westward deformation affects all the sites considered while the northern horizontal displacements decreases until changing direction for more continental stations.

A comparison was performed between the gravity variations at Membach detected by the SG and the gravity changes computed by our model during the periods in which the two main surge events previously investigated happened. The time series agree quite well during the time intervals considered, in particular the maximums in the gravity measurements happened at the same time in which the maximum peaks of the storm surge events are registered. It has to be said that the observed time series showed some "noisy" effects but they are probably related with the hydrogeology of the region. Since the Membach geophysical station is not located near the coast, it was concluded that if the SG site was about 100 km closer to the coastline the storm surge signal would stand out much more clearly above the other noise in the data.

The EPN GPS time series were compared with the total vertical deformation elaborated by our model. The agreement between GPS data and modelled values was in general not very good. EPN curves were obtained averaging over a period of a week the observed coordinates, which significantly reduces the effect of a single surge event. Furthermore the modelled time series represent just the effect of atmospheric pressure and storm surge loading while other components are surely present in the values observed. In particular, it was pointed out that the large scale hydrological and barometric loading can affect the whole processed network since similar effects affect a wide area. These errors can "spread" to various stations as a results of the processing strategy used. It was concluded that even if the signal due to the loading deformation induced by atmospheric pressure and storm surge is present in the GPS coordinates, it is very difficult to directly measure it because of the confusing signals (noise) in the weekly observed time series at the 5 - 10 mm level.

Finally the effect of storm surge and atmospheric pressure loading at the UK CGPS station of Lowestoft over the period of the main surge event of 2000 was investigated in a more detailed analysis, in order to assess whether the GPS data were sensitive or not to the loading effects produced. It was concluded that there is some evidence that daily and sub-daily GPS results for this surge event exhibit a pattern that follow the vertical deformation predicted at Lowestoft when hourly loading modelled effects are considered i.e. at Lowestoft GPS time series confirm the model predictions in amplitude and phase. Given both the SG and the GPS results, the signal due to storm surge loading is detectable and can be predicted using our derived models.

Chapter 7

Conclusions and recommendations

The aim of this thesis was to better understand the effects of atmospheric pressure loading and non-tidal ocean loading from shallow seas with particular attention during the periods of large storm surge events. Several models were developed in order to model the crustal displacements and the gravity variations induced and therefore to reduce the noise in geodetic observations and gravity measurements by correcting for the modelled loading effects.

From the general case of a disc loading the surface, it was pointed out that the choice of different Green's functions is not very important in the definition of the final result since compared with the uncertainties in the load distribution, the uncertainties in the Green's functions can be neglected.

The time series of the modelled vertical displacement induced by sea level atmospheric pressure variations at a few coastal sites, show that the magnitude of the radial deformation increases when a broader area is considered to contribute to the deformation for both the case of a NIBO or IBO ocean model. In particular, the main contribution to the displacement comes from an area within 2000 km from the point of interest so this is the minimum spatial extension of the pressure variations that has to be considered in order to perform accurate loading computations.

In the case of an IBO model the vertical displacements are generally smaller if compared with the results for an oceanless model, because with the first assumption, ocean floors do not experience any of the forces associated with barometric pressure variations and therefore the total incremental mass load over the ocean basins is set to zero. For both the assumptions, the perturbation results are bigger in amplitude during winter months when also the atmospheric pressure variations are bigger.

From the time series of vertical and horizontal displacements computed

at four European stations, it was noted, that when surface pressure data are used for computing the deformations, the displacements induced are very similar even if the mean pressure removed from the data set is averaged over different periods of time (3, 10, 23 years). On the other hand, when the deformation is induced by the sea level pressure field, the modelled time series are affected by a diurnal variation that is more evident during the summer months. This oscillation is probably related with the daily temperature excursion that is particularly big between May and August and since it does not appear in the time series considered for comparison (Sherneck, 2002; Petrov, 2003) and derived from surface pressure values, it was concluded that it is related to the sea level pressure data set. As a consequence particular attention has to be paid in the choice of the pressure data set (i.e. sea level or surface NCEP or ECMWF), used for the calculation. On the contrary, the dissimilarities between grids of interpolation have negligible effects on the final result. Another important source of disagreement between results when the surface pressure field is considered may derive from the dimensions of the land-sea mask chosen.

Even if in general it is not possible to produce a unique admittance coefficient for a certain station (this coefficient slightly changes with time for the same site), it has been noted, comparing the results from different years, that the coefficients uncertainty is only about ± 0.01 mm/mbar. This fact allows the use of averaged admittances for the locations considered. These transfer functions are also generally similar for the same site when they are derived from an area extending 2000 km or more from the point of interest.

The reasonable agreement found between our admittance coefficients (especially for Wettzell) and those published by other authors (Van Dam and Herring, 1994; Manabe et al., 1991; Van Dam et al., 1994; Van Dam and Wahr 1987, Van Dam 2002) and the good agreement of our time series of the vertical and tangential deformation and those proposed in particular by Petrov (Petrov, 2003), represent an important validation of our model. The variations in the coefficients at the other stations is mainly related with the sea-land mask chosen by the different authors.

For both an oceanless Earth model and an IBO model the simple admittance formula, calculated when an area extending 4000 km from the site is considered, gives a better approximation of the displacement at the sites considered than the Rabbel and Zschau formula (IERS conventions 1996) so their equation is generally not sufficient for correctly evaluating the vertical displacement at the coastal stations examined. The same result is valid when a worldwide distribution of point loads contribute to the deformation. It is suggested either the use of the convolution or the admittance derived from the convolution over the TCCE method.

In general the main contribution to the variation in the vertical deformation at a station situated in the south east region of the UK and along or nearby the north-west European coastline, is due to the storm surge effect. These areas exhibit the largest deformation effects due to non-tidal ocean loading (up to -30 mm of radial displacement, 10 mm in the tangential north-west direction and gravity changes of about 8μGal during extreme meteorological conditions). The effect decreased gradually inland with values of almost -10 mm in the vertical deformation, 1-2 mm in the horizontal and gravity variations of 2-3 μGal at distances of 150 km from the coast. Atmospheric pressure loading and storm surge loading have almost the same magnitude but opposite signs in the northern regions of the British Isles since in these areas the sea level responds approximately as an inverse barometer to pressure fluctuations, so it can be concluded that here in particular, it is very important to correct the geodetic measurements for both the effects of storm surge and atmospheric pressure loading. At coastal sites, atmospheric pressure loading correction alone might degrade the results. For stations situated well inland in Europe, atmospheric pressure loading is responsible for most of the deformation induced.

The loading effect induced by storm surges, varies faster (within hours), compared with that due to the atmospheric pressure loading (within 2-5 days). Furthermore, storm surge loading effects are generally larger (especially at high latitudes) but they affect small regions at a time (about 500 km of extension). Pressure variations usually affect very broad areas (1000-2000 km of extension).

The results from the seasonal and longer period vertical deformations and gravity variations due to storm surge loading bring us to the conclusion that if the long period deformation is considered for very extended periods of time, the meteorological disturbances can probably be neglected but in the cases studied here it is still important to consider the effect of meteorological factors. It was pointed out that generally a significant monthly mean displacement can also be achieved when several surge events happen in the same averaged period.

The effects of storm surge loading and atmospheric pressure loading on the deformations and gravity variations during two winter seasons characterized by extremely opposite NAO indices were investigated. It was concluded that when the NAO index is positive the vertical displacements produced by the storm surge loading alone are negative in sign i.e a sinking of the areas investigated. A tangential movement towards the center of the North Sea is also detected. The gravity variations associated are positive. When NAO index is negative the deformation produced is positive indicating a general rise of the regions interested. The tangential deformation has opposite di-

rection and the associated gravity change is negative. When the effects of atmospheric pressure loading are also considered, a general reduction in the deformation and gravity variation is common since in most of the regions considered the sea responds to pressure fluctuations as an inverted barometer. The inter-annual variability between such extreme winter seasons should be detectable in the vertical displacements measured by GPS, VLBI and SLR.

The comparison between the observed time series of the gravity variations at Membach, detected by the SG, and the modelled gravity changes during the periods of two main North Sea storm surge events, show that the maximums in the gravity measurements were contemporary with the modelled maximum peaks. The noisy effects in the observed time series were probably related with the hydrogeology of the region and therefore it was concluded that if the SG site was about 100 km closer to the coastline or in locations as Helgoland Island or Lowestoft where the signal is up to 4 times larger during storm events, the storm surge signal would stand out much more clearly above the other noise in the data. Gravity measurements corrected for atmospheric pressure loading may represent a good tool for detecting loading vertical deformation induced by storm surges especially when the gravimetric station is located near to the coastline.

The differences found between GPS data from the EPN and modelled values, can be explained by the fact that hourly modelled data were compared with weekly observed values. Furthermore the GPS time series do not represent just the effect of atmospheric pressure and storm surge loading but other components are surely present in the values observed. Large scale hydrological loading can affect the whole processed network and the errors can "spread" to various stations as a results of the processing strategy used. The results from a more detailed analysis carried out for the UK CGPS station of Lowestoft over the period of the main surge event of 2000 were more encouraging. It was concluded that there is some evidence that daily and sub-daily GPS results exhibit a pattern that is similar to the vertical deformation predicted at Lowestoft when hourly loading modelled effects are considered. The signal due to the loading deformation induced by atmospheric pressure and storm surges present in the GPS coordinates needs to be removed also in order to detect smaller transient or tectonics deformations.

7.1 Recommendations for future work

Significant work has been performed in this research project but there are some aspects that need further refinement. In this section some suggestions concerning the remaining problems or the future work are presented.

- In Chapter 4 it was shown that the time series of the loading deformations derived from the NCEP/NCAR pressure field are slightly different from those predicted using the ECMWF data set. The differences are between 1 and 5 mm. The main discrepancy in the loading results when a different pressure field is used is mainly related with the inaccuracy in the atmospheric pressure models. In the future it will be necessary to develop better meteorological models in order to reduce the discrepancies in the loading results. Furthermore the pressure field data should be available every hour in order to directly sum the associated loading effects with those induced by non-tidal ocean loading, even if the variation in atmospheric pressure is usually quite smooth.

- The transfer functions between the vertical displacement induced by atmospheric pressure loading and the pressure variation, derived from the convolution method (IBO hypothesis), represent an important tool for determining with good approximation the radial deformation at a site from the local pressure change. The admittance coefficients can be used when an accuracy of about 1 mm is required since the uncertainty in the results is smaller than that due to the use of different meteorological models. In particular the coefficients presented in this thesis (Table 4.4), are more accurate with respect to those previously available from the literature since a more detailed sea-land mask was used in the loading models.

- Admittances can be successfully used for correcting to a first order the geodetic measurements for the vertical loading deformation induced by atmospheric pressure and the non-tidal ocean in the northern part of the UK. In the areas situated in the south and especially on the east coast of England, the full convolution results are required, in particular during the winter season. In fact, in those regions the response of the sea level to pressure fluctuations is more complex than the inverted barometer response. For the tangential displacements the full convolution method is required in all the areas investigated.

- The use of GPS should be further investigated in the future, comparing the predicted and observed time series of the vertical and horizontal deformation as well, in order to validate and verify the models first and then for routinely correct the observations for the loading effects associated with atmospheric pressure and storm surge loading. In particular, if an experiment could be set up in the area of the north west Europe, a profile of GPS stations perpendicular to the Dutch-German-Danish coastlines should be set at 10-30 km spacing plus some GPS or/and

SG and AG stations at coastal sites, in order to detect the variation of storm surge and atmospheric pressure loading signals moving inland. Furthermore, the time series of the vertical and horizontal displacements induced should be compared, when possible, with observational data from other geodetic techniques such VLBI and SLR.

- A very large part of the gravity atmospheric effect is associated with the Newtonian attraction of the atmospheric mass within 50 km from the observation point. Empirical admittance factors are usually considered in order to account for this effect (typically -0.3 μGal/mbar for combined effects of attraction and loading). For SG stations where very precise atmospheric corrections are required for particular studies, the mass distribution within the vertical atmospheric column needs to be taken into account and therefore the method described by Merriam (1992) is required.

- Models of the loading effects associated with groundwater/soil moisture variations need to be developed and validated in particular for investigating the associated seasonal variations. The induced deformations and gravity changes averaged during the cold seasons characterized by opposite NAO indices should be studied as well. Furthermore predicted deformations and gravity variations due to groundwater loading should be removed from the geodetic measurements. At present there is still a great uncertainty in modelling the distribution of groundwater/soil moisture and therefore as a first step the accuracy of such models should be improved.

- At the present the Special Bureau for Loading (SBL) provides atmospheric pressure loading corrections for many GPS, VLBI and SLR stations. It is planned that in the future also corrections for the groundwater loading and the non-tidal ocean loading will be provided. However, the non-tidal ocean loading effects will be computed from a global ocean model with a fairly crude resolution in shelf sea areas, as for example the North Sea or the Gulf of Mexico. For the future it is suggested that more detailed resolution models be used, especially in those regions around the world where the storm surge loading effects are particularly important.

- Models of storm surge loading and attraction are also required for the GRACE satellite gravity mission. In the field of hydrological studies in north west Europe (in particular in areas like the North Sea characterized by stormy winter seasons), it would be beneficial to remove ocean

effects such as storm surge loading. Conversely there is much speculation of the ability of GRACE to remove loading signals in GPS, VLBI and SLR; this will need to be verified by storm surge and atmospheric pressure models.

Bibliography

Agnew D.C. 1997. *NLOADF: A program for computing ocean tide loading*, J. Geophys. Res., 102, no.B3, 5109-5110.

Amin M. 1982. *On analysis and prediction of tides on the west coast of Great Britain*, Geophysical Journal of the Royal astronomical Society, 68, 57-78.

Appenzeller C., Schwander J., Sommer S. and Stocker T.F. 1998. *The North Atlantic Oscillation and its imprint on precipitation and ice accumulation in Greenland*, Geophysical Research Letters, vol. 25, no. 11, pp. 1939-1942.

Ashkenazi V., Bingley R.M., Whitmore G.M. and Baker T.F. 1993. *Monitoring changes in mean-sea-level to millimeters using GPS*, Geophysical Research Letters, vol. 20, no. 18, pp. 1951-1954.

Baker T. F. 1984. *Tidal deformations of the Earth*, Sci. Prog., Oxf. 69: 197-233.

Baker T. F. 1985. *Methods of tidal loading computation*, Bull. D'Inform. Marees Terrestres (1985) 94: 6365-6373.

Baker T. F., Edge R. J. and Jeffries G., 1991. *Tidal gravity and ocean loading in Europe*, Geophys. J. Int. 107, 1-11.

Baker T. F. 1993. *Absolute sea level measurements, climate change and vertical crustal movements*, Global and Planetary Change, 8 (1993): 149-159 Elsevier Science Publishers B.V., Amsterdam.

Baker T.F., Curtis D.J. and Dodson A.H., 1995. *Ocean tide loading and GPS*, GPS world, March 1995, 54-59.

Baker T.F., Woodworth P.L., Blewitt G., Boucher C. and Woppelmann G. 1997. *A European network for sea level and coastal land level monitoring*, Journal of Marine Systems, 13(1-4): 163-171.

Bos M.S., 2000. *Ocean tide loading using improved ocean tide models*, PhD thesis, University of Liverpool.

Bos M.S., Baker T.F., Rothing K. and Plag H.-P. 2002. *Testing ocean tide models in the Nordic seas with tidal gravity observations*, Geophys. J. Int. 150, 687-694.

Boy JP., Gegout P. and Hinderer J. 2002. *Reduction of surface gravity data from global atmospheric pressure loading*, Geophys. J. Int. 149, 534-545.

Bruyninx C., Gurtner W. and Muls A. 1997. *The EUREF Permanent GPS Network*, Proceedings of EUREF Symposium, Ankara, Turkey, May 1996 EUREF Publication No. 5, ed. E. Gubler and H. Hornik, pp. 123-130.

Bruyninx C. 2000. *Status and Prospects of the EUREF Permanent Network*, Proceedings of EUREF Symposium, Prague, Czech Republic, June 1999 EUREF Publication No. 8, ed. E. Gubler, J.A. Torres and H. Hornik, pp. 42-46.

Bruyninx C. 2001. *Overview of the EUREF Permanent Network and Network coordination activities*, Proceedings of EUREF Symposium, Tromso, Norway, June 2000 EUREF Publication No. 9, ed. J.A. Torres and H. Hornik, pp. 24-30.

Bruyninx C. and Roosbeek F. 2002. *Network coordination of the EUREF Permanent Network*, EUREF Publication no.10, ed. J.A. Torres and H. Hornik, pp.42-48.

Bruyninx C., Carpentier G. and Roosbeek F. 2003. *EPN Monitoring: status and plans*, Proceedings of EUREF Symposium, Ponta Delgada, Portugal, June 2002.

Bruyninx C., Carpentier G. and Roosbeek F. 2004. *Today's EPN and its network coordination*, Proceedings of EUREF Symposium, Toledo, Spain, June 2003.

Bruyninx C. and Carpentier G. 2004.
http://www.epncb.oma.be/_dataproducts/timeseries/series_sm.html

Carrere L. and Lyard F. 2003. *Modeling the barotropic response of the global ocean to atmospheric wind and pressure forcing - comparison with observations*, Geophys. Res. Letters, vol.30, no.6, doi:10.1029/2002GL016473.

Crossley D., Hinderer J., Francis O., Hsu H.-T., Imanishi Y., Jentzsch G., Kaarianen J., Merriam J., Meurers B., Neumeyer J., Richter B., Shibuya K., Sato T. and Van Dam T. 1999. *Network of superconducting gravimeters benefits a number of disciplines*, Eos Trans. AGU, 80(11), pp.121-132.

Curtis D.J. 1996. *Ocean tide loading for geodetic applications*, PhD thesis, The University of Nottingham.

de la Vega-Leinert A. and Nicholls R. 2000. *North Sea vulnerability and adaptation - Implications of accelerated sea-level rise (ASLR) for UK*, in Proceeding of SURVAS Expert Workshop on European Vulnerability and Adaptation to impacts of Accelerated Sea-Level Rise (ASLR), Hamburg Germany, 19-21 June 2000.

Dickman S.R. 1988. *Theoretical investigation of the oceanic inverted barometer response*, J. Geophys. Res., 93: 14941-14946.

Dixon T. H., 1991. *An introduction to the Global Positioning System and some geological applications*, Rev. Geophys., 29: 249-276.

Dong D., Fang P., Bock Y., Cheng M.K. and Miyazaki S. 2002. *Anatomy of apparent seasonal variations from GPS-derived site position time series*, Journal of Geophysical Research vol. 107, no. B4 pages 1-9.

Donnelly J.P., Cleary P., Newby P. and Ettinger R. 2004. *Coupling instrumental and geological records of sea-level change: evidence from southern New England of an increase in the rate of sea-level rise in the late 19th century*, Geophys. Res. Letters, vol.31, L05203, doi:10.1029/2003GL018933.

Douglas B. C., 1991. *Global sea level rise*, Geophys. Res. Letters, 96(C4): 6981-6992.

Dziewonski A.M. and Anderson D.L. 1981. *Preliminary reference Earth model*, Phys. Earth Planet Int., 25:297-356.

Esselborn S. and Eden C. 2001. *Sea surface height changes in the North Atlantic Ocean related to the North Atlantic Oscillation*, Geophysical Research Letters, vol. 28, no. 18, pp.3473-3476.

Etkins R. and Epstein E. S. 1982. *The rise of Global Mean Sea Level as an Indication of Climate Change*, Science, 215 pp.287-289.

Farrell, W. E., 1972. *Deformation of the earth by surface loads*, Rev. Geophys Space Phys., 10(3), pages 761-797.

Flather R.A. and Davies A.M. 1976. *Note on a preliminary scheme for storm surge prediction using numerical models*, Quart. J. R. M. Soc., 102, pp.123-132.

Flather R.A. 1984. *A numerical model investigation of the storm surge of 31 January and 1 February 1953 in the North Sea*, Quart. J. R. M. Soc., 110, pp.591-612.

Flather R.A. and Williams J.A. 2001. *Investigation of operational model performance during 2000/2001*, Proudman Oceanographic Laboratory, Internal Document, No 139, 11 pp.

Flather R.A., Williams J.A., Blackman D.L. and Carlin L. 2001. *Fine grid surge model evaluation: Final report on MAFF/DEFRA contract FD 1203*, Proudman Oceanographic Laboratory, Internal Document, No 141, 52 pp.

Garland 1979. *The Earth's Shape and Gravity*, Pergamon Press, 183pp.

Goodkind J. M., 1986. *Continuous measurement of non-tidal variations of gravity*, J. Geophys. Res., 91: 9125-9134.

Heaps N. S. 1967. *Storm surge*, Oceanography and marine biology-an annual Review, 5, 11-47.

Hilmer M. and Jung T. 2000. *Evidence for a recent change in the*

link between the North Atlantic Oscillation and Arctic sea ice export, Geophysical Research Letters, vol. 27, no. 7, pp.989-992.

Hopewell H. 1999. *Environmental and instrumental effects of high precision gravimetry - A case study in Britain*, PhD thesis, The University of Edinburgh.

Hurrell J.W. 1995. *Decadal trend in the North Atlantic Oscillation - regional temperature and precipitation*, Science 269: 676-679.

Jones P.D., Jonsson T. and Wheeler D. 1997. *Extension to the North Atlantic Oscillation using early instrumental pressure observations from Gibraltar and south-west Iceland*, Int. J. Climat. vol. 17, 1433-1450.

Kaniuth K. and Huber S. in press. *Modelling vertical site displacements due to atmospheric pressure loading with Bernese software. A demonstration using EUREF data*, in EUREF Permanent Network (EPN); Developments and applications.

Lanzano P. 1982. *Deformations of an elastic Earth*, International Geophysical Series, vol.31 Academic Press. 226 pages.

Longman I.M. 1962. *A Green's function for determining the deformation of the Earth under surface Mass Loads - 1 Theory*, Journal of Geophysical Research, vol.67, No. 2 845-850.

Longman I.M. 1963. *A Green's function for determining the deformation of the Earth under surface Mass Loads - 2 Computations and numerical results*, Journal of Geophysical Research, vol.68, No. 2 485-496.

Lu J. and Greatbatch R.J. 2002. *The changing relationship between the NAO and northern hemisphere climate variability*, Geophysical Research Letters, vol. 29, no. 7, doi.10.102972001GL014052.

Lutherbacher J., Schmutz C., Gyalistras D., Xoplaki E. and Wanner H. 1999. *Reconstruction of monthly NAO and EU indices back to AD 1675*, Geophysical Research Letters, vol. 26, no. 17, pp. 2745-2748.

MacMillan D. S. and Gibson J. M. 1994. *Atmospheric pressure loading parameters from very long baseline interferometry observations*, Journal of Geophysical Research vol. 99, no.B9 pages 18081-18087.

Malkin Z.M. and Voinov A.V. 2000. *Preliminary results of processing of EUREF observations using non-fiducial strategy*, presented at the IGS Network Workshop 2000, Oslo, Norway, Jul 12-15, 2000.

Manabe S., Sato T., Sakai S. and Yokoyama K. 1991. *Atmospheric loading effect on VLBI observations*, in Proceeding of the AGU Chapman Conference on Geodetic VLBI: Monitoring Global Change, NOAA Tech. Rep., NOS 137 NGS 49, 111-122.

Mathers E.L. and Woodworth P.L. 2001. *Departures from the local inverse barometer model observed in altimeter and tide gauge data and in a global barotropic numerical model*, Journal Geophys. Research, vol.106, No.C4 6957-6972.

Melchior P. 1983. *The tides of the planet Earth*, 641 pp., Pergamon, New York.

Merriam J.B. 1992. *Atmospheric pressure and gravity*, Geophys. J. Int. 109:488-500.

Mehta V.M., Suarez M.J., Manganello J.V. and Delworth T.L. 2000. *Oceanic influence on the North Atlantic Oscillation and associated northern Hemisphere climate variations: 1959-1993*, Geophysical Research Letters, vol. 27, no. 1, pp.121-124.

Munekane H. and Matsuzaka S. 2004. *Nontidal ocean mass loading detected by GPS observations in the tropical Pacific region*, Geophysical Research Letters, vol. 31, L08602, doi.10.1029/2004GL019773.

Munk W. and MacDonald G. 1960. *The rotation of the Earth*, Cambridge University Press. New York 323 pages.

Nerem R. S. and Mitchum 2001. *Sea level change*, in : Fu L. and Cazenave A. (Eds.), Satellite Altimetry and earth Science, pp.329-349. Academic Press, San Diego.

Okubo S., Yoshida S., Sato T., Tamura Y. and Imanishi Y.1997. *Verifying the precision of a new generation absolute gravimeter FG5 - Comparison with superconducting gravimeters and detection of oceanic loading tide*, Geophysical Research Letters, vol. 24, no. 4, pp.489-492.

Paeth H., Hense A., Glowienka-Hense R. and Voss R. 1999. *The North Atlantic Oscillation as an indicator for greenhouse-gas induced regional climate change*, Climate Dynamics, 15:953-960.

Pagiatakis S.D. 1992. *Program LOADSDP for the calculation of ocean load effects*, Manusc. Geod., 17 315-320.

Peixoto J.P. and Oort A.H., 1992. *Physics of climate*, American Institute of Physics, New York 520 pp.

Peltier W. R. and Tushingham A. M., 1989. *Global sea level rise and the greenhouse effect: might they be related?*, Science, 244: 806-810.

Peltier W. R. and Tushingham A. M., 1991. *Influence of glacial isostatic adjustment on tide gauge measurements of secular sea level change*, Journal of Geophysical Research, vol.96, No. B4 6779-6796.

Petrov L. 2003.
http : //gemini.gsfc.nasa.gov/aplo/aplo.shtm

Petrov L. and Boy JP. 2004. *Study of the atmospheric pressure signal in VLBI observations*, Journal Geophys. Research, vol.109, No.B03405, doi:10.1029/2003JB002500, 2004.

Ponte R.M., Salstein A. and Rosen R.D. 1991. *Sea level response to pressure forcing in a barotropic numerical model*, Journal Physical Oceanography vol.21 1043-1057.

Ponte R.M. and Ray R., D. 2002. *Atmospheric pressure corrections in geodesy and oceanography: a strategy for handling air tides*, Geophysical Research Letters, vol. 29, no. 24, pp.2153-2159.

Ponte R.M. 1992. *The sea level response to a stratified ocean to barometric pressure forcing*, Journal Physical Oceanography vol.22 109-113.

Pugh D. T. 1987. *Tides, Surges and mean sea level*, John Wiley, Chichester, 472 pp.

Rabbel W. and Schuh H. 1986. *The influence of atmospheric loading on VLBI-experiments*, in J. Geophys., 59, 164-170.

Rabbel W. and Zschau J. 1985. *Static deformations and gravity changes at the earth's surface due to atmospheric loading*, J. Geophys., 56, 81-99.

Rodwell M.J., Rowell D.P. and Folland C.K. 1999. *Oceanic forcing of the wintertime North Atlantic Oscillation and European climate*, Science, 398: 320-323.

Sasagawa G.S., Klopping F., Niebauer T.M., Faller J.E. and Hilt R.L.1995. *Intracomparison tests of the FG5 absolute gravity meters*, Geophysical Research Letters, vol. 22, no. 4, pp.461-464.

Sherneck H.G. 1991. *A parameterized solid Earth tide model and ocean tide loading effects for global geodetic baseline measurements*, Geophys. J. Int., 106, 677-694.

Sherneck H.G. 2002.
http://www.oso.chalmers.se/ hgs/apload.html

Schmutz C., Lutherbacher J., Gyalistras D., Xoplaki E. and Wanner H. 2000. *Can we trust proxy-based NAO index reconstructions?*, Geophysical Research Letters, vol. 27, no. 8, pp.1135-1138.

Sclater, J. G. and Christie P.A.F. 1980. *Continental stretching and explanation of the post mid-Cretaceous subsidence of the central North Sea Basin*, Journal Geophys. Research, vol.85, pp.3711-3739.

Stepanov V.N. and Hughes C.W. 2004. *Parameterization of ocean self-attraction and loading in numerical models of the ocean circulation*, Journal Geophys. Research, vol.109, doi:10.1029/2003JC002034.

Stephenson D.B. 1999.
http://www.met.rdg.ac.uk/cag/NAO

Stolz A. and Larden D.R. 1979. *Seasonal displacement and deformation of the Earth by the atmosphere*, Journal of Geophysical Research, vol.84, No. B11 6185-6194.

Sun H.P., Ducarme B., Dehant V. 1993. *Preliminary Investigation of the atmospheric pressure effect on vertical displacement and gravity observations*, Bulletin dInformations des Marees terrestres, 114 pp.

8134-8162.

Sun H.P., Ducarme B. and Dehant V. 1994. *Theoretical calculation of the atmospheric gravity Green functions*, paper presented at Working Group on High Precision Tidal Data Processing, Calibration, Theoretical Tide Model, Aug. 30th - Sep. 2nd 1994, Bonn, Germany.

Sun H.P. 1995. *Static deformation and gravity changes at the Earth's surface due to atmospheric pressure*, PhD. Thesis Cath. Univ. Louvain.

Sun H.P., Ducarme B. and Dehant V. 1995. *Effect of the atmospheric pressure on surface displacements*, Journal of Geodesy, 70:131-139.

Takacs B. and Bruyninx C. 2002. *Quality checking in the raw data of the EUREF Permanent Network*, EUREF Publication No. 10, ed. J.A. Torres and H. Hornik, pp. 53-61.

Teferle F.N., Bingley R.M., Dodson A.H., Penna N.T., Baker T.F. 2001. *Using GPS to separate crustal movements and sea level changes at tide gauges in the UK*, Vertical reference system, Cartagena, Colombia 20-23 February 2001, IAG Symposia vol.124 pp.264-269, edited by Drewes et al., Springer - Verlog.

Ulbrich U. and Christoph M. 1999. *A shift of the NAO and increasing storm track activity over Europe due to anthropogenic greenhouse gas forcing*, Climate Dynamics, 15:551-559.

Van Camp M., Camelbeeck T. and Richard P. 2003. *The FG5 absolute gravimeter: metrology and geophysics*, Physicalia magazine (Journal of the Belgian Physical Society), 25 (3), pp. 161-174.

Van Dam T.M. and Wahr J.M. 1987. *Displacements of the Earth's surface due to atmospheric loading: effects on gravity and baseline measurements*, Journal of Geophysical Research, vol.92, No. B2 1281-1286.

Van Dam T.M. 1991. *Atmospheric loading response of the solid Earth and oceans*, PhD thesis, University of Colorado at Boulder.

Van Dam T.M., Bewitt G. and Heflin M.B. 1994. *Atmospheric pressure loading effects on Global Positioning System coordinate determinations*, Journal of Geophysical Research, vol.99, No. B12 23939-23950.

Van Dam T.M. and Herring T. A. 1994. *Detection of atmospheric pressure loading using very long baseline interferometry measurements*, J. Geophys. Res., 99, B3, pages 4505-4517.

Van Dam T.M., Wahr J., Chao Y. and Leuliette E. 1997. *Predictions of crustal deformation and of geoid and sea-level variability caused by oceanic and atmospheric loading*, Geophys. J. int., 129:507-517.

Van Dam T.M. and Francis O. 1998. *Two years of continuous measurements of tidal and nontidal variations of gravity in Boulder, Colorado*, Geophys. Res. Lett., 25 pp. 393-396.

Van Dam T.M., Wahr J.M., Milly P.C.D., Shmakin A.B., Blewitt G., Lavallee D. and Larson K.M. (2001). *Crustal displacements due to continental water loading*, Geophysical Research Letters, vol.28, No. 4 pages 651-654.

Van Dam T.M. 2002.
http://www.abl.statkart.no/products/regression/iers_regression.dat

Vanicek P. & Krakiwsky E., 1986. *Geodesy: the concepts*, Elsevier Science Publishers B.V., Amsterdam pp.691.

Wadhams P. and Munk W. 2004. *Ocean freshening, sea level rise, sea ice melting*, Geophysical Research Letters, vol. 31, L11311, doi.10.1029/2004GL020039.

Wakelin S.L., Woodworth P.L., Flather R. A. and Williams J. A. 2003. *Sea level dependence on the NAO over the NW European continental shelf*, Geophysical Research Letters, vol. 30, no 7:561-564.

Wells N. 1997. *The atmosphere and ocean. A physical introduction*, John Wiley & Sons, Chichester pp.394.

Wessel P. and Smith W.H.F. 1991. *Free software helps map and display data*, Eos Trans. AGU, 72, 441.

Wessel P. and Smith W.H.F. 1995. *A new version of generic mapping tools (GMT)*, Eos Trans. AGU, 76(33), 329.

Williams S.D.P., Baker T. F. and Jeffries G., 2001. *Absolute gravity measurements at UK tide gauges*, Geophysical Research Letters, 28, 2317-2320.

Williams S. D. P., Bock Y., Fang P., Jamason P., Nikolaidis R.M., Prawirodirdjo L., Miller M. and Johnson D.J., 2004. *Error analysis of continuos GPS position time series*, Journal of Geophysical Research , vol.109, B03412, doi:10.1029/2003JB002741.

Woodworth P.L. and Player R. 2003. *The permanent service for mean sea level. An update to the 21st century*, Journal of Coastal research, 19(2), pp. 287-295.

Woolf D.K., Shaw A.G.P. and Tsimplis M.N. 2003 *The influence of the North Atlantic Oscillation on sea-level variability in the north Atlantic region*, The global atmosphere and Ocean system, vol.9, no. 4:145-167.

Wunsch C.1972. *Bermuda sea level in relation to times, weather and baroclinic fluctuation*, Rev. Geophys. Space Phys., 10, 1-49.

Yan Z., Tsimplis M.N. and Woolf D.K. 2004. *Analysis of the relationship between the North Atlantic Oscillation and sea-level changes in northwest Europe*, Int. J. of Climatol. 24: 743-758.

Appendix A

Describing the elastic deformation of the solid Earth

A.1 Integration of the equation of motion

The elastic deformation of the Earth is governed by the equations of motion. They are the linearized equation for the conservation of linear momentum and Poisson's equation:

$$\rho\frac{\partial^2 \mathbf{u}}{\partial t^2} = \nabla\cdot\tau - \nabla(\rho g\ \mathbf{u}\cdot\ \mathbf{e_r}) - \rho\nabla\ \phi + g\nabla\cdot(\rho\ \mathbf{u})\ \mathbf{e_r}$$
$$\nabla\phi^2 = -4\pi G\nabla\cdot(\rho\ \mathbf{u}) \qquad \text{(A.1)}$$

ρ and g are the density and the gravitational acceleration in the absence of motion (hydrostatic equilibrium state) while G is the Newtonian's gravitational constant. $\mathbf{u}$ represents the displacement, τ is the stress tensor and $\mathbf{e_r}$ is the unit vector in the radial direction ($\mathbf{e_\theta}$ for the tangential direction) since a spherical system is considered.

The gravitational potential ϕ, is the sum between the perturbation in the ambient gravitational potential (ϕ_1) i.e. the potential of the distorted density field of the Earth and the potential of any externally applied gravitational force (ϕ_2) as for example is a surface load.

The potential of the applied force satisfies the Laplace's equation within the Earth.

Equation (A.1) is solved in the hypothesis of a spherically symmetric Earth model and its properties are then only a function of the radius r.

If it is also imposed the condition that at the free surface the tangential stress vanishes, equation (A.1) reduces to a spheroidal system of equations

in the three scalar variables u_r, u_θ and ϕ. Expanding $\mathbf{u}$ and ϕ in vector spherical harmonics we have:

$$\mathbf{u} = \sum_{n=0}^{\infty} \left(U_n(r) P_n(\cos\theta)\ \mathbf{e_r} + V_n(r) \frac{\partial P_n(\cos\theta)}{\partial \theta}\ \mathbf{e}_\theta \right)$$

$$\phi = \sum_{n=0}^{\infty} \Phi_n(r) P_n(\cos\theta) \qquad \text{(A.2)}$$

The solution of equation (A.2) depends just upon the latitude because the surface load was assumed axially symmetric. The terms $P_n(\cos\theta)$ are called the Legendre polynomials with n denoting their degree and m their order. Only the particular Legendre polynomial order $m = 0$ was used in the expansion.

The radial and tangential components of the stress tensor, τ_{rr} and $\tau_{r\theta}$, and the variable q related with the potential gradient are then introduced. They are dependent variables derived from the stress-strain relations. In particular q is defined as:

$$q = \frac{\partial \phi}{\partial r} + \frac{(n+1)}{r}\phi + 4\pi G \rho u_r$$

When τ_{rr}, $\tau_{r\theta}$, and q are expressed in terms of their Legendre transforms, they are represented by $T_{r,n}$, $T_{\theta,n}$ and Q_n. Transforming equation (A.1) leads to the matrix equation:

$$\frac{d\,\mathbf{Y}}{dr} = \mathbf{AY} \qquad \text{(A.3)}$$

where $\mathbf{Y} = (U_n, V_n, T_{r,n}, T_{\theta,n}, \Phi_n, Q_n)$ and $\mathbf{A}$ is a 6x6 coefficients matrix depending upon the radial distance r, the order of the harmonic approximation n, the compressibility $\lambda(r)$, the rigidity $\mu(r)$ and the density $\rho(r)$.

Choosing the appropriate boundary conditions equation (A.3) is solved by numerical integration of the six simultaneous differential equations within the Earth (from $r = 0$ to $r = r_{Earth}$). For the computation, non-dimensional variables are introduced and the numerical integration starts from a certain $r = r_0$ below which the Earth is assumed to be an homogeneous sphere (λ, μ, ρ are constants). The choice of r_0 depends upon the accuracy required.

A.2 Surface boundary conditions

For the solution of the body force problem regularity of the solution at the origin is required, continuity of stresses, deformations, potentials and their gradients across internal boundaries. The surface loading problem involves additional boundary conditions that are instead not needed in the body force problem.

The boundary conditions at the deformed surface of the Earth are:

1. The normal stress must equal the applied load acting at the surface ($\tau_{rr}(r_{Earth}) = -g\gamma$ with γ applied surface mass);
2. The tangential stress must vanish $\tau_{r,\theta}(r_{Earth}) = 0$;
3. The potentials ϕ_1, ϕ_2 and $(\nabla\phi_1 + 4\pi G\rho u) \cdot e_r$ are continuous while $e_r \cdot \nabla\phi_2$ must change by $4\pi g\gamma$ across the boundary $r = r_{Earth}$.

Since the transformed potential at the Earth's surface for a point mass load is:

$$\Phi_{2,n} = \frac{r_{Earth} \cdot g}{m_e} \tag{A.4}$$

with m_e mass of the Earth. The transformed boundary conditions became:

$$\begin{aligned} T_{r,n}(r_{Earth}) &= -g\frac{2n+1}{4\pi r_{Earth}^2} \\ T_{\theta,n}(r_{Earth}) &= 0 \\ Q_n(r_{Earth}) &= -4\pi G\frac{2n+1}{4\pi r_{Earth}^2} \end{aligned} \tag{A.5}$$

With these conditions, U_n, V_n and $\Phi_n(r)$ are determined for the point mass load.

A.3 Love numbers (load deformation coefficients)

Generally in geophysical literature the load numbers are introduced as non-dimensional quantities related to the solution of the spherical deformation.

Since these solutions are functions of the boundary conditions assumed, there can be a variety of load numbers according to the loading conditions assumed.

The Love numbers are h_n, l_n and k_n, they are functions of the two variables n and r. The Love number h_n is used for describing the vertical deformation while l_n is applied in the determination of the tangential displacement. A combination of Love numbers is instead employed in the formulation of the gravity response.

For U_n, V_n and $\Phi_{1,n}$ arising from an axially symmetric force field, Love numbers are described as follows:

$$\begin{bmatrix} U_n(r) \\ V_n(r) \\ \Phi_{1,n}(r) \end{bmatrix} = \Phi_{2,n}(r) \begin{bmatrix} \frac{h_n(r)}{g} \\ \frac{l_n(r)}{g} \\ k_n(r) \end{bmatrix}$$

where $\Phi_{2,n}$ was defined in equation (A.4).

Farrell (1972) solved the equations of motion for a spherical, layered, self gravitating, elastic Earth loaded by a n^{th} degree surface mass layer. He evaluated the loading Love numbers up to a degree n= 10000.

Longman (1963) has described the load Love numbers as load deformation coefficients, while Munk and MacDonald (1960) have distinguished between tidal Love numbers and load Love numbers, adding to the latter a superscript prime. Since in this thesis we are only interested on the surface loading problem, we will not distinguish between the two types. Everytime we refer to the load deformation coefficients, we will always consider the load Love numbers.

A.4 Green's functions

The determination of the Love numbers is just the first step in the computation of the deformation of the Earth by a surface load distribution and the response of our planet to a point load has to be considered.

Longman (1962) was the first scientist who instead of expressing the surface distribution of mass as a sum of surface zonal harmonics, introduced the Green's functions for calculating the deformation of the spherical Earth.

The Green's functions give the response of the Earth to a point mass load derived from a certain model Earth. They describe the radial and tangential displacements and the gravitational potential perturbation caused by the point surface mass load as a function of the angular distance from the load. The proper weighted sums of the load Love numbers for each degree n must be added up to form the Green's functions.

Longman (1963) numerically calculated these functions for distances greater than 30 degrees from the point load, using load Love numbers up to a degree n equal 40. Farrell (1972), using Love numbers up to degree 10000, calculated the Green's functions at all distances for a Gutenberg-Bullen A Earth model. He considered the response of the Earth to a circular disc load, in the limit as the radius of the disc goes to zero. So a distribution of point loads is generated and the total loading can be calculated by summing the deformation produced by each one of them.

The Green's functions for the surface point mass load are formed by substituting the expression of Love numbers and $\Phi_{2,n}$ (see Equation A.4) in equation (A.2) :

$$u(\theta) = \frac{r_{Earth}}{m_e} \sum_{n=0}^{\infty} h_n P_n(\cos\theta)$$
$$v(\theta) = \frac{r_{Earth}}{m_e} \sum_{n=1}^{\infty} l_n \frac{\partial P_n(\cos\theta)}{\partial\theta} \tag{A.6}$$

Equation (A.6) represents the Green's functions for the radial and the tangential displacements.

It has to be noted that in the second expression of the equation (A.6) the summation for the displacement starts at $n = 1$. This can be explained by the fact that a load of P_0 form is uniform over the whole Earth and causes radial displacement but neither tangential displacement nor potential perturbation.

The Green's functions depend both on r and the angular distance θ, but in this particular case just the dependence upon θ is considered since the radius r is equal to r_{Earth} at the geodetic measurement sites.

When n becomes large, h_n, nl_n and nk_n approach constant values h_∞, $k_\infty$and l_∞ and the Green's functions become:

$$u(\theta) = \frac{r_{Earth} h_\infty}{m_e} \sum_{n=0}^{\infty} P_n(\cos\theta) + \frac{r_{Earth}}{m_e} \sum_{n=0}^{\infty} (h_n - h_\infty) P_n(\cos\theta)$$
$$v(\theta) = \frac{r_{Earth} l_\infty}{m_e} \sum_{n=1}^{\infty} \frac{1}{n} \frac{\partial P_n(\cos\theta)}{\partial\theta} + \frac{r_{Earth}}{m_e} \sum_{n=1}^{\infty} (nl_n - l_\infty) \frac{1}{n} \frac{\partial P_n \cos\theta}{\partial\theta} \tag{A.7}$$

The first part of the sum in both the expressions is known analytically, while the second summation terminates after a finite number of terms since

$(h_n - h_\infty)$ and $(nl_n - l_\infty)$ are zero above $n = N$, the maximum Legendre degree. It follows then (Farrell, 1972):

$$u(\theta) = \frac{r_{Earth}}{2m_e \sin\frac{\theta}{2}} h_\infty + \frac{r_{Earth}}{m_e} \sum_{n=0}^{N} (h_n - h_\infty) P_n \cos\theta$$

$$v(\theta) = -\frac{r_{Earth}}{m_e} l_\infty \frac{\cos\frac{\theta}{2}[1 + 2\sin\frac{\theta}{2}]}{2\sin\frac{\theta}{2}[1 + \sin\frac{\theta}{2}]} + \frac{r_{Earth}}{m_e} \sum_{n=1}^{N} (nl_n - l_\infty) \frac{1}{n} \frac{\partial P_n \cos\theta}{\partial\theta} \tag{A.8}$$

Equation (A.8) is now a finite sum (equation A.7 was an infinite sum), but it still converges quite slowly because the term P_n falls out only as $n^{-\frac{1}{2}}$. Different contrivances such as the use of Euler transformation of series or other appropriate numerical transforms can be employed to accelerate the convergence and this is especially applied when n is large and θ is quite small, in fact in this case h_n, l_n and P_n are slowly varying functions of n.

For forming the Green's functions, the Love numbers must be known over a large range of Legendre degree n, typically up to $n = 10000$ but it is not necessary to integrate the equations of motion for each degree n but an interpolation can instead be used on a sparse table of load coefficients.

A similar expression can be written also for the gravitational potential perturbation caused by the surface mass load and the third Green's function $g(\theta)$ can be defined.

The computation of the gravity Green's functions is performed summing up the effects due to the loading deformation produced, the Newtonian gravitational attraction of the extra mass determining the loading and the changes in potential due to the redistribution of mass within the Earth. This results in a combination of Love numbers.

$$g(\theta) = \frac{g}{m_e} \sum_{n=0}^{\infty} (n + 2h_n - (n+1)k_n) P_n(\cos\theta) \tag{A.9}$$

In Equation (A.9), the acceleration is assumed positive upward. The first term in bracket is the component of the direct gravitational attraction perpendicular to the surface at the station and is called the Newtonian acceleration g^N and it is summed exactly to give:

$$g^N(\theta) = -\frac{g}{4m_e \sin\frac{\theta}{2}}$$

Also the elastic acceleration g^E can be defined, it arises from the Earth's elastic deformation.

$$g^E = g - g^N$$

In the case of a perfect rigid Earth this contribution would vanish.

Green's functions are also defined for tilt and strain but they will not be discussed here.

Appendix B

Vertical deformation induced by sea level atmospheric pressure and derived admittance coefficients (NIBO and IBO hypotheses)

In this Appendix are presented the plots representing the relationships between vertical deformation and sea level pressure for the sites of Lowestoft and Herstmonceux in both the NIBO and the IBO assumptions. When an oceanless Earth model is assumed, an air pressure correction of -0.5 mm/mbar can be consider in a first approximation as the coefficient for determining the vertical displacement induced from the sea level pressure value at the centre of the cell in which the site is situated. It can be noted that for the IBO hypothesis, the transfer function between air pressure and deformation is smaller than in the NIBO case.

The plots representing the admittance coefficients computed fitting a linear curve to the results obtained with the convolution method in the NIBO ad IBO hypotheses, are also presented for the two stations.

Finally the graphics with residuals are presented; for the convolution method compared to multiplying the admittance characteristics for a certain year by the local derived pressure, and for the convolution method compared to Rabbel & Zschau (1985) method.

B.1 Relationships between vertical deformation and sea level pressure variations

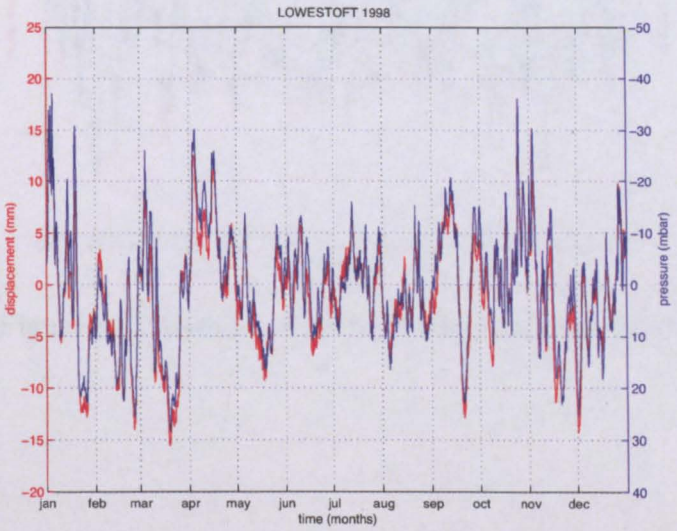

Figure B.1: Vertical displacement and pressure variations at Lowestoft during 1998. The red curves are the vertical displacement (in mm) during the year 1998, from all the cells within an area of 4000 km from Lowestoft. The blue curves are the pressure variation (in millibar) inducing the deformation (NIBO hypothesis)

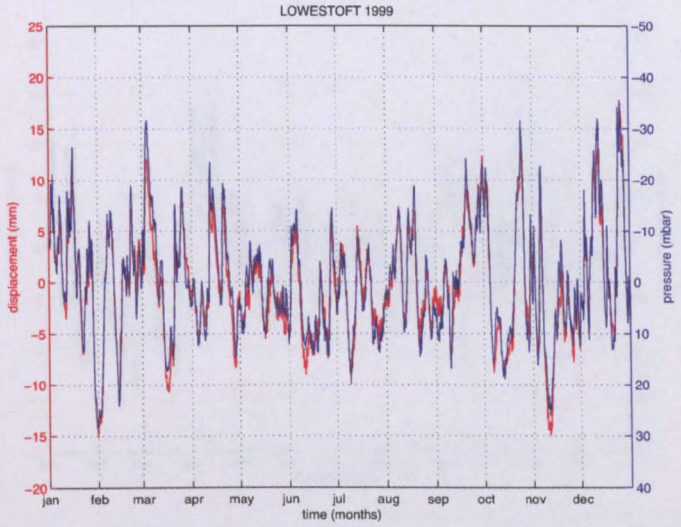

Figure B.2: Same as Figure B.1 but for year 1999.

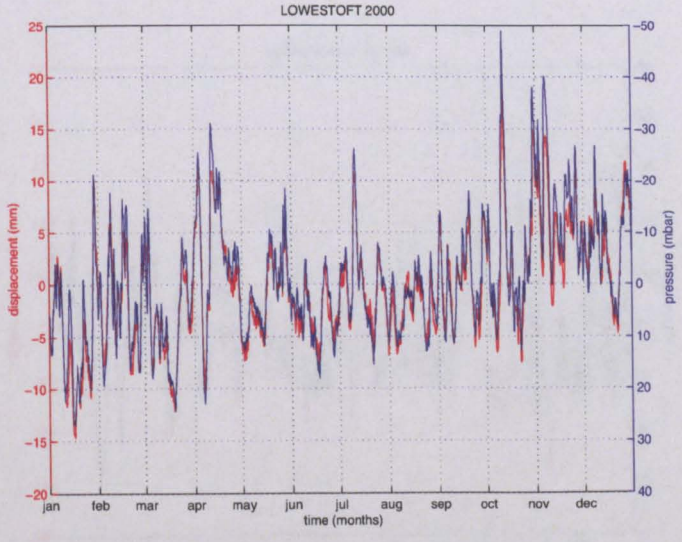

Figure B.3: Same as Figure B.1 but for year 2000.

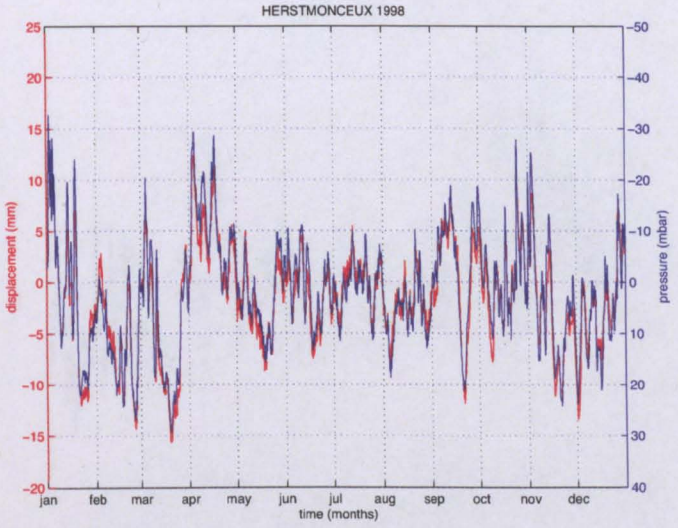

Figure B.4: Vertical displacement and pressure variations at Herstmonceux during 1998. The red curves are the vertical displacement (in mm) during the year 1998, from all the cells within an area of 4000 km from Herstmonceux. The blue curves are the pressure variation (in millibar) inducing the deformation (NIBO hypothesis)

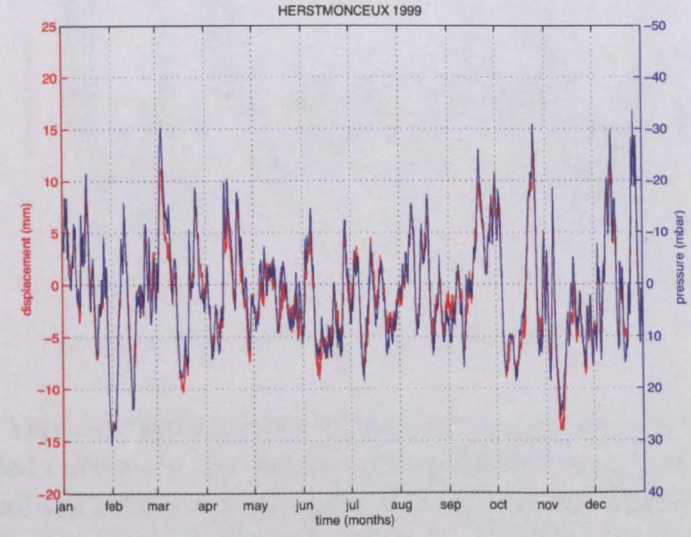

Figure B.5: Same as Figure B.4 but for year 1999.

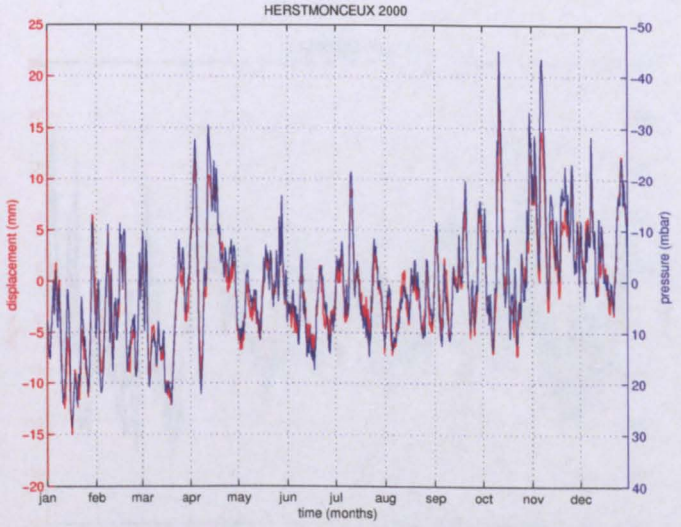

Figure B.6: Same as Figure B.4 but for year 2000.

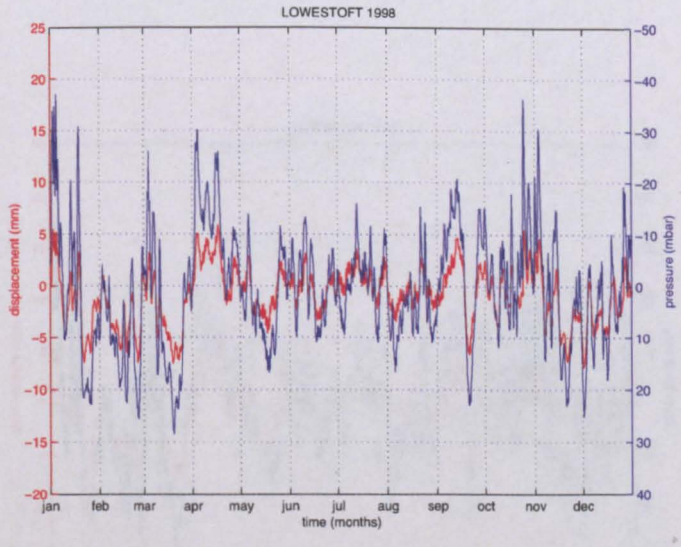

Figure B.7: Vertical displacement and pressure variations at Lowestoft during 1998. The red curves are the vertical displacement (in mm) during the year 1998, from all the cells within an area of 4000 km from Lowestoft. The blue curves are the pressure variation (in millibar) inducing the deformation (IBO hypothesis)

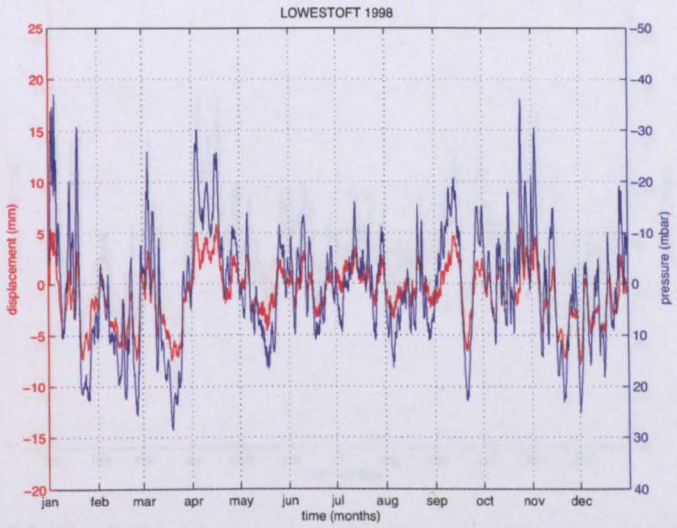

Figure B.8: Same as Figure B.7 but for year 1999.

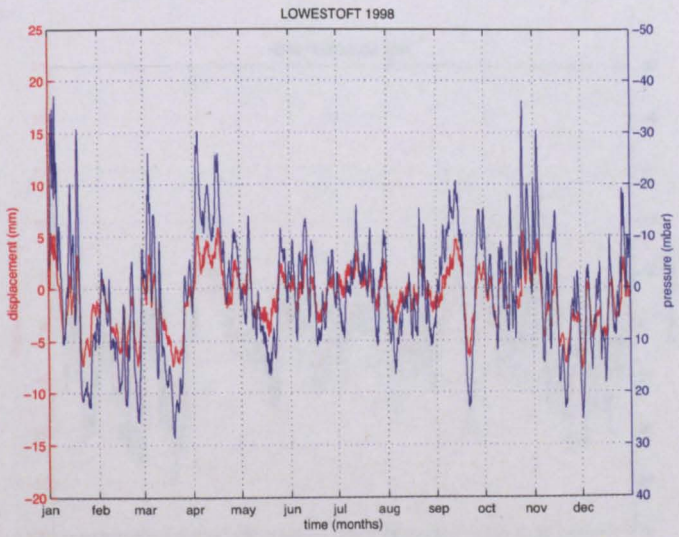

Figure B.9: Same as Figure B.7 but for year 2000.

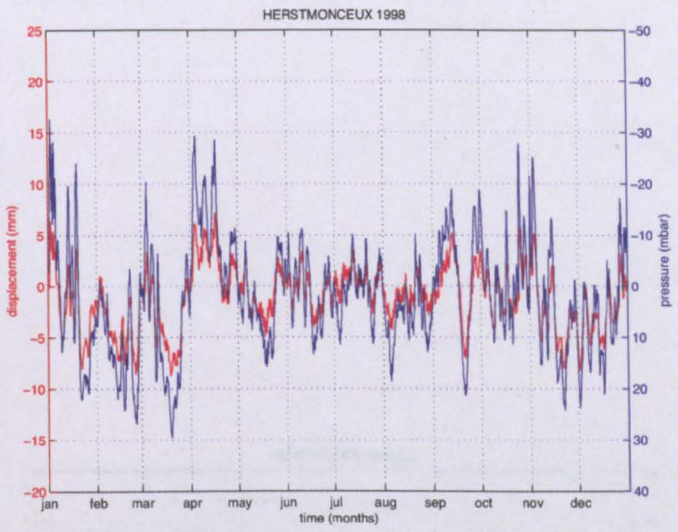

Figure B.10: Vertical displacement and pressure variations at Herstmonceux during 1998. The red curves are the vertical displacement (in mm) during the year 1998, from all the cells within an area of 4000 km from Herstmonceux. The blue curves are the pressure variation (in millibar) inducing the deformation (IBO hypothesis)

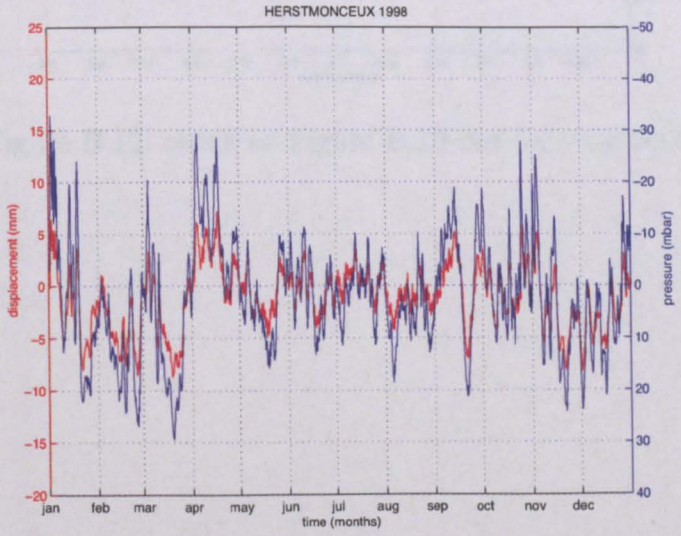

Figure B.11: Same as Figure B.10 but for year 1999.

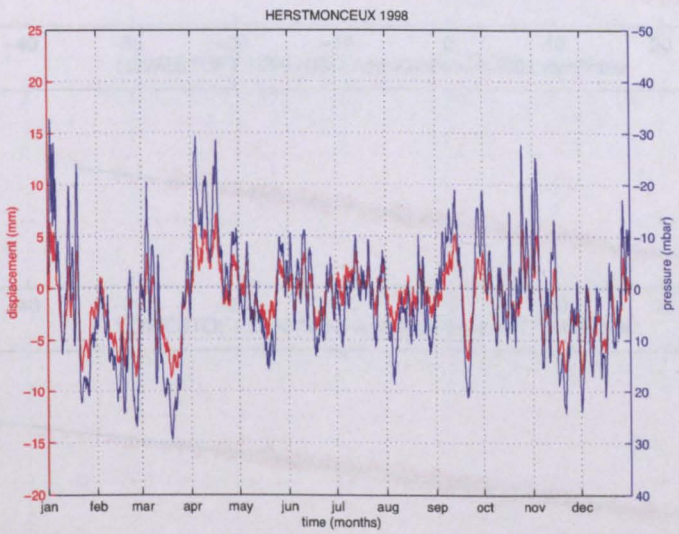

Figure B.12: Same as Figure B.10 but for year 2000.

B.2 Admittance coefficients

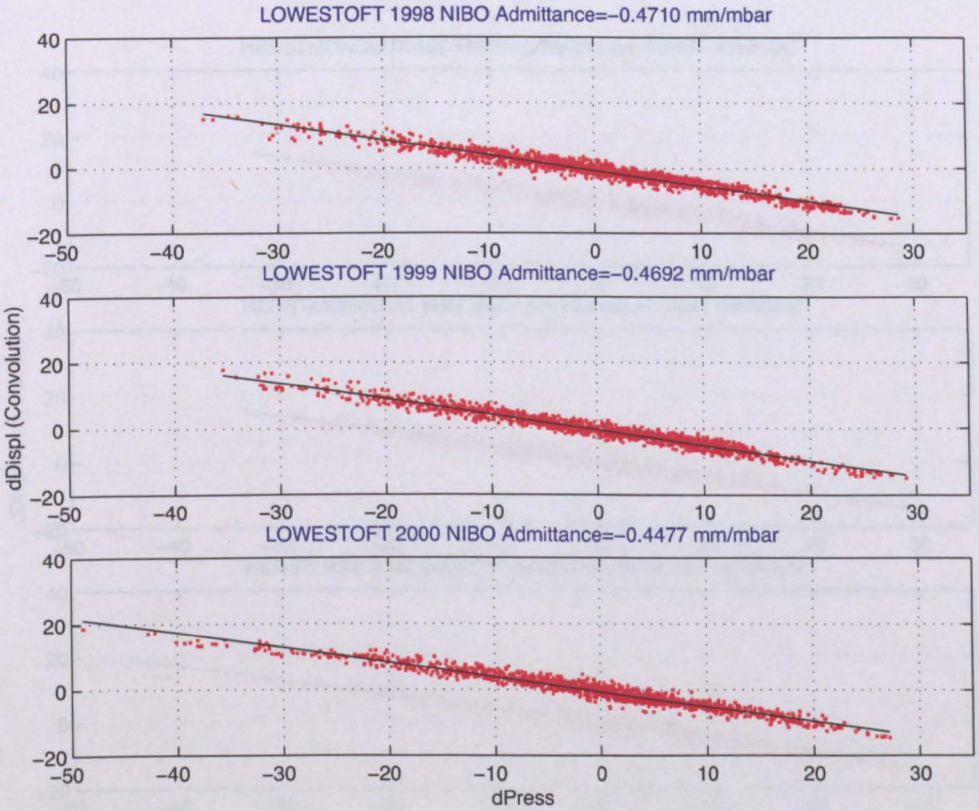

Figure B.13: Admittance coefficients for the period considered for the sites of Lowestoft (CONV method applied to an area of 4000 km from the site - NIBO hypothesis).

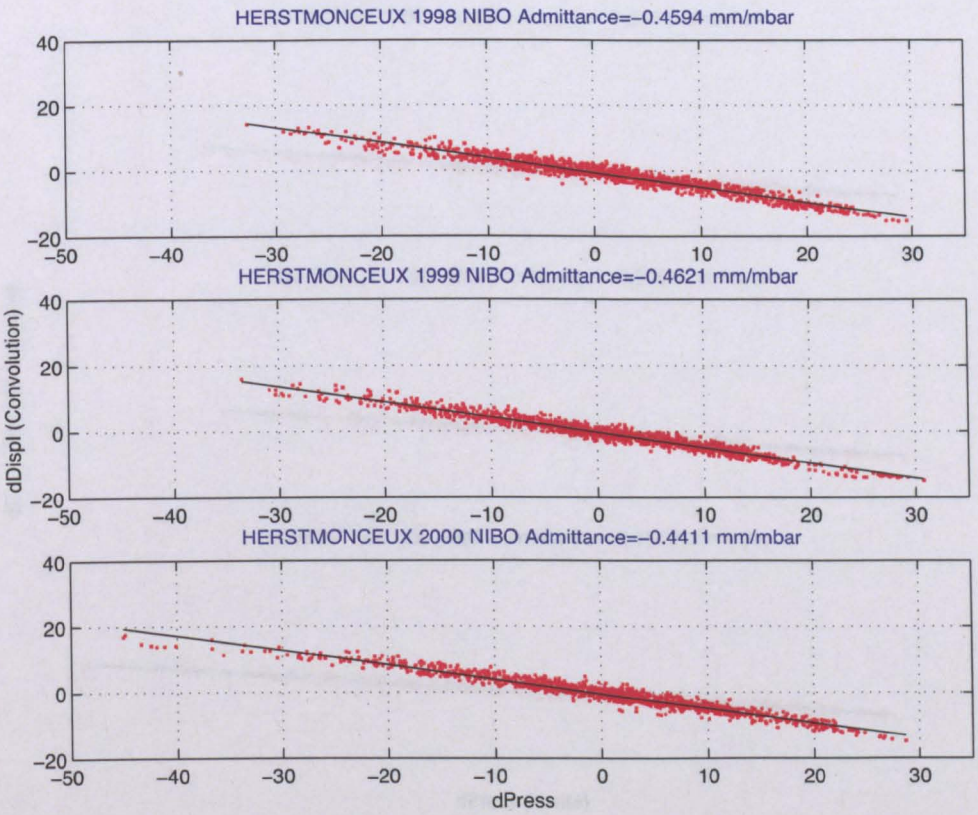

Figure B.14: Admittance coefficients for the period considered for the sites of Herstmonceux (CONV method applied to an area of 4000 km from the site - NIBO hypothesis).

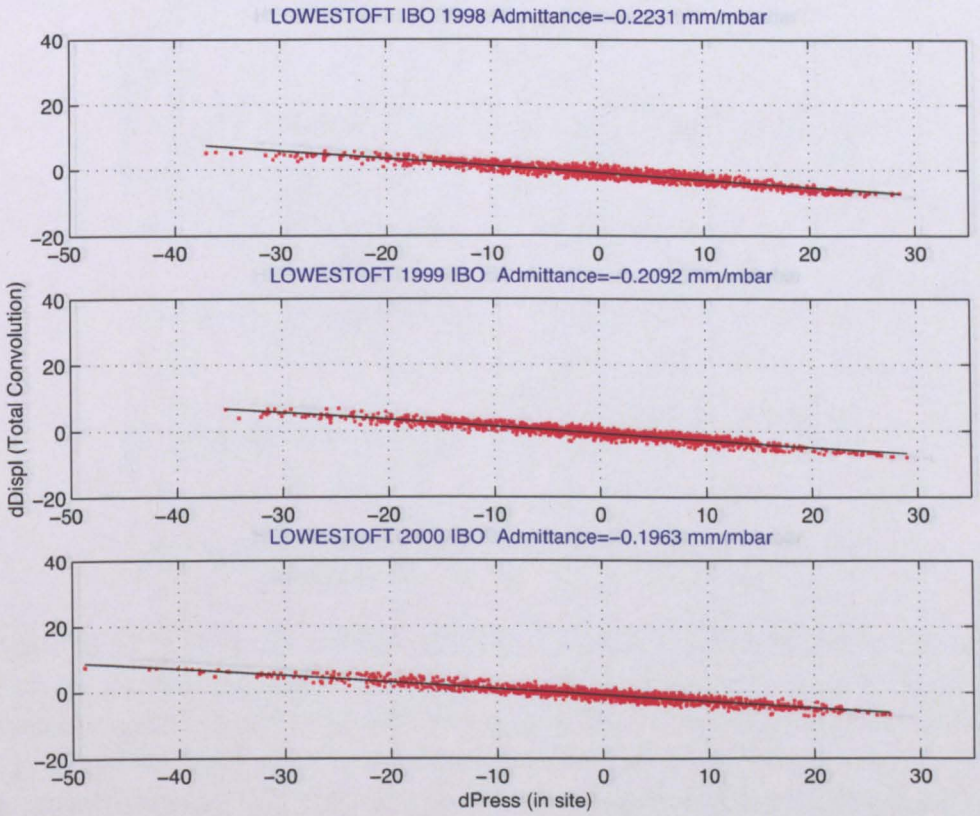

Figure B.15: Admittance coefficients for the period considered for the sites of Lowestoft (CONV method applied to an area of 4000 km from the site - IBO hypothesis).

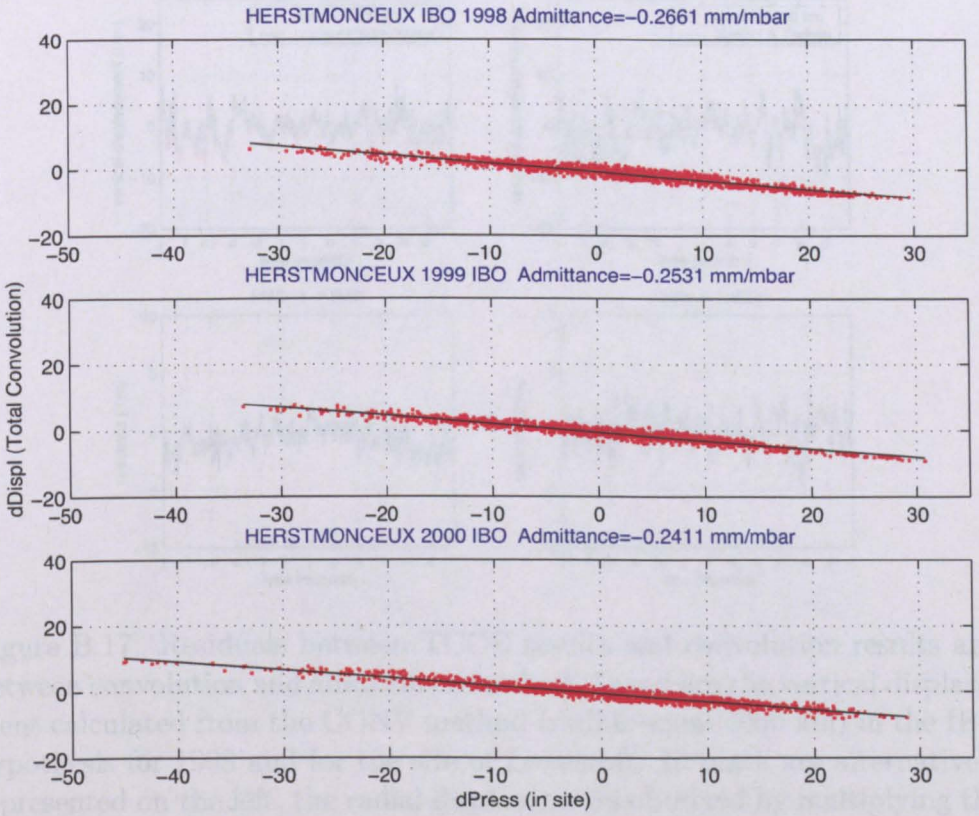

Figure B.16: Admittance coefficients for the period considered for the sites of Herstmonceux (CONV method applied to an area of 4000 km from the site - IBO hypothesis).

B.3 Residuals

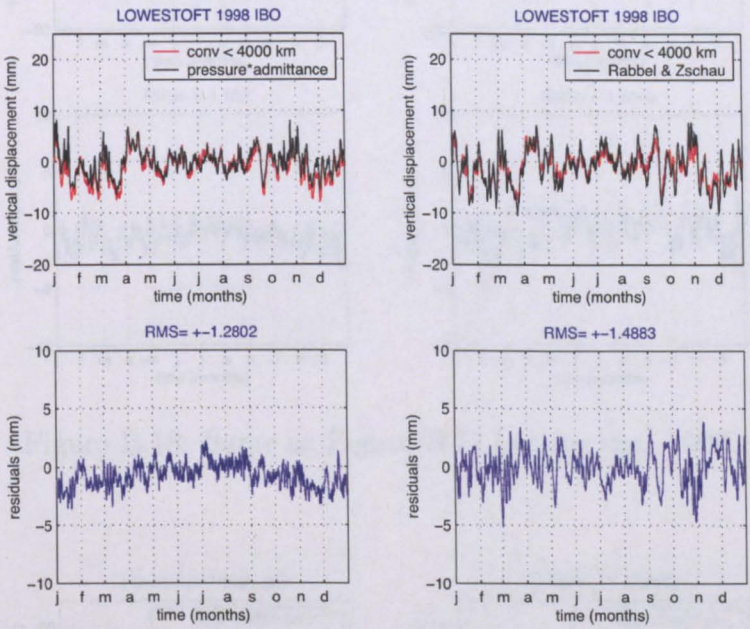

Figure B.17: Residuals between TCCE results and convolution results and between convolution and admittance method. In red are the vertical displacement calculated from the CONV method (radius equal 4000 km) in the IBO hypothesis for 1998 and for the site of Lowestoft. In black are alternatively represented on the left, the radial displacements obtained by multiplying the admittance characteristic for the station and for the year considered by the local derived pressure (pressure value of the cell in which Lowestoft is situated), and on the right, the vertical displacements obtained from the TCCE method. In blue are the residuals between convolution and admittance (left) and convolution and TCCE method (right).

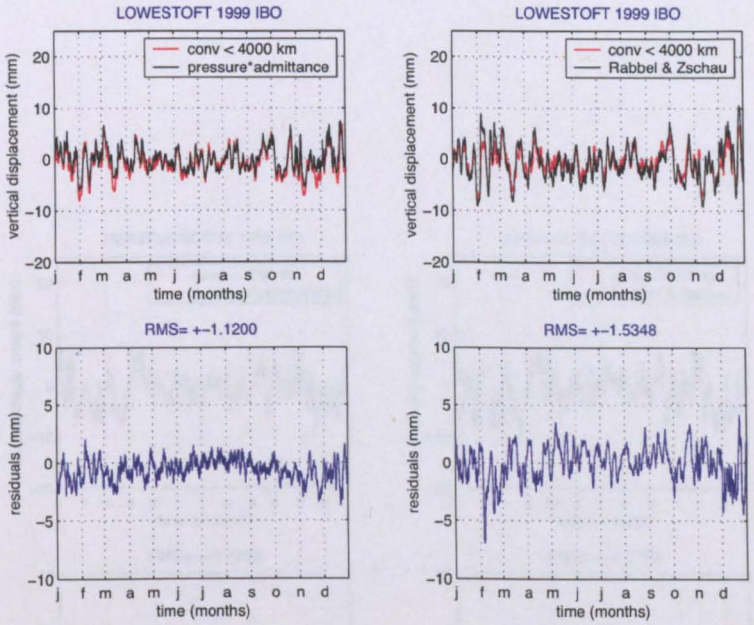

Figure B.18: Same as Figure B.17 but for year 1999.

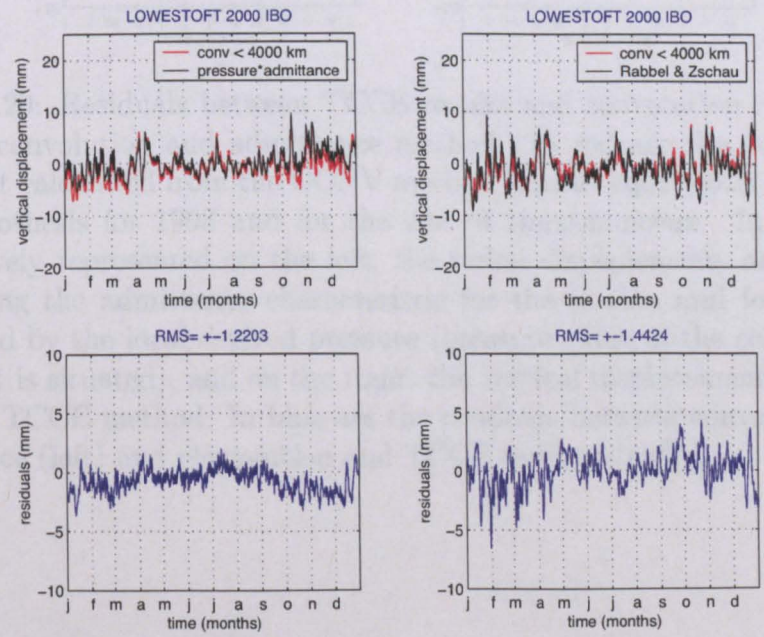

Figure B.19: Same as Figure B.17 but for year 2000.

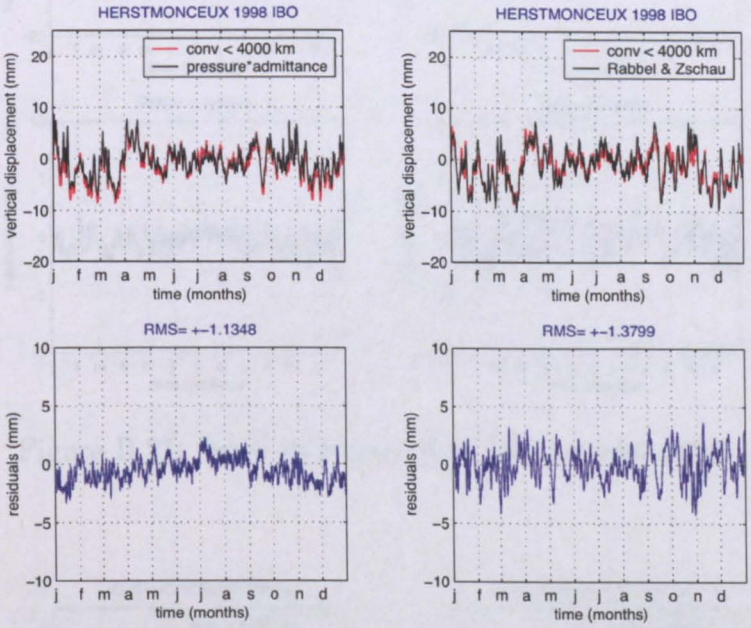

Figure B.20: Residuals between TCCE results and convolution results and between convolution and admittance method. In red are the vertical displacement calculated from the CONV method (radius equal 4000 km) in the IBO hypothesis for 1998 and for the site of Herstmonceux. In black are alternatively represented on the left, the radial displacements obtained by multiplying the admittance characteristic for the station and for the year considered by the local derived pressure (pressure value of the cell in which Lowestoft is situated), and on the right, the vertical displacements obtained from the TCCE method. In blue are the residuals between convolution and admittance (left) and convolution and TCCE method (right).

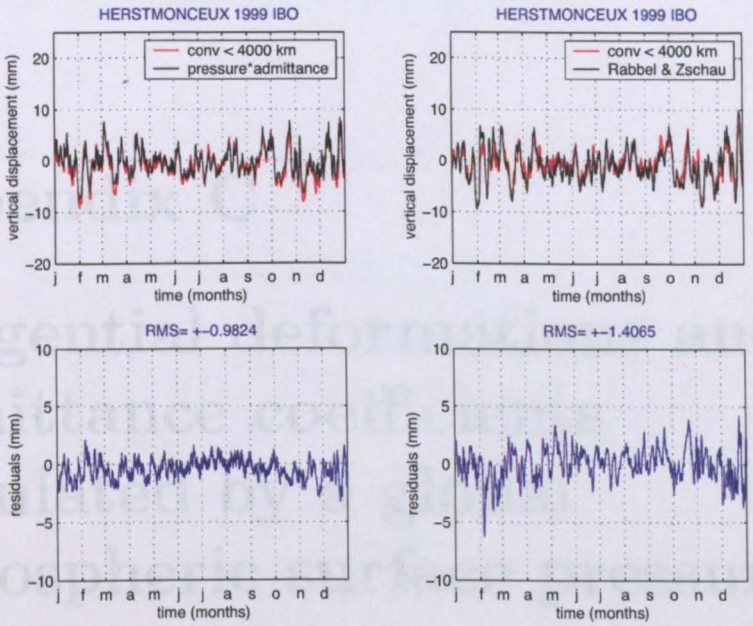

Figure B.21: Same as Figure B.20 but for year 1999.

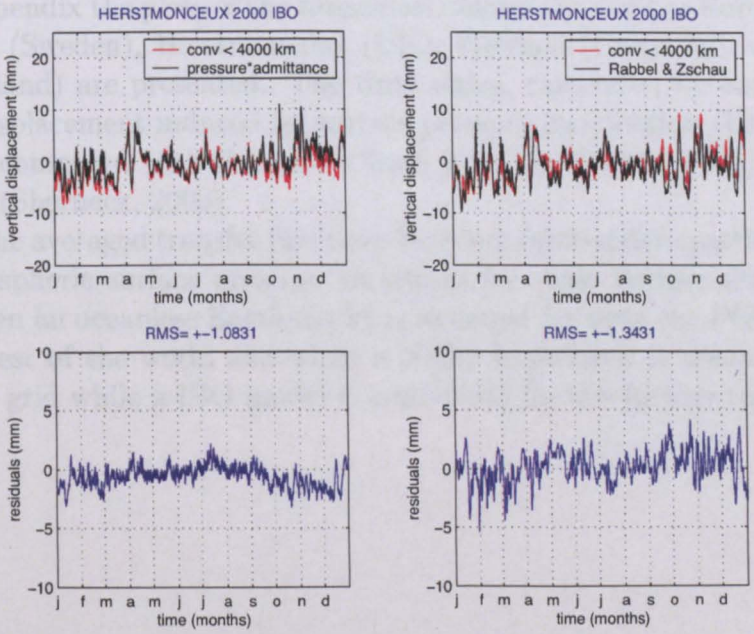

Figure B.22: Same as Figure B.20 but for year 2000.

Appendix C

Tangential deformations and admittance coefficients calculated by a global atmospheric surface pressure loading model

In this appendix the plots of the tangential deformation at the European sites of Onsala (Sweden), Herstmonceux (UK), Wettzell (Germany) and Metsahovi (Finland) are presented. The time series, calculated by our model of surface displacement induced by surface pressure distribution (IBO hypothesis), are compared with the curves from NASA's (Petrov, 2004) and OSO web sites (Sherneck, 2003).

Also the averaged transfer functions between vertical deformation induced and atmospheric surface pressure variations for some British sites are proposed when an oceanless Earth model is assumed for both the POLSSM grid and the rest of the world and when a NIBO hypothesis is assumed for the POLSSM grid while a IBO model is considered for the further regions.

C.1 Tangential deformation

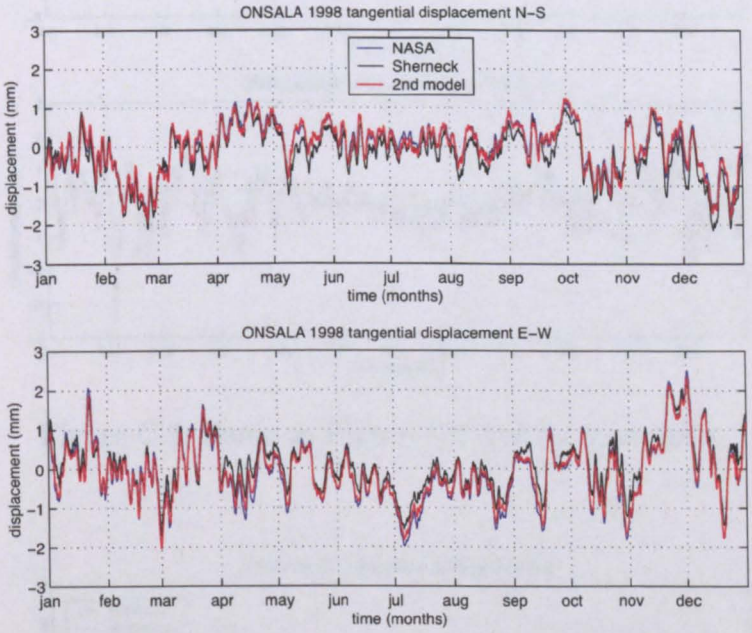

Figure C.1: Tangential displacements (north-south components and east-west components) calculated by the models of surface deformations due to atmospheric surface pressure forcing (red curves) at Onsala for the year 1998. In blue are represented the time series from NASA's web sites while in black are drawn the curves that refer to the data from OSO web site. It has to be noted that the blue and the red curves are almost superimposed.

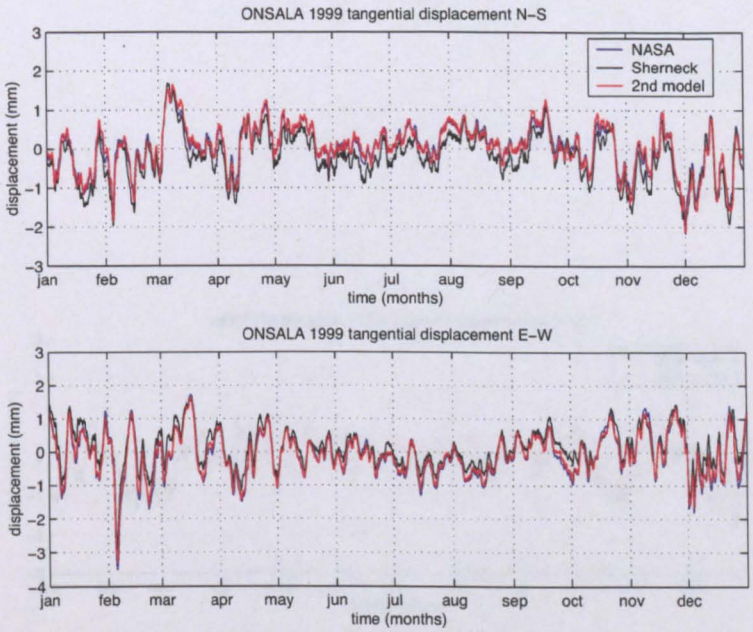

Figure C.2: Same as Figure C.1 but for year 1999.

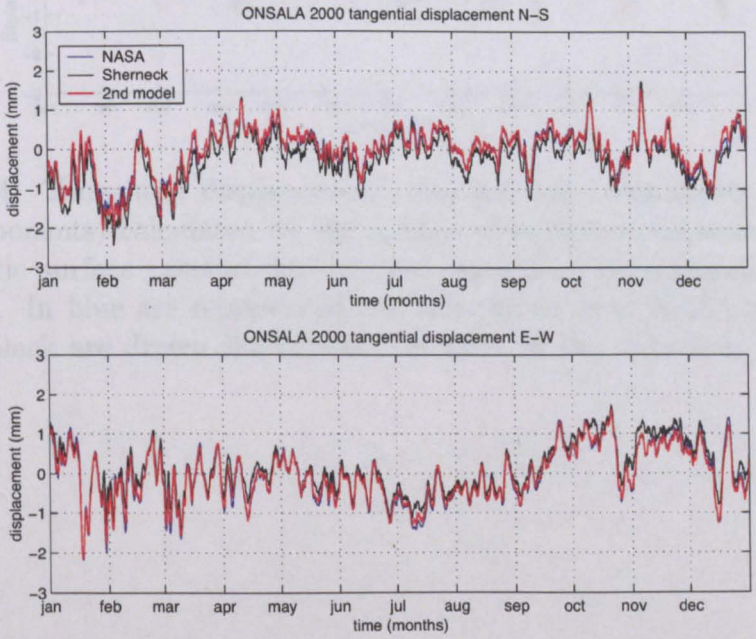

Figure C.3: Same as Figure C.1 but for year 2000.

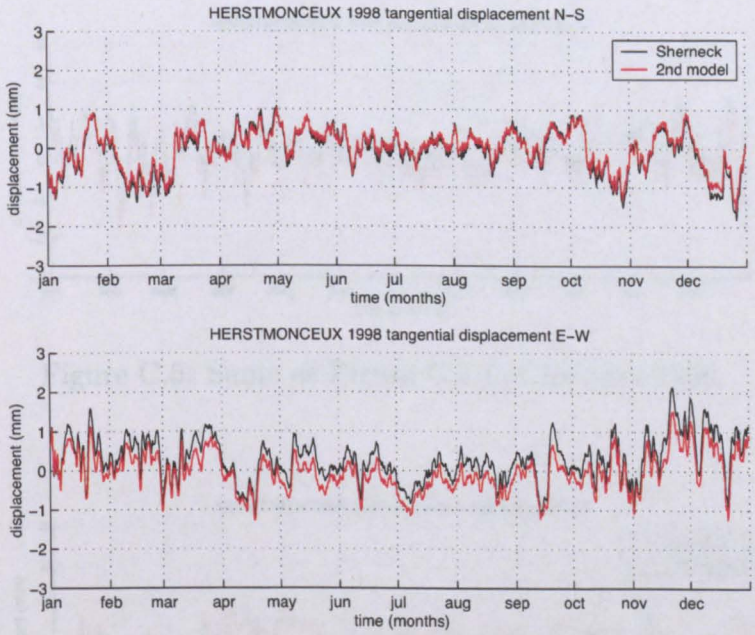

Figure C.4: Tangential displacements (north-south components and east-west components) calculated by the models of surface deformations due to atmospheric surface pressure forcing (red curves) at Herstmonceux for the year 1998. In blue are represented the time series from NASA's web sites while in black are drawn the curves that refer to the data from OSO web site.

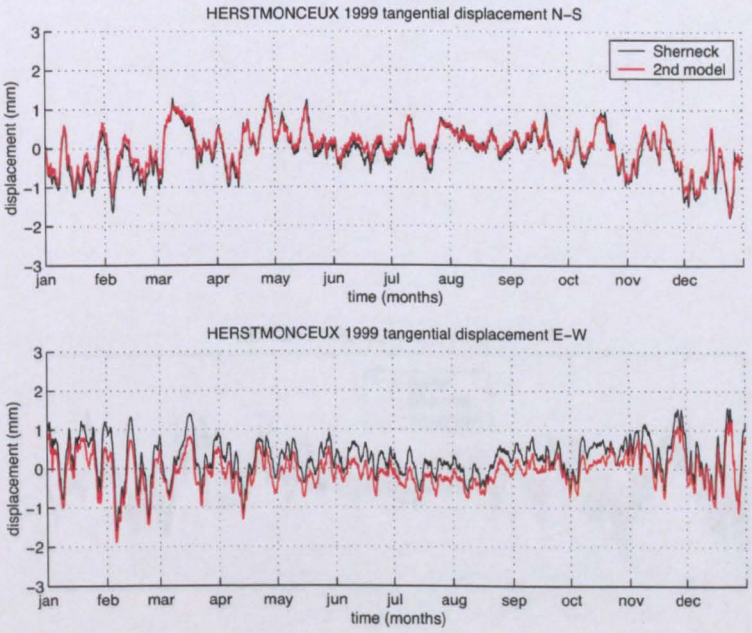

Figure C.5: Same as Figure C.4 but for year 1999.

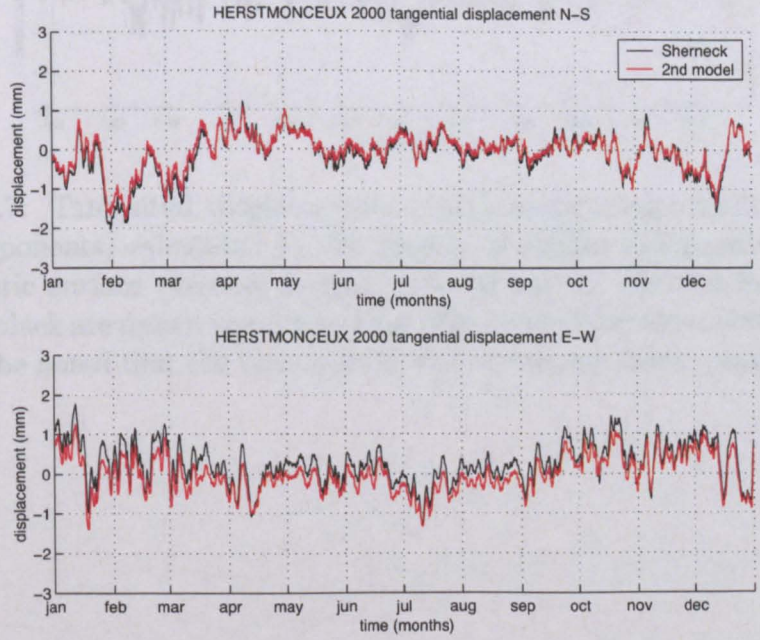

Figure C.6: Same as Figure C.4 but for year 2000.

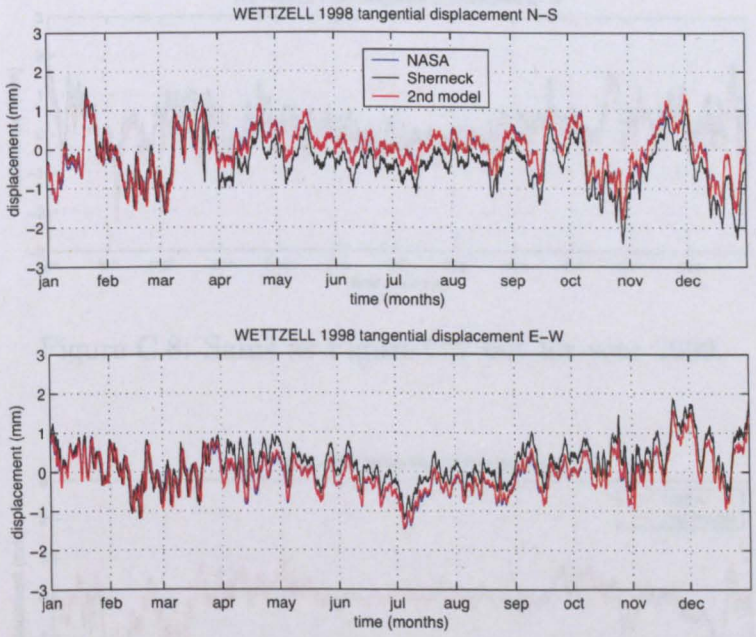

Figure C.7: Tangential displacements (north-south components and east-west components) calculated by the models of surface deformations due to atmospheric surface pressure forcing (red curves) at Wettzell for the year 1998. In black are drawn the curves that refer to the data from OSO web site. It has to be noted that the blue and the red curves are almost superimposed.

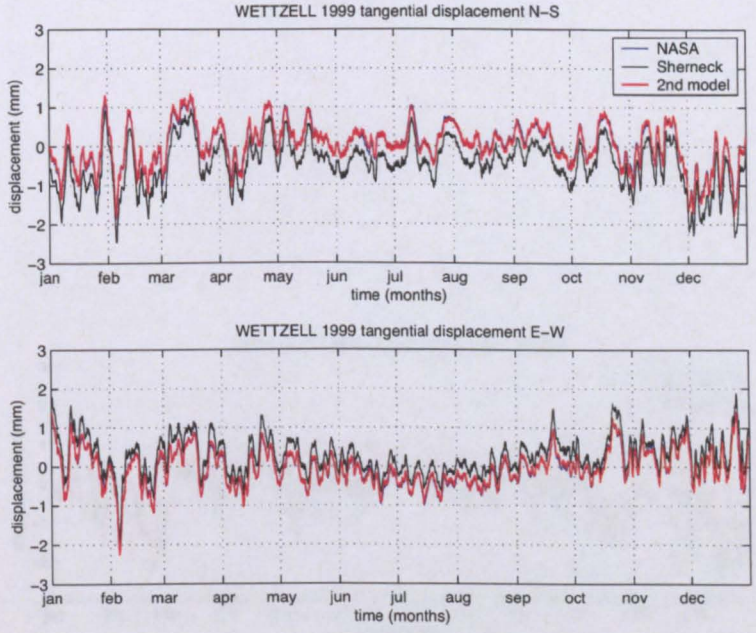

Figure C.8: Same as Figure C.7 but for year 1999.

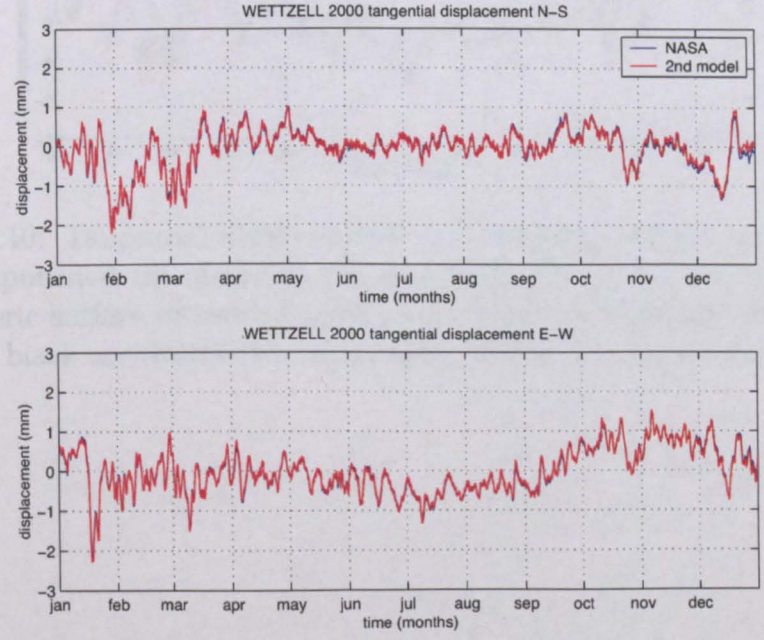

Figure C.9: Same as Figure C.7 but for year 2000. The time series for the year 2000 were not available from OSO web site for the station of Wettzell.

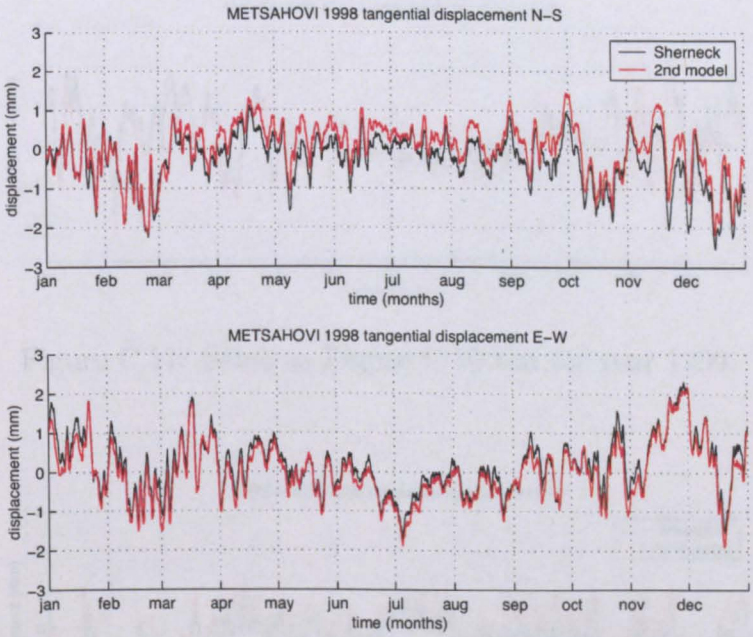

Figure C.10: Tangential displacements (north-south components and east-west components) calculated by the models of surface deformations due to atmospheric surface pressure forcing (red curves) at Metsahovi for the year 1998. In black are drawn the curves that refer to the data from OSO web site.

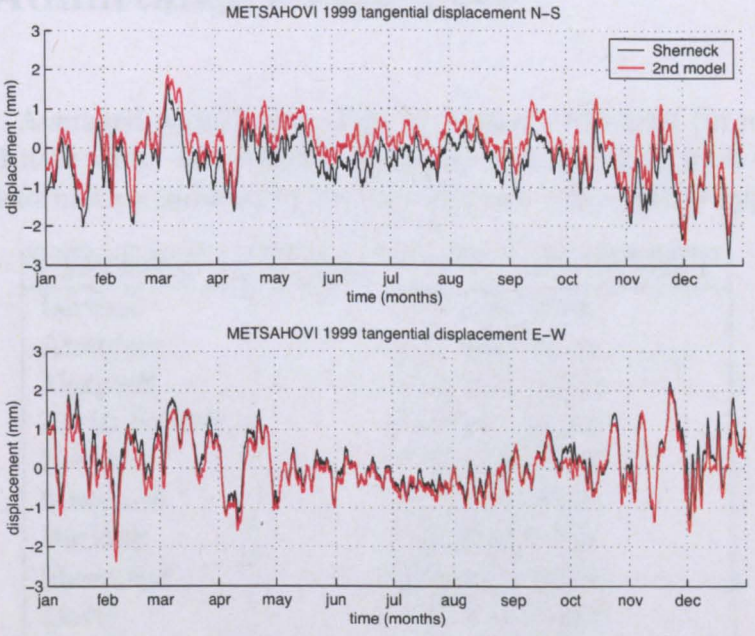

Figure C.11: Same as Figure C.10 but for year 1999.

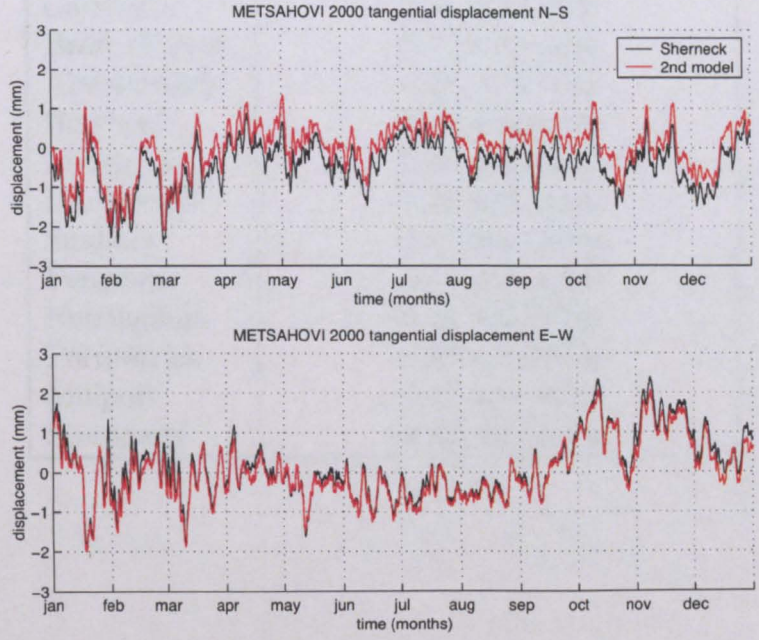

Figure C.12: Same as Figure C.10 but for year 2000.

C.2 Admittance coefficients

Table C.1: Averaged admittances over the period 1998-2000 (in mm/mbar) for some British sites. The transfer functions were obtained from the model of radial deformation induced by surface pressure (sfp) (NIBO hypothesis).

STATIONS	ADMITTANCE COEFFICIENT
Lerwick	-0.47 mm/mbar
Aberdeen	-0.47 mm/mbar
Morpeth	-0.48 mm/mbar
North Shields	-0.48 mm/mbar
Hemsby	-0.48 mm/mbar
Lowestoft	-0.47 mm/mbar
Barking	-0.47 mm/mbar
Sheerness	-0.48 mm/mbar
Dover	-0.48 mm/mbar
Herstmonceux	-0.48 mm/mbar
Portsmouth	-0.49 mm/mbar
Hurn	-0.49 mm/mbar
Newlyn	-0.48 mm/mbar
Camborne	-0.48 mm/mbar
Brest (France)	-0.48 mm/mbar
Aberystwyth	-0.48 mm/mbar
Holyhead	-0.48 mm/mbar
Liverpool	-0.48 mm/mbar
Dunkeswell	-0.48 mm/mbar
Sunbury	-0.47 mm/mbar
Pershore	-0.49 mm/mbar
Nottingham	-0.49 mm/mbar
Portpatrick	-0.47 mm/mbar
Millport	-0.47 mm/mbar
Stornoway	-0.48 mm/mbar

Table C.2: Averaged admittances over the period 1998-2000 (in mm/mbar) for some British sites. The transfer functions were obtained from the model of radial deformation induced by surface pressure (sfp) (NIBO hypothesis inside POLSSM grid and IBO hypothesis for the rest of the world).

STATIONS	ADMITTANCE COEFFICIENT
Lerwick	-0.38 mm/mbar
Aberdeen	-0.40 mm/mbar
Morpeth	-0.42 mm/mbar
North Shields	-0.42 mm/mbar
Hemsby	-0.43 mm/mbar
Lowestoft	-0.42 mm/mbar
Barking	-0.42 mm/mbar
Sheerness	-0.43 mm/mbar
Dover	-0.43 mm/mbar
Herstmonceux	-0.43 mm/mbar
Portsmouth	-0.43 mm/mbar
Hurn	-0.42 mm/mbar
Newlyn	-0.38 mm/mbar
Camborne	-0.38 mm/mbar
Brest (France)	-0.32 mm/mbar
Aberystwyth	-0.41 mm/mbar
Holyhead	-0.41 mm/mbar
Liverpool	-0.42 mm/mbar
Dunkeswell	-0.40 mm/mbar
Sunbury	-0.42 mm/mbar
Pershore	-0.43 mm/mbar
Nottingham	-0.43 mm/mbar
Portpatrick	-0.39 mm/mbar
Millport	-0.40 mm/mbar
Stornoway	-0.38 mm/mbar

Appendix D

Daily, weekly and monthly averages of the vertical deformations and associated gravity variations calculated from a storm surge loading model

This appendix presents the daily, weekly and monthly averaged values of the radial displacements and of the gravity changes induced by storm surge loading. The plots refer to the stations of Lowestoft and Sheerness and the years 1997, 1998, 2001, 2002 and 2003.

A different section is dedicated to the plots of the deformations and gravity changes induced by storm surge loading at the station of Herstmonceux and to the seasonal and longer period deformations and gravity changes predicted during 1999 and 2000.

D.1 Daily, weekly and monthly averages

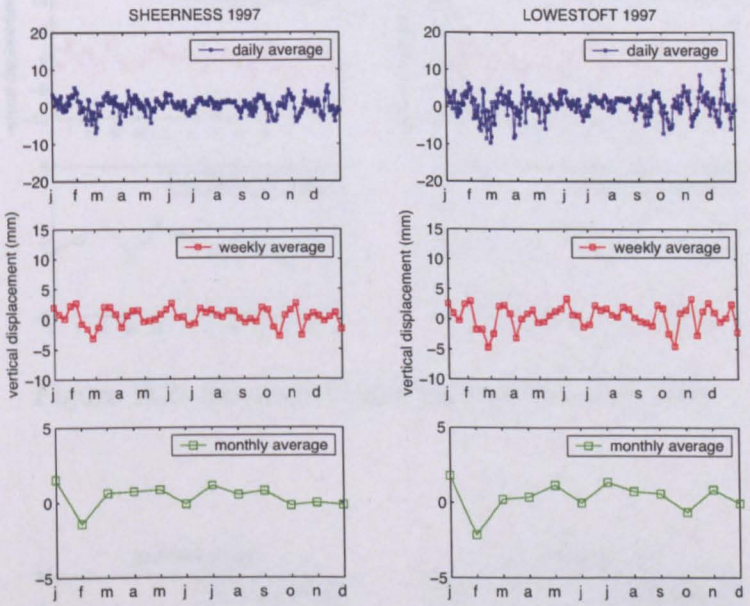

Figure D.1: Daily averages of the vertical displacement (in blue) for the year 1997 at Sheerness and Lowestoft respectively. In red are represented the weekly averages of the displacement while in green the monthly averages are shown.

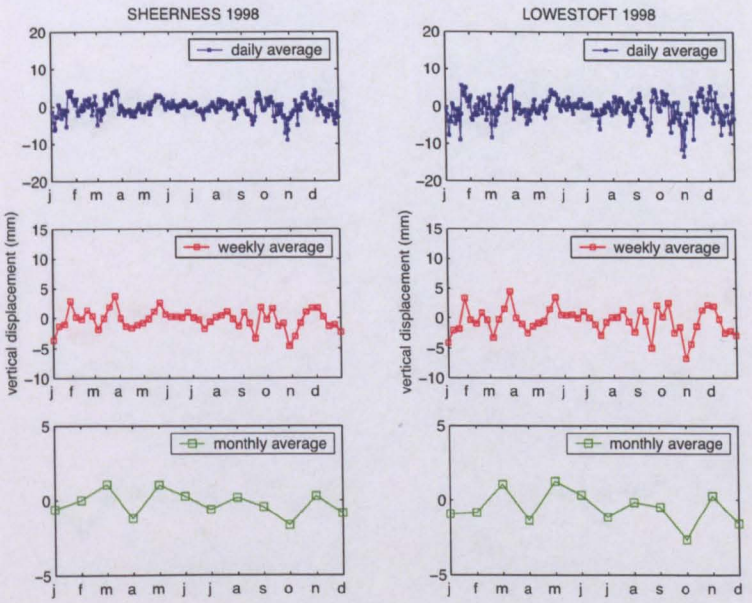

Figure D.2: Same as Figure D.1 but for year 1998.

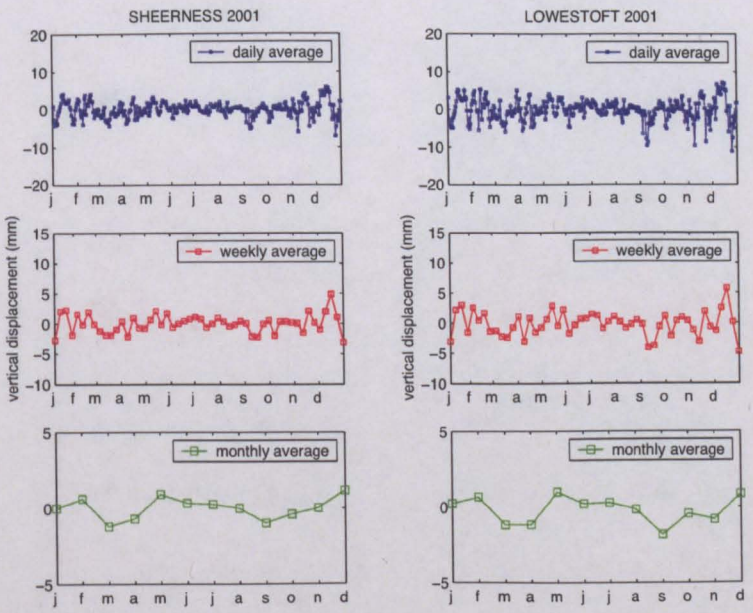

Figure D.3: Same as Figure D.1 but for year 2001.

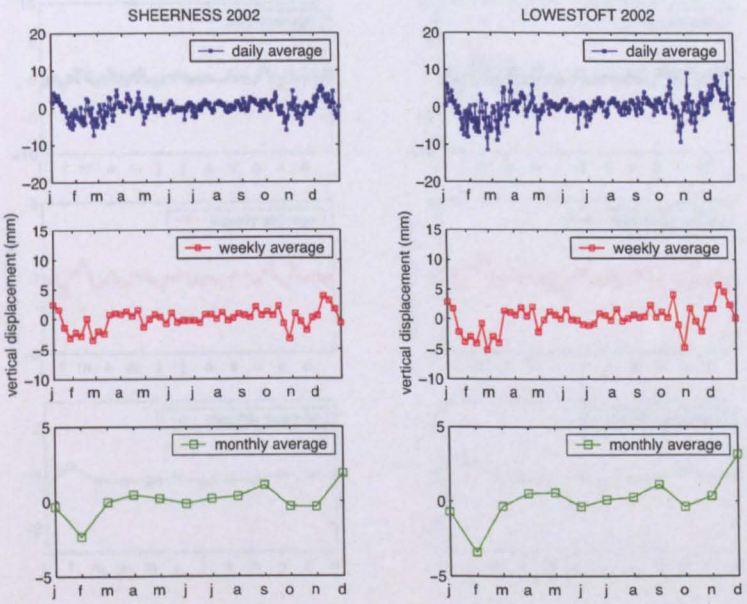

Figure D.4: Same as Figure D.1 but for year 2002.

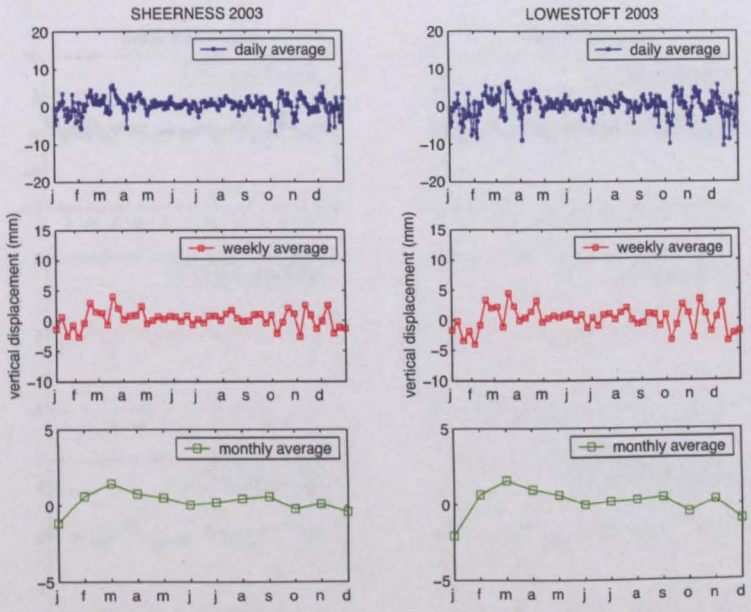

Figure D.5: Same as Figure D.1 but for year 2003.

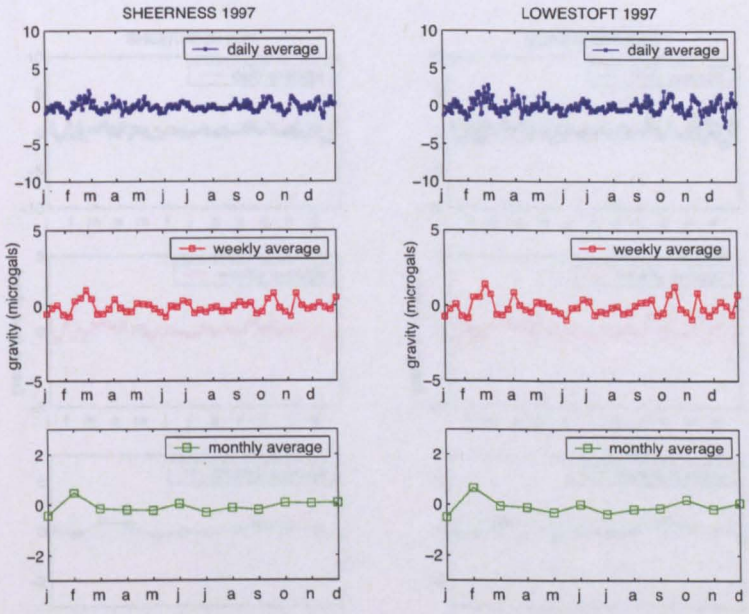

Figure D.6: Daily averages of the total gravity variation (in blue) for the year 1997 at Sheerness and Lowestoft respectively. In red are represented the weekly averages of the gravity chance while in green the monthly averages are shown.

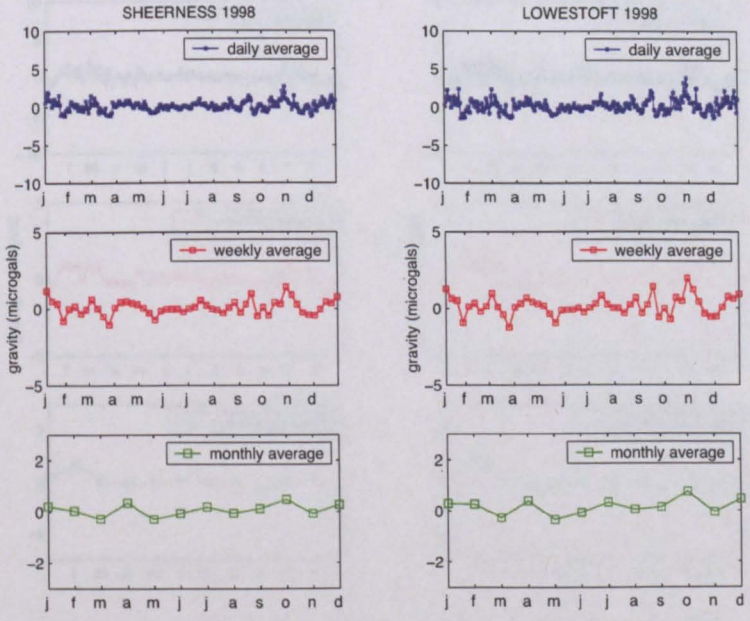

Figure D.7: Same as Figure D.6 but for year 1998.

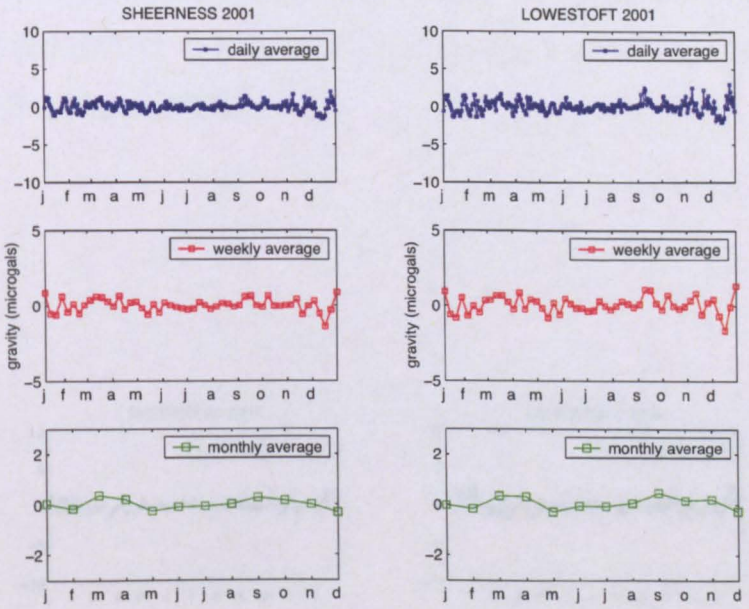

Figure D.8: Same as Figure D.6 but for year 2001.

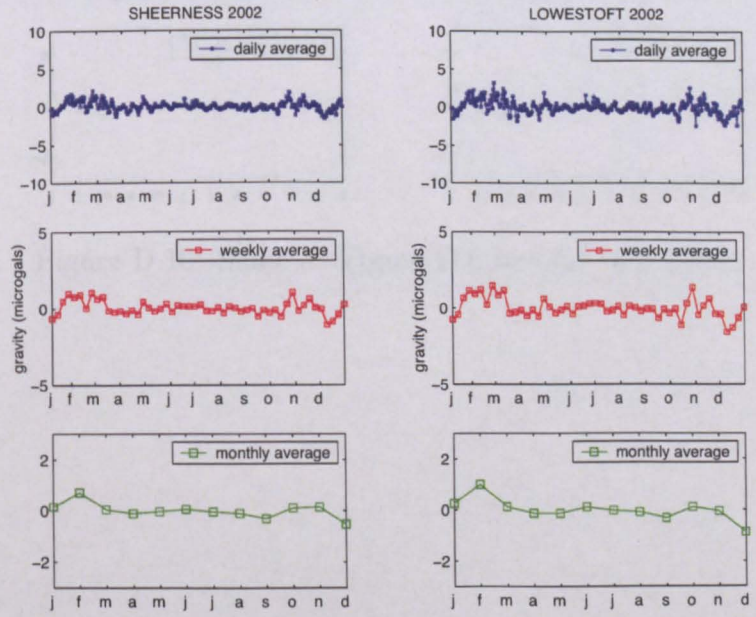

Figure D.9: Same as Figure D.6 but for year 2002.

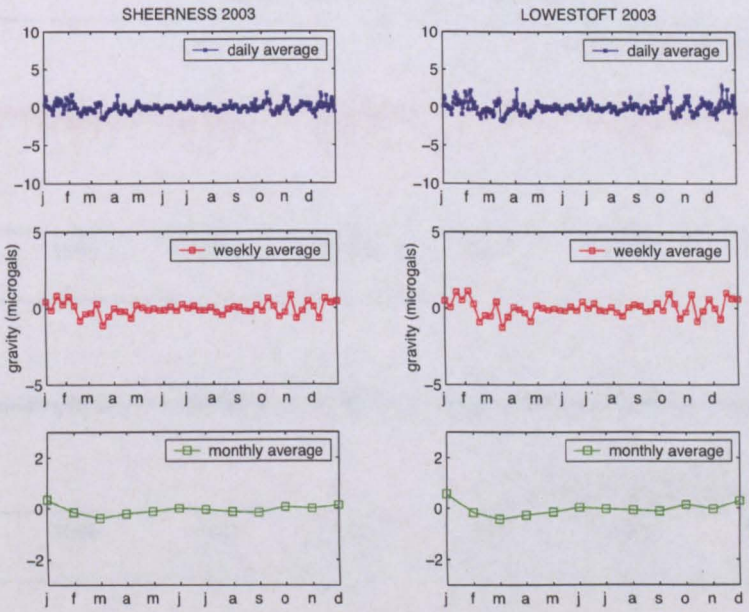

Figure D.10: Same as Figure D.6 but for year 2003.

D.2 Modelled deformations and gravity changes induced by storm surge loading at Herstmonceux

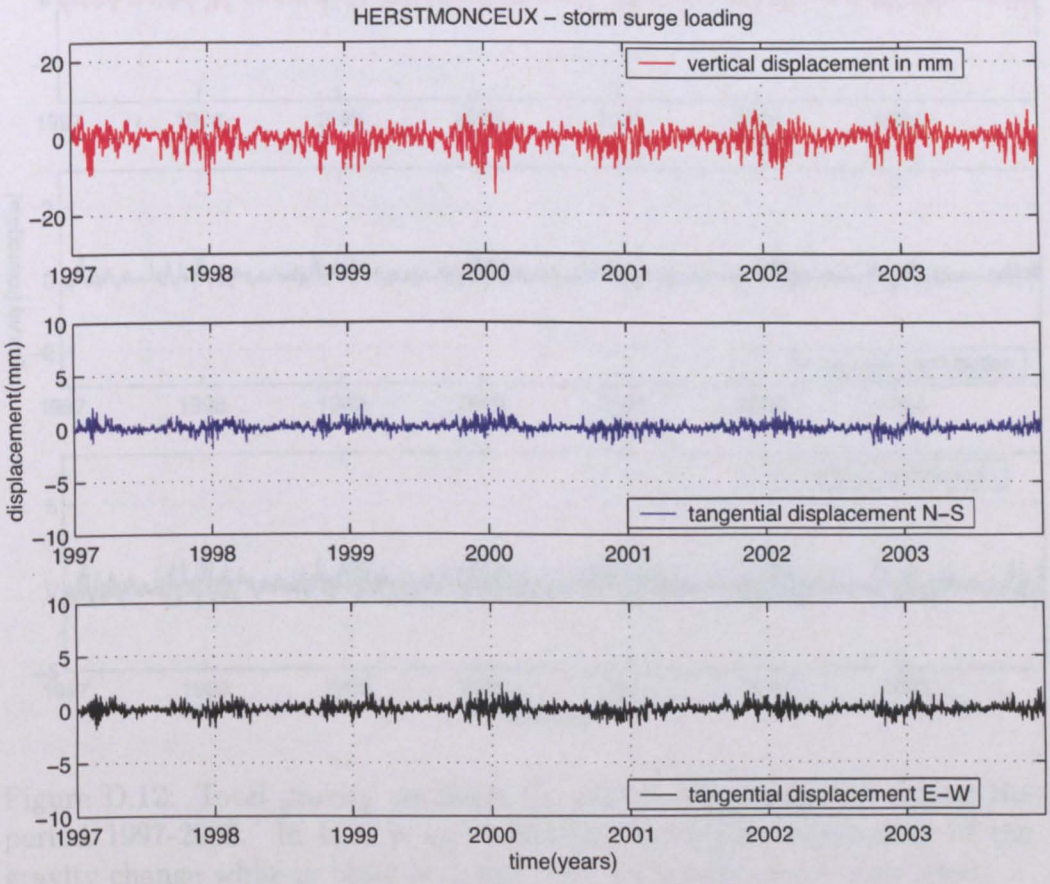

Figure D.11: Radial deformation (in red) and associated tangential displacement as a North-South component (blue curve) and East-West component (in black) during the period 1997-2003. The results refer to the station of Herstmonceux.

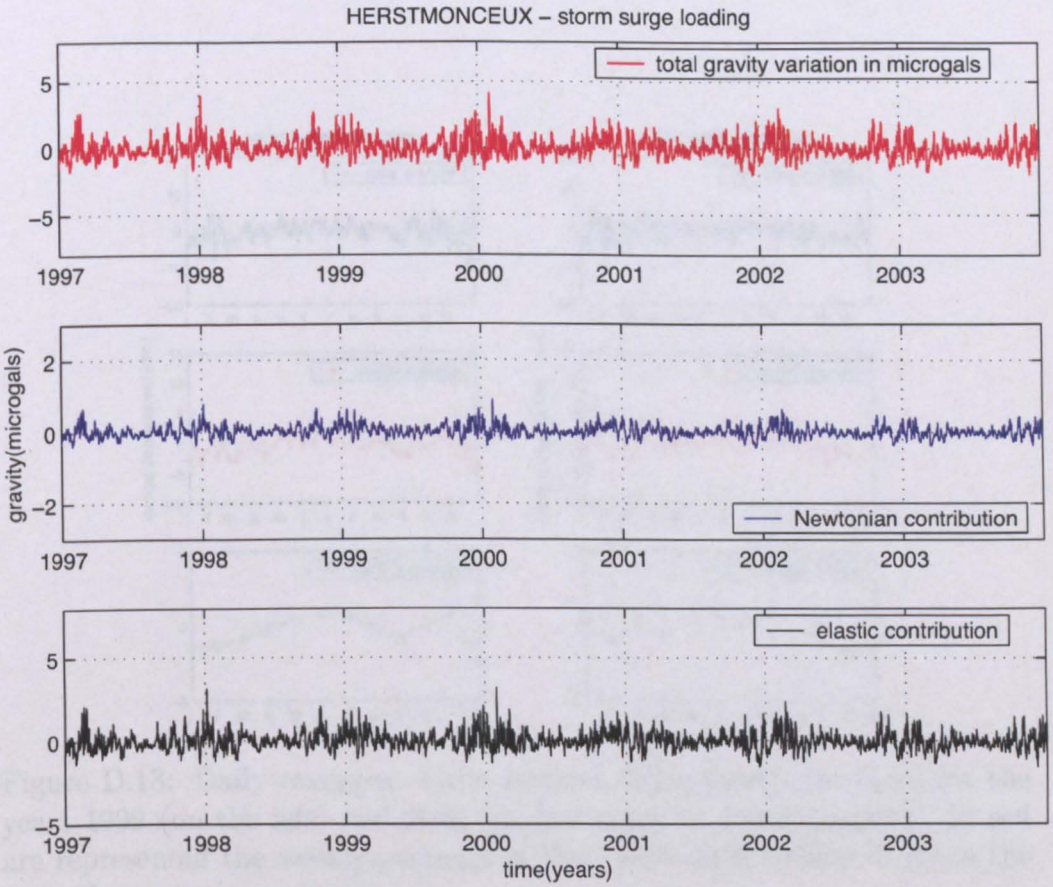

Figure D.12: Total gravity variation (in red) at Herstmonceux during the period 1997-2003. In blue is presented the Newtonian component of the gravity change while in black is drawn the elastic component associated.

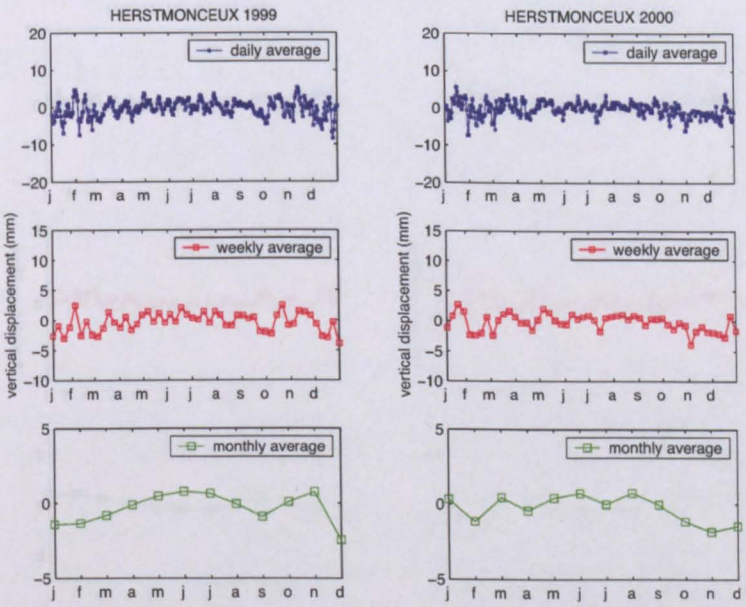

Figure D.13: Daily averages of the vertical displacement (in blue) for the years 1999 (on the left) and 2000 (on the right) at Herstmonceux. In red are represented the weekly averages of the displacement while in green the monthly averages are shown.

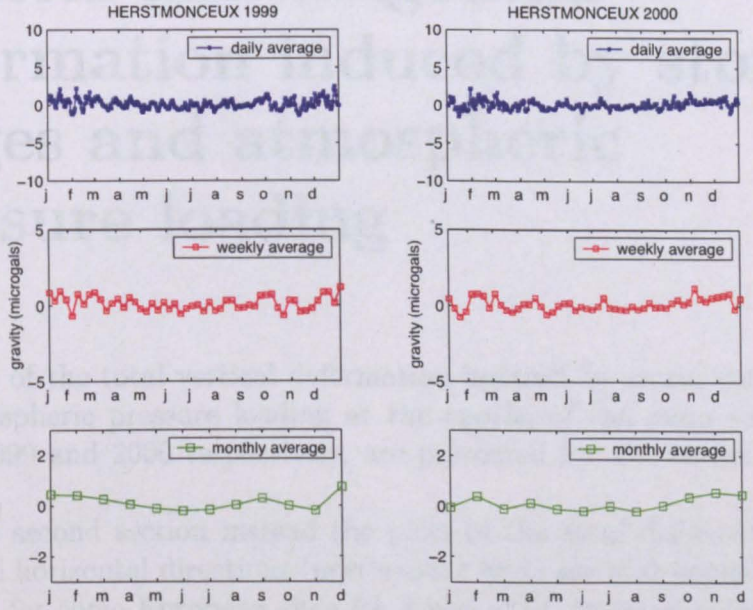

Figure D.14: Daily averages of the gravity variations (in blue) for the years 1999 (on the left) and 2000 (on the right) at Herstmonceux. In red are represented the weekly averages of the gravity change while in green the monthly averages are shown.

Appendix E

Vertical and tangential deformation induced by storm surges and atmospheric pressure loading

The plots of the total vertical deformation induced by storm surge loading and atmospheric pressure loading at the epochs of the main surge events of year 1999 and 2000 respectively, are presented for a selection of British stations.

In the second section instead the plots of the total deformation in the radial and horizontal directions (north-south and east-west components) are presented for some European sites for a period up to seven years (between 1997 and 2003).

Where available, also the EPN weekly GPS time series are presented for visual comparison (in these plots a blue line always indicates a receiver change or a firmware update and a red one refers to a replaced antenna).

Finally in the last section, it is presented a comparison between the gravity residuals at Membach (Belgium) observed by a superconducting gravimeter operating at the station and corrected for Earth tides, polar motion effect and linear drift, and the gravity variations induced by storm surge loading modelled for the two periods of the main surge events previously investigated. The air pressure effect was not removed from the observations.

E.1 Total vertical deformation during the main surge events at some British stations

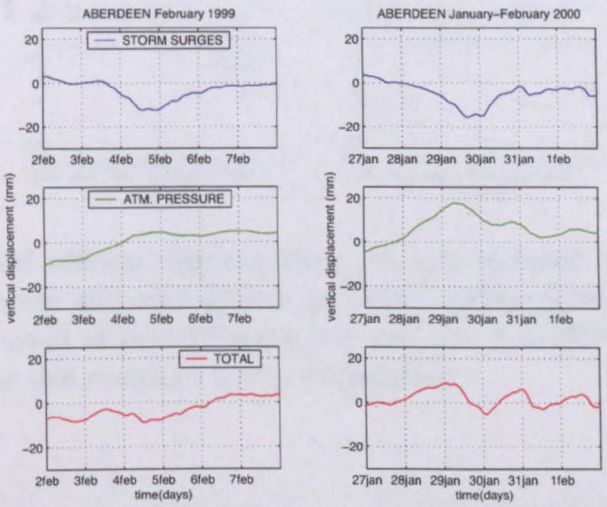

Figure E.1: Total vertical displacements (in red) induced by storm surges loading (blue curve) and atmospheric pressure loading (green curve) during the main surge event of year 1999 (on the left) and year 2000 (on the right) at Aberdeen. The deformations are in millimeters.

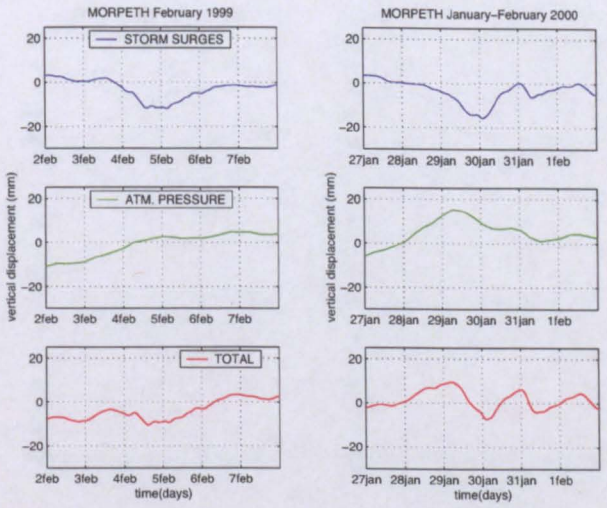

Figure E.2: Total vertical displacements (in red) induced by storm surges loading (blue curve) and atmospheric pressure loading (green curve) during the main surge event of year 1999 (on the left) and year 2000 (on the right) at Morpeth. The deformations are in millimeters.

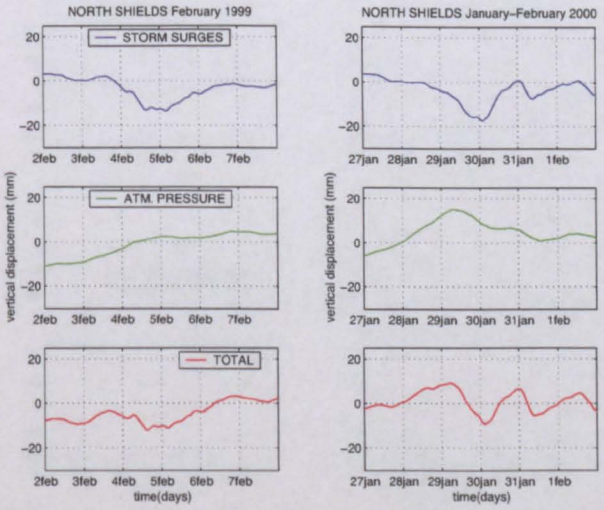

Figure E.3: Total vertical displacements (in red) induced by storm surges loading (blue curve) and atmospheric pressure loading (green curve) during the main surge event of year 1999 (on the left) and year 2000 (on the right) at North Shields. The deformations are in millimeters.

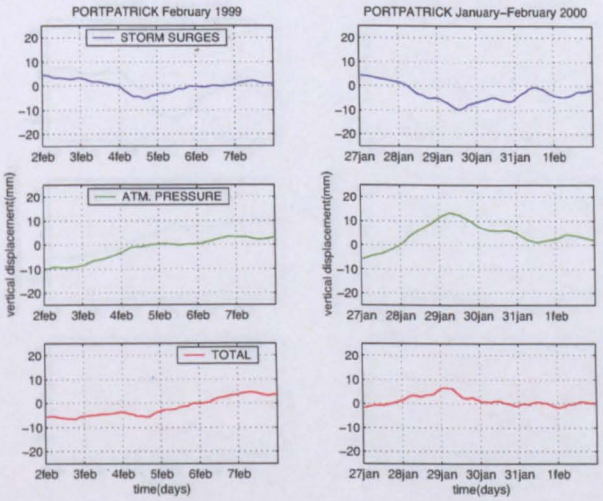

Figure E.4: Total vertical displacements (in red) induced by storm surges loading (blue curve) and atmospheric pressure loading (green curve) during the main surge event of year 1999 (on the left) and year 2000 (on the right) at Portpatrick. The deformations are in millimeters.

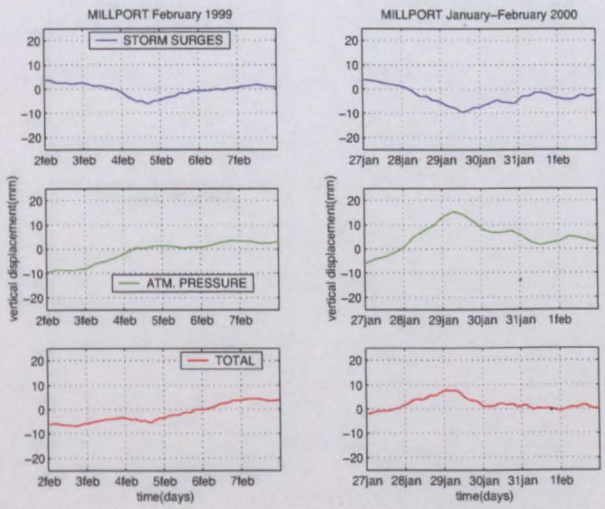

Figure E.5: Total vertical displacements (in red) induced by storm surges loading (blue curve) and atmospheric pressure loading (green curve) during the main surge event of year 1999 (on the left) and year 2000 (on the right) at Millport. The deformations are in millimeters.

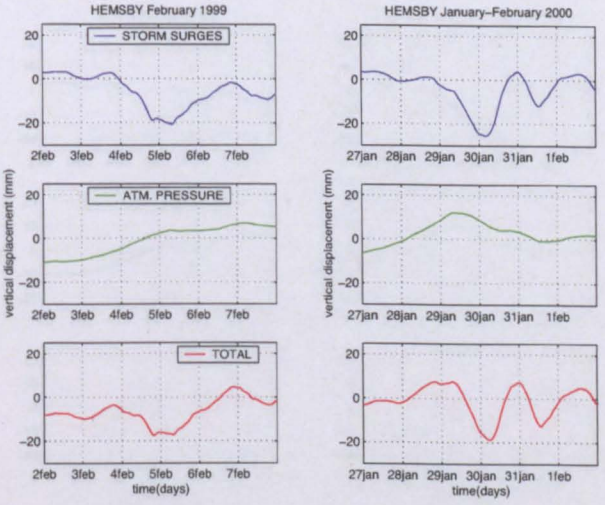

Figure E.6: Total vertical displacements (in red) induced by storm surges loading (blue curve) and atmospheric pressure loading (green curve) during the main surge event of year 1999 (on the left) and year 2000 (on the right) at Hemsby. The deformations are in millimeters.

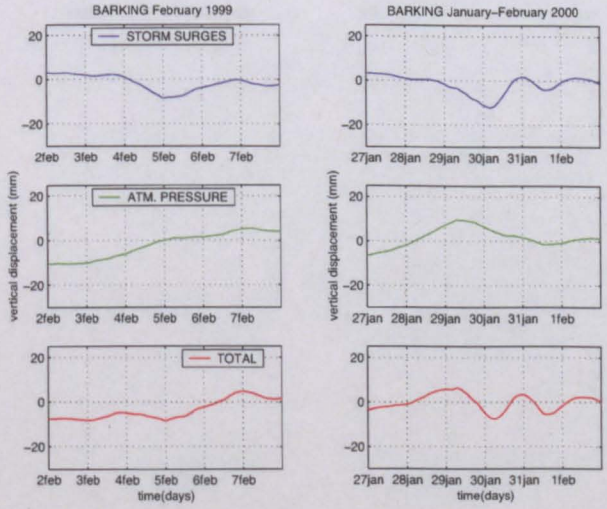

Figure E.7: Total vertical displacements (in red) induced by storm surges loading (blue curve) and atmospheric pressure loading (green curve) during the main surge event of year 1999 (on the left) and year 2000 (on the right) at Barking. The deformations are in millimeters.

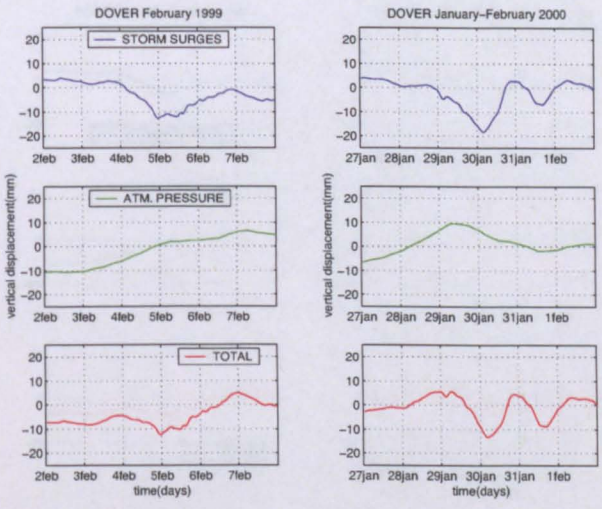

Figure E.8: Total vertical displacements (in red) induced by storm surges loading (blue curve) and atmospheric pressure loading (green curve) during the main surge event of year 1999 (on the left) and year 2000 (on the right) at Dover. The deformations are in millimeters.

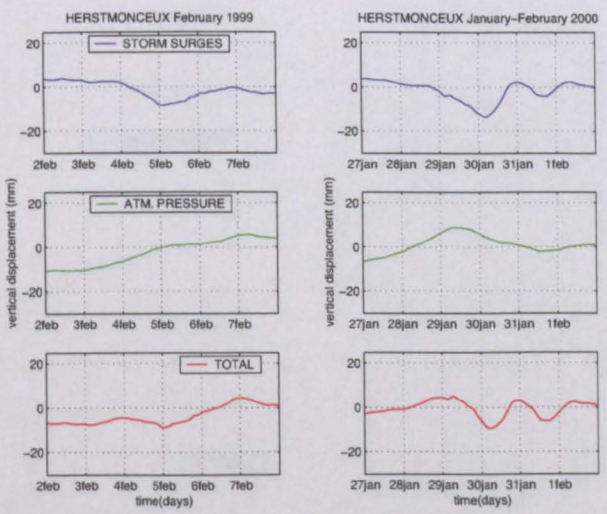

Figure E.9: Total vertical displacements (in red) induced by storm surges loading (blue curve) and atmospheric pressure loading (green curve) during the main surge event of year 1999 (on the left) and year 2000 (on the right) at Herstmonceux. The deformations are in millimeters.

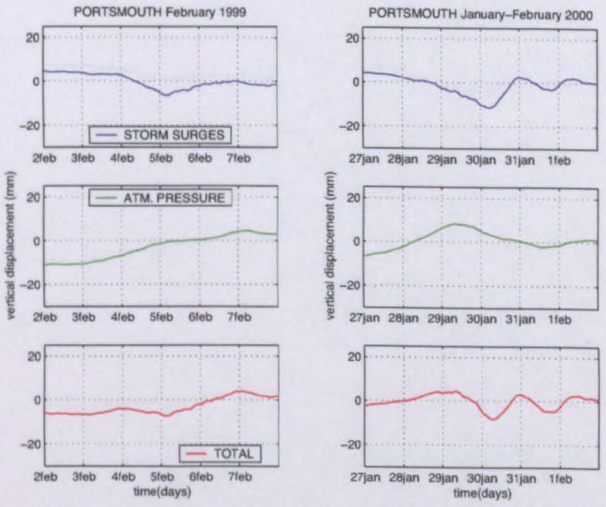

Figure E.10: Total vertical displacements (in red) induced by storm surges loading (blue curve) and atmospheric pressure loading (green curve) during the main surge event of year 1999 (on the left) and year 2000 (on the right) at Portsmouth. The deformations are in millimeters.

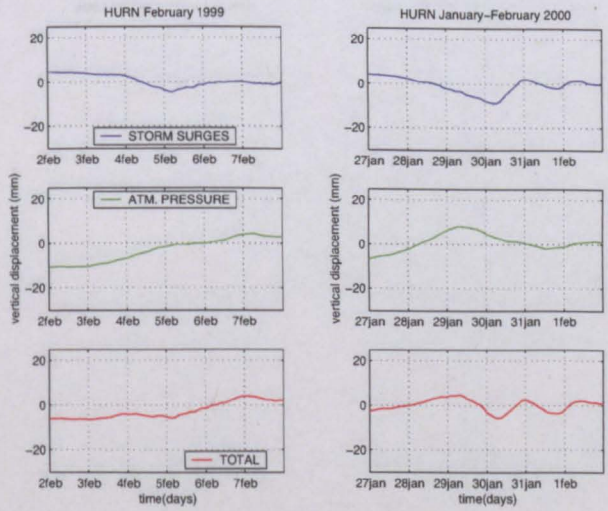

Figure E.11: Total vertical displacements (in red) induced by storm surges loading (blue curve) and atmospheric pressure loading (green curve) during the main surge event of year 1999 (on the left) and year 2000 (on the right) at Hurn. The deformations are in millimeters.

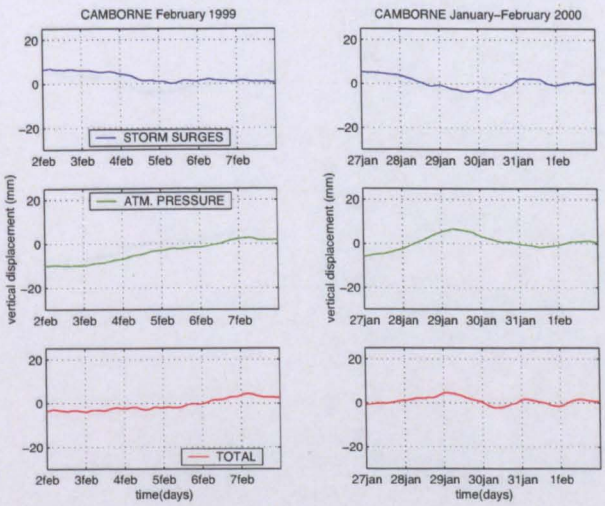

Figure E.12: Total vertical displacements (in red) induced by storm surges loading (blue curve) and atmospheric pressure loading (green curve) during the main surge event of year 1999 (on the left) and year 2000 (on the right) at Camborne. The deformations are in millimeters.

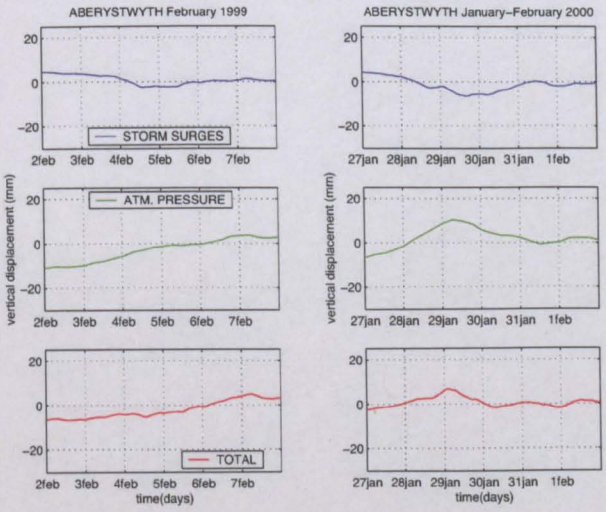

Figure E.13: Total vertical displacements (in red) induced by storm surges loading (blue curve) and atmospheric pressure loading (green curve) during the main surge event of year 1999 (on the left) and year 2000 (on the right) at Aberystwyth. The deformations are in millimeters.

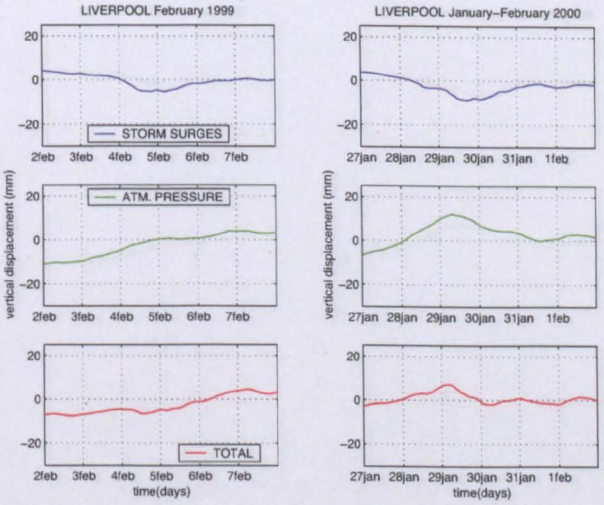

Figure E.14: Total vertical displacements (in red) induced by storm surges loading (blue curve) and atmospheric pressure loading (green curve) during the main surge event of year 1999 (on the left) and year 2000 (on the right) at Liverpool. The deformations are in millimeters.

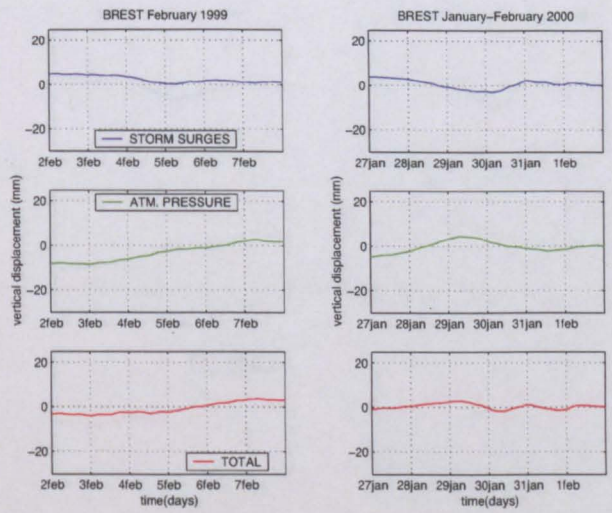

Figure E.15: Total vertical displacements (in red) induced by storm surges loading (blue curve) and atmospheric pressure loading (green curve) during the main surge event of year 1999 (on the left) and year 2000 (on the right) at Brest (France). The deformations are in millimeters.

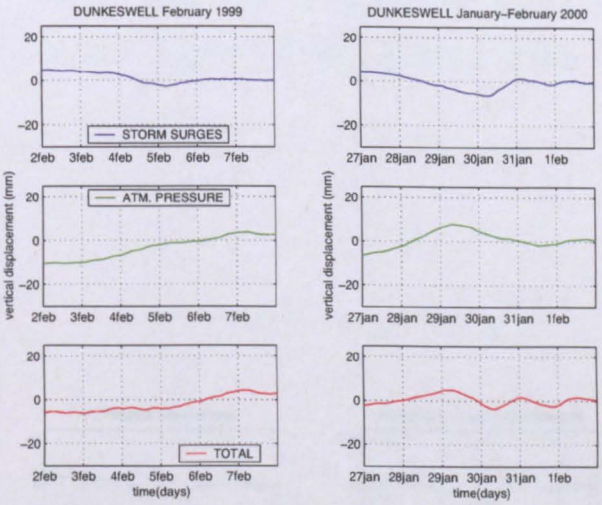

Figure E.16: Total vertical displacements (in red) induced by storm surges loading (blue curve) and atmospheric pressure loading (green curve) during the main surge event of year 1999 (on the left) and year 2000 (on the right) at Dunkeswell. The deformations are in millimeters.

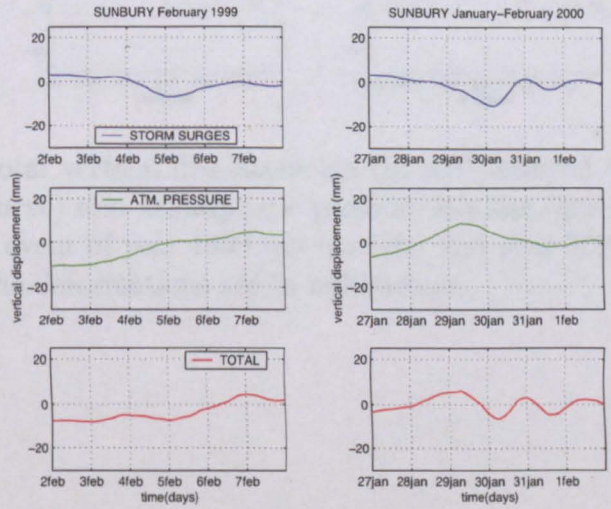

Figure E.17: Total vertical displacements (in red) induced by storm surges loading (blue curve) and atmospheric pressure loading (green curve) during the main surge event of year 1999 (on the left) and year 2000 (on the right) at Sunbury. The deformations are in millimeters.

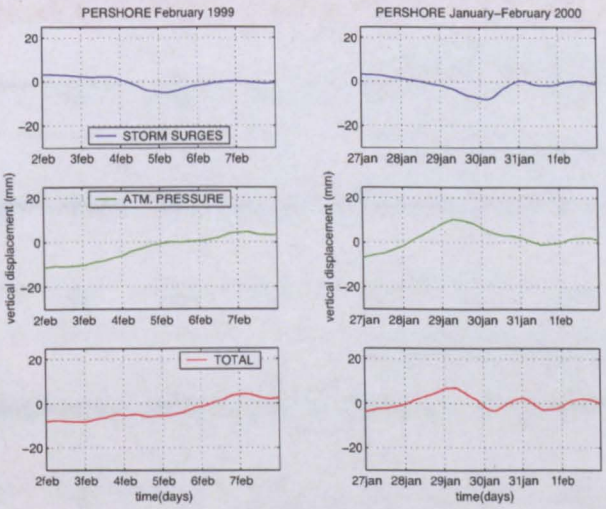

Figure E.18: Total vertical displacements (in red) induced by storm surges loading (blue curve) and atmospheric pressure loading (green curve) during the main surge event of year 1999 (on the left) and year 2000 (on the right) at Pershore. The deformations are in millimeters.

E.2 The total vertical and tangential deformation at some European sites

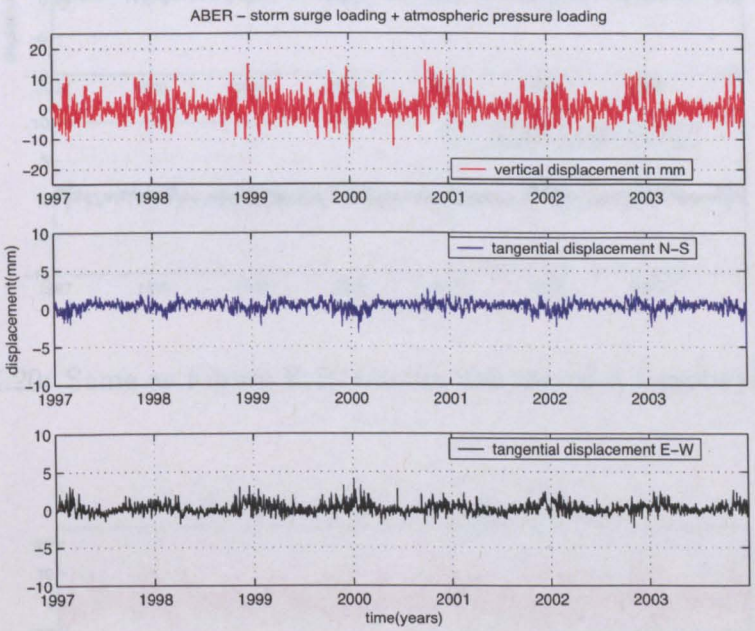

Figure E.19: Total vertical (in red) and tangential displacements (in blue the north-south component and in black the east-west component) induced by storm surges loading and atmospheric pressure loading at Aberdeen (UK). The deformations are in millimeters.

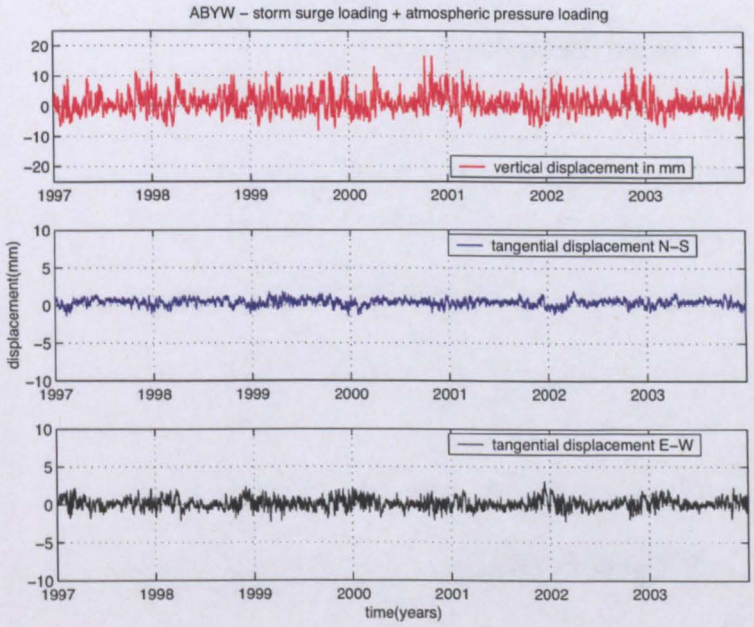

Figure E.20: Same as Figure E.19 but for the site of Aberystwyth (UK).

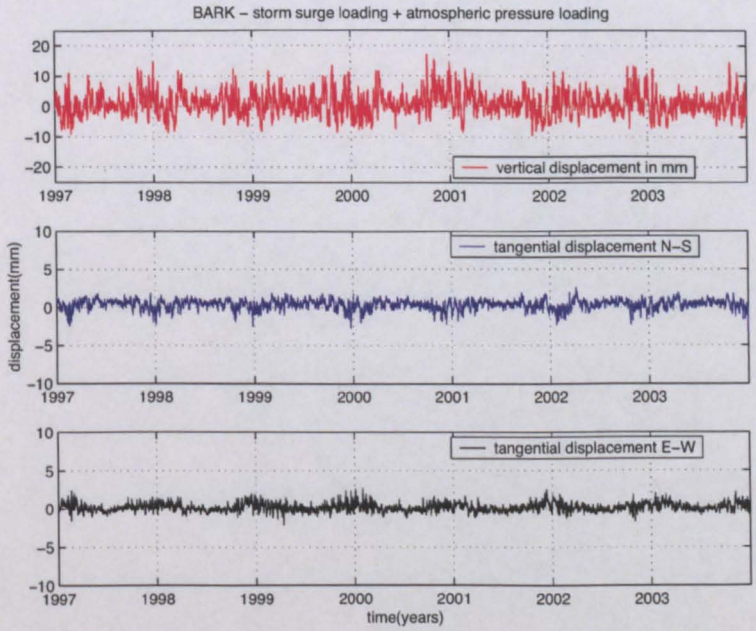

Figure E.21: Same as Figure E.19 but for the site of Barking (UK).

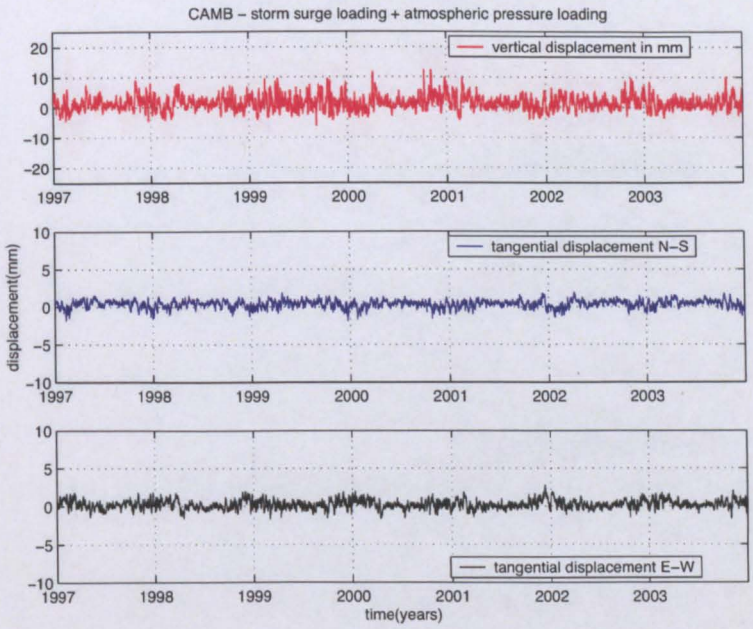

Figure E.22: Same as Figure E.19 but for the site of Camborne (UK).

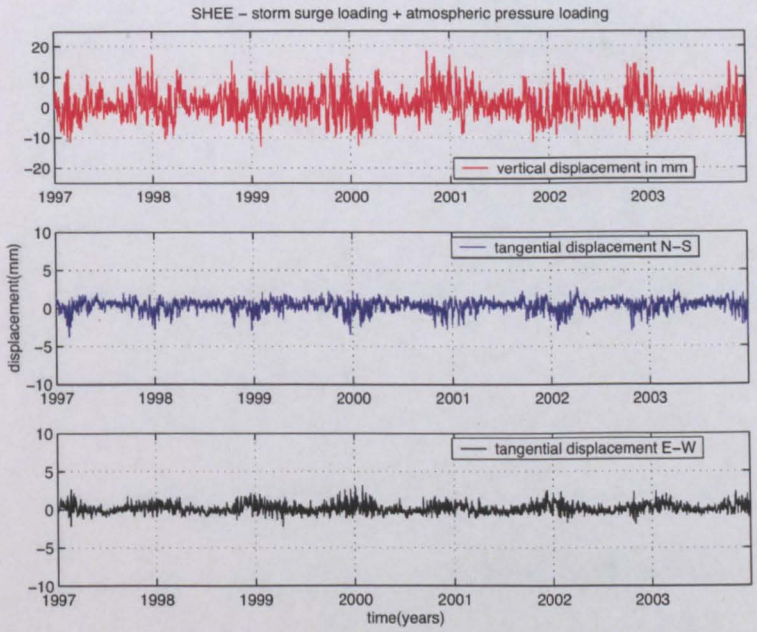

Figure E.23: Same as Figure E.19 but for the site of Sheerness (UK).

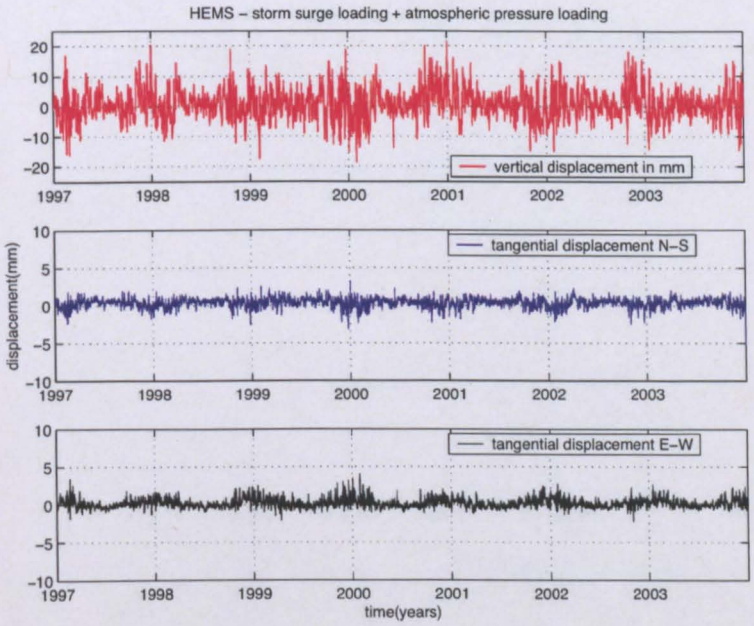

Figure E.24: Same as Figure E.19 but for the site of Hemsby (UK).

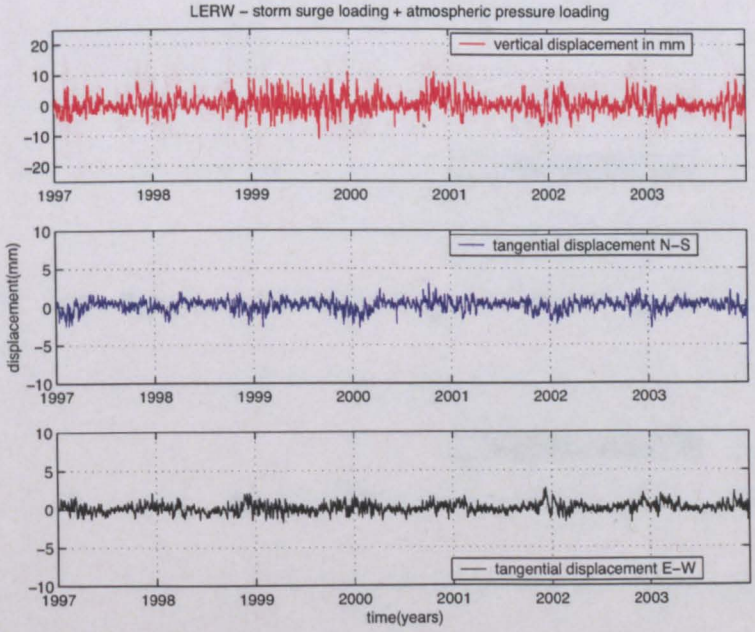

Figure E.25: Same as Figure E.19 but for the site of Lerwick (UK).

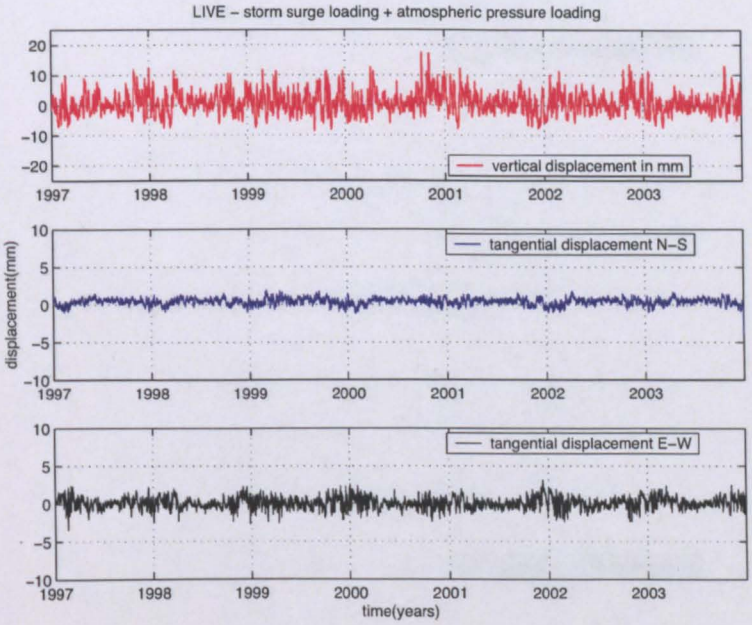

Figure E.26: Same as Figure E.19 but for the site of Liverpool (UK).

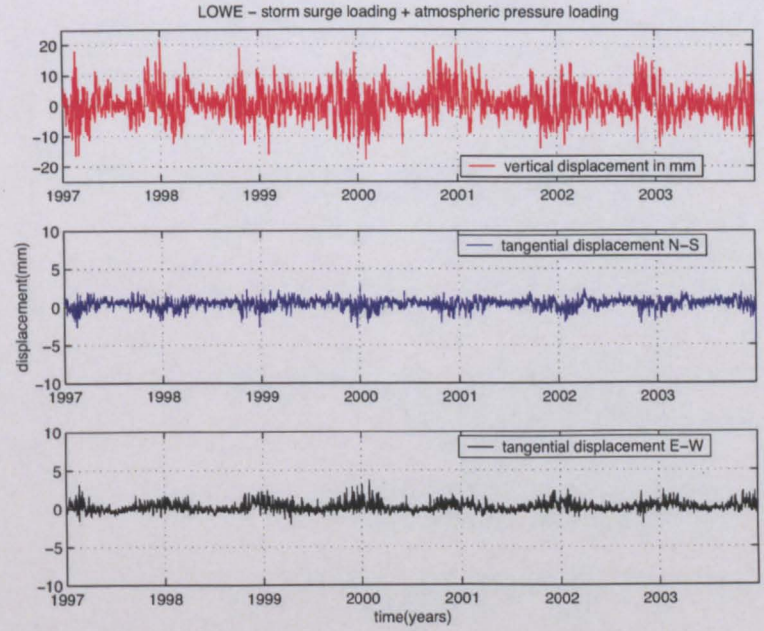

Figure E.27: Same as Figure E.19 but for the site of Lowestoft (UK).

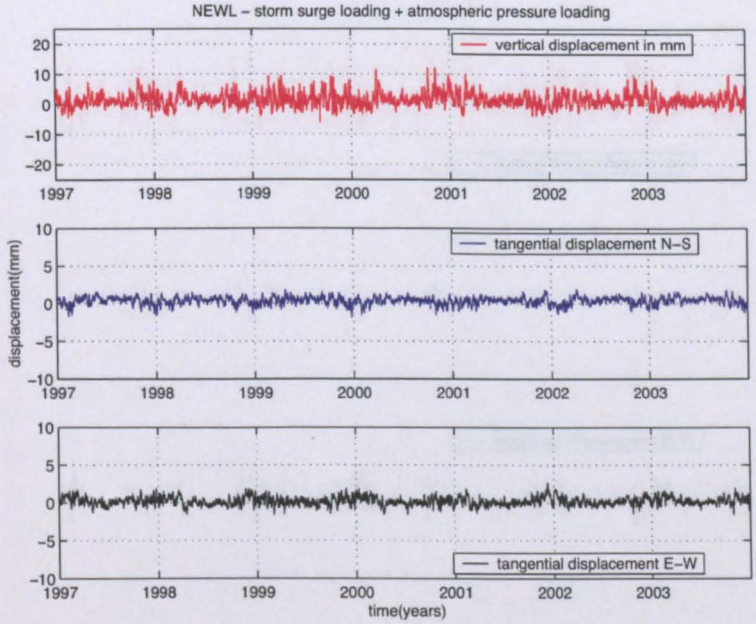

Figure E.28: Same as Figure E.19 but for the site of Newlyn (UK).

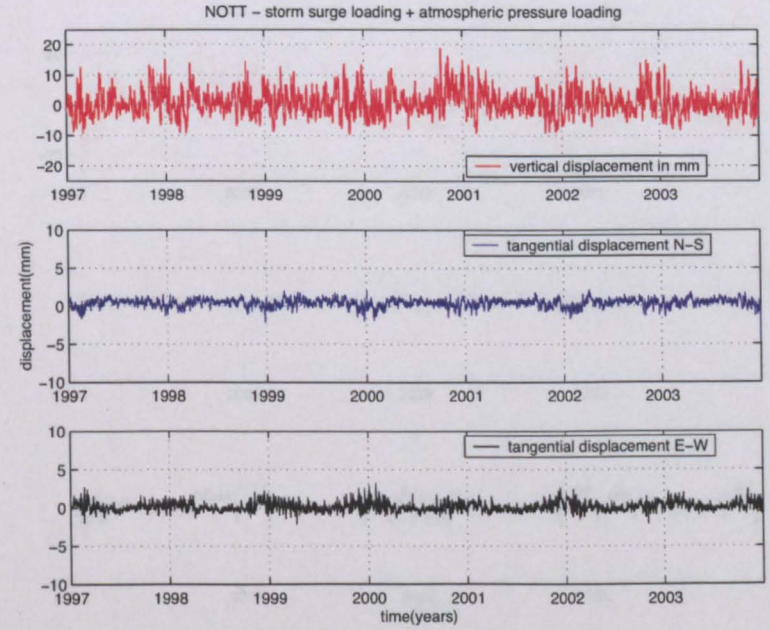

Figure E.29: Same as Figure E.19 but for the site of Nottingham (UK).

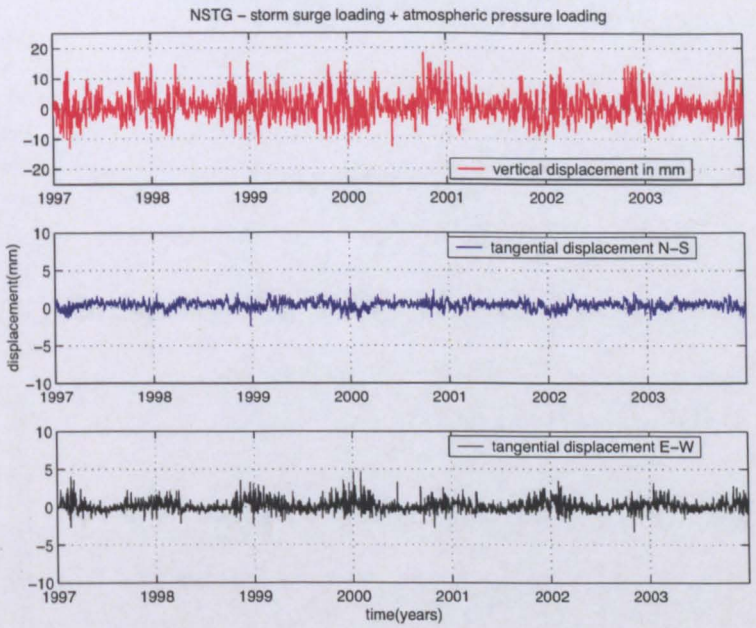

Figure E.30: Same as Figure E.19 but for the site of North Shields (UK).

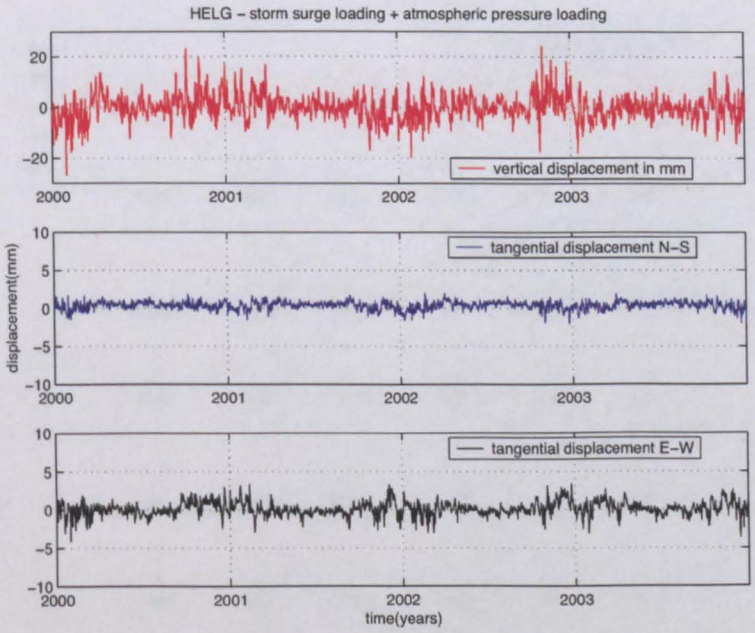

Figure E.31: Same as Figure E.19 but for the site of Helgoland (Germany).

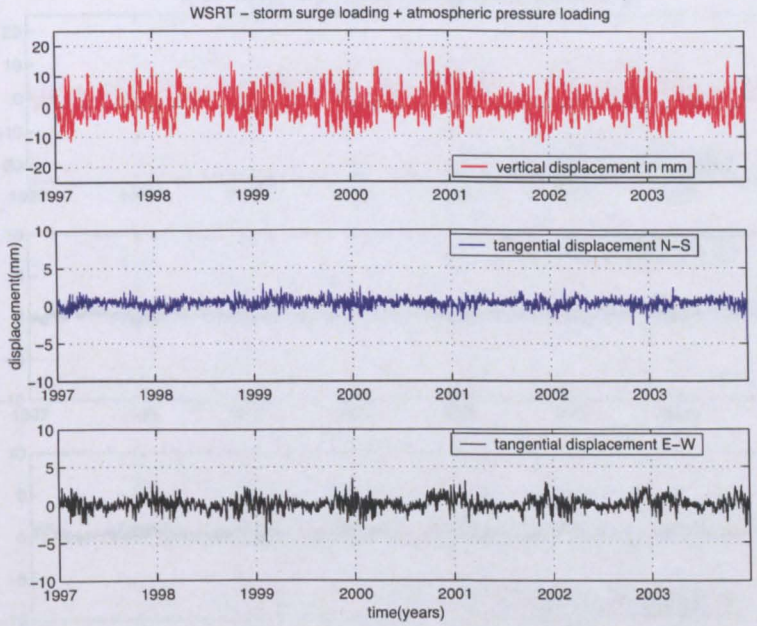

Figure E.32: Same as Figure E.19 but for the site of Westerbork (Germany).

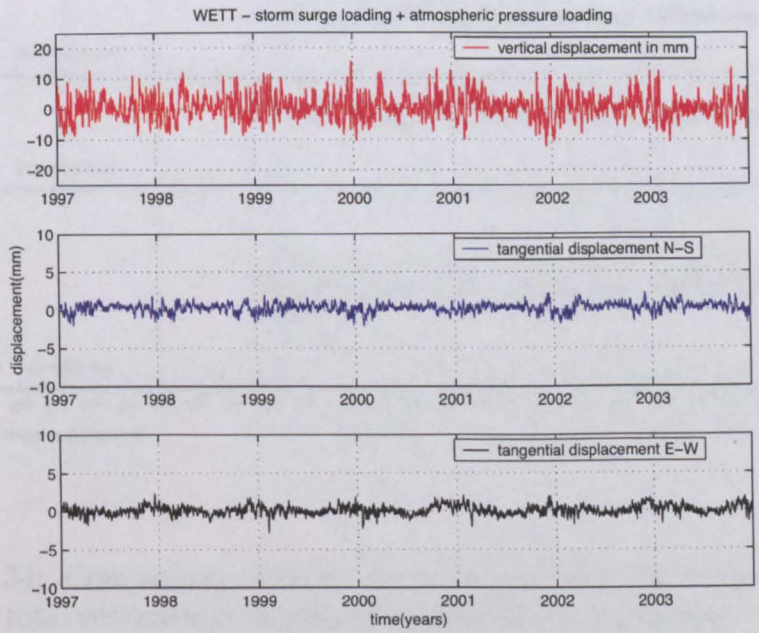

Figure E.33: Same as Figure E.19 but for the site of Wettzell (Germany).

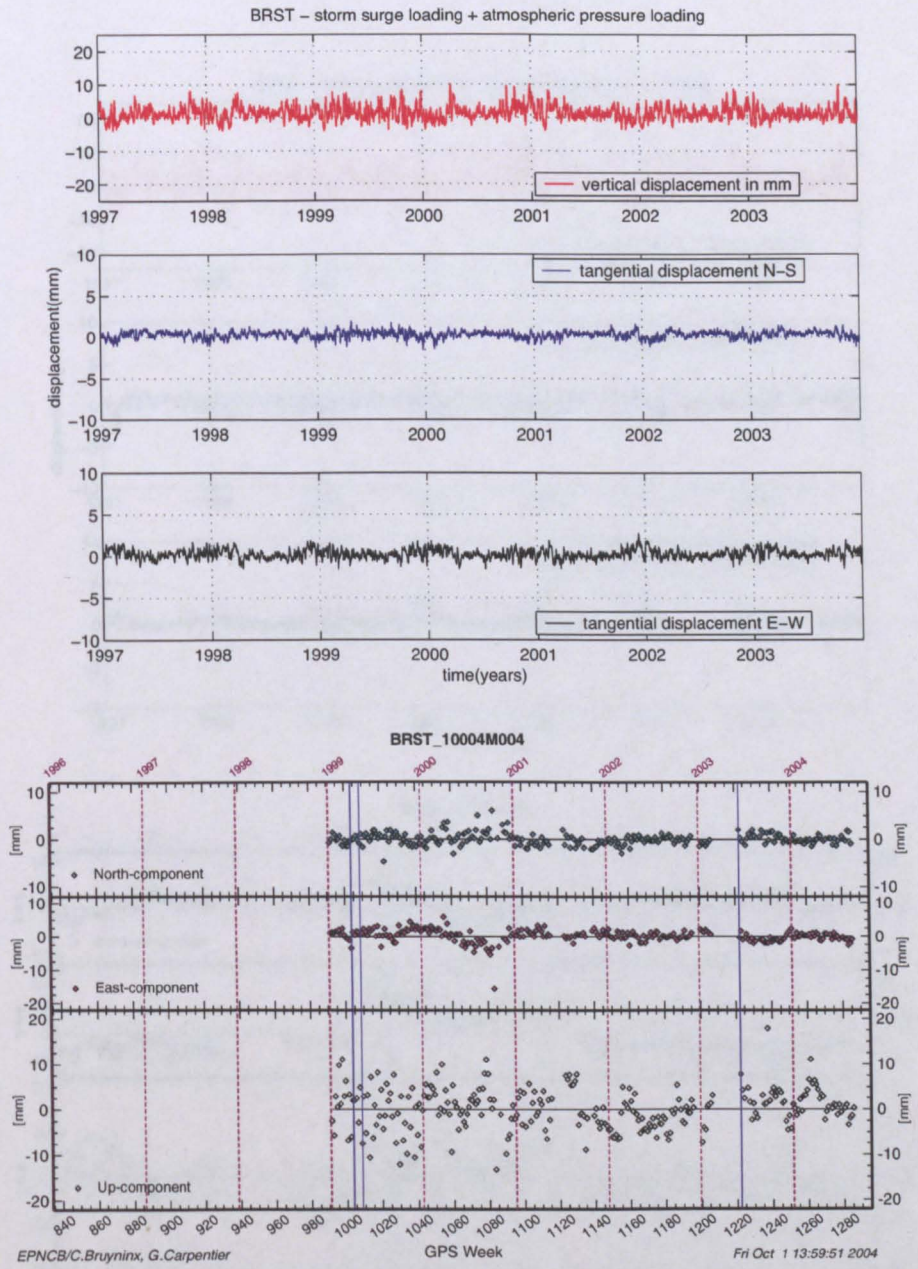

Figure E.34: Comparison between the standard EPN time series and the predicted total vertical and tangential displacements. In the upper part of the figure are the modelled total vertical (in red) and tangential displacements (in blue the north-south component and in black the east-west component) induced by storm surges loading and atmospheric pressure loading at Brest (France). The predicted displacements are compared with the standard EPN time series for the site considered (lower part). All the deformations are in millimeters.

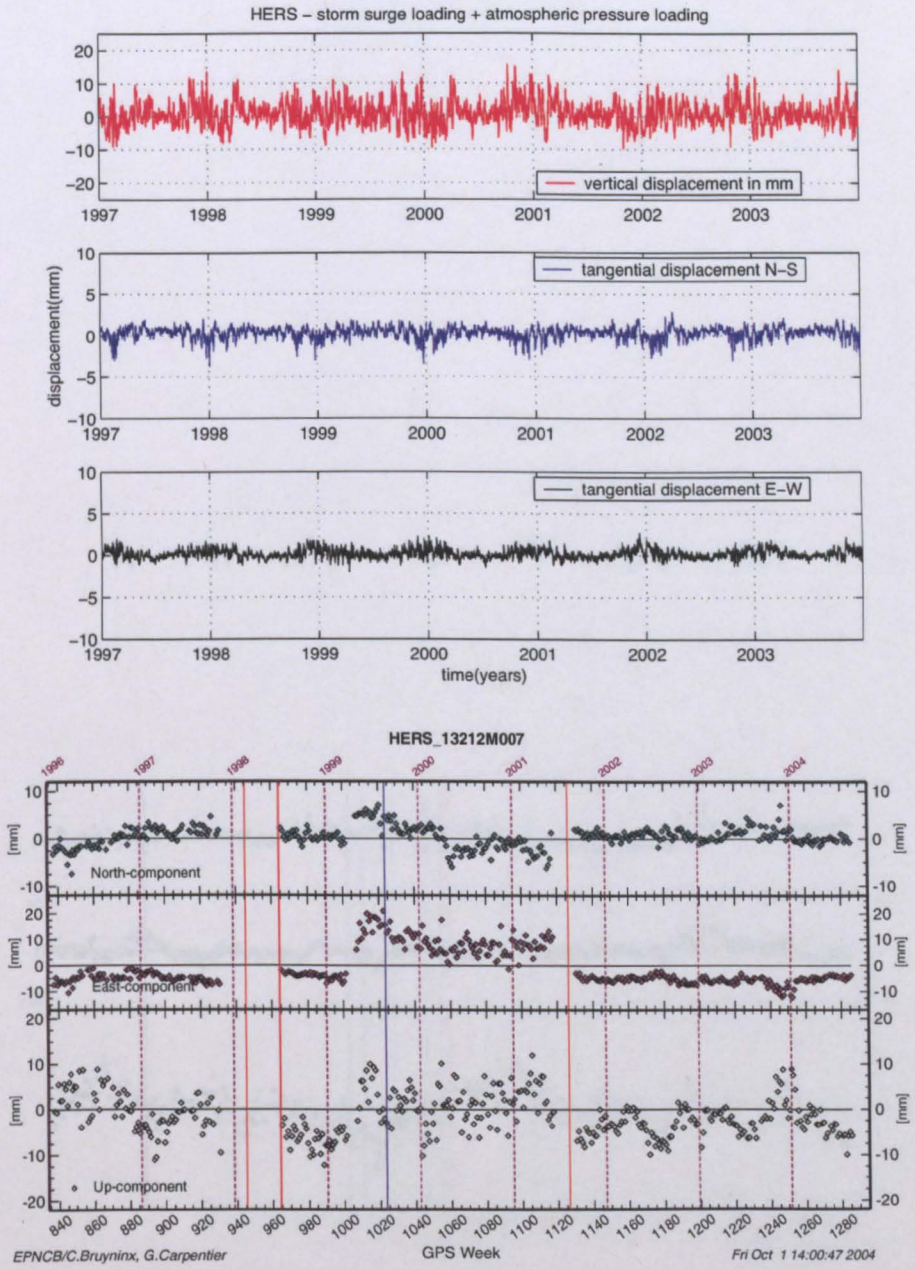

Figure E.35: Same as Figure E.34 but for the site of Herstmonceux (UK).

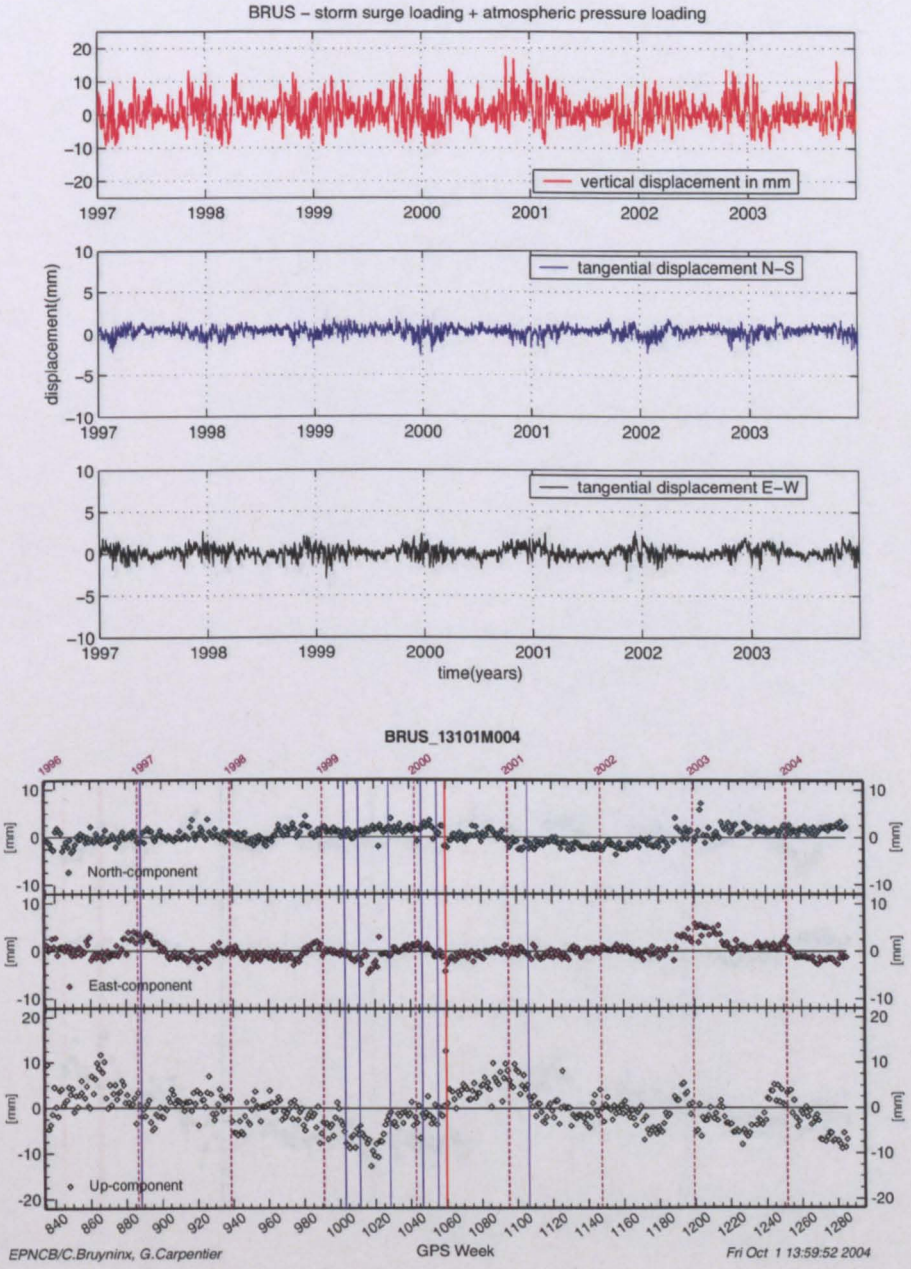

Figure E.36: Same as Figure E.34 but for the site of Brussels (Belgium).

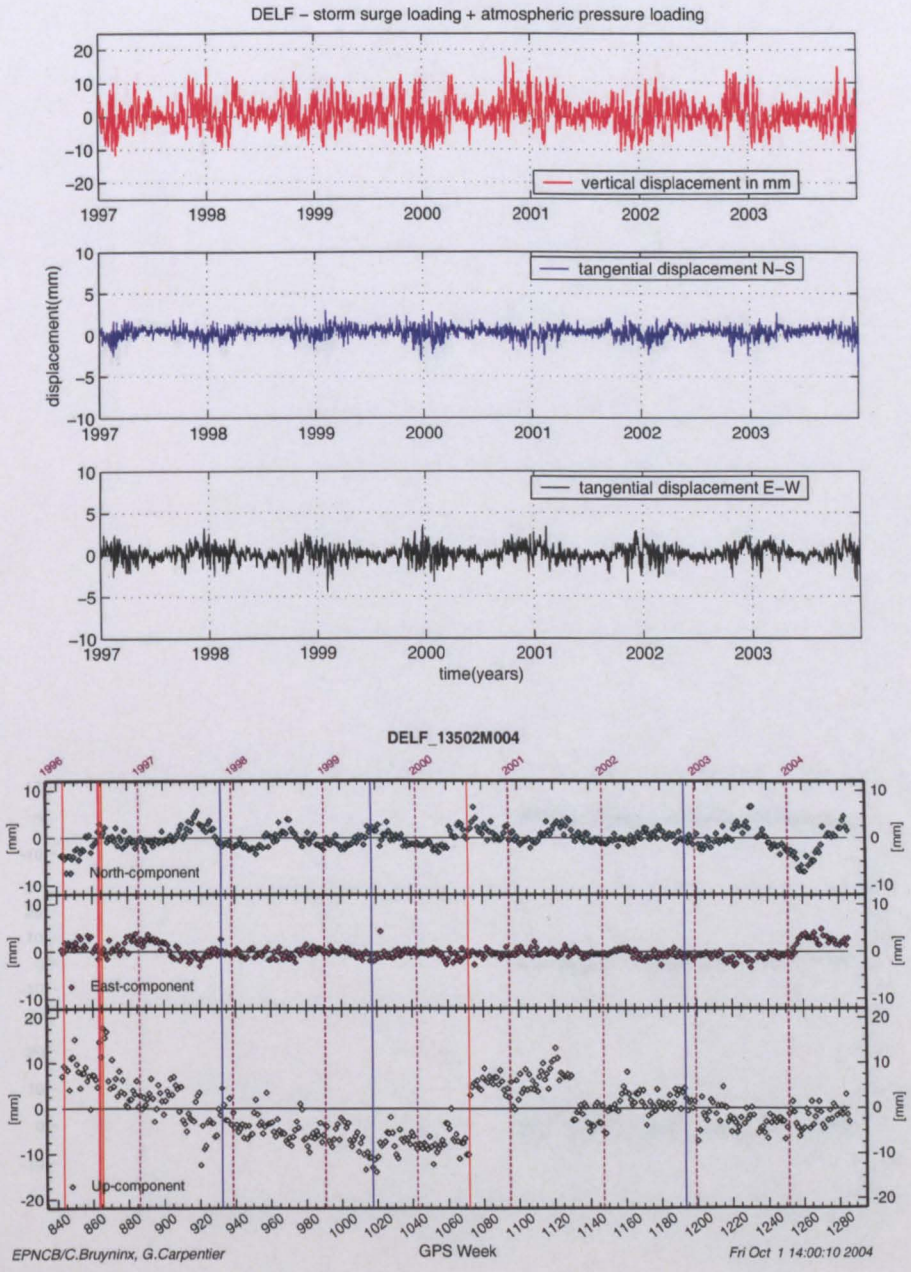

Figure E.37: Same as Figure E.34 but for the site of Delft (Netherland).

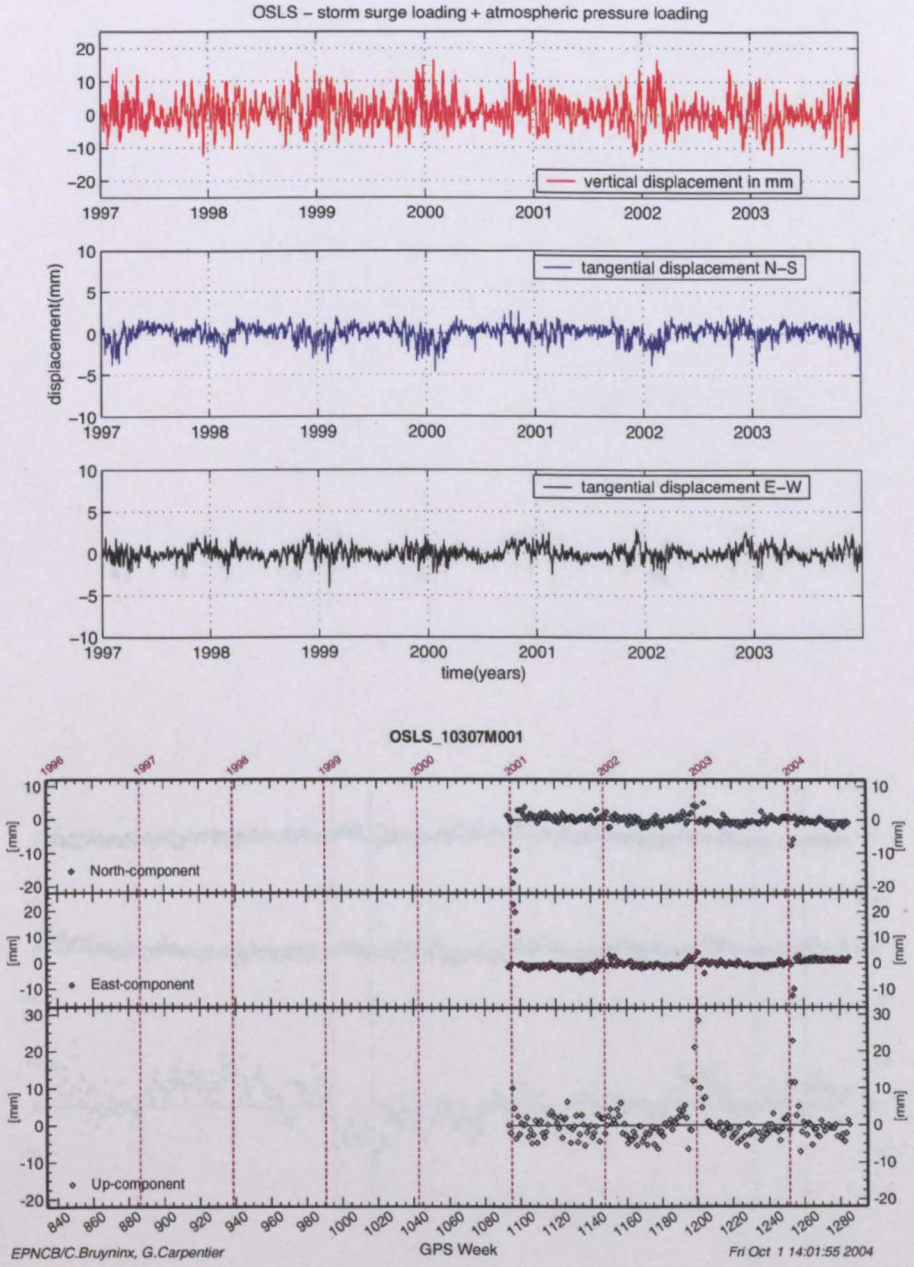

Figure E.38: Same as Figure E.34 but for the site of Oslo (Norway).

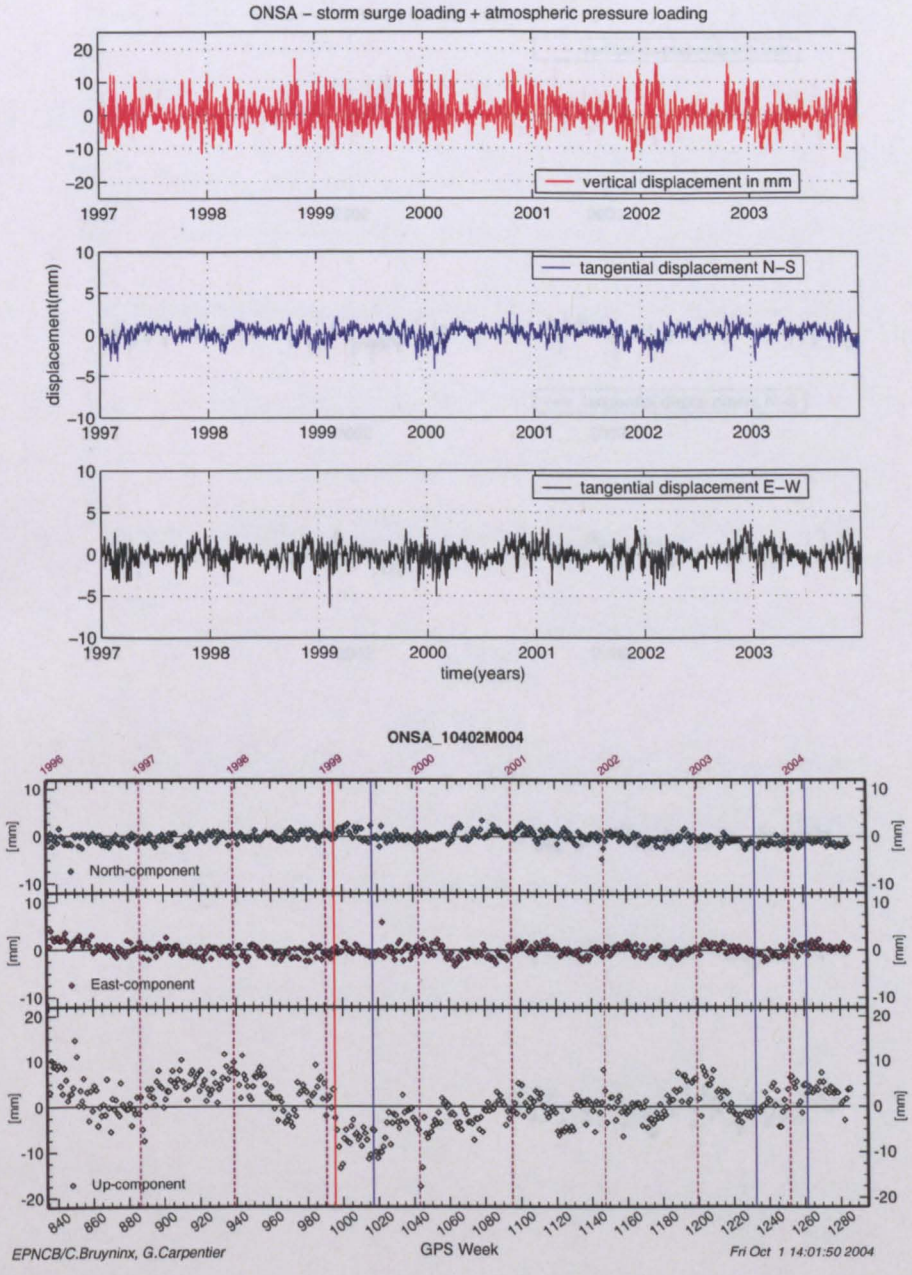

Figure E.39: Same as Figure E.34 but for the site of Onsala (Sweden).

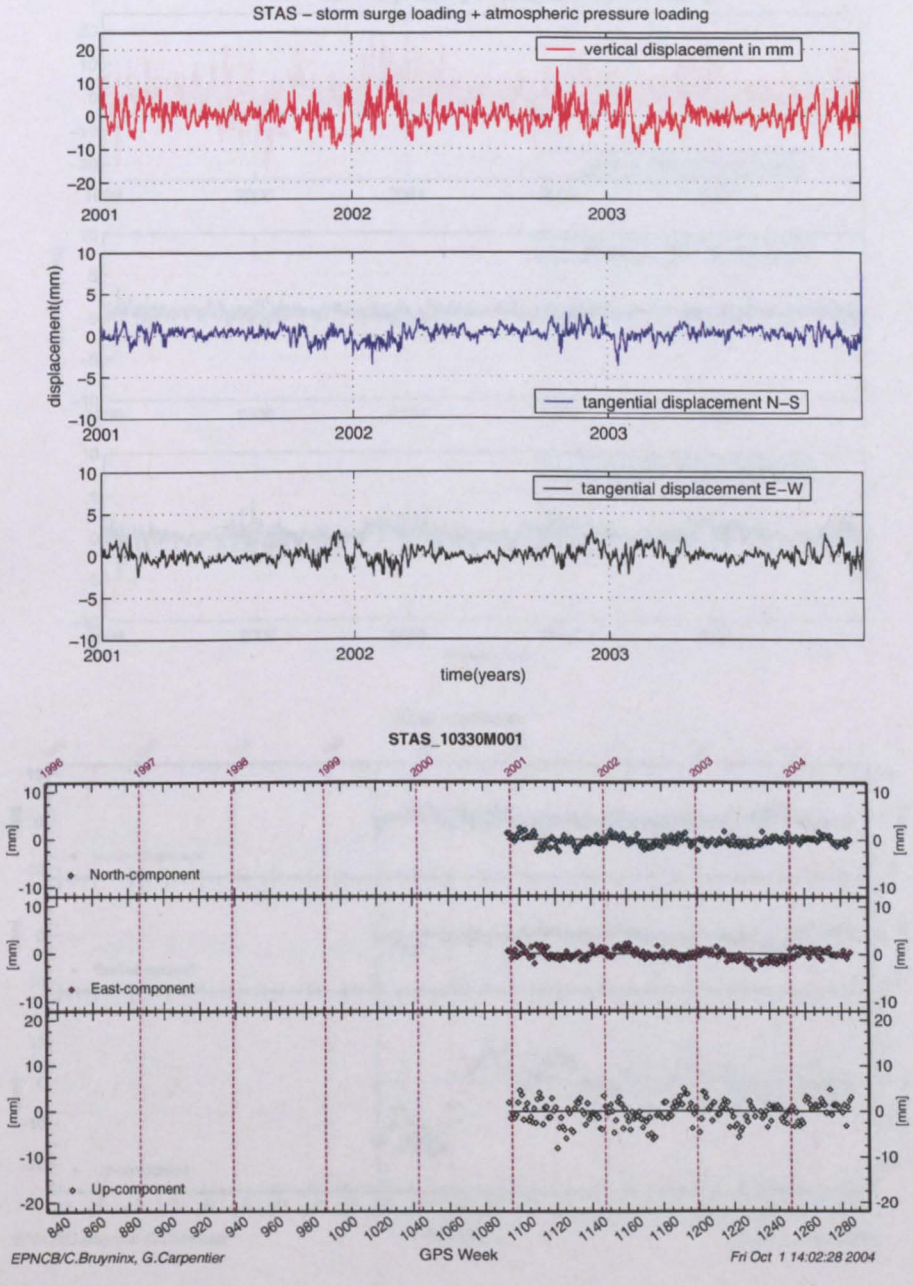

Figure E.40: Same as Figure E.34 but for the site of Stavanger (Norway).

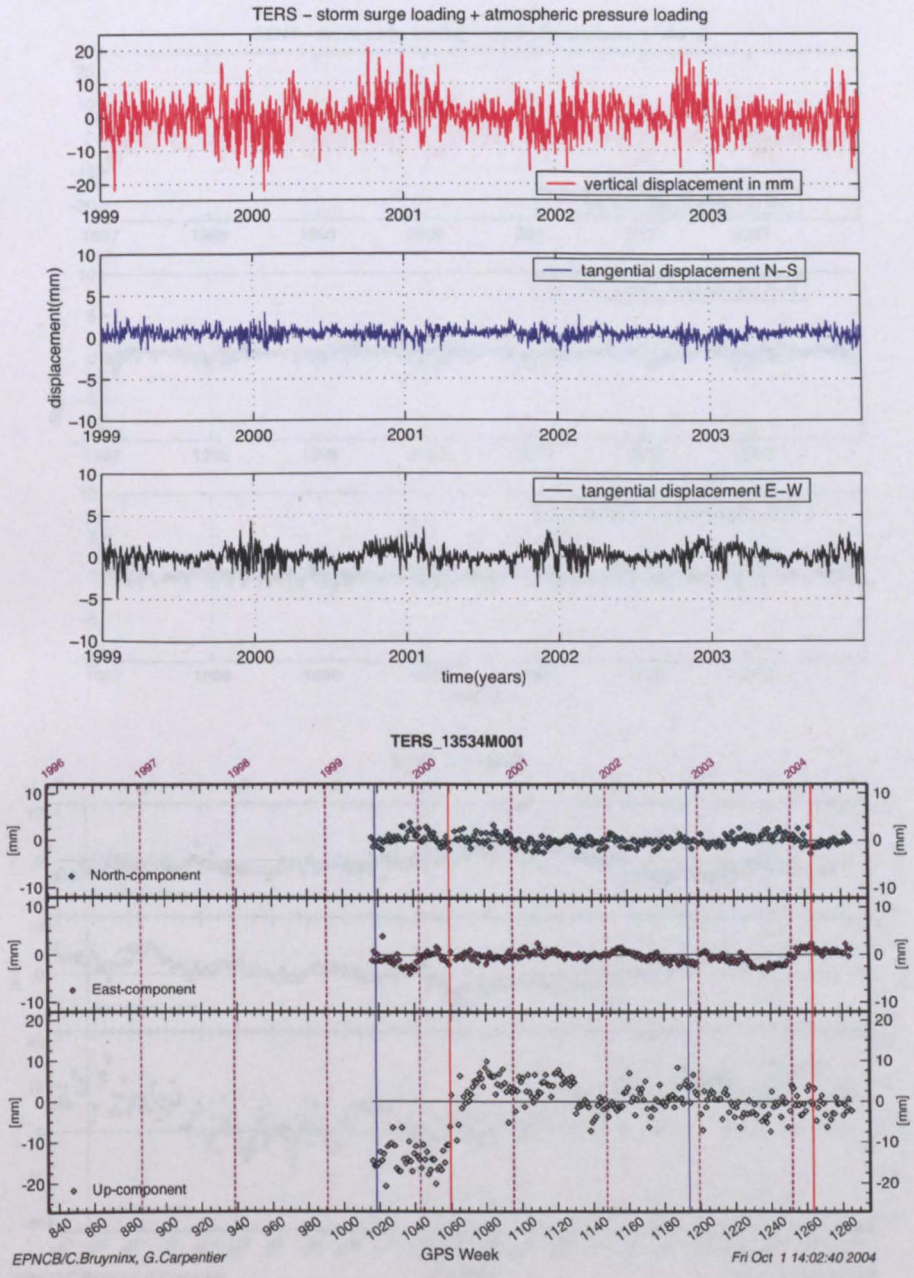

Figure E.41: Same as Figure E.34 but for the site of Terschelling (Netherland).

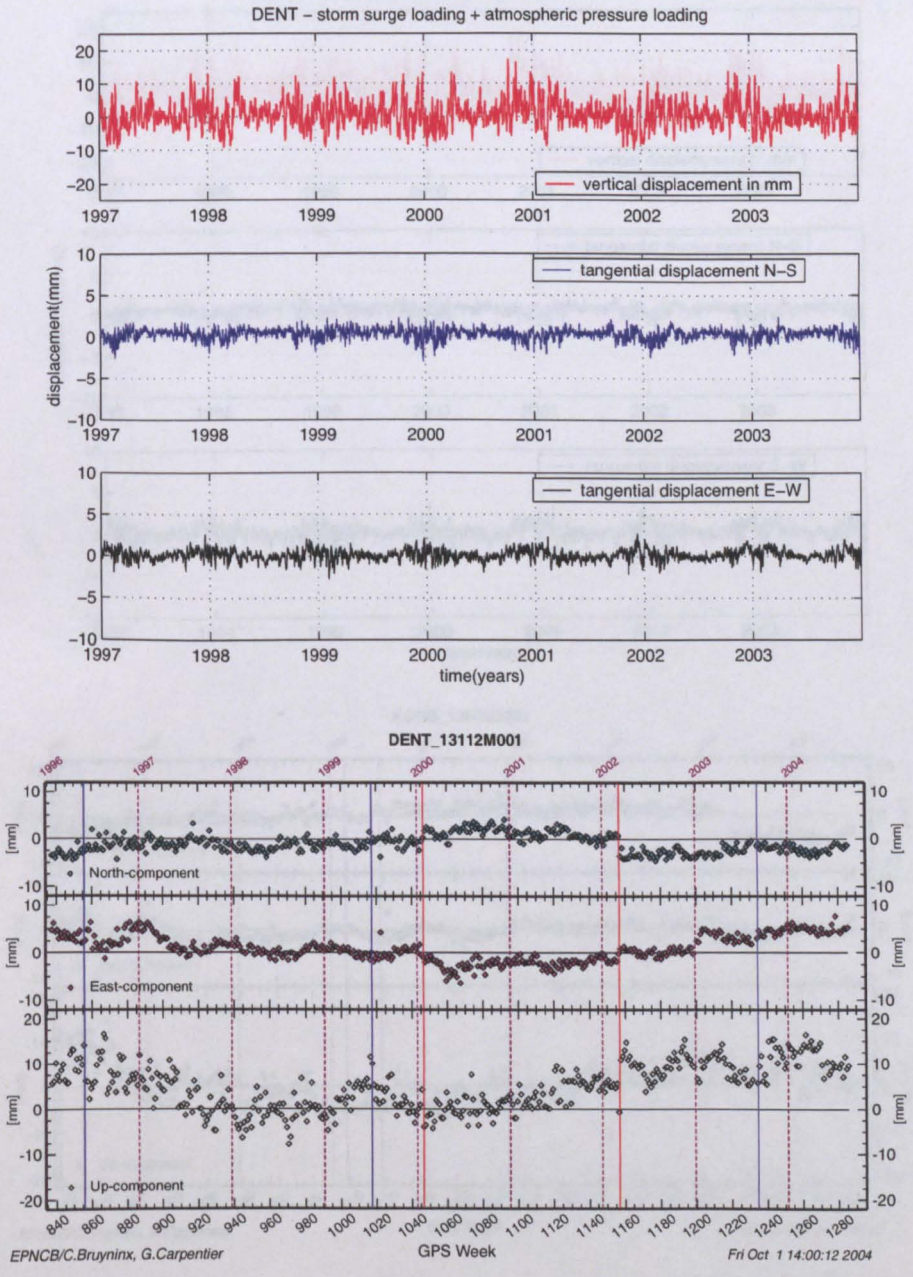

Figure E.42: Same as Figure E.34 but for the site of Dentergem (Belgium).

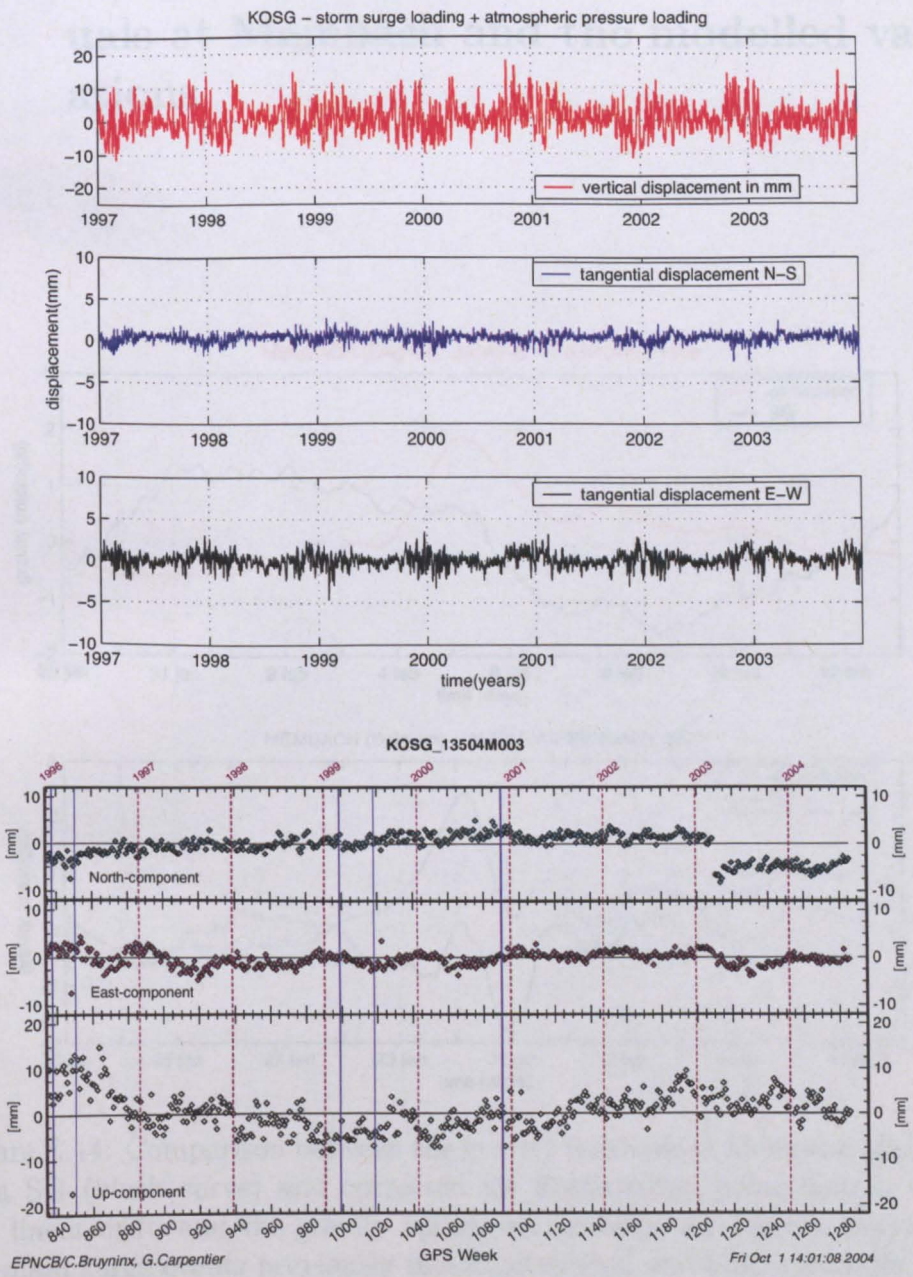

Figure E.43: Same as Figure E.34 but for the site of Kootwijk Observatory (Netherland).

E.3 Comparison between the SG gravity residuals at Membach and the modelled variations

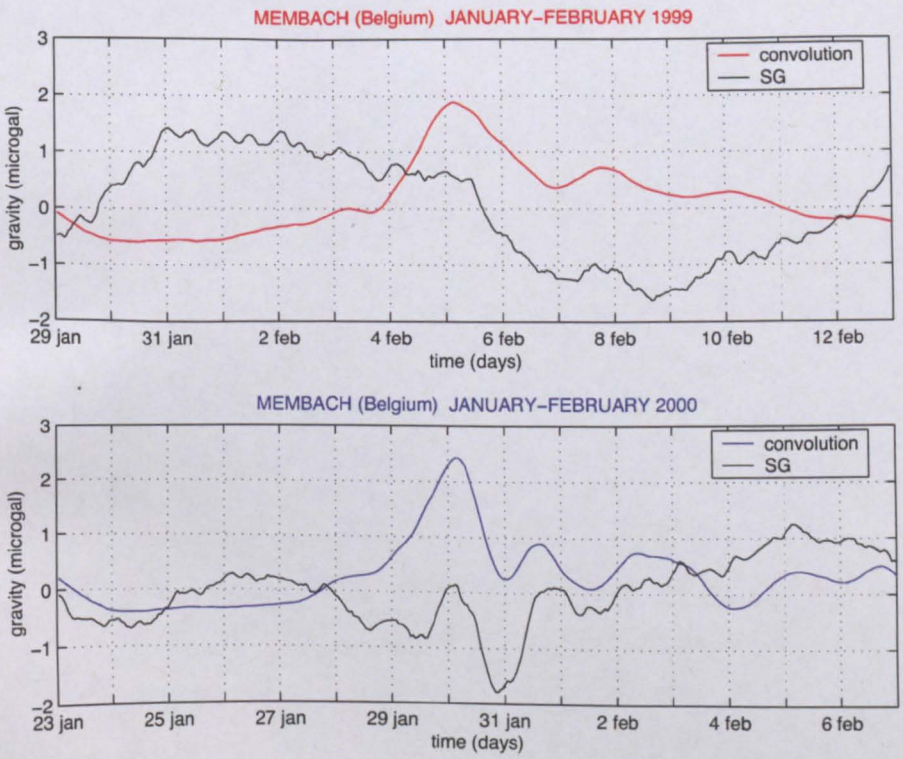

Figure E.44: Comparison between the gravity residuals at Membach observed by a SG (black curve) and corrected for Earth tides, polar motion effect and linear drift, and the gravity variations modelled for the two periods of the main surge events previously investigated (red and blue curves for 1999 and 2000 respectively). The air pressure effect was not removed from the observations.